The development and characterisation of a novel reverse-phase wet granulation process

Wade, Jonathan

Awarding institution:
King's College London

The development and characterisation of a novel reverse-phase wet granulation process

Jonathan Brett Wade
(BSc, MSc)

A thesis submitted for the degree of

Doctor of Philosophy
Of
King's College London

Institute of Pharmaceutical Science

2013

To Vicki, Ben & Sam

The happiness of a man in this life does not consist in the absence but in the mastery of his passions

Alfred Lord Tennyson

ACKNOWLEDGEMENTS

I am deeply grateful to my supervisors, Professor Gary Martin and Dr. Dave Long, for their expert supervision, continual support and encouragement. It has been the leadership and feedback provided by Professor Martin, and the challenging comments and playful tone of Dr. Long, which have encouraged me throughout this work.

I would especially like to thank my family. My wife Victoria who has endured many years of days, evenings and weekends hearing about "powders sticking together" all the while bringing our son Ben into this world part way through the Raman spectroscopy study, and then our son Sam during the thesis submission. I would also like to thank my father Lindsay for providing me with the competitive spark to achieve my research and educational goals, and my mother Anne for her continued voice of calm throughout.

My gratitude also goes to Sharon Deram from SBI Analytical Inc. for her assistance and training on the RXN2-785 Raman spectrometer, P^{h}AT probe and iC Raman^{TM} software and to Kaiser Optics for the loan of the instrument.

Finally, I would like to acknowledge Eli Lilly for their financial support and my industrial sponsor Dr. Kurt Van Scoik for his support of my personal development.

LIST OF PUBLICATIONS

MANUSCRIPTS

Wade J.B., Martin G.P. and Long D.F., A methodological approach for determining the effect of moisture content on the compaction properties of powders: granular hydroxyapatite, Powder Technology, 246 (2013) 511-519.

Wade J.B., Martin G.P. and Long D.F., An assessment of powder pycnometry as a means of determining granule envelope density. Pharmaceutical Development and Technology, DOI:10.3109/10837450.2013.860550.

POSTER PRESENTATIONS

Wade J.B., Martin G.P. and Long D.F., Effects of moisture on the compaction properties of granular anhydrous tricalcium phosphate (TRI-CAL WG^{TM}), Poster M1010, AAPS Workshop on Advances and Opportunities in Drug Product Manufacturing, Baltimore, MD, USA. 20th September 2010.

Wade J.B., Martin G.P. and Long D.F., Development of a novel reverse-phase wet granulation process: effect of liquid saturation and impeller speed. Poster W4150, 2012 AAPS Annual Meeting and Exposition, Chicago, IL, USA. 17th October 2012.

Wade J.B., Martin G.P. and Long D.F., Determination of granule envelope density using the GeoPyc® apparatus. Poster W5336, 2012 AAPS Annual Meeting and Exposition, Chicago, IL, USA. 17th October 2012.

Wade J.B., Martin G.P. and Long D.F., Development of a growth regime map for a novel reverse-phase wet granulation process. Poster 58, 6th international Granulation Workshop, Sheffield, UK. 27th June 2013.

ABSTRACT

Conventional wet granulation processes involve controlled coalescence of moist particles through the addition of binder liquid to dry powder particles such that the process proceeds in the direction of increasing liquid saturation. The process is terminated immediately prior to an undesirable state of uncontrolled granule growth and batch loss. The ideal conventional wet granulation process is stated to require tight control over granule nucleation conditions which are often not possible to execute commercially. Consequently, a novel reverse-phase granulation process was developed and studied involving immersion of dry powder into the binder liquid, thus eliminating the traditional granule nucleation process. The reverse-phase process proceeds in the direction of reduced liquid saturation, thus decreasing the risk of uncontrolled growth and batch loss.

The effects of binder liquid quantity, binder liquid viscosity and impeller speed on the granules produced using the reverse-phase and conventional processes were compared. The conventional process exhibited induction growth behaviour and uncontrolled granule growth at elevated liquid saturation. In contrast the reverse-phase process demonstrated steady granule growth behaviour at all liquid saturations indicating greater robustness to process failure. The primary mechanism of the reverse-phase granulation process was breakage of large moist agglomerates and mechanical dispersion of the binder liquid throughout the powder formulation. The size and porosity of reverse-phase granules were controlled by the liquid saturation and impeller speed, with these physical properties being best described by the dimensionless Stokes deformation number and the growth regime map.

Two potentially negative consequences associated with the reverse-phase granulation approach were evaluated. First, the compaction properties of reverse-phase granules were shown to be similar to those of conventional granules. Second, the rate and extent of hydration of the model drug anhydrous theophylline was shown to be similar for both the reverse-phase and conventional granulation processes. Based upon these findings it was concluded that the reverse-phase process may represent a feasible alternative to the conventional process, particularly should scale-up to the industrial scale prove applicable.

CONTENTS

LIST OF FIGURES

LIST OF TABLES

ABBREVIATIONS AND SYMBOLS USED COMMONLY

ABBREVIATIONS

A: Area
ANOVA: analysis of variance
BCS: Bio Classification System
BET: Brunauer Emmett Teller theory
D: Diameter
DSC: differential scanning calorimetry
G: Gibbs free energy
H: Enthalpy
HA: Hydroxyapatite
HPC: Hydroxypropyl cellulose
HPMC: Hydroxypropylmethyl cellulose
MCC: Microcrystalline cellulose
NIR: Near Infra Red
P: Pressure
PAA: Poly (acrylic acid)
PEG: Polyethylene glycol
PVP: Poly (vinyl pyrrolidone)
R^2: linear correlation coefficient
RH: relative humidity
rpm: revolution per minute
S: Entropy
SD: standard deviation
SEM: scanning electron microscopy
t: thickness
T: Temperature
TER: Total elastic recovery
TGA: thermogravimetric analysis
YM: Young's Modulus of elasticity

SYMBOLS

Ca^*: Modified capillary number
d: pore size
$d_{3,2}$: surface mean particle size
d_{pm}: mass mean diameter
d_{10}: 10 % of particles have size ≤ d
d_{50}: 50 % of particles have size ≤ d
d_{90}: 90 % of particles have size ≤ d
ε: porosity
ε_{min}: minimum porosity reached
k: tablet bonding capacity
θ: contact angle
σ: wet granule strength
σ_g: dry granule strength
σ_{To}: tablet tensile strength at zero porosity
ρ_{bulk}: bulk density
ρ_c: tablet density
ρ_e: envelope density
ρ_t: true density
ρ_{tap}: tapped density
P_y: mean yield pressure
S_{max}: liquid saturation
St_{def}: Stokes deformation number
v: powder surface velocity
v_o: particle relative velocity
w: Walker compressibility constant
ψ_a: dimensionless spray flux
γ: surface tension
μ: viscosity

CHAPTER ONE: INTRODUCTION

1 General introduction

Tablets are the most popular dosage form for drug delivery in the pharmaceutical industry, occupying over two thirds of the global market [1-3]. Convenience of administration, accurate dosing, ease of manufacture, long term storage stability and good tolerance to changes in temperature and humidity contribute to this popularity [4].

Tablets are prepared by compressing a powder blend in a die, at high compression force, to form a solid compact. The powder blend contains the drug and generally a diluent, a binder, a disintegrant and a lubricant. The large scale production of high quality tablets requires a powder blend with excellent properties regarding homogeneity, flow and compaction that will yield a tablet with the desired mechanical properties, dose uniformity and drug release profile. Often the powder blend does not possess all of these properties and therefore some form of agglomeration process, such as dry or wet granulation, extrusion, or spray drying, is employed to enhance the tableting properties.

1.1 Overview of common agglomeration techniques

1.1.1 Dry granulation

The term dry granulation encompasses both slugging and roller compaction agglomeration processes. These processes are primarily used to improve powder flow properties. Slugging is a lesser used technique involving the compaction of powder, at intermediate pressure, to form a large “slug” in the order of 2.5 cm diameter and 0.75 cm thickness [5]. Roller compaction involves compressing the powder between two counter-rotating rolls, under pressure, to form a “ribbon” of compacted powder. The resulting slug or ribbon is then milled to obtain granules of the desired size distribution for further processing. Dry granulation processes are relatively simple, fast, easily controlled and are often favoured in the processing of moisture or temperature sensitive drugs. However, the resulting tablets often show inferior tensile strength compared to other granulation techniques due to the limited bonding potential of the powder, which is partially consumed during the compaction stage of the dry granulation step [6].

Powders which undergo plastic deformation [7] have been shown to be more sensitive to this phenomenon than powders that undergo deformation by brittle fracture [8].

1.1.2 Extrusion

Extrusion (or spheronisation) involves six steps [9]; (i) dry mixing of ingredients, (ii) wet granulation to form a sufficiently plastic wet mass, (iii) extrusion to form rod-shaped particles of uniform diameter, (iv) rounding of rod-shaped particles in a spheroniser, (v) drying to a prescribed moisture content, (vi) milling to achieve the desired particle size distribution. The major advantage of extrusion is the ability to form granules with very high levels of drug without producing granules of excessive size [10]. Extruded pellets offer flexibility in dosage form design and can be coated with functional or aesthetic coatings, compressed into tablets or filled into capsules. However, extrusion is considered to be more labour and time consuming than the other agglomeration approaches and is typically only used in circumstances where other techniques cannot form granules of the required properties [9].

1.1.3 Spray drying

Spray drying occurs in three main stages [11]: (i) atomisation of the feed liquid, (ii) mixing of spray droplets with a heated air stream to form dried particles by evaporation, (iii) separation of the dried particles from the air stream. Spray drying offers good control over particle size, shape and moisture content. The main advantage of spray drying is the ability to increase the solubility of drugs through stabilisation of the amorphous form in a solid dispersion [12]. However, spray drying is not well suited to forming particles >200 μm, has poor thermal efficiency and the exhaust air stream contains significant heat which requires removal [11].

1.1.4 Wet granulation

Wet granulation typically involves an initial dry blending of the powders, to give an homogeneous distribution, followed by the addition of a granulation liquid to the powders. Continued mixing ensures wetting of the powder surfaces and promotes agglomeration of the particles to form granules. Mixing is continued until the desired

end point is reached. The end point may be defined by a number of parameters including mixing time, quantity of binder liquid added and power or torque reading on the mixing impeller. The wet granules are then passed through a coarse screen to break large lumps, dried to remove the binder liquid, and milled to produce granules of the desired particle size distribution. The milled granules are then often blended with a lubricant, and potentially a portion of extra-granular binder and disintegrant, to form the final granule blend which is homogeneous, free flowing and possesses sufficient compaction properties to form a suitable tablet under compression.

Wet granulation is used to enhance powder flowability and compaction properties and reduce segregation potential. The main advantage offered by wet granulation is the ability to increase the bioavailability of poorly soluble drugs. A surface active agent can be readily incorporated into the binder liquid, where it is brought into intimate contact with the surfaces of the drug particles during the granulation process, to enhance solubility and dissolution rate. It is estimated that approximately 40 % of the world's top oral drugs are classified as BCS (Bio Classification System) class II (low solubility, high permeability) and IV (low solubility, low permeability) compounds [13], and that the problem is considered even worse in drug discovery pipelines [14]. Consequently, the use of wet granulation processes to simultaneously form granules of the desired physical properties and enhanced bioavailability remains a popular option.

1.2 Introduction to wet granulation

Wet granulation processes have been a topic of research for several decades with Newitt and Conway-Jones [15] pioneering some of the earliest work in 1958, where they investigated the agglomeration behaviour of sand in a drum granulator. Since then a substantial volume of work has been published studying a wide range of materials such as detergents, minerals and pharmaceuticals, which have been granulated in a variety of equipment ranging from coffee grinders, food processors, rotating drums, fluidised beds and high shear mixers. Several comprehensive review papers have been written over the decades to summarise the state of knowledge in the discipline; notably in the 1970's where Kapur [16] reviews the "balling" process, the 1980's [17-19] and 1990's [20] where authors review "agglomeration" and "size enlargement", and finally the 2000's where Iveson *et al* [21] review the "nucleation, growth and breakage phenomena in

agitated wet granulation processes". These earlier reviews provide the basis for the current understanding that wet agglomeration processes involve three simultaneous rate processes [22] as shown in Figure 1-1; (A) wetting and nucleation; (B) consolidation and coalescence; (C) attrition and breakage. Each has received considerable attention in the literature and are discussed separately in the following sections.

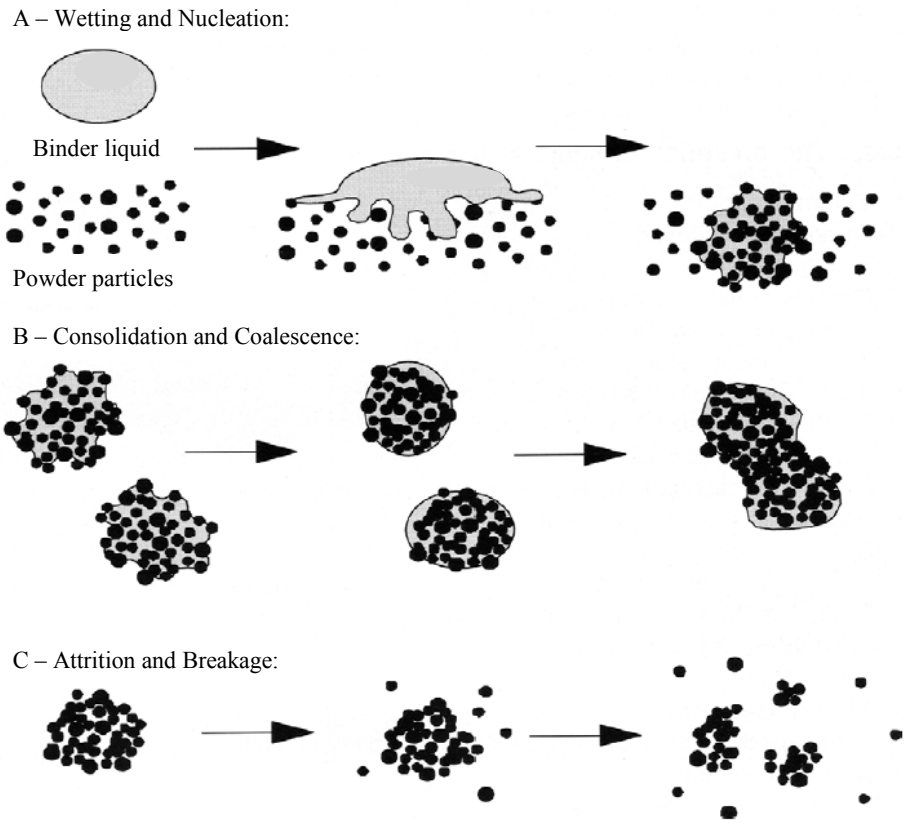

Figure 1-1. Representation of wet granulation rate processes: A - Wetting and Nucleation. B - Consolidation and Coalescence, C - Attrition and Breakage. Taken from [23].

1.3 Wetting and nucleation

Wetting is the process of displacing air from the powder surface with binder liquid. Nucleation is the process of bringing two or more surface wet particles into contact to form nuclei (Figure 1-1A). The area where the binder liquid and powder surface come into contact to form initial nuclei is termed the nucleation zone. Both nuclei formation and binder liquid dispersion are important in the nucleation zone. The size of the binder liquid droplet relative to the powder particles onto which it is deposited will influence the nucleation mechanism. Two different nucleation mechanisms have been proposed

[24, 25]; if the droplet is large compared to the particles, nucleation will occur by immersion of the smaller particles into the larger droplet to form nuclei with saturated pores. Alternatively, nucleation with relatively small droplets will occur by distribution of the drops on the surface of the particles, which will then start to coalesce.

1.3.1 Drop penetration time

When a binder liquid contacts the powder bed surface it penetrates into the capillary pores, both within and between particles, to form nuclei. The time taken for the drop to penetrate completely into a powder bed with no liquid remaining on the surface is defined as the drop penetration time. Denesuk *et al* [26] developed a simple drop penetration time model taking into account the liquid surface tension, liquid viscosity, solid-liquid contact angle and the pore size of the powder bed. They applied the Washburn equation, where wetting is driven by capillary pressure and resisted by viscous dissipation of the flow, and assumed the powder bed behaved as a bundle of parallel cylindrical capillaries. They also assumed the drop penetration behaviour follows the constant drawing area (CDA) model where the three-phase contact line remains stationary (i.e. constant drop radius) and the apparent contact angle slowly decreases as the liquid drains from the droplet into the porous surface. The CDA model is more commonly used than the decreasing drawing area (DDA) model where the apparent contact angle at the substrate surface remains constant throughout the penetration process and the liquid contact line retards toward the centre of the drop [27]. Hapgood *et al* [27] modified the approach by introducing terms for the effective porosity and effective pore size of the powder bed to account for the fact that the assumption of parallel capillary pores is unlikely to represent a moving powder where particles are loosely packed resulting in the following equation:

$$t_p = 1.35 \frac{{V_d}^{2/3}}{{\varepsilon_{eff}}^2 R_{eff}} \frac{\mu}{\gamma \cos\theta} \qquad \textit{Equation 1-1}$$

where t_p is the predicted drop penetration time, V_d is the drop volume, ε_{eff} is the effective porosity of the powder bed, R_{eff} is the effective pore radius, μ is the liquid viscosity, γ is the liquid surface tension and θ is the liquid-solid contact angle.

Hapgood *et al* [28] later revised the model to incorporate the effects of hydrophobic powder components and defined drop penetration time as:

$$t_p = 1.37 \frac{V_d^{2/3}}{((1-\zeta)\varepsilon^*_{eff})^2 R_{eff}} \frac{\mu}{\gamma \cos\theta} \qquad \textit{Equation 1-2}$$

Where the modified effective porosity, ε^*_{eff}, is defined as:

$$\varepsilon^*_{eff} = \varepsilon_{tap} \left(1 - \varepsilon + \varepsilon_{tap} - \varepsilon \frac{fSA_{phobic}}{SA_{blend}}\right)^y \qquad \textit{Equation 1-3}$$

and the effective pore radius, R_{eff}, is defined as:

$$R_{eff} = \frac{\varphi d_{3,2}}{3} \frac{\varepsilon_{eff}}{(1-\varepsilon_{eff})} \qquad \textit{Equation 1-4}$$

where ζ is the proportion of the powder surface comprised of hydrophobic particles, ε_{tap} is the tapped porosity of the powder bed, ε is the porosity of the powder bed, fSA_{phobic} is the ratio of hydrophobic particle surface area to the total surface area of the powder blend, SA_{blend}, y is the percolation factor, φ is the shape factor and $d_{3,2}$ is the surface mean particle size. Short penetration times are thus facilitated by small droplet size, low binder viscosity, porous non-hydrophobic powders, large powder pore size, high surface tension and low contact angle.

In order to apply drop penetration time measurements between different formulations and granulation equipment a dimensionless drop penetration time, τ_p, was proposed [29]:

$$\tau_p = \frac{t_p}{t_c} \qquad \textit{Equation 1-5}$$

where t_p is the drop penetration time and t_c is the circulation time, which is the time interval between a quantity of powder leaving and re-entering the spray zone. The circulation time is a function of powder flow patterns, the quantity of powder in the granulator and impeller speed [29].

1.3.2 Binder liquid delivery

It has been hypothesised that if all particles contain an equal amount of binder, their physical properties should be the same and produce a narrow size distribution [30], provided the primary particles are the same size to begin with. If the binder liquid is unevenly distributed, some nuclei will be more saturated than others and will grow preferentially resulting in heterogeneous granule properties. There are three operating variables in binder liquid delivery; droplet size distribution, flow rate and spray area. When the binder liquid is poured into the granulator the initial liquid distribution is poor with localised areas of high moisture content resulting in an initial bimodal size distribution and an increased fraction of coarse granules [25, 31]. Over the course of the granulation process a uni-modal distribution can result depending upon the mechanical dispersion conditions [32].

It is possible to alter the nucleation zone by changing the type, position and settings of the spray nozzle. Large spray angles and high nozzle to bed distance increase the spray area and decrease the spray density reducing the likelihood of binder droplets coalescing, and hence reduces the size and spread of the nuclei produced [33].

1.3.3 Powder mixing

Effective powder mixing is critical to binder liquid dispersion in all granulator types. A high rate of fresh powder passing through the nucleation zone facilitates uniform distribution of the binder liquid throughout the powder. Increasing the impeller speed aids binder liquid dispersion by increasing both the shear forces in the granulator, which induces granule breakage of large wet granules, and promotes powder flux through the nucleation zone [31, 34, 35].

1.3.4 Dimensionless spray flux

Tardos *et al* [36] attempted to standardise the description of the nucleation zone conditions across equipment scales. They suggested measuring binder flow-rate compared to the size of the spray zone and the powder flux through the spray zone. A decreased flow rate, increased spray zone or increased flux would therefore be expected

to reduce the granule size since there is a lower probability of drop coalescence and a lower liquid volume available for agglomeration per unit of powder [33].

More recently Litster *et al* [37] quantified spray conditions in a high shear mixer through the development of a dimensionless spray flux, Ψ_a, defined as:

$$\psi_a = \frac{3V}{2\, d_d\, v\, w_s} \qquad \textit{Equation 1-6}$$

where V is the liquid volumetric flow rate ($m^3\ s^{-1}$), d_d is the average droplet size (m), v is the powder surface velocity beneath the nozzle ($m\ s^{-1}$) and w_s is the width of the spray (m) 90° to powder flow direction. A high Ψ_a, >1.0, indicates that the ratio of binder liquid addition rate to the powder flux rate is high and the probability of droplets overlapping on the powder surface and coalescing is increased. The surface of the powder bed will become saturated and form large wet areas and nucleation will occur by immersion resulting in a wide nuclei size distribution. A low Ψ_a, <0.1, indicates that the ratio of binder liquid addition rate to the powder flux is sufficiently low that individual droplets are unlikely to coalesce and will therefore form single nuclei which leave the nucleation zone before being re-wet by another droplet.

Some authors have argued that fast dispersion of the binder liquid is taken for granted in high shear granulators and that the binder liquid addition conditions are not critical [38]. It is proposed that the coalescence into granules is mainly affected by the mixing conditions and the binder liquid amount, and that the system usually "recovers" even when binder liquid is added as a single event since the shear forces in the granulator break the initial nuclei and distribute the binder liquid by mechanical dispersion [31, 39, 40]. Plank *et al* [41] also highlight several practical limitations in achieving a spray flux <0.1 upon scale up of the process to commercial scales such as the need to either decrease volumetric binder liquid flow rate or increase impeller tip speed, both of which have significant effects on granule consolidation and growth. Another option considered was to increase the number of spray nozzles, however in the scale up example used this resulted in over 14 nozzles in a 300 L scale granulator which is impractical due to space limitations. As a result Plank *et al* [41] predict that wet granulation processes executed beyond the laboratory scale routinely operate outside the drop-controlled regime. They

do acknowledge the practical benefits of quantifying liquid coverage relative to powder flux, however challenge the relevance of using drop size measurements to quantify liquid coverage when routinely operating outside the drop-controlled regime, and therefore propose that the area over which the binder liquid is delivered is more influential resulting in the development of an empirical equation:

$$\Psi_{\text{alt}} = \frac{V}{vA} \qquad \textit{Equation 1-7}$$

where A is the area of the spray zone. It is proposed that the most reliable method to determine V/A is via direct measurement, such as collecting liquid from a spray nozzle into a collection device such as a grid of adjacent square cuvettes and weighing the amount of liquid collected over a given period of time.

1.3.5 Nucleation regime map

Nucleation can be considered a combination of single drop behaviour (dimensionless drop penetration time, τ_p) and multiple drop interactions (dimensionless spray flux, Ψ_a) with the specific formulation properties and equipment operating conditions determining the nucleation regime [21]. Three nucleation regimes have been proposed [37]; drop controlled, intermediate and mechanical dispersion. Based on these regimes, Hapgood et al [29] proposed the nucleation regime map (Figure 1-2) which considers both the dimensionless drop penetration time and the dimensionless spray flux. While exact values for the regime map boundaries are unknown at present the regime map provides a logical basis for investigation and development of granulation processes. Further quantification of the regime map transition boundaries is a clear area for future investigation which would further advance the field of controlled nucleation.

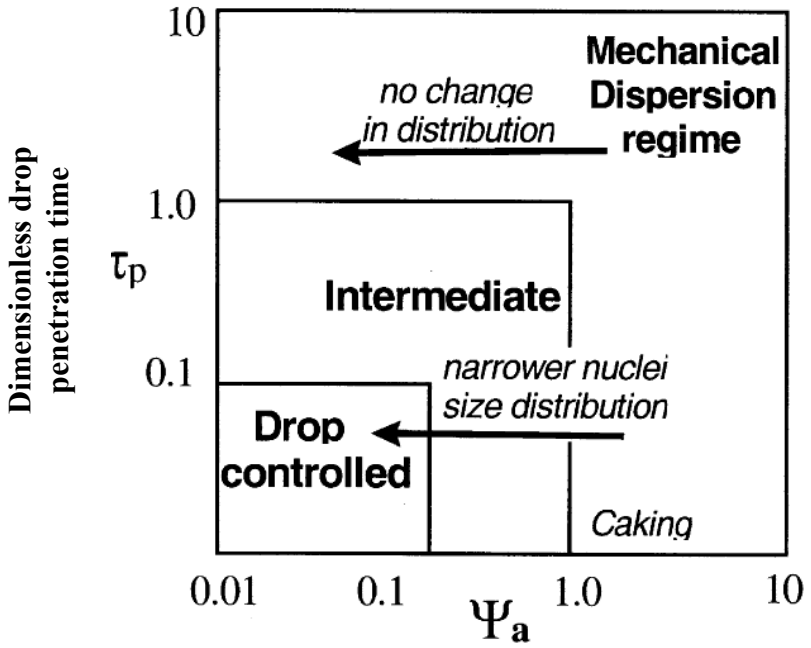

Figure 1-2. Nucleation regime map where Ψ_a is the dimensionless spray flux and τ_p is the dimensionless drop penetration time. Taken from [29].

In the drop controlled regime, binder liquid droplets penetrate the powder bed immediately and the individual droplet size determines the nuclei size distribution. As the drop penetration time slows and/or the dimensionless spray flux increases nucleation moves towards the mechanical dispersion regime. In the mechanical dispersion regime mixing intensity relative to capillary and viscous forces determine nucleation. The retarding effect of viscosity on the nucleation process has been frequently reported [24, 42-44]. In these cases nucleation and binder liquid distribution occur by mechanical mixing and the liquid addition method has minimal effect on the particle size distribution. In the intermediate regime, both drop penetration time and mechanical dispersion are influencing factors making the granulation process difficult to control. If the binder liquid addition rate exceeds the binder liquid dispersion rate local overwetting will occur. In practice, control of the nucleation process requires measurement and understanding of a number of important variables such as the wetting behaviour of the binder liquid on the powder bed (i.e. formulation), the binder droplet size (i.e. method of addition), binder spray width (i.e. spray nozzle design) and powder surface velocity (i.e. impeller speed and design).

1.4 Consolidation and coalescence

As granules are agitated in a granulator they experience many collisions with other granules, walls of the granulator and the impeller and chopper blades. These collisions can cause either dilation of the granule structure which creates a more porous assembly, or consolidation (also called densification or compaction) which reduces their porosity and size, squeezes out entrapped air, and possibly even squeezes binder liquid to the granule surface (Figure 1-1B) [45]. Granule porosity controls granule deformability and liquid saturation, both of which have a strong influence on granule growth mechanisms [46].

1.4.1 Liquid saturation

Newitt and Conway-Jones [15] first described the effect of increased binder liquid content on the wet granule structure (Figure 1-3). As the binder liquid content increases the number of liquid bridges between primary particles increases and the granule moves from a pendular state to a funicular state. At increased binder liquid content liquid bridges merge into a continuous network leading to the capillary state. Further increase in binder liquid content leads to oversaturation and the static strength of the granules drops to zero [47]. It has been suggested that if air is entrapped in the granules it may be feasible for surface liquid to become available at liquid saturation <100 % [48] as represented by the pseudo-droplet state.

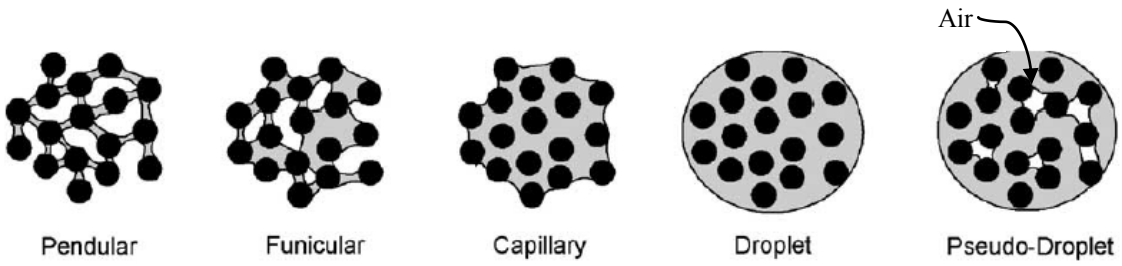

Figure 1-3. Representation of the different pore saturation states of liquid-bound granules. Taken from [47].

The increase in pore liquid saturation as a function of binder liquid content may vary during the granulation process, depending upon formulation and equipment variables which both affect the extent of granule consolidation. Therefore, the maximum granule

liquid saturation (S_{max}) is used as a dimensionless measure of binder liquid content [46, 49] which can be used as a means of comparison between different granulation systems:

$$S_{max} = \frac{m\,\rho_s\,(1-\varepsilon_{min})}{\rho_l\,\varepsilon_{min}} \qquad \textit{Equation 1-8}$$

where m is the mass ratio of liquid to solid, ρ_s, is the density of solid particles, ρ_l, is the liquid density and ε_{min} is the minimum porosity the formulation reaches under given operating conditions. The term m should take into account liquid volume changes due to solids dissolution [48]. ε_{min} is a complex function of formulation properties and operating conditions [45, 50] and cannot be predicted without performing actual measurements of granule porosity [49]. Porosity has commonly been determined by using low pressure mercury porosimetry [51], however mercury is a toxic substance with associated handling problems, the method is relatively time consuming, and the apparatus is relatively costly. More recently, a powder pycnometry method has been shown to be a robust method for determining the porosity of larger bodies such as rectangular roller compacted ribbons of 10 mm width x 22 mm length x 2 mm thickness [52] and spherical green iron ore pellets of 10–12.5 mm diameter [53]. Powder pycnometry has also been used to determine the porosity of pharmaceutical granules with a size less than 5 mm [54, 55], however evaluation of the appropriateness of powder pycnometry for granules of this size has not been investigated to date. A comprehensive study is presented in Chapter 2 to address this need.

Tardos *et al* [36] noted that nucleation is the predominant granulation mechanism at low liquid saturation with the rate of nucleation being proportional to the strength of the nuclei formed. Kristensen *et al* [46] investigated the granulation of lactose monohydrate and found that when liquid saturation was less than 0.6 growth proceeded slowly. Above a liquid saturation of 0.6 the growth rate rapidly increased due to rapid coalescence of moist agglomerates. Similarly, the power consumption of the granulation increased significantly at the same time, thereby providing a basis for an instrumented endpoint where the process could be ended immediately prior to the uncontrolled growth stage. Kristensen [56] studied the granulation of calcium hydrogen phosphate and showed that as liquid saturation increased so did the geometric mean diameter of

the agglomerates, with a rapid increase in growth occurring above a liquid saturation of approximately 0.8.

1.4.2 Coalescence forces in liquid bound granules

Granule consolidation, and the resultant liquid bound granule strength, is controlled by at least three forces; capillary forces, viscous forces and interparticulate friction [47]. Interparticulate friction and viscous forces are dissipative in that they resist particle motion, whereas capillary forces are conservative in that they always act to pull particles together and therefore aid consolidation and resist dilation [47]. Other forces such as van der Waals and electrostatic forces can also be important in some cases. However, in liquid-bound systems, electrostatic forces are usually minimal since the conductive binder liquid dissipates charge density therefore van der Waals forces are usually negligible compared to liquid bridge forces for systems with particle size greater than 10 μm [57].

1.4.3 Coalescence models

Granule growth behaviour is fundamentally determined by whether colliding granules coalesce or rebound. This simple concept is difficult to model because of the complex nature of granules. Ennis *et al* [42] developed a model for granule coalescence based on the dynamic liquid bridge. They defined a dimensionless Stokes viscous number, St_v, to predict whether a collision between two spherical granules will result in coalescence or rebound (Equation 1-9), depending upon their kinetic energy and the energy dissipated during the collision:

$$St_v = \frac{8\rho_g v_p r}{9\mu} \qquad \textit{Equation 1-9}$$

where ρ_g is the granule density, v_p the relative velocity between two spheres estimated as the impeller tip speed, r is the radius of the sphere, and μ is the binder viscosity. The model predicts that the collision will result in coalescence if the St_v is less than the critical Stokes viscous number, St^*_v:

$$St^*_{v} = \left(1 + \frac{1}{e}\right) ln\left(\frac{h}{h_a}\right) \qquad \textit{Equation 1-10}$$

where e is the coefficient of restitution, h is the thickness of the surface liquid layer, and h_a is the characteristic height of surface asperities. Three regimes were defined; (1) $St_v << St^*_v$ – the non-inertial regime where all collisions result in coalescence regardless of the size of the colliding granules; (2) $St_v = St^*_v$ – the inertial regime where some collisions result in coalescence; collisions between two large granules are less likely to result in coalescence and (3) $St_v >> St^*_v$ – the coating regime where no collisions result in coalescence. As shown by the model the probability of coalescence increases with decreasing particle density, impeller speed and granule size and increasing surface liquid layer thickness and binder viscosity. Practical difficulty in applying the model is in the estimation of the coefficient of restitution, thickness of the surface liquid layer and the height of the surface asperities as these are experimentally difficult to quantify and are a function of time and binder liquid content and will be dynamic during the course of the granulation process [58].

The model of Liu *et al* [58] builds on this model and is written in terms of bulk parameters of the formulation-binder mixture and of process intensity, including dimensionless groups such as viscous and Stokes deformation numbers, and the ratio of the plastic yield stress to elastic modulus. The model gives the conditions for two types of coalescence: type I and type II. For type I coalescence granules coalesce by viscous dissipation in the surface liquid layer before the granule surfaces contact. In type II coalescence granule surfaces contact and deform. Relative granule velocity is reduced to zero by viscous forces during rebound. The model considers coalescence between two surface wet granules to occur in three stages. The approach stage describes the squeezing of surface liquid from between granules in the collision contact area. The deformation stage describes the collision impact velocity between two granules and their separation distance. In this stage granules begin to deform and at a critical separation distance and collision velocity excess kinetic energy is stored elastically, some of which is dissipated by interparticulate movement and viscous forces. When the collision velocity is reduced to zero a contact area has formed between the two granules. The separation stage describes the rebound of the two granules with an initial velocity equal to the stored elastic energy of the impact. Granules will coalesce if the

collision kinetic energy is completely dissipated by either viscous losses in the surface liquid layer or plastic deformation in the granule matrix. The model predicts that granules will rebound if the energy attributable to the granule velocity at the end of the separation stage exceeds the strength of the liquid bridge.

1.4.4 Growth behaviour

Granule growth behaviour can be divided into two broad classes: steady growth and induction growth (Figure 1-4) [49]. The type of growth depends on the deformability and consolidation rate of the granules.

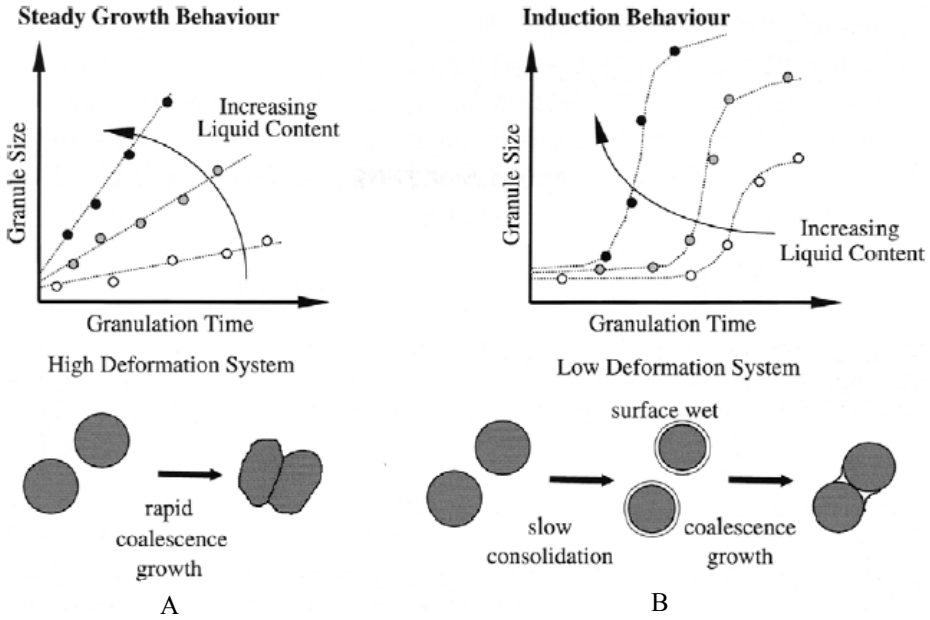

Figure 1-4. Schematic of steady and induction growth mechanisms. Taken from [49].

Steady growth occurs when weak, deformable particles form a large contact area during collision and liquid may be squeezed into the contact zone. If this bond is strong enough to resist the separating forces within the granulator, then the pair of granules will coalesce to form a new larger granule (Figure 1-4A). This behaviour leads to a steady increase in granule size and is common in systems with coarse, narrowly-sized particles and low surface tension and/or low viscosity binders [15, 59, 60]. Induction growth occurs when strong, slowly consolidating granules do not deform sufficiently during collision to form a large contact area or strong contact bonds. Pairs of collided granules

quickly break apart, and there is a period of little or no growth, so named the induction period (Figure 1-4B). The length of this induction period decreases with increasing liquid content, and will become zero above a critical liquid content. If granules consolidate sufficiently the binder liquid may eventually be squeezed to the surface of the granules. This surface liquid enables bonds to form between granules without the need for large amounts of deformation. This triggers rapid granule growth until granules become so large that further coalescence is prevented by the impact force of the granulator impeller. This type of growth behaviour is often seen in systems with fine particles and/or viscous binders [16, 60, 61].

Other types of behaviour include: nucleation only when granule nuclei form, but there is insufficient binder liquid to promote further growth; crumb behaviour when the formulation is too weak to form permanent granules but instead forms a loose crumb material which cushions a few large granules which are constantly breaking and reforming; and overwetting where excess binder liquid is present and the system exhibits uncontrolled growth [49].

1.4.5 Effect of primary particle size

Since free surface liquid is necessary in order to obtain agglomeration, the optimum amount of liquid required for granulation will depend upon the accessible surface area of the powders. A smaller particle size results in a larger surface area of the powder. Therefore for a given constant binder liquid volume a decreasing particle size will result in a smaller granule size or alternatively a larger volume of binder liquid will be required to keep granule size constant when powder particle size decreases.

Kristensen *et al* [46], and later Iveson and Litster [45], found that dicalcium phosphate granule strength increased with decreasing powder particle size. Since the deformability of the granule determines the probability of coalescence a higher strength granule deforms less and slows the growth rate. Supporting data were reported by Hsiau *et al* [62] who found that as the primary particle size (d_{50}) of calcium carbonate increased from 1.5 to 82.5 μm the rate of granule growth increased. They also proposed that granules comprising smaller primary particle size were stronger and suffered a lesser degree of breakage. Hunter and Ganderton [63] found a similar trend for lactose

granulations. They explained the observations as being due to the fact that the attractive force for finer agglomerates is greater per unit volume than the larger particles and therefore a stronger granule is obtained. Such nuclei will be brittle and will tend to rebound off each other when they collide resulting in a lower growth rate when compared to granules comprised of larger particles, which will be more plastic and deform readily upon collision and coalesce to form larger granules. This was only the case when the experiments were performed with a constant volume of binder liquid but a changing dry powder particle size and the differences were overcome by bringing all granulations to the same liquid saturation [63].

It has been suggested that a bimodal particle size distribution will favour coalescence and growth through a layering mechanism of smaller particles onto the surface of larger ones [36, 64, 65]. Smaller particles will have lower collision energy than larger particles. This lower energy is more likely to be dissipated upon collision for smaller agglomerates resulting in a greater probability of coalescence between a small and a large particle, than between a collision of two large particles.

When the excipients are semi-soluble in the binder liquid the amount of liquid has to be decreased to account for the reduced powder surface area and increased liquid volume caused by dissolution of excipients. Since the smallest particles will dissolve faster the reduction in surface area can be large and must be reflected in the reduction in binder liquid amount. When preparing lactose granules, that were partially soluble in the binder liquid, the liquid saturation required for significant growth was within the range of 0.3–0.6 [66]. However when experiments were carried out using a polyethylene glycol (PEG) binder liquid, in which the lactose was not soluble, rapid growth by coalescence required liquid saturations in the markedly higher range of 0.8–0.9 [67].

1.4.6 Binder liquid properties

The powder bed can be considered as a porous surface consisting of a series of capillary pores into which binder liquid will only penetrate when the wetting thermodynamics are favourable, i.e. the contact angle between the powder surface and the binder liquid droplet is less than 90 ° [21]. A high contact angle between the binder liquid and the dry powder can result in difficult to control, and highly variable, granulation processes [27,

28]. Provided that wetting thermodynamics are favourable then the binder liquid properties that will influence the granulation process are viscosity and surface tension.

An increase in binder liquid viscosity has been found to promote granule growth up to a certain critical value above which granule growth decreases [68]. For example the minimum silicone oil binder liquid viscosity necessary to form granules from various particle sizes of calcium carbonate has been reported [69]. A silicone oil viscosity of 10 mPa.s was necessary to from granules when considering calcium carbonate primary particles with a mean size of 8 μm, a viscosity of 100 mPa.s was necessary for particles of 50 to 80 μm and a viscosity of 1 mPa.s was necessary for particles of 230 μm. Granulation with low viscosity binder liquids is thought to be controlled by a layering growth mechanism while granulation with higher viscosity binder liquids is thought to be controlled by a coalescence mechanism [44].

A decrease in binder liquid surface tension can decrease granule growth by decreasing the strength of liquid bridges between particles meaning dilation or breakage is more likely [47]. A decrease in surface tension therefore typically produces granules of a smaller size and higher porosity. This effect was demonstrated for glass ballotini with surface mean diameters of 19 μm which were granulated with glycerol binder liquids of varying surface tension which was manipulated using sodium dodecylbenzene sulphonate surfactant. As surface tension was increased from 48 to 72 mN m^{-1} the granule porosity decreased from ~0.39 to ~0.35 with the rate of consolidation also decreasing as the surface tension increased [45].

1.4.7 Wet granule strength

Rumpf [57] first calculated wet granule strength, σ, with the assumption that capillary forces in wet granules were dominant:

$$\sigma = 6S_{max}\frac{1-\varepsilon}{\varepsilon}\frac{\gamma cos\theta}{d_p} \qquad \textit{Equation 1-11}$$

where S_{max} is the liquid saturation, ε is the granule porosity, γ is the liquid surface tension, θ is the liquid-solid contact angle and d_p is the particle size of the primary particles,

Ennis *et* al [42] postulated that in a dynamic situation viscous forces are likely to be dominant and therefore proposed a modified version of the Rumpf equation to calculate granule strength in the wet state:

$$\sigma = \frac{9}{8}\frac{(1-\varepsilon)^2}{\varepsilon^2}\frac{9\pi\mu v_p}{16 d_{3,2}} \qquad \textit{Equation 1-12}$$

where μ is the liquid viscosity, v_p is the relative velocity of particles within the granulator and $d_{3,2}$ is the surface mean particle size of the primary particles.

However, it has been shown that both static and dynamic forces contribute to granule growth [70] therefore an additive model derived by Liu and Litster [71] has been proposed.

$$\sigma = S_{max}\left[6\frac{1-\varepsilon}{\varepsilon}\frac{\gamma cos\theta}{d_p} + \frac{9}{8}\frac{(1-\varepsilon)^2}{\varepsilon^2}\frac{9\pi\mu v_p}{16 d_{3,2}}\right] \qquad \textit{Equation 1-13}$$

This model (Equation 1-13) considers both the capillary strength and dynamic strength of the liquid bridges when calculating granule strength in the wet state.

1.4.8 Stokes deformation number

The dimensionless Stokes deformation number, St_{def}, first proposed by Tardos *et al* [36] and later adapted by Iveson *et al* [48], is the ratio between the externally applied kinetic energy of the wet granules just before collision to the energy dissipated by the liquid bonds between the particles [36, 42].

$$St_{def} = \frac{\rho_g {v_c}^2}{2\sigma} \qquad \textit{Equation 1-14}$$

where ρ_g is the granule's density and v_c is the representative collision velocity. A small Stokes deformation number implies that significant energy is dissipated in deforming the granule during a collision. The use of Stokes deformation number has been reported in the literature for both drum granulators and high shear mixers [48, 72-75].

1.4.9 Growth regime map

The growth regime map (Figure 1-5), originally proposed by Iveson and Litster [49] and later modified by Iveson *et al* [48], considers the granule liquid saturation, S_{max}, and the Stokes deformation number, St_{def}, as the two variables that determine the growth regime that a given granulation process will operate within. The model is considered useful in that it ties easily measureable material properties (e.g. binder viscosity, wet granule strength, granule density and size) to operating conditions such as particle collision velocity or shear rate [76].

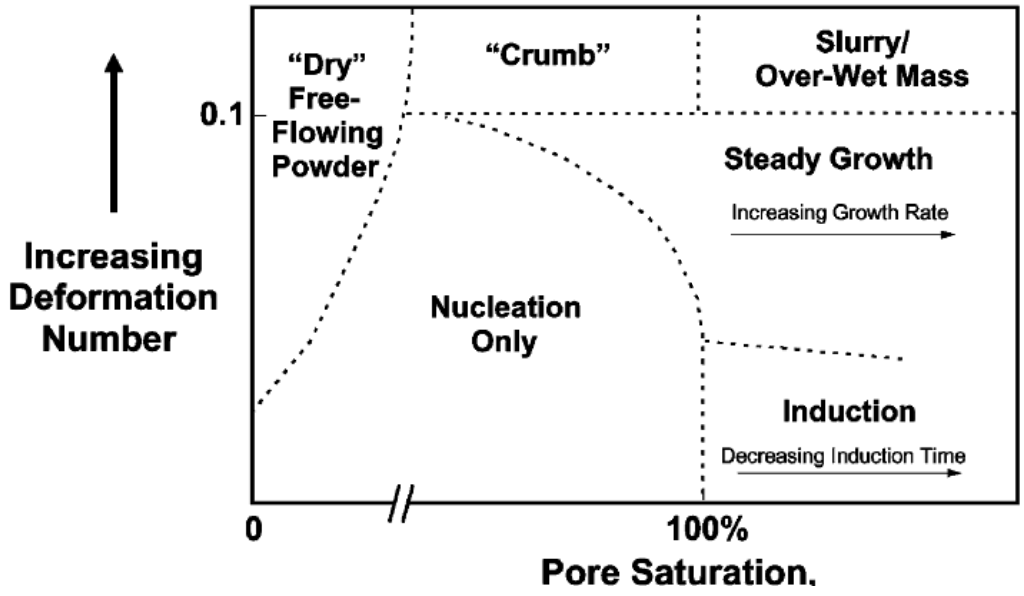

Figure 1-5. Growth regime map for liquid bound granules. Taken from [48].

The regime map does have limitations. It does not consider wetting and nucleation effects and by consequence does not consider control of drop penetration time and dimensionless spray flux [49]. These are of particular importance in the nucleation and induction regimes where they can influence the size distribution and porosity of granules. The regime map is also not able to predict the rate or extent of granule growth,

but does give an indication of the dominant growth mechanism and gives an informed directional approach to process scale-up, transfer and process control strategies.

The regime map does not replace experimentation with a given formulation or piece of equipment since variables such as temperature, which will affect binder liquid viscosity, surface tension and also solids dissolution, and the extent of consolidation that a given formulation will reach, cannot currently be predicted [48]. Therefore some degree of experiments with a given formulation and piece of granulation equipment are necessary.

1.5 Attrition and breakage

Wet granule breakage (Figure 1-1C) is understood less thoroughly than either the wetting and nucleation or consolidation and coalescence mechanisms. The breakage mechanism is however very important as it will influence, and potentially control, the final granule size distribution especially in high shear granulators [71]. Iveson *et al* [48] discussed the relevance of granule consolidation in breakage, and suggested that an increase in impeller speed will increase the collision velocity between granules. If the increase in collision energy is greater than the dissipation capacity of the system then colliding granules will rebound and potentially break which reduces the probability of granule coalescence and growth. An increase in wet massing time results in repeated impacts with the impeller blades which can cause increased breakage and densification of granules. Generally an increase in massing time narrows the granule size distribution and decreases the porosity [24, 25, 32, 40, 77]. Over time the granules consolidate and increase in strength, resulting in an equilibrium between granule growth and breakage and a plateau in granule size is reached [32]. This assumes that heat generation and further dissolution of formulation components does not take place during the equilibrium phase.

Tardos *et al* [36] developed a criteria where a granule will break if the applied kinetic energy during an impact exceeds the energy required for breakage. The breakage condition was posed such that if St_{def} was greater than the critical St^*_{def} then breakage would occur. In this work these workers [36] defined a very similar Stokes deformation number to that adopted to describe the growth mechanisms in wet granulation processes [48]. The St^*_{def} is likely to be higher for granule breakage than for coalescence as

granules undergo plastic deformation upon collision prior to breakage. Increasing impeller speed will increase the impact velocity and hence the Stokes deformation number. Granule consolidation also increases as a function of both frequency and energy of impacts up to a point at which collision energy is excessive and breakage over-rides consolidation [42, 78]. Therefore increasing impeller speed should shift a system's behaviour from a nucleation regime to steady or induction growth; and from steady growth to crumb, rapid, or over-wetted growth. Granule breakage has been postulated to be related closely to granule yield strength [71]. The rate of breakage of glass ballotini and lactose particles was found to be significantly influenced by liquid saturation, binder liquid viscosity and surface tension, and primary powder particle size. The calculated Stokes deformation number gave a good prediction of the breakage probability for each formulation and an upper boundary value of >0.2 was proposed to represent the point at which breakage increased [71].

Granule breakage has also been investigated through the addition of dyed tracers, either in the granules or binder liquid. Using an 8-L high shear granulator and amaranth dye to colour a fraction of pellets, the dye concentration across several sieve size classifications was tracked, and it was found that an increase in impeller speed increased the rate of granule breakage [79]. A similar study in a 30-L high shear granulator was conducted using blue Patent V80 dye [80], where an initial fast movement of dye to smaller granule size fractions was followed by a slower increase. The movement of dye was shown to be dependent upon the age of the granules, with the younger granules experiencing a greater extent of breakage [80]. This was proposed to be consistent with the fact that larger granules tend to be weaker than smaller granules, and are present in greater quantity earlier in the granulation process, therefore breakage is greater in the earlier stages of the process [81]. The reduced breakage over time is also consistent with the fact that granules will consolidate to a greater extent as the process proceeds resulting in reduced porosity and increased strength of the granules.

1.6 Alternative Wet Granulation Methods

Optimisation limits for conventional wet granulation have essentially been reached and the opportunity now exists for the development of alternative and streamlined wet granulation techniques, which eliminate variables that currently present barriers to the control of the granulation process, or can reduce the costs of production. Recent examples include development of melt granulation techniques to allow the processing of hygroscopic sodium valproate drug substances [82] and to improve moisture stability of dipeptidylpeptidase IV [83]. Fluidised bed granulation offers more uniform particle characteristics and higher granule porosity compared to conventional high shear mixer processes [84]. These two techniques have also been combined in a co-melt fluidised bed granulation process developed to enhance ibuprofen bioavailability [85]. Foam granulation has also recently been introduced with the advantages of improved binder distribution, shorter processing times and elimination of spray nozzles [86]. Presently a reverse-phase granulation process is proposed as a novel approach where dry powder is immersed into the binder liquid, thus eliminating the traditional granule nucleation variables. Such a reverse-phase process would form granules by a controlled breakage mechanism which would proceed in the direction of reduced liquid saturation, thus decreasing the risk of uncontrolled growth and batch loss.

1.7 Aims and Scope of the Thesis

The aim of the present study was to investigate the feasibility of developing a novel "reverse-phase" wet granulation process. Such a reverse-phase process would involve the controlled addition of the powder formulation into the agitated binder liquid to create saturated moist granules. It is hypothesised that the addition of further powder mass would reduce the liquid saturation of the granules and enable mechanical distribution of the binder liquid to take place until the desired particle size was obtained through controlled breakage. This is in contrast to the conventional granulation approach where the binder liquid is added to the dry powder and addition of further binder liquid increases the liquid saturation of the granules and granule growth takes place by controlled coalescence. A number of advantages motivate the development of the reverse-phase process.

First, the wetting and nucleation mechanisms in conventional granulation processes are very sensitive. Drop penetration time is sensitive to formulation properties such as powder bed porosity and effective pore size, both of which depend upon agitation intensity and variations in powder particle size. Dimensionless spray flux is sensitive to binder addition variables such as droplet size, spray area and powder flux which are difficult to control. As a result the control of the nucleation process in a laboratory environment is challenging, and often not even possible on the commercial scale [41]. Since the proposed reverse-phase process would follow an immersion mechanism the drop penetration time and dimensionless spray flux would not be relevant. Instead binder liquid is likely to be dispersed by a breakage mechanism, controlled by the liquid saturation, wet granule strength and agitation intensity in the granulator.

Second, granule growth in the conventional granulation process involves a careful progression in granule pore saturation so as to promote consolidation and coalescence, but to terminate the process immediately prior to the point of uncontrolled growth. In a commercial conventional granulation process the binder liquid typically contains a predetermined quantity of polymer binder, dissolved in a fixed quantity of water to form the binder liquid, which is subsequently sprayed onto the powder formulation in its entirety. Careful control of several, often poorly understood and uncontrolled variables, including primary powder particle size, powder flow patterns and collision energies, is required to ensure that the fixed quantity of binder liquid results in granules of the desired properties and that the appropriate process endpoint criteria are met. Any variation in these, or other, variables can result in over saturation of the powder, uncontrolled granule growth and batch loss. In the commercial manufacturing environment batch loss incurs not only the financial expense of the drug and raw materials which can be very significant, but also the direct and indirect labour hours invested and the equipment depreciation cost allocated against the batch. Additionally, the supply chain and sales implications of missing customer orders is significant and can damage the company or product brand. Therefore process robustness is of utmost importance.

A reverse-phase process would start at a state of complete pore saturation and use controlled breakage to reduce granule size and disperse the binder liquid throughout the powder. As the reverse-phase process advances, the liquid saturation would decrease

and the process would move away from a point of over-wetting, uncontrolled growth and batch loss. In contrast the conventional granulation process is designed to proceed in the opposite direction. As the conventional process advances the liquid saturation increases and the process is terminated immediately prior to the point at which uncontrolled growth is triggered.

In the context of the previously described theory this means the reverse-phase process begins at a very undesirable point operating under an immersion nucleation regime where the dimensionless spray flux is very large and the liquid saturation is such that slurry growth conditions exist. However, it is hypothesised that under this mechanism the manipulation of a few easier to control variables (binder quantity, binder viscosity and impeller speed) is sufficient to reach the desired granule properties without the risk of uncontrolled growth and batch rejection.

Two potentially negative consequences of the reverse-phase approach are acknowledged. First, it is thought that due to the nature of the immersion mechanism employed in the reverse-phase process the granules may undergo greater consolidation and therefore have a greater strength than conventional granules, which may detrimentally affect the compaction characteristics. Second, this approach will be likely to increase the potential for drug dissolution during the process. Therefore transformation of the drug to a new polymorphic or hydration state is possible which has potential negative processing, bioavailability and regulatory implications. Both of these considerations are investigated in the present work to understand possible limitations of the novel approach.

Accordingly, the objectives for each chapter of this thesis were:

Chapter (1): To evaluate the current state of wet granulation understanding as summarised in the present chapter. The popularity and application of regime maps and dimensionless numbers was discussed. In particular granule porosity was noted as an important material attribute in understanding granulation mechanisms and was also highlighted as a critical measurement used to calculate granule liquid saturation and Stokes deformation number.

Chapter (2): To assess powder pycnometry as a method for the measurement of granule porosity. Porosity is traditionally measured by mercury porosimetry, however powder pycnometry offers cycle time, cost and safety advantages. An assessment of the powder pycnometry experimental procedure and any methodological limitations has not yet been reported for granules with diameter <10 mm.

Chapter (3): To study the effect of moisture on the compaction properties of the selected model raw material, hydroxyapatite. Hydroxyapatite is exposed to moisture during the wet granulation process and can also absorb moisture from the environment. Minimal investigation into the compaction properties of hydroxyapatite, in particular the effects of moisture, have been reported.

Chapter (4): To study the effect of binder liquid quantity and viscosity on the reverse-phase process and contrast the results with the conventional granulation process. Liquid saturation and binder liquid viscosity are significant variables in the consolidation and coalescence of wet granules. The conventional granulation process is susceptible to uncontrolled growth at elevated liquid saturation, however it was hypothesised that the reverse-phase process may be less sensitive.

Chapter (5): To study the effect of impeller speed and binder liquid viscosity on the reverse-phase process and contrast the results with the conventional granulation process. It was hypothesised that impeller speed can be used to control the size distribution of granules prepared by a reverse-phase process. Additionally, it is hypothesised that the reverse-phase process may produce granules of greater strength which would form tablets of lower tensile strength when compared to the conventional process.

Chapter (6): To develop a growth regime map for the reverse-phase granulation process. The growth regime map, developed for the conventional process, considers the granule liquid saturation and Stokes deformation number as the two variables that determine the growth regime that a given granulation process will operate within. The model is considered very useful since it links measureable material properties to process conditions and therefore its application to the reverse-phase process is of interest.

Chapter (7): To monitor the in-situ hydration of anhydrous theophylline during the reverse-phase granulation process using Raman spectroscopy, and compare the results with a conventional granulation process. It is hypothesised that the reverse-phase process represents a higher risk solid state transformations due to the immersion of formulation components in the binder liquid.

Chapter (8): To give a general discussion of the thesis and provide context for the direction of future research initiatives.

1.8 References

[1] Wu, C.Y., Seville, J.P.K., A comparative study of compaction properties of binary and bilayer tablets, Powder Technology, 189 (2009) 285-294.

[2] Patel, S., Bansal, A.K., Prediction of mechanical properties of compacted binary mixtures containing high-dose poorly compressible drug, Int. J. Pharm., 403 (2011) 109-114.

[3] York, P. The design of dosage forms in: Aulton M.E., (Eds.) *Pharmaceutics: The Science of Dosage Forms*, 2nd ed, Elsevier, 2002, pp. 1-12.

[4] Gohel, M.C., Jogani, P.D., A review of co-processed directly compressible excipients, J. Pharm. Sci., 8 (2005) 76-93.

[5] Miller, R.W. Roller Compaction Technology in: Parikh D.M., (Eds.) *Handbook of Pharmaceutical Granulation Technology, 2nd Ed.*, Taylor & Francis Group, 2005, pp. 159-190.

[6] Kleinebudde, P., Roll compaction/dry granulation: pharmaceutical applications, Eur. J. Pharm. Biopharm., 58 (2004) 317-326.

[7] Sun, C.C., Himmelspach, M.W., Reduced tabletability of roller compacted granules as a result of granule size enlargement, J. Pharm. Sci., 95 (2006) 200-206.

[8] Wu, S.J., Sun, C.C., Insensitivity of compaction properties of brittle granules to size enlargement by roller compaction, J. Pharm. Sci., 96 (2007) 1445-1450.

[9] Mehta, K.A., Rekhi, G.S., Parikh, D.M. Extrusion/Spheronization as a Granulation Technique in: Parikh D.M., (Eds.) *Handbook of Pharmaceutical Granulation Technology, 2nd Ed*, Taylor & Francis Group, 2005, pp. 333-368.

[10] Mehta, K.A., Kislalioglu, M.S., Phaupradit, W., Malick, A.W., Shah, N.H., Effect of formulation and process variables on matrix erosion and drug release from a multiunit erosion matrix of a poorly soluble drug, Pharmaceutical Technology, February (2002) 26-34.

[11] Celik, M., Wendel, S.C. Spray Drying and Pharmaceutical Applications in: Parikh D.M., (Eds.) *Handbook of Pharmaceutical Granulation Technology, 2nd Ed*, Taylor & Francis Group, 2005, pp. 129-157.

[12] VandenMooter, G., Paudel, A., Worku, Z.A., Meeus, J., Guns, S., Manufacturing of solid dispersions of poorly water soluble drugs by spray drying: Formulation and process considerations, Int. J. Pharm., 453 (2013) 253-284.

[13] Amidon, G.L., Dahan, A., Miller, J.M., Prediction of solubility and permeability class membership: Provisional BCS Classification of the world's top oral drugs, AAPS Journal, 11 (2009) 740-746.

[14] Lipinski, C., Poor aqueous solubility - an industry wide problem in drug discovery, American Pharmaceutical Review, 5 (2002) 82-85.

[15] Newitt, D.M., Conway-Jones, J.M., A contribution to the theory and practice of granulation, Trans. I. Chem. Eng., 36 (1958) 422-430.

[16] P.C. Kapur. Balling and Granulation *Advances in Chemical Engineering*, 1978, pp. 55-123.

[17] Schubert, H., Principles of agglomeration, Int. Chem. Eng., 21 (1981) 363-377.

[18] Kristensen, H.G., Schaefer, T., Granulation: A review of pharmaceutical wet-granulation, Drug Dev. Ind. Pharm., 13 (1987) 803-872.

[19] Kristensen, H.G., Agglomeration of powders, Acta Pharm. Suec., 25 (1988) 187-204.

[20] Ennis, B.J., Agglomeration and size enlargement session summary paper, Powder Technology, 88 (1996) 203-225.

[21] Iveson, S.M., Litster, J.D., Hapgood, H., Ennis, B.J., Nucleation, growth and breakage phenomena in agitated wet granulation processes: a review, Powder Technology, 117 (2001) 3-39.

[22] Ennis, B.J., Litster, J.D. Particle Size Enlargement in: Perry R., Green D., eds, *Perry's Chemical Engineers' Handbook*, 7th ed, 1997, pp. 73-117.

[23] Hapgood, K.P., Iveson, S.M., Litster, J.D., Liu, L.X. Granulation rate processes in: Salman A.D., Hounslow M.J., Seville J.P.K., eds, *Granulation*, Elsevier, Oxford, UK, 2007, pp. 897-977.

[24] Schaefer, T., Mathiesen, C., Melt pelletization in a high shear mixer VIII: Effects of binder viscosity, Int. J. Pharm., 139 (1996) 125-138.

[25] Scott, A.C., Hounslow, M.J., Instone, T., Direct evidence of heterogeneity during high-shear granulation, Powder Technology, 113 (2000) 205-213.

[26] Denesuk, M., Smith, G.L., Zelinski, B.J.J., Kreidl, N.J., Uhlmann, D.R., Capillary penetration of liquid droplets into porous materials, Journal of Colloid Interface Science, 158 (1993) 114-122.

[27] Hapgood, K.P., Litster, J.D., Biggs, S.R., Howes, T., Drop penetration time into porous powder beds, Journal of Colloid and Interface Science, 253 (2002) 353-366.

[28] Hapgood, K.P., Nguyen, T., Shen, W., Drop penetration time in heterogeneous powder beds, Chem. Eng. Sci., 64 (2009) 5210-5221.

[29] Hapgood, K.P., Litster, J.D., Smith, R., Nucleation regime map for liquid bound granules, AIChE J., 49 (2003) 350-361.

[30] Mort, P.R., Tardos, G.I., Scale-up of agglomeration processes using transformation, Kona, 17 (1999) 64-75.

[31] Holm, P., Jungerson, O., Schaefer, T., Kristensen, H.G., Granulation in High Speed Mixers Part I: Effects of process variables during kneading, Pharm. Ind., 45 (1983) 806-811.

[32] Knight, P.C., Instone, T., Pearson, J.M.K., Hounslow, M.J., An investigation into the kinetics of liquid distribution and growth in high shear mixer agglomeration, Powder Technology, 97 (1998) 246-257.

[33] Rankell, A.S., Scott, M.W., Lieberman, H.A., Chow, F.S., Battista, J.V., Continuous production of tablet granulations in fluidized bed II. Operation and performance of equipment, J. Pharm. Sci., 53 (1964) 320-324.

[34] Holm, P., Jungerson, O., Schaefer, T., Kristensen, H.G., Granulation in High Speed Mixers Part II: Effects of process variables during kneading, Pharm. Ind., 46 (1984) 97-101.

[35] Kokubo, H., Sunada, H., Effect of process variables on the properties and binder distribution of granules prepared by high-speed mixer, Chem. Pharm. Bull., 44 (1996) 1546-1549.

[36] Tardos, G.I., Khan, M.I., Mort, P.R., Critical parameters and limiting conditions in binder granulation of fine powers, Powder Technology, 94 (1997) 245-258.

[37] Litster, J.D., Hapgood, K.P., Michaels, J.N., Sims, A., Roberts, M., Kameneni, S.K., Hsu, T., Liquid distribution in wet granulation: dimensionless spray flux, Powder Technology, 114 (2001) 29-32.

[38] Faure, A., York, P., Rowe, R.C., Process control and scale-up of pharmaceutical wet granulation processes: a review, Eur. J. Pharm. Biopharm., 52 (2001) 269-277.

[39] Terashita, K., Watano, S., Miyanami, K., Determination of end-point by frequency analysis of power consumption in agitation granulation, Chem. Pharm. Bull., 38 (1990) 3120-3123.

[40] Knight, P.C., Johansen, A., Kristensen, H.G., Schaefer, T., Seville, J.P.K., An investigation of the effects on agglomeration of changing the speed of a mechanical mixer, Powder Technology, 110 (2000) 204-209.

[41] Plank, R., Diehl, B., Grinstead, H., Zega, J., Quantifying liquid coverage and powder flux in high-shear granulators, Powder Technology, 134 (2003) 223-234.

[42] Ennis, B.J., Tardos, G.I., Pfeffer, R., A microlevel-based characterization of granulation phenomena, Powder Technology, 65 (1991) 257-264.

[43] Schaefer, T., Johnsen, D., Johansen, A., Effects of powder particle size and binder viscosity on intergranular and intra-granular particle size heterogeneity during high shear granulation, Eur. J. Pharm. Sci., 21 (2004) 525-531.

[44] Mills, P.J.T., Seville, J.P.K., Knight, P.C., Adams, M.J., The effect of binder viscosity on particle agglomeration in a low shear mixer/agglomerator, Powder Technology, 113 (2000) 140-147.

[45] Iveson, S.M., Litster, J.D., Fundamental studies of granule consolidation Part 2: Quantifying the effects of particle and binder properties, Powder Technology, 99 (1998) 243-250.

[46] Kristensen, H.G., Holm, P., Schaefer, T., Mechanical properties of moist agglomerates in relation to granulation mechanisms: Part 1. Deformability of moist, densified agglomerates, Powder Technology, 44 (1985) 227-238.

[47] Iveson, S.M., Beathe, J.A., Page, N.W., The dynamic strength of partially saturated powder compacts: the effect of liquid properties, Powder Technology, 127 (2002) 149-161.

[48] Iveson, S.M., Wauters, P.A.L., Forrest, S., Litster, J.D., Meesters, G.M.H., Scarlett, B., Growth regime map for liquid-bound granules: further development and experimental validation, Powder Technology, 117 (2001) 83-97.

[49] Iveson, S.M., Litster, J.D., Growth regime map for liquid-bound granules, AIChE J., 44 (1998) 1510-1518.

[50] Iveson, S.M., Litster, J.D., Ennis, B.J., Fundamental studies of granule consolidation Part 1: Effects of binder content and binder viscosity, Powder Technology, 88 (1996) 15-20.

[51] Giesche, H., Mercury Porosimetry: A General (Practical) Overview, Part. Part. Syst. Charact., 23 (2006) 9-19.

[52] Zinchuk, A., Mullarney, M., Hancock, B., Simulation of roller compaction using a laboratory scale compaction simulator, Int. J. Pharm., 269 (2004) 403-415.

[53] Forsmo, S.P.E., Vuori, J.P., The determination of porosity in iron ore green pellets by packing in silica sand, Powder Technology, 159 (2005) 71-77.

[54] Ghadiri, M., Rahmanian, N., Jia, X., Stepanek, F., Characterisation of granule structure and strength made in a high shear granulator, Powder Technology, 192 (2009) 184-194.

[55] Litster, J.D., Ramachandran, R., Poon, J., Sanders, C., Glaser, T., Immauel, C., III, F.D., Stepanek, F., Wang, F., Cameron, I., Experimental studies on distributions of granule size, binder content and porosity in batch drum granulation: Inferences on process modelling requirements and process sensitivities, Powder Technology, 188 (2008) 89-101.

[56] Kristensen, H.G., Particle agglomeration in high shear mixers, Powder Technology, 88 (1996) 197-202.

[57] Rumpf, H. The strength of granules and agglomerates in: Knepper W.A., (Eds.) *Agglomeration*, Interscience-Wiley, New York, 1962, pp. 379-418.

[58] Liu, L.X., Litster, J.D., Iveson, S.M., Ennis, B.J., Coalescence of deformable granules in wet granulation processes, AIChE J., 46 (2000) 529-539.

[59] Capes, C.E., Danckwerts, P.V., Granule formation by the agglomeration of damp powders: 1. The mechanism of granule growth, Trans. I. Chem. Eng., 43 (1965) 116-122.

[60] Linkson, P.B., Glastonbury, J.R., Duffy, G.J., The mechanism of granule growth in wet pelletisation, Trans. I. Chem. Eng., 51 (1973) 251-257.

[61] Sastry, K.V., Panigraphy, S.C., Fuerstenau, D.W., Effect of wet grinding and dry grinding on the batch balling behaviour of particulate materials, Trans. Soc. Mining Engineers, 262 (1977) 325-331.

[62] Hsiau, S.S., Tu, W.D., Ingram, A., Seville, J., The effect of powder size on induction behaviour and binder distribution during high shear melt agglomeration of calcium carbonate, Powder Technology, 184 (2008) 298-312.

[63] Hunter, B.M., Ganderton, D., The effect of particle size on the granulation of lactose by massing and screening, J. Pharm. Pharmac. Suppl., 24 (1972) 17-24.

[64] Hounslow, M., Pearson, J., Instone, T., Tracer studies of high-shear granulation: II. Population balance modelling, AIChE J., 47 (2001) 1984-1998.

[65] Litster, J.D., Waters, A., Influence of the material properties of iron ore sinter feed on granulation effectiveness, Powder Technology, 55 (1988) 141-151.

[66] Kristensen, H.G., Holm, P., Jaegerskou, A., Schaefer, T., Granulation in high shear mixers, Part 4: Effect of liquid saturation on the agglomeration, Pharm. Ind., 46 (1984) 763-766.

[67] Schaefer, T., Holm, P., Kristensen, H.G., Melt granulation in a laboratory scale high shear mixer, Drug Dev. Ind. Pharm., 16 (1990) 1249-1277.

[68] Johansen, A., Schaefer, T., Effects of interactions between powder particle size and binder viscosity on agglomerate growth mechanisms in a high shear mixer, Eur. J. Pharm. Sci., 12 (2001) 297-309.

[69] Keningly, S., Knight, P., Marson, A., An investigation into the effects of binder viscosity on agglomeration behaviour, Powder Technology, 91 (1997) 95-103.

[70] Benali, M., Gerbaud, V., Hemati, M., Effect of operating conditions and physico-chemical properties on the wet granulation kinetics in a high shear mixer, Powder Technology, 190 (2009) 160-169.

[71] Liu, L.X., Litster, J.D., Wet granule breakage in a breakage only high-shear mixer: Effect of formulation properties on breakage behaviour, Powder Technology, 189 (2009) 158-164.

[72] Iveson, S., Page, N., Dynamic strength of liquid-bound granular materials; The effect of particle size and shape, Powder Technology, 152 (2005) 79-89.

[73] Bouwman, A.M., Visser, M.R., Meesters, G.M.H., Frijlink, H.W., The use of Stokes deformation number as a predictive tool for material exchange behaviour of

granules in the 'equilibrium' phase in high shear granulation, Int. J. Pharm., 318 (2006) 78-85.

[74] Cavinato, M., Franceschinis, E., Cavallari, S., Realdon, N., Santomaso, A., Relationship between particle shape and some process variables in high shear wet granulation using binders of different viscosity, Chem. Eng. J., 164 (2010) 292-298.

[75] Kayrak-Talay, D., Dale, S., Wassgren, C., Litster, J., Quality by design for wet granulation in pharmaceutical processing: Assessing models for *a priori* design and scaling, Powder Technology, 240 (2013) 7-18.

[76] Mort, P.R., Scale-up and control of binder agglomeration processes - Flow and stress fields, Powder Technology, 189 (2009) 313-317.

[77] Vonk, P., Guillaume, C.P.F., Ramaker, J.S., Vromans, H., Kossen, N.W.F., Growth mechanisms of high-shear pelletisation, Int. J. Pharm., 157 (1997) 93-102.

[78] Ouchiyama, N., Tanaka, T., Stochastic model for compaction of pellets in granulation, Ind. Eng. Chem. Fundam., 19 (1980) 555-264.

[79] Ramaker, J., Albada-Jelgersma, M., Vonk, P., Kossen, N., Scale-down of a high shear pelletisation process: flow profile and growth kinetics, Int. J. Pharm., 166 (1998) 89-97.

[80] Pearson, J., Hounslow, M., Instone, T., Tracer studies of high-shear granulation: I. Experimental results, AIChE Journal, 47 (2001) 1978-1983.

[81] Reynolds, G.K., Fu, J.S., Cheong, Y.S., Hounslow, M.J., Salman, A.D., Breakage in granulation: A review, Chem. Eng. Sci., 60 (2005) 3969-3992.

[82] Thies, R., Kleinebudde, P., Melt pelletisation of a hygroscopic drug in a high shear mixer: Part 1. Influence of process variables, Int. J. Pharm., 188 (1999) 131-143.

[83] Kowalski, J., Kalb, O., Joshi, Y.M., Serajuddin, A.T.M., Application of melt granulation to enhance stability of a moisture sensitive immediate-release drug product, Int. J. Pharm., 381 (2009) 56-61.

[84] Turton, R., Tardos, G.I., Ennis, B.J. Fluidized bed coating and granulation in: Yang W.C., (Eds.) *Selected Topics on Fluidization, Solids Handling and Processing*, Noyes Publications, 1999, pp. 331-429.

[85] Walker, M., Bell, S.E.J., Andrews, G., Jones, D., Co-melt fluidised bed granulation of pharmaceutical powders: improvements in drug bioavailability, Chem. Eng. Sci., 62 (2007) 451-462.

[86] Keary, C.M., Sheskey, P.J., Preliminary report of the discovery of a new pharmaceutical granulation process using foamed aqueous binders, Drug Dev. Ind. Pharm., 30 (2004) 831-845.

CHAPTER TWO: AN ASSESSMENT OF POWDER PYCNOMETRY AS A MEANS OF DETERMINING GRANULE POROSITY

2 Introduction

Porosity is an important property of pharmaceutical granules which can affect strength [1], compactibility [2] and dissolution behaviour [3]. Porosity is also an important physical property used to characterise granule consolidation behaviour during wet granulation processes [4, 5]. The calculation of important parameters such as granule liquid saturation (Section 1.4.1) and wet granule strength (Section 1.4.6) both require determination of the granule porosity. These parameters are used in the present thesis and therefore a practical and efficient method for the determination of granule porosity was investigated.

The porosity of a granule sample can be calculated from its envelope, or apparent density, and true density as follows:

$$\varepsilon = 1 - \left(\frac{\rho_e}{\rho_t}\right) \times 100 \qquad \textit{Equation 2-1}$$

where ε is the sample porosity, ρ_t is the sample true density and ρ_e is the sample envelope density. The envelope density of a solid is defined by the American Society for Testing Materials (ASTM D3766) as the ratio of the mass of a particle to the sum of the volumes of the solid in each piece and the voids within each piece, that is, within close-fitting imaginary envelopes completely surrounding each piece.

Envelope density is generally determined by using low pressure mercury porosimetry [6], however mercury is a toxic substance with associated handling problems, the method is relatively time consuming, and the apparatus relatively costly. As an alternative a powder pycnometer has been developed, the GeoPyc® 1360 apparatus, which is designed to measure envelope density. The apparatus is marketed with claims of offering improved safety, shorter cycle times, whilst also providing instrument cost advantages. The use of the GeoPyc® apparatus involves the addition of a measured sample mass to a known volume of quasi-fluid media (Dry*Flo*®). The apparent sample envelope volume is measured by displacement theory allowing the calculation of the sample envelope density.

When considering powder pycnometry the packing behaviour between the displacement media and the sample is a potential limitation in the method and must be considered. The addition of a solid sample particle to a bed of displacement media increases the total volume by an amount attributable to both the volume of the added sample particle and the volume due to steric repulsion induced by the presence of the new sample particle [7]. While the volume of the added sample particle can be considered a constant, the volume increase associated with packing density will be expected to be a function of the particle size of both the sample particles and the displacement media, i.e. packing efficiency. Changes in packing efficiency could therefore potentially cause deviations in the envelope density measurements obtained when compared to a reference method, such as mercury porosimetry where packing efficiency is consistently achieved. It is important to investigate these limitations and consider whether certain circumstances exist where the advantages of the powder pycnometry method outweigh the disadvantages of the mercury porosimetry method.

The use of the GeoPyc® powder pycnometry method has previously been shown to be robust for envelope density measurement of larger bodies. The envelope density for rectangular roller compacted ribbons of 10 mm width x 22 mm length x 2 mm thickness measured using the GeoPyc® was shown to be consistent with manual caliper measurements [8]. Similarly, envelope density measurement of spherical green iron ore pellets of 10–12.5 mm diameter measured using the GeoPyc® were shown to have an excellent correlation with envelope density results obtained by mercury porosimetry (R^2 0.972) [9].

The method has also been used to measure the envelope density of pharmaceutical granules. Litster *et al* [10] used the GeoPyc® apparatus to measure the porosity of 17 different size fractions of calcite / aqueous polyvinyl alcohol granules in the range 53–4750 μm. These researchers concluded that the porosity values calculated from the granule envelope density measurements of the GeoPyc® were reproducible for each granule size fraction as indicated by the narrow error bars. Carvajal and Macias [11] measured the envelope density of microcrystalline cellulose granules, comprising 12 sieve fractions in the size range 53–1190 μm, using the GeoPyc®. They modelled the relationship between granule density and granule strength using an exponential fit model and obtained an R^2 of 0.9535, indicating the validity of the envelope density

results generated using the GeoPyc®. Ghadiri *et al* [12, 13] used the GeoPyc® apparatus to measure the porosity of calcium carbonate granules prepared with 65 % *w/w* aqueous PEG 4000 in the size range 500–600 μm prepared at different impeller speeds. In the earlier work [12] these researchers generated envelope density results using both the GeoPyc® and mercury porosimetry methods and while they did not perform a comparative analysis of the methods they presented the raw data for each method. Linear correlation of their data, as part of this present study, yielded an R^2 of 0.9556. These data only represented three paired data points for each method so the correlation is tentative, but does indicate that the method shows promise and may be able to be used in place of mercury porosimetry.

These published results indicate that the GeoPyc® powder pycnometer has found application for the measurement of envelope density of pharmaceutical granules of varying size. However, none of these studies has fully evaluated the comparability of this method to the reference mercury porosimetry method for granules. Nor did any of these studies explore the limitations of the powder pycnometry method in terms of the effect of sample particle size on packing efficiency, which would be seen as a deviation from an ideal linear correlation with the mercury porosimetry method. The experimental procedure and physical properties of the Dry*Flo*® displacement media have also received little attention and have not been thoroughly investigated.

Accordingly, the present aims of the study were to: 1) investigate Dry*Flo*® particle size reproducibility and consolidation properties, 2) determine the number of *preparation cycles* required before test measurements should be taken, 3) compare the results obtained by powder pycnometry to those generated using mercury porosimetry, and 4) investigate the effect of granule size on the envelope density measurement.

2.1 Materials and Methods

2.1.1 Materials

Pharmaceutical grade hydroxyapatite (HA) (TRI-CAL WG^{TM}, tricalcium phosphate anhydrous granular) was obtained from Innophos, Chicago Heights, Illinois, USA. Poly (vinyl pyrrolidone) (PVP) (Plasdone K29/32) was obtained from ISP Pharmaceuticals, Covington, Kentucky, USA. Dry*Flo*® displacement media was obtained from Micromeritics, Norcross, Georgia, USA.

2.1.2 Granule preparation and physical characterisation

2.1.2.1 Granulation process

Aqueous granulation binder liquid was prepared by dissolving 10 or 20 % *w/w* PVP in water. Following dissolution of the PVP, the solution was held without agitation for at least 12 h to allow deaeration. Granules were prepared using the novel reverse-phase granulation process in a 1-L high shear granulator (P1-6, Diosna Dierks & Sohne GmbH, Osnabruck, Germany) as shown in Figure 2-1.

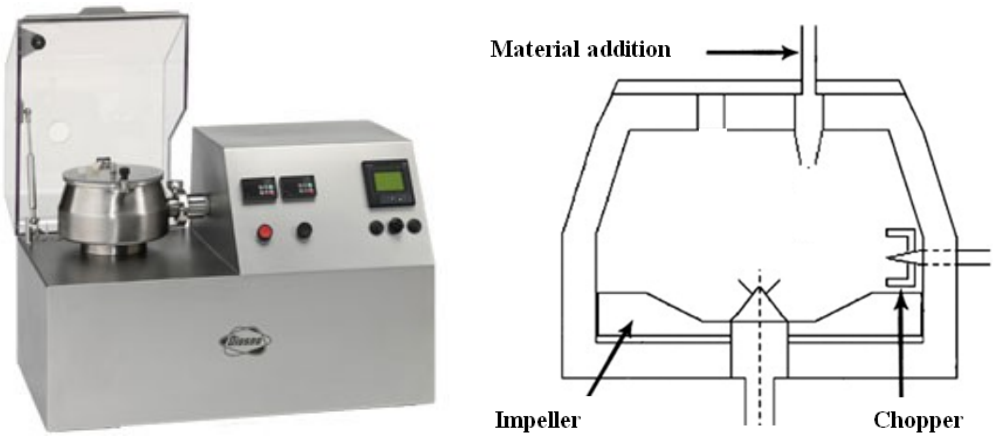

Figure 2-1. Illustrations of Diosna P1-6 granulator.

For the reverse-phase granulation process the total volume of binder liquid was added directly to the granulator bowl. Separate experiments were performed employing 50, 100, 150, 200 and 250 cm^3 of the 10 or 20 % *w/w* aqueous PVP binder liquid. The binder liquid was mixed for 30 s using an impeller speed of 400 rpm (3.14 m s^{-1}) and chopper speed of 1000 rpm (0.89 m s^{-1}). Following mixing 600 g of dry HA powder was added to the moving liquid using a vibratory feeder with a feed rate of approximately 5 g s^{-1} (Syntron F-T0, FMC Technologies Inc., Tupelo, Mississippi, USA). Wet massing was performed for 10 s following complete addition of the HA powder.

The resultant granules were dried as a thin layer in a hot air convection oven (Lindberg/Blue, SPX Thermal Solutions, Rochester, New York, USA) at 60 ºC to a moisture content of ≤ 1.2 %, as measured by loss on drying at 105 ºC (Computrac MAX2000-XL, Arizona Instruments, Chandler, Arizona, USA).

Granules generated from each granulation experiment were sampled and the envelope density measured using the GeoPyc® powder pycnometer. From these initial results six experimental conditions were selected (Table 2-1) which represented a range of envelope density values. Granules generated under these conditions were characterised further for particle size, bulk and tapped density and envelope density measured by mercury porosimetry as described subsequently.

2.1.2.2 Envelope density using powder pycnometry

The envelope density of granule samples (n=4) was determined by a powder pycnometry method (GeoPyc® 1360, Micromeritics, Norcross, Georgia, USA) which uses displacement theory to determine the sample volume. Dry*Flo*®, a quasi-fluid powder is used as the displacement media. Dry*Flo*® (~2.5 cm^3) is added to the sample chamber (25.4 mm diameter) and a stepper motor inserts a piston into the rotating chamber until a pre-determined force (51 N) is reached. Each count on the stepper motor is equivalent to a known displacement of the piston allowing the use of a conversion factor to calculate a volume measurement. A pre-determined number of *preparation cycles* are completed to allow consistent consolidation of the Dry*Flo*®. These *preparation cycles* are disregarded by the software. A pre-determined number of

blank cycles are then performed to obtain a volume measurement of the Dry*Flo*® media. An accurately weighed sample (~4 g) is then added to the sample chamber and the pre-determined number of *preparation cycles* repeated. Subsequently a pre-determined number of *sample measurements* are performed to obtain a total volume measurement for the Dry*Flo*® and sample. The sample weight is divided by the difference between the *sample* and *blank* volume measurements to obtain an envelope density result. The following equations were used to calculate sample envelope density:

$$V_c = d_o \times CSA \qquad \textit{Equation 2-2}$$

$$C_v = [\pi D^2 / ((200)(4)(6.297)(3))] \qquad \textit{Equation 2-3}$$

$$V_b = V_c - (C_v \text{ x } C_e) \qquad \textit{Equation 2-4}$$

$$V_s = C_v (C_p - C_e) \qquad \textit{Equation 2-5}$$

$$p_e = \frac{W}{Vs} \qquad \textit{Equation 2-6}$$

where V_c is the chamber volume (33.523 cm^3), d_o the zero depth calibration value of 6.6259 cm, *CSA* the sample chamber cross sectional area (5.067 cm^2), C_v the volume equivalent to one count of the piston motor (cm^3/count) [14], *D* the chamber diameter (25.4 mm), V_b the Dry*Flo*® blank volume (cm^3), C_e the motor count with no sample present, V_s the sample volume (cm^3), C_p the motor count with the sample present, p_e the sample envelope density (g cm^{-3}) and *W* the sample weight (g).

2.1.2.3 Granule size analysis

Approximately 100 g of dried granules (n=4) were placed onto tared 8 inch diameter ASTM certified screens (pan, 75, 150, 250, 425, 600, 850, 1000, 1700, 2000, 3350, 4750 and 8000 µm). The sieve stack was then mounted on a single intensity sieve tester (RoTap RX-29, W.S. Tyler, Mentor, Ohio, USA) and the granules sieved Preliminary work indicated that sieving times of 5, 10 and 15 minutes showed no differences in the granule mass retained on each sieve therefore a sieving time of 5 min was selected.

After sieving 13 size fractions were collected and the mass mean diameter, d_{pm}, was determined using the following equation:

$$d_{pm} = \frac{(\Sigma f_i \cdot d_{pi})}{(\Sigma f_{i-n})} \qquad \textit{Equation 2-7}$$

where f_i is the mass fraction of size interval i, d_{pi} is the mean diameter of size interval i (μm).

2.1.2.4 Bulk and tapped density

Bulk and tapped densities (n=4) were measured using a tap density meter (Vankel, Cary, North Carolina, USA). A weight of granule, W, with an apparent volume of at least 50 cm^3 was placed into a graduated cylinder secured in its holder. The unsettled apparent volume, V_0, was determined to the nearest cm^3. Bulk density calculated as W/V_0.

The sample was then tapped 300 and 600 times and the corresponding volumes V_{300} and V_{600} recorded to the nearest cm^3. If the difference between V_{300} and V_{600} was ≥1 cm^3 another 300 taps were performed until a constant volume, V_x, was recorded. Tapped density was calculated as W/V_x.

2.1.2.5 Envelope density using mercury intrusion porosimetry

The envelope density of granule samples (n=3) was determined by mercury intrusion porosimetry (AutoPore, Micromeritics, Norcross, Georgia, USA) and was employed in accordance with the method described by Alderborn *et al* [6]. A sample holder (penetrometer) of a bulb and stem volume of 6 cm^3 and 1.13 cm^3 respectively was used. The empty penetrometer was placed into the porosimeter and filled with mercury to determine the fill volume of the penetrometer. The penetrometer was then emptied of mercury, cleaned and dried. The penetrometer was then loaded with granule samples of approximately 1 g (weighed to 0.0001 g) and filled with mercury at a pressure of 14.7 psi (corresponding to atmospheric pressure of 0.10 MPa). The volume of the granule sample was determined as the difference between the volume of the empty penetrometer

and the volume of mercury intruded into the penetrometer containing the sample. The pore size, *d*, intruded by mercury was estimated using the Washburn equation [15] to be 12 µm:

$$d = -\left(\frac{4\gamma}{P}\right) cos\ \theta \qquad \textit{Equation 2-8}$$

where γ is the surface tension of mercury (0.485 N m^{-1}) [6], P is the applied pressure (0.10 MPa) and θ is the contact angle between mercury and the pore wall (130°) [6].

2.1.2.6 Scanning electron microscopy

Scanning Electron Microscopy (SEM) images were captured using a scanning electron microscope (FEI Company, Hillsboro, Oregon, USA). Samples were platinum coated prior to analysis to reduce sample charging using the following parameters: target type = noble, 45 mA current, 90 s sputter time and 2 min pump hold. Sputter coated samples were analysed under high vacuum with 10 kV accelerating voltage and spot size 3.0.

2.1.2.7 Dry*Flo*® particle size analysis

Dry*Flo*® displacement media particle size (n=3) was measured by a dry dispersion laser light scattering method (Scirocco 2000, Malvern, Worcestershire, UK) with a micro volume tray (2–10 g) operated with 29 % vibration feed and 0.1 bar dispersive air pressure such that a final obscuration range of 0.5–6.0 was attained. The size range of the output was 0.02–2000 µm. Data were analysed using the general purpose Fraunhofer diffraction model and the $d_{10\%}$, $d_{50\%}$ and $d_{90\%}$ particle size results were reported for each sample where d represents the particle diameter and 10, 50 or 90 represents the percent of particles in the distribution with a size equal to or less than that diameter.

2.1.2.8 Statistical analysis

Statistical analysis was performed using JMP® version 9.0.3 (SAS Institute Inc., Cary, North Carolina, USA). Each data set was evaluated prior to analysis. Data sets with a

sample size of n ≥6 [16] were tested for normality using the Shapiro-Wilk test for normality [17]. The null hypothesis for the Shapiro-Wilk test stated that the data were normally distributed and a p-value <0.05 rejected the null hypothesis. If the null hypothesis for normality was accepted the data were analysed using the parametric ANOVA with Tukeys honestly significant difference (HSD) post-hoc test (referred to as ANOVA subsequently). The null hypothesis stated that there was no significant difference between means and a two-tailed p-value <0.05 rejected the null hypothesis. If the null hypothesis for normality was rejected, or the sample size was <6 [16], the data were analysed using the non-parametric Wilcoxon each pair test [18] (referred to as Wilcoxon subsequently). The null hypothesis stated that there was no significant difference between means and a two-tailed p-value <0.05 rejected the null hypothesis for a sample size of n ≥4 and a two-tailed p-value <0.10 rejected the null hypothesis for a sample size of n=3.

2.2 Results and Discussion

2.2.1 Physical characterisation

HA granule bulk and tapped density, mass mean diameter and envelope density were determined for each sample (Table 2-1). Bulk density showed an initial increase ($p < 0.05$ Wilcoxon) with binder volumes of 50–150 cm^3, followed by a decrease when 250 cm^3 of binder liquid was used for both binder liquid concentrations. Tapped density decreased ($p < 0.05$ Wilcoxon) with increasing binder liquid volume, indicating a reduction in packing efficiency, which is likely a result of the increase in mass mean diameter ($p < 0.05$ Wilcoxon). Envelope density increased with increasing binder liquid volume when measured using the GeoPyc® ($p < 0.05$ Wilcoxon) and was confirmed by mercury porosimetry ($p < 0.10$ Wilcoxon).

Mass mean diameter and envelope density both increased as a result of increased binder liquid quantity. This is consistent with previous findings where larger sized granules tended to be less porous [5, 19, 20] and this observation has been attributed to two factors. First, the deformability of the granules is greater at higher liquid contents resulting in larger and more compact granules [10, 19]. Second, larger granules are generally composed of smaller particles [21, 22] and as a result of the closely packed nature of the granule structure the pore volume is smaller [23, 24].

Table 2-1. Summary of granulation process conditions and granule physical properties. Mean ± SD, n=4 (except mercury porosimetry envelope density where n=3).

Granulation process	Binder liquid volume (cm^3)	Binder liquid PVP conc (% *w/w*)	Bulk density (g cm^{-3})	Tapped density (g cm^{-3})	Mass mean particle size (µm)	GeoPyc® envelope density (g cm^{-3})	Mercury porosimetry envelope density (g cm^{-3})
Un-granulated	0	0	0.79 ± 0.004	1.16 ± 0.014	202 ± 1.5	0.93 ± 0.015	1.23 ± 0.027
Reverse-Phase	50	10	0.81 ± 0.005	1.13 ± 0.008	360 ± 18.7	0.99 ± 0.029	1.26 ± 0.017
Reverse-Phase	100	10	0.85 ± 0.003	1.12 ± 0.011	760 ± 13.3	1.08 ± 0.006	1.29 ± 0.019
Reverse-Phase	150	10	0.88 ± 0.010	1.09 ± 0.012	842 ± 10.8	1.13 ± 0.012	1.34 ± 0.016
Reverse-Phase	250	20	0.75 ± 0.007	0.86 ± 0.007	1810 ± 91.4	1.19 ± 0.029	1.46 ± 0.009
Reverse-Phase	250	10	0.75 ± 0.008	0.87 ± 0.015	1814 ± 36.3	1.22 ± 0.010	1.48 ± 0.011

The displacement media, Dry*Flo*®, is composed of silica beads lubricated by fine graphite particles. Scanning electron micrographs (Figure 2-2) show the silica beads to be spherical in shape, smooth surfaced and hollow in some cases. Small irregular particles are present on the surface of the spheres.

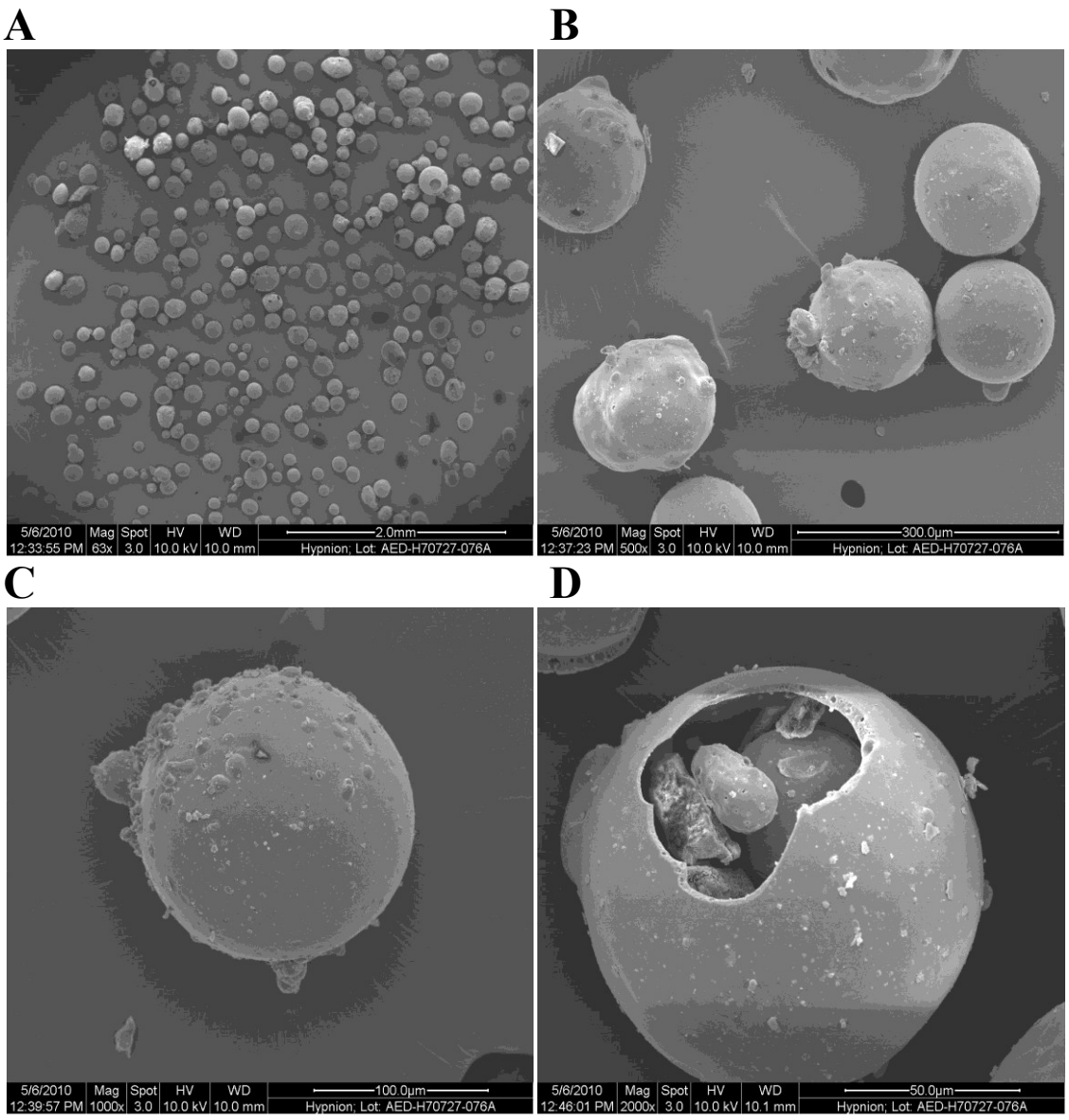

Figure 2-2. Scanning electron micrograph of DryFlo® media, A – 63 x magnification, B – 500 x magnification, C – 1000 x magnification, D – 2000 x magnification.

Dry*Flo*® samples (~1 g) were taken in triplicate, using a stainless steel sample thief (Sampling Systems Ltd., Warwickshire, UK), from locations at the top, middle and bottom of each of three separate 3 L Dry*Flo*® bottles received from the vendor. The $d_{10\%}$ and $d_{50\%}$ (Figure 2-3) results are similar ($p > 0.05$ Wilcoxon) across all of the samples taken, however the $d_{90\%}$ values for the size of the Dry*Flo*® show clear differences in both the mean and standard deviation for three of the sample locations (Bottle 1 Bottom, Bottle 1 Middle and Bottle 3 Middle). Evaluation of the particle size distribution in Figure 2-4 shows evidence of a bimodal distribution in replicate 3. Visual observations of the sample during analysis confirmed that the sample with a bimodal distribution contained black agglomerates approximately 1–2 mm in diameter.

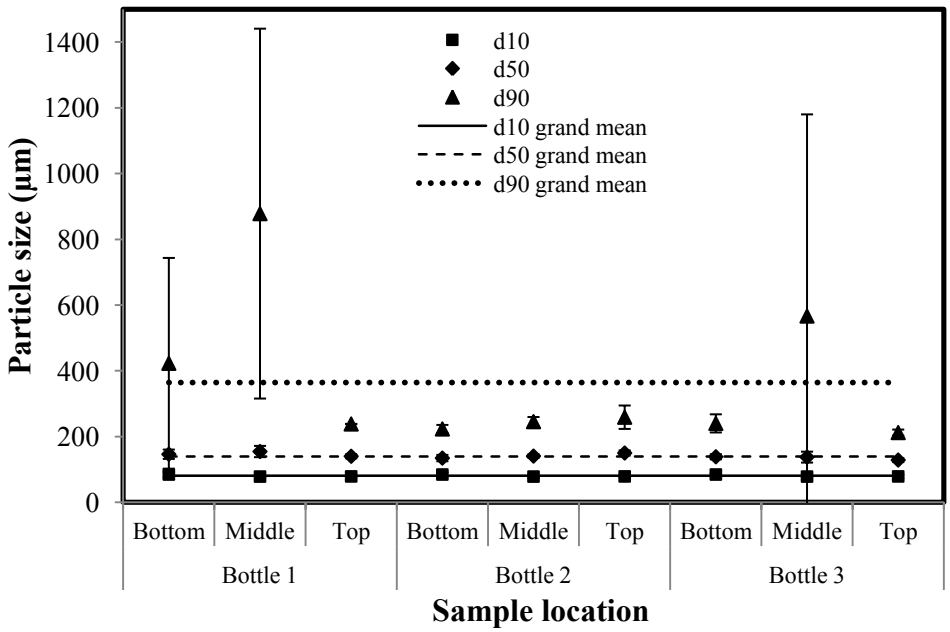

Figure 2-3. $d_{10\%}$, $d_{50\%}$, $d_{90\%}$ particle size results for DryFlo® displacement media. Error bars represent 1 SD, n=3.

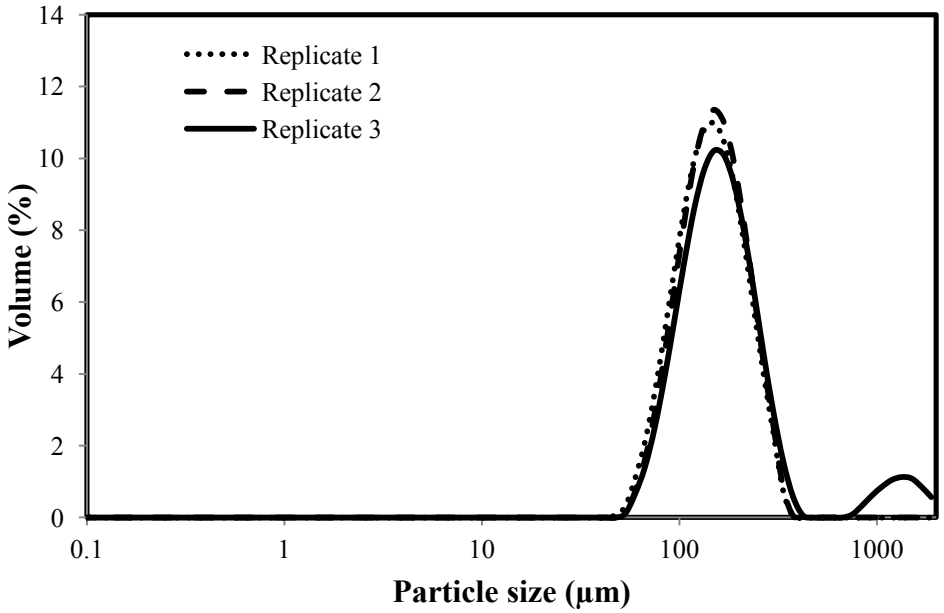

Figure 2-4. Example particle size distributions obtained for DryFlo® displacement media showing a bimodal peak in some samples which appeared to be associated with the presence of graphite agglomerates.

Scanning electron micrographs (SEM) and energy dispersive spectrographs (SEM-EDS) of the agglomerates were obtained. A mixture of large smooth graphite agglomerates (Figure 2-5A and Figure 2-5B) and smaller irregular agglomerates (Figure 2-5C and Figure 2-5D) were observed. In all cases the integrity of the structure of the particles was extremely weak and did not survive the SEM low-vacuum platinum sputter coating procedure and micrographs were therefore obtained using uncoated samples only. As a result silica beads on the surface of the agglomerates in Figure 2-5A and Figure 2-5B appear silver in colour due to static charging. SEM-EDS indicated that carbon was the principal elemental component of the agglomerates, consistent with the graphite component of Dry*Flo*® (Figure 2-5E).

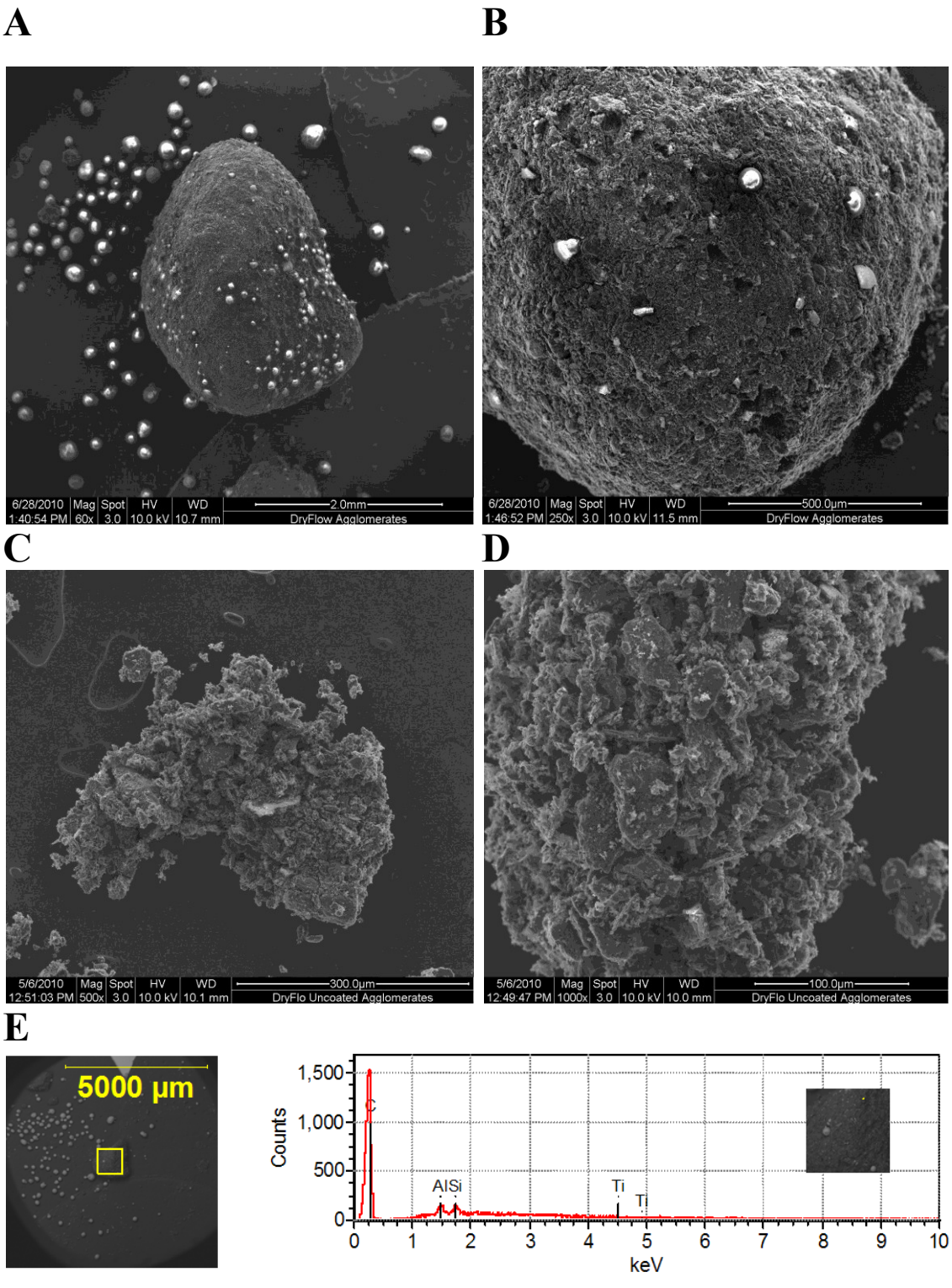

Figure 2-5. Scanning electron micrograph of agglomerates identified in DryFlo® media, A – 60 x magnification, B – 240 x magnification, C – 500 x magnification, D – 1000 x magnification. E – Energy dispersive spectrograph of agglomerate identified in DryFlo® media.

As a precaution the Dry*Flo*® media used for further analysis was sieved through a 500 µm screen to remove or break up, any agglomerates prior to use. Particle size analysis was repeated for the sample locations that displayed a bimodal distribution using sieved Dry*Flo*®. Similar $d_{90\%}$ results ($p > 0.05$ Wilcoxon) were then obtained across all sample locations (Figure 2-6).

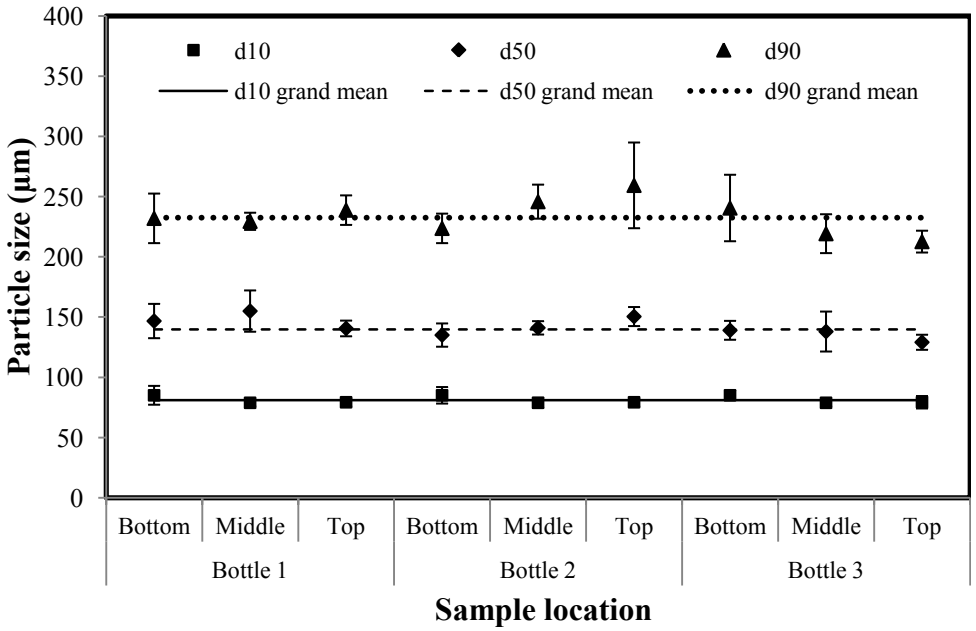

Figure 2-6. $d_{10\%}$, $d_{50\%}$, $d_{90\%}$ particle size results for DryFlo® displacement media. Error bars represent 1 SD, n=3.

2.2.2 Dry*Flo*® and sample consolidation

An important GeoPyc® variable is the number of preparation cycles that the software disregards when calculating the sample statistics. Preparation cycles are used to ensure that the Dry*Flo*® achieves a stable packing configuration before any test measurements are taken. The vendor recommends using two preparation cycles, and a maximum of 20 preparation cycles is allowed by the software. A change of ≤ 0.01 g cm^{-3} is considered acceptable for this application. During the initial cycles consolidation is less consistent as the piston first travels the length of the test chamber resulting in variable count measurements. After a number of cycles repeatable consolidation occurs and representative volume measurements are obtained.

Approximately 6–7 g samples of Dry*Flo*® media were analysed using zero preparation cycles and 20 test cycles using consolidation forces of 10, 20, 30, 40, 51, 60, 70, 80, 90 and 100 N. Dry*Flo*® density was calculated for each of the 20 cycles (Figure 2-7).

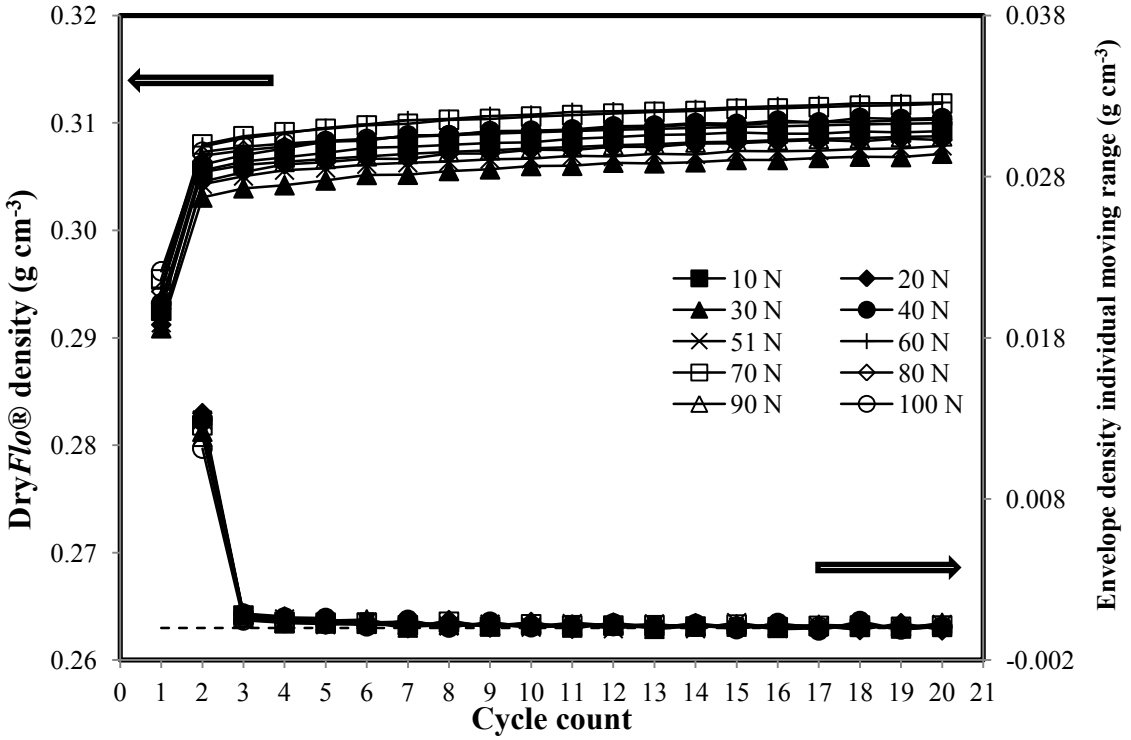

Figure 2-7. Plot of DryFlo® density as a function of cycle count and consolidation force (n=6).

For all consolidation forces cycle one generated density results that were markedly different ($p < 0.05$ ANOVA) from those obtained in the subsequent cycle results. The individual moving range (IMR), where IMR = [X1 – X2], between cycle 1 and cycle 2 varies from 0.0111–0.0133 g cm^{-3}. Cycles 2 to 20 exhibit an acceptable (<0.01 g cm^{-3}) individual moving range difference of -0.0002–0.0009 g cm^{-3}. The study was similarly performed using samples of HA granules at the 51 N consolidation force, recommended by the vendor. HA granule density was calculated for each of 20 cycles (Figure 2-8). Cycle 1 results were again markedly different ($p < 0.05$ ANOVA) to the values obtained in subsequent cycles with samples having an IMR of -0.1729–0.0048 g cm^{-3}. Cycles 2 to 20 exhibit an acceptable (<0.01 g cm^{-3}) IMR difference of -0.0094 – 0.0104 g cm^{-3}.

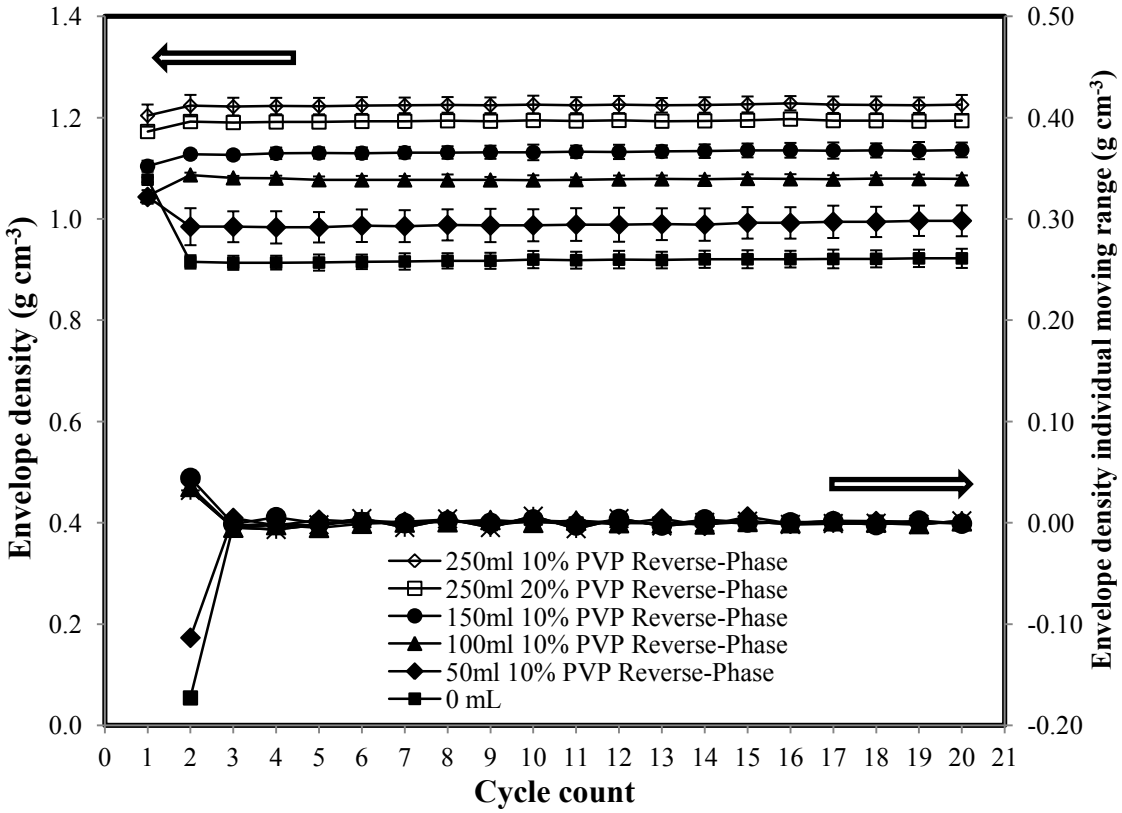

Figure 2-8. Plot of envelope density for HA granules prepared by reverse-phase granulation process as a function of cycle count using a 51 N compression force. Error bars represent 1 SD, n=4.

A second variable to consider is the consolidation force used to determine the endpoint for each cycle. The vendor recommends a force of 51 N with the 25.4 mm diameter sample chamber with an operating range of 0–180 N. The maximum Dry*Flo*® density achieved at cycle 20 was plotted as a function of consolidation forces (Figure 2-9) and the standard deviation of the densities at each force calculated.

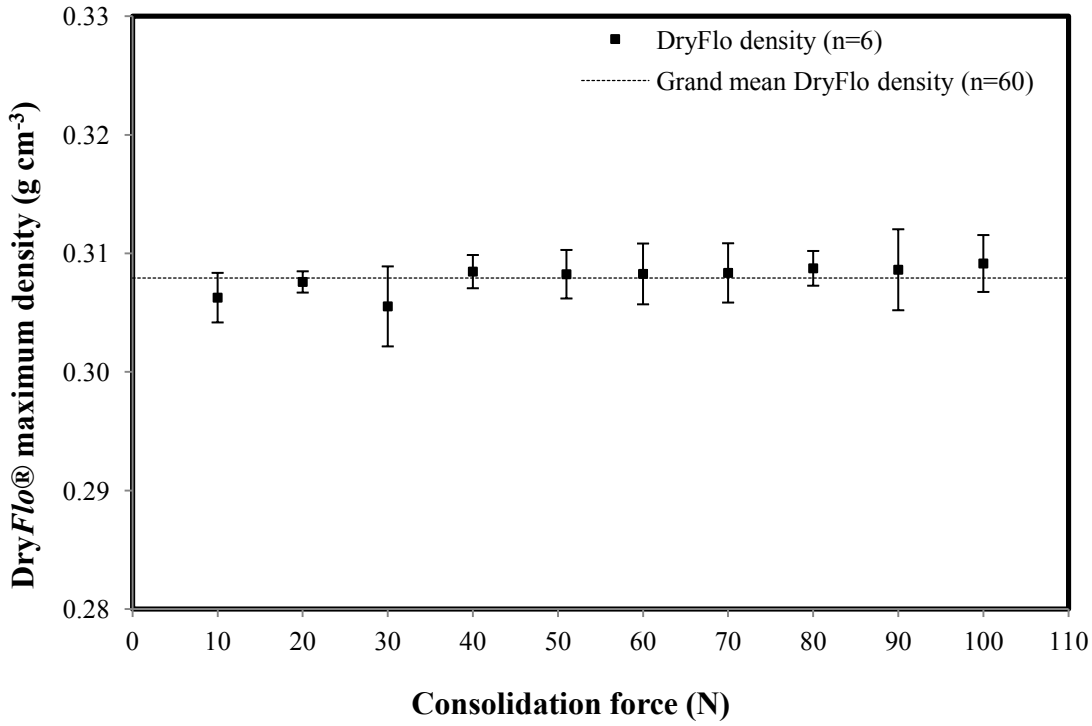

Figure 2-9. Plot of DryFlo® density as a function of consolidation force. Error bars represent 1 SD, n=6.

The cycle 20 mean density (range 0.3055–0.3091 g cm^{-3}) and standard deviation (range 0.0009–0.0034 g cm^{-3}) were found to be similar ($p > 0.05$ ANOVA) at all consolidation forces supporting the vendor recommended default setting of 51 N.

2.2.3 Comparison to mercury intrusion porosimetry

The envelope density of granules prepared as described in Section 2.1.2.1 was measured using both the mercury porosimetry (Section 2.1.2.5) and powder pycnometry (Section 2.1.2.2) methods. The results are shown in Figure 2-10.

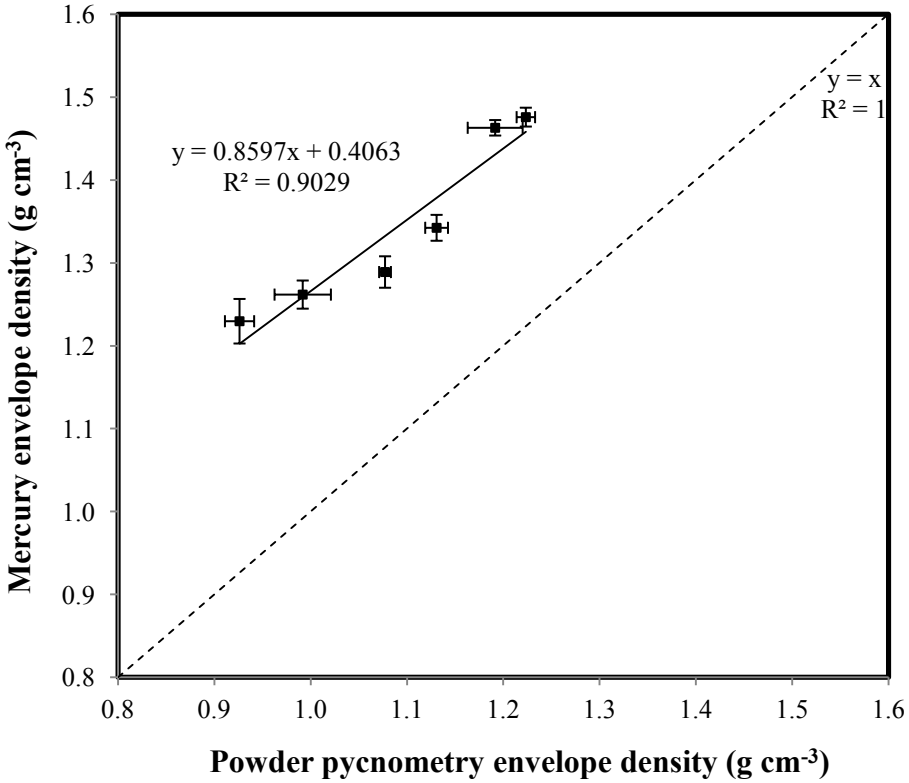

Figure 2-10. Calibration plot of powder pycnometry and mercury porosimetry envelope density measurements of hydroxyapatite granules. Dashed line represents perfect agreement in the values between the two methods. Error bars represent 1 SD, n=3.

The GeoPyc® envelope density measurements are lower than the corresponding results obtained using mercury porosimetry, which is consistent with the limited results that have been previously reported comparing the two methods [12]. The difference is likely to be attributable to the differences in the pore size intruded by each method. Dry*Flo*® media has a larger particle size (mean [SD] d_{10} 82 µm [5.2 µm], d_{50} 142 µm [11.8 µm], d_{90} 227 µm [20.8 µm]) than the pore size (12 µm) intruded by mercury at 0.10 MPa intrusion pressure.

Despite the differences in the intruded pore size, the GeoPyc® method yields results with a linear correlation (R^2 0.9029) to those generated using the reference mercury porosimetry method. While the correlation is not perfect it is sufficient to indicate that the GeoPyc® method is suitable for measuring the envelope density of the HA granules as well as the un-granulated material. The observed correlation between the methods is likely due to the fact that both the Dry*Flo*® displacement media and the HA granules are polydisperse in nature, which facilitates packing [25], meaning that introduction of

the sample to the Dry*Flo*® displacement media causes minimal change in packing efficiency. The linear regression fit in Figure 2-10 could be used to convert the GeoPyc® envelope density results to those obtained from mercury porosimetry.

2.2.4 Effect of granule particle size

Granules prepared by the reverse-phase granulation process using 250 cm^3 of 10 % *w/w* PVP binder liquid were sieved and the following fractions collected: 0–75, 75–150, 150–250, 250–425, 425–600, 600–850, 850–1000, 1000–1700, 1700–2000, 2000–3350, 3350–4750, 4750–8000 µm. The envelope density of each sieve fraction was measured by powder pycnometry and mercury porosimetry methods (Figure 2-11).

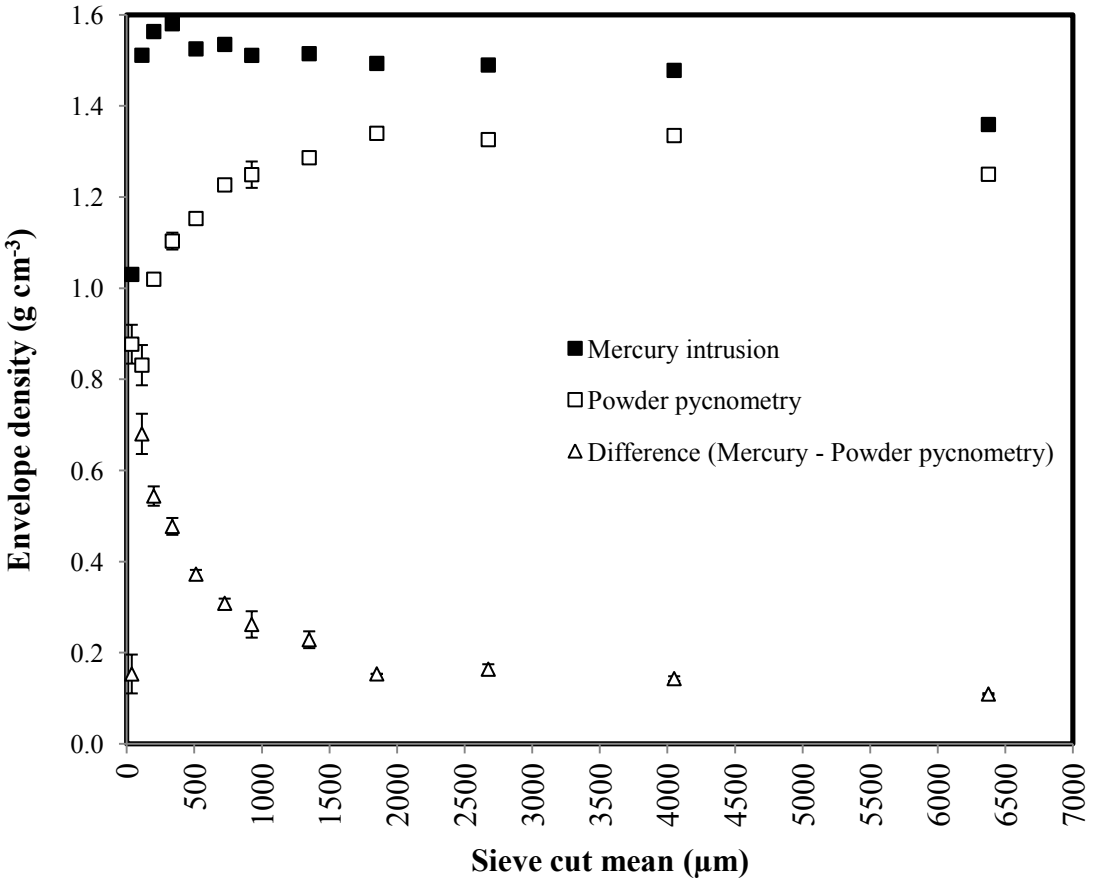

Figure 2-11. Plot of mean particle size fraction envelope density values for powder pycnometry and mercury porosimetry methods. Error bars represents 1 SD, n=3.

The GeoPyc® powder pycnometry envelope density values increased steadily as the size fraction mean increased from 37.5–1350 µm and then stabilised for granule size

fractions within the range 1850–6375 μm. The mercury porosimetry envelope density results plotted as a function of granule size demonstrated a similar profile. Nevertheless, there was a relatively large increase in the density from that obtained for the 37.5 μm to the 112.5 μm size fraction. This was followed by a region from 112.5 μm to 925 μm where the value for the envelope density was more variable, whereas the value remained almost constant above this particle size. A constant difference in the envelope densities obtained by the two methods, represented by the open triangles in Figure 2-11, was determined for granules within the 1850–6375 μm size range. Narrow size fractions below this range do not appear to yield comparable measurements making calibration for this range challenging, indicating that the GeoPyc® powder pycnometry method for narrow size fractions of smaller particles may be less appropriate for quantitative measurements and requires case by case determination. This is likely due to the particle size of the Dry*Flo*® media which affects packing around the sample particles relative to mercury intrusion, which reliably penetrates pores ≥12 μm regardless of sample particle size. As the sample particle size is reduced the sample particles and the Dry*Flo*® particles approach a similar size. As this occurs the packing efficiency is reduced creating a more open packing structure [26], resulting in inaccurate measurements of envelope density. As the sample particle size increases the packing efficiency is increased since the Dry*Flo*® media can effectively pack around the sample. Above a critical sample particle size reproducible packing of the Dry*Flo*® can occur and a calibration to the mercury porosimetry measurement can be undertaken for narrow size fractions.

2.3 Conclusions

GeoPyc® powder pycnometry proved to provide a repeatable method to measure HA granule envelope density for polydisperse samples, where efficient packing between the sample and Dry*Flo*® can take place. Dry*Flo*® media was shown to have a consistent particle size when sampled across three separate containers and multiple locations within each container. Relatively large graphite agglomerates were identified in the Dry*Flo*® media which could be removed, or broken up, by screening the media before use. A minimum of 1 preparation cycle should be used before blank or sample measurements are recorded.

Dry*Flo*® density was found to be insensitive to consolidation forces in the range of 10–100 N indicating that the vendor-recommended 51 N force was suitable for carrying out the envelope density determination. The GeoPyc® powder pycnometry method could be calibrated against the reference mercury porosimetry method when considering polydisperse HA granule samples. However, when analysing narrow particle size fractions, limitations in the GeoPyc® powder pycnometry method were noted which indicated that the correlation between the results obtained by mercury porosimetry was only valid between the particle size range of 1850–6375 μm. The results demonstrated the limitations of the GeoPyc® powder pycnometry method in measuring the envelope density of granules of narrow size fractions but indicated that these limitations were overcome when using polydisperse (i.e. un-sieved) granule samples.

While porosity is an important attribute that can affect granule strength and compactibility [1, 2, 11] so is moisture content [27]. Only limited characterisation of HA compaction properties has been reported previously, whilst the role of moisture in HA compaction properties has received notably less attention. Consequently, it is recommended that the effect of moisture content on the compaction properties of hydroxyapatite be studied further.

2.4 References

[1] Rumpf, H. The strength of granules and agglomerates in: Knepper W.A., (Eds.) *Agglomeration*, Interscience-Wiley, New York, 1962, pp. 379-418.

[2] Wikberg, M., Alderborn, G., Compression characteristics of granulated materials. IV. The effect of granule porosity on the fragmentation propensity and the compactibility of some granulations., Int. J. Pharm., 69 (1991) 239-253.

[3] M. Ansari, Stepanek, F., The effect of granule microstructure on dissolution rate, Powder Technology, 181 (2008) 104-114.

[4] Iveson, S.M., Litster, J.D., Ennis, B.J., Fundamental studies of granule consolidation Part 1: Effects of binder content and binder viscosity, Powder Technology, 88 (1996) 15-20.

[5] Iveson, S.M., Litster, J.D., Fundamental studies of granule consolidation Part 2: Quantifying the effects of particle and binder properties, Powder Technology, 99 (1998) 243-250.

[6] Alderborn, G., Nordstrom, J., Persson, A.-S., Lazarova, L., Frenning, G., The degree of compression of spherical granular solids controls the evolution of microstructure and bond probability during compaction, Int. J. Pharm., 442 (2013) 3-12.

[7] Plantard, G., Goetz, V., Py, X., A direct method for porous particle density characterization applied to activated carbon, Advanced Powder Technology, 21 (2010) 592-598.

[8] Zinchuk, A., Mullarney, M., Hancock, B., Simulation of roller compaction using a laboratory scale compaction simulator, Int. J. Pharm., 269 (2004) 403-415.

[9] Forsmo, S.P.E., Vuori, J.P., The determination of porosity in iron ore green pellets by packing in silica sand, Powder Technology, 159 (2005) 71-77.

[10] Litster, J.D., Ramachandran, R., Poon, J., Sanders, C., Glaser, T., Immauel, C., III, F.D., Stepanek, F., Wang, F., Cameron, I., Experimental studies on distributions of granule size, binder content and porosity in batch drum granulation: Inferences on process modelling requirements and process sensitivities, Powder Technology, 188 (2008) 89-101.

[11] Carvajal, M.T., Macias, K.A., The influence of granule density on granule strength and resulting compact strength, Chem. Eng. Sci., 72 (2012) 205-213.

[12] Ghadiri, M., Rahmanian, N., Jia, X., Stepanek, F., Characterisation of granule structure and strength made in a high shear granulator, Powder Technology, 192 (2009) 184-194.

[13] Ghadiri, M., Rahmanian, N., Naji, A., Effects of process parameters on granule properties produced in a high shear granulator, Chemical Engineering Research and Design, 89 (2011) 512-518.

[14] Orr, C., Method and apparatus for measuring envelope density, Micromeritics Instrument Corporation US Patent 5,608,157, (1997).

[15] Allen, T. Surface Area and Pore Size Determination *Particle Size Measurement*, 5th ed, Chapman & Hall, London, 1997, pp. 251-302.

[16] Jones, D. Statistical hypothesis testing in *Pharmaceutical Statistics*, Pharmaceutical Press, London, 2002, pp. 133.

[17] Shapiro, S.S., Wilk, M.B., An analysis of variance test for normality (complete samples), Biometrika, 52 (1965) 591-611.

[18] Wilcoxon, F., Individual comparisons by ranking methods, Biometrics Bulletin, 1 (1945) 80-83.

[19] El-Hagrasy, A.S., Hennenkamp, J.R., Burke, M.D., Cartwright, J.J., Litster, J.D., Twin screw wet grnaulation: Influence of formulation parameters on granule properties and growth behavior, Powder Technology, 238 (2013) 108-115.

[20] Mackaplow, M.B., Rosen, L.A., Michaels, J.N., Effect of primary particle size on granule growth and endpoint determination in high-shear wet granulation, Powder Technology, 108 (2000) 32-45.

[21] Scott, A.C., Hounslow, M.J., Instone, T., Direct evidence of heterogeneity during high-shear granulation, Powder Technology, 113 (2000) 205-213.

[22] Ramachandran, R., Ansari, M.A., Chaudhury, A., Kapadia, A., Prakesh, A.V., Stepanek, F., A quantitative assessment of the influence of primary particle size polydispersity on granule inhomogeneity, Chem. Eng. Sci., 71 (2012) 104-110.

[23] Kristensen, H.G., Holm, P., Schaefer, T., Mechanical properties of moist agglomerates in relation to granulation mechanisms: Part 1. Deformability of moist, densified agglomerates, Powder Technology, 44 (1985) 227-238.

[24] Hsiau, S.S., Tu, W.D., Ingram, A., Seville, J., The effect of powder size on induction behaviour and binder distribution during high shear melt agglomeration of calcium carbonate, Powder Technology, 184 (2008) 298-312.

[25] Furnas, C.C., Grading aggregates. I. Mathematical relations for beds of broken solids of maximum density, Ind. Eng. Chem., 23 (1931) 1052-1058.

[26] Orband, L.R., Geldart, D., The Use of an Antistatic Agent to Improve Powder Flowability, Particle Particle System Characterization, 12 (2005) 204-206.

[27] Carstensen, J.T., Effect of moisture on the stability of solid dosage forms, Drug Dev. Ind. Pharm., 14 (1988) 1927-1969.

CHAPTER THREE: THE EFFECT OF MOISTURE CONTENT ON THE COMPACTION PROPERTIES OF HYDROXYAPATITE

3 Introduction

The reverse-phase granulation process involves the mixing of powdered materials with an aqueous binder liquid to form moist granules, which are subsequently dried to a pre-determined moisture content. The presence of moisture in pharmaceutical powders can have a marked effect on their compaction properties, and the mechanical strength of the resulting tablet [1-6]. The mechanical strength of a tablet is critical to the success of downstream processes such as film coating, imprinting and packaging, and also plays a role in tablet disintegration and drug dissolution. The effect of moisture on the compaction properties of pharmaceutical powders is therefore of interest.

Hydroxyapatite (HA) was selected as the model raw material for the development of the reverse-phase granulation process. HA is a plastically deforming material [7-9] which has gained prominence in pharmaceutical and dietary supplement formulations due to low toxicity, desirable flow properties, good compaction characteristics, reasonably low cost and high orally available calcium content [1, 9, 10]. HA is anhydrous and does not form a hydrate upon exposure to water [1]. Aqueous solubilities between 0.017 and 0.025 mg L^{-1} at 20 ˚C [9, 10] and melting points between 1550 ºC and 1614 ºC [11, 12] have been reported. It is worth noting that HA has a Ca/P molar ratio of 1.667 and chemical formula of $Ca_5(PO_4)_3(OH)$ or $Ca_{10}(PO_4)_6(OH)_2$, but has often been erroneously referred to as tricalcium phosphate [13], tricalcium orthophosphate or tribasic calcium phosphate [14] which all have a Ca/P ratio of 1.5 [15] and the chemical formula $Ca_3(PO_4)_2$. A number of pharmaceutical grade HAs are commercially available for use in direct compression and wet granulation manufacturing processes. TRI-CAL WG™ (Section 2.1.1), a granular form of HA, is specifically designed for use in aqueous wet granulation processes and is the focus of this study.

The mechanical strength of a tablet is commonly described by its tensile strength and is considered to be primarily determined by two parameters: the bonding force between powder particles and the area over which these bonding forces act [16]. Three types of bonding forces are generally accepted to act between pharmaceutical powder particles: solid bridges, mechanical interlocking and distance forces [17]. Solid bridges describe the continuous solid phase formed between two, or more, particles and contribute markedly to the strength of materials with a simple structure, low melting point, some

degree of solubility in adsorbed moisture, or have a glass transition temperature similar to that experienced during compaction [18-20]. Mechanical interlocking is considered possible for some materials with a rough texture and/or irregular shape, which allow for hooking or twisting together of particles [21], however the pharmaceutical relevance of this mechanism has been challenged [22]. Interparticulate distance forces, i.e. van der Waals forces, hydrogen bonds, and electrostatic interactions, are generally considered to be the dominant bonding mechanism for most pharmaceutical powders [23]. Additionally, capillary forces between particles, caused by the condensation of moisture, have also been reported to contribute to the interparticulate bonding force of powder particles [24].

An increase in moisture content has been reported to increase the bonding area of plastically deforming materials during compaction due to plasticising and lubricant effects [25, 26]. Moisture facilitates particle rearrangement and deformation during compaction resulting in tablets with a lower porosity at constant compaction pressure and therefore increases the area over which interparticulate bonding can take place. This effect has frequently been reported for pharmaceutical powders as a reduction in the mean yield pressure derived from the Heckel equation [2, 4, 6, 27-34] and also by an increase in the compressibility coefficient derived from the Walker equation [35].

Moisture on particle surfaces has been proposed to enhance interparticulate interactions. Moisture adsorption can mediate molecular attraction forces if the layers touch or penetrate each other [3, 36]. Surface moisture can also be seen as part of the particle surface thus reducing interparticulate distance, leading to an increase in interparticulate bonding and tensile strength [3, 37, 38]. Adsorbed moisture can also function as a surface-restructuring medium, increasing the contribution of solid bridges [30], particularly for salts and soluble materials.

However, moisture has also been reported to have a negative effect by disrupting certain bonding forces. For example dissolution of solid bridges can take place at elevated relative humidity, which acts to reduce tensile strength [39]. Sodium chloride and saccharose tablets stored at 100 % RH for 15 days demonstrated complete loss of tensile strength due to this phenomenon [40]. Similarly, for anhydrous dextrose an increase in moisture content from 0.34 to 8.90 % *w/w* resulted in increased tensile strength due to

recrystallisation effects, however the tensile strength was significantly reduced at moisture contents of 9.20 and 9.66 % *w/w* as a result of condensation of moisture and dissolution of solid bridges [41]. Adsorbed moisture on the particle surface can also interfere with intermolecular forces, thus reducing the bond strength and resultant tablet tensile strength [16, 42, 43].

Studies with HPMC polymers suggest the effect of moisture on tablet tensile strength is a balance between the relative quantities of each physical form of moisture [29]. Tensile strength increased to a maximum at 6 % *w/w* moisture content, but decreased with further increases in moisture content [30]. The first 6 % *w/w* moisture content is suggested to strongly bind by hydrogen bonds to the hydroxyl groups in the cellulose structure, rather than being present as monolayer or multilayer moisture on the surface of the particles. Moisture in the hydrogen bonded state acts as a plasticiser to facilitate plastic deformation and increases the area over which interparticulate bonds can act [44]. Above 6 % *w/w* moisture forms a monolayer at the surface of the particles acting to disrupt intermolecular bonds [45] and facilitate elastic recovery, through a lubrication effect, resulting in decreased tensile strength of tablets at a solid fraction of 0.9 [30]. The interplay between plasticity and the positive or negative effects of moisture on bond strength have also been the topic of study for a number of other researchers [25, 30, 45-47].

Investigation of the compaction of microcrystalline cellulose found that below a critical moisture content (~3.3 % *w/w*) tablet tensile strength was at a maximum [6]. This was attributed to the plasticising effect of moisture distributed within the relatively porous particles; moisture forms hydrogen bonds with the surfaces of microfibrils and is concentrated in amorphous regions, resulting in a decreased glass transition temperature [48]. Increases above the critical moisture content, postulated to be represented by the monolayer moisture coverage, resulted in decreased tensile strength, despite the decreased tablet porosity that was achieved [5].

Similar findings were reported for pregelatinised starch [47] where an increase in the sample water activity from 0.22 to 0.70 resulted in an increase in tensile strength, but a further increase to 0.95 water activity caused a decrease in tensile strength. When constant tablet porosity was considered, by applying the Ryshkewitch-Duckworth

equation, it became evident that increasing moisture content resulted in a steady decrease in bonding capacity and tensile strength at zero porosity. In addition, the observed increase in tensile strength at constant compaction pressure was due to the decreased mean yield pressure and therefore increased bonding area.

Increased moisture content reduced amylodextrin tablet porosity when compressed at a pressure of 250–300 MPa [25]. However, despite the increased bonding area, the tablets of higher moisture content had lower tensile strength, due to a reduction in bond strength caused by multiple water-layers on the particle surfaces. Similar results were obtained for crystalline materials also. Ibuprofen tablets exhibited a maximum tensile strength at ~2.5 % *w/w* moisture content, which decreased as the moisture was increased to 10 % *w/w* [4]. Non-hygroscopic paracetamol tablets yielded maximum tensile strength at 6 % *w/w* moisture, but decreased at 8 % *w/w* [33]. However, both these latter studies only evaluated the effect on tabletability and tablet porosity, therefore the interplay between bonding area and bond strength was not considered.

The quantity and distribution of moisture will depend upon the chemical properties of the powder, various physical properties such as particle size and pore structure, and the RH at which the material is handled and stored [33]. The relative importance and contribution of bonding area and bond strength to tablet tensile strength varies as a function of moisture content and should be evaluated on a material-by-material basis [6].

Only limited characterisation of HA compaction properties has been reported previously. Published results are restricted to studying the effect of compaction force on tablet breaking strength and Heckel analysis [8, 9, 49-51], whilst the role of moisture in HA compaction properties has received notably less attention. An aqueous wet granulated formulation comprising 84 % HA, 10 % starch, 5 % naproxen and 1 % magnesium stearate has been investigated [52]. As moisture content increased over the range of 1.5–4.9 % *w/w* the mean tablet breaking strength decreased. Nevertheless, these findings can be considered preliminary since the focus of the study was on the effect of relative humidity conditions during storage upon changes in tablet breaking strength. Over the moisture content range studied there was no difference in tablet breaking strength upon storage at 23 °C / 44 % RH. However, storage of tablets

compressed at lower initial moisture contents of 1.5–3.1 % at 23 °C / 93 % RH showed a decrease in tablet breaking strength, despite tablets with a higher initial moisture content of 4.0 % and 4.9 % displaying negligible change in breaking strength under the same storage conditions. Clearly, although moisture is important in the compaction properties of HA and the resultant tablet tensile strength, there is much that remains to be investigated; specifically the effect of moisture on the simultaneous relationships between compaction pressure, tablet porosity and tensile strength.

3.1 Materials and Methods

3.1.1 Materials

Hydroxyapatite (HA) (TRI-CAL WG^{TM}) was obtained as detailed in Section 2.1.1.

3.1.2 Micromeritic characterisation

Bulk and tapped densities of HA were measured as described in Section 2.1.2.4, SEM images were captured as described in Section 2.1.2.6 and particle size of HA was determined as described in Section 2.1.2.7.

3.1.2.1 True density

In the present study true density was determined by helium pycnometry (AccuPyc 1330, Micromeritics, Norcross, Georgia, USA). The volume of a large capacity sample chamber was determined by placing two spherical NIST traceable calibration standards with a volume of 6.3720 cm^3 into the sample chamber and performing the calibration cycle. The sample chamber was then loaded with a sample of approximately 4.8 g (weighed to 0.0001 g) of HA and placed into the instrument. An equilibration rate criteria of <0.0020 psig min^{-1} was applied between 20 consecutive measurements, with the mean of the values being reported as the true density.

3.1.2.2 Specific surface area

Specific surface area of HA (n=3) was measured using a nitrogen adsorption method (TriStar 3000, Micromeritics, Norcross, Georgia, USA). The mass of three 3/8 ” sample tubes with rubber stoppers was recorded to the nearest 0.0001 g, with and without the sample present. Samples were then outgassed using nitrogen gas at 40 ºC for 2 h and cooled for 15 min. Analysis was performed using a 7 point BET nitrogen isotherm at relative pressures of 0.050, 0.075, 0.100, 0.125, 0.150, 0.175 and 0.200. The following instrument settings were used: absolute pressure tolerance of 5 mm Hg, relative pressure tolerance of 5 %, evacuation rate of 10 mm Hg s^{-1}, evaluation time 6 min, leak

test of 120 s, measurement intervals of 120 min, analysis bath temperature of 77.3 K and equilibration interval of 10 s.

3.1.3 Moisture sorption behaviour

Moisture sorption isotherms (n=3) were generated using a gravimetric analyser (SGA-100 gravimetric analyser, VTI Scientific Instruments, Hialeah, Florida, USA). HA samples (~50 mg) were held in open aluminium crucibles at 25 °C. Moisture sorption and desorption isotherms were generated over the relative humidity range of 5–95 % with a 10 % RH step. Equilibration criteria were 0.01 % in 10 min with a maximum equilibration time of 120 min. At each RH condition the sample weight was recorded allowing a linear regression plot of $a/[(1-a)M]$ versus a to be constructed, where M is the moisture content (in g/100 g dry solid) and a is the activity of water (which is approximated as RH/100) [53, 54]. The monolayer water coverage, M_o, can be calculated by linear regression as follows:

$$M_o = \frac{1}{(S+I)} \qquad \textit{Equation 3-1}$$

where S is the slope and I is the y-intercept.

3.1.4 Manipulation of moisture content

HA moisture content was altered by thermal treatment. A sample was also stored under ambient conditions (20 ºC / 30 % RH) for 72 h to be used as a reference. Samples of ~500 g were heated at 60, 100 or 325 ºC in a drying oven (Lindberg/Blue, SPX Thermal Solutions, Rochester, New York, USA) for at least 72 h prior to compaction. A 250 g sub-sample of the material heated to 100 ºC was re-equilibrated to ambient conditions for at least 72 h. Moisture content was determined using thermogravimetric analysis (TGA) (Q1000, TA Instruments, New Castle, DE, USA). Samples (~12 mg) were placed in standard aluminium pans and heated to 450 ºC at a rate of 10 °C min^{-1} to determine the loss on drying for each of the samples.

3.1.5 Tablet preparation and characterisation

Flat-faced tablets (n=10) of approximately 220 mg and a diameter of 8 mm were prepared on an instrumented single-punch tablet press (Korsch EK-0, Korsch AG, Berlin, Germany) at a speed of 60 tablets per min. HA tablets were produced using compression forces across the range 2–25 kN (~100–500 MPa). Tablet weight, thickness and breaking strength were determined at each compression force. Tablet weight was measured using an electronic balance (PM200, Mettler Toledo, OH, USA). Tablet breaking force and thickness were determined using a tablet hardness and thickness tester (PH-4HT hardness and thickness tester, CI Electronics, Salisbury, UK).

3.1.6 Determination of tablet tensile strength

To eliminate the undesirable effect of variations in tablet thickness on measured breaking force, tensile strength (n=10) was calculated using the equation [55]:

$$\sigma = \frac{2BA}{\pi Dt} \qquad \textit{Equation 3-2}$$

where σ is the tensile strength (MPa), B is the tablet breaking strength (kp), A is gravitational acceleration (9.81 m s^{-2}), D is the diameter (m) and t is the thickness (m) of the compact.

3.1.7 Determination of tablet porosity

Tablet porosity (n=10) was calculated by the following equation:

$$\varepsilon = 1 - \frac{\rho_c}{\rho_t} \qquad \textit{Equation 3-3}$$

where ρ_c is the density of the tablet, which was calculated from the weight and geometric volume of the tablet, and ρ_t is the true density of the sample.

3.1.8 Walker analysis

The Walker equation [35] was used derive the compressibility coefficient using data generated over the 37–133 MPa compaction pressure range:

$$logP = -L \times \frac{V`}{V_o} + C \qquad \textit{Equation 3-4}$$

where P is the compaction pressure, $V`$ is the tablet volume, $V_o$ is the volume at zero porosity, $L$ is the pressing modulus and $C$ is a constant. Calculation of $V`$ was performed using the out-of-die method [56]. Expressed in terms of the relative volume, $V_R = V`/V_o$ = 1/Density, as the dependent variable then Equation 3-5 results, where for practical reasons the relative volume is multiplied by 100:

$$100\, V_R = -w \times logP + C \qquad \textit{Equation 3-5}$$

The compressibility coefficient, w, expresses the percentage change in volume when the pressure is increased by a factor of 10 and is considered a measure of the irreversible compressibility of the compact [56].

3.1.9 Heckel analysis

The Heckel equation [57, 58] was used to determine the mean yield pressure using data generated over the 133–523 MPa compaction pressure range. The out-of-die method was used in order to eliminate the effects of elastic recovery on the calculated mean yield pressure [6, 59, 60].

$$ln\left(\frac{1}{\varepsilon}\right) = K\,P + E \qquad \textit{Equation 3-6}$$

where P is the compaction pressure (MPa), E is a constant (no units) and K is the slope of the linear part of the curve and represents the material-dependent constant. The reciprocal of K is the mean yield pressure, P_y (MPa), which is considered to be the pressure at which yielding starts to occur during compaction [57, 58].

3.1.10 Determination of elastic behaviour

Flat-faced compacts (n=3) of approximately 300 mg and a diameter of 10 mm were prepared using an Instron Universal Testing System with a 50 kN load cell (Model 5569, Instron Corporation, Norwood, Massachusetts). Tablets were compressed and

decompressed at 50 mm min^{-1} up to a specified compression load ranging from 2.5–20 kN (~30–250 MPa). The punches and die were lubricated with a 5 % *w/v* magnesium stearate suspension in methanol and these were allowed to dry before each set of tablets were prepared. Tablet dimensions were determined 24 h after ejection using a dial caliper (Mitutoyo Corporation, Mizonokuchi, Japan). All compacts were stored at 20–22 ºC and 22–33 % RH. Total elastic recovery (TER) was calculated using the following equation [61]:

$$TER = \left(\frac{t_2 - t_1}{t_1}\right) \times 100 \qquad \textit{Equation 3-7}$$

where t_1 is the minimum thickness (mm) of the powder bed achieved during the compression event and t_2 is the tablet thickness (mm) 24 h after ejection.

The Young's modulus of elasticity (n=3) was calculated from the gradient of the stress-strain relationship during tablet compaction using the following equation [62]:

$$YM = \left(\frac{Stress}{Strain}\right) = \frac{\left(\frac{F}{A}\right)}{\left(\frac{\Delta H}{Ho}\right)} \qquad \textit{Equation 3-8}$$

where YM is the Young's modulus (GPa), F is the force (kN) applied during tableting, A is the cross-sectional area (mm^2) of the punch tip, H_0 is the height (mm) of the compact at zero force, and ΔH is the change in height (mm) due to applied force. Young's modulus was calculated at a constant tablet porosity of 0.1 [63, 64].

3.1.11 Statistical analysis

Statistical analysis to determine whether significant differences existed between sample means was performed as described in Section 2.1.2.8.

3.2 Results and Discussion

3.2.1 Micromeritic characterisation

SEM micrographs of HA (Figure 3-1) show that the particles appear irregular in shape and have a wide size range. Multiple smaller particles are adhered to larger irregularly shaped particles. Many of the smaller particles have an irregular surface but crystalline appearance.

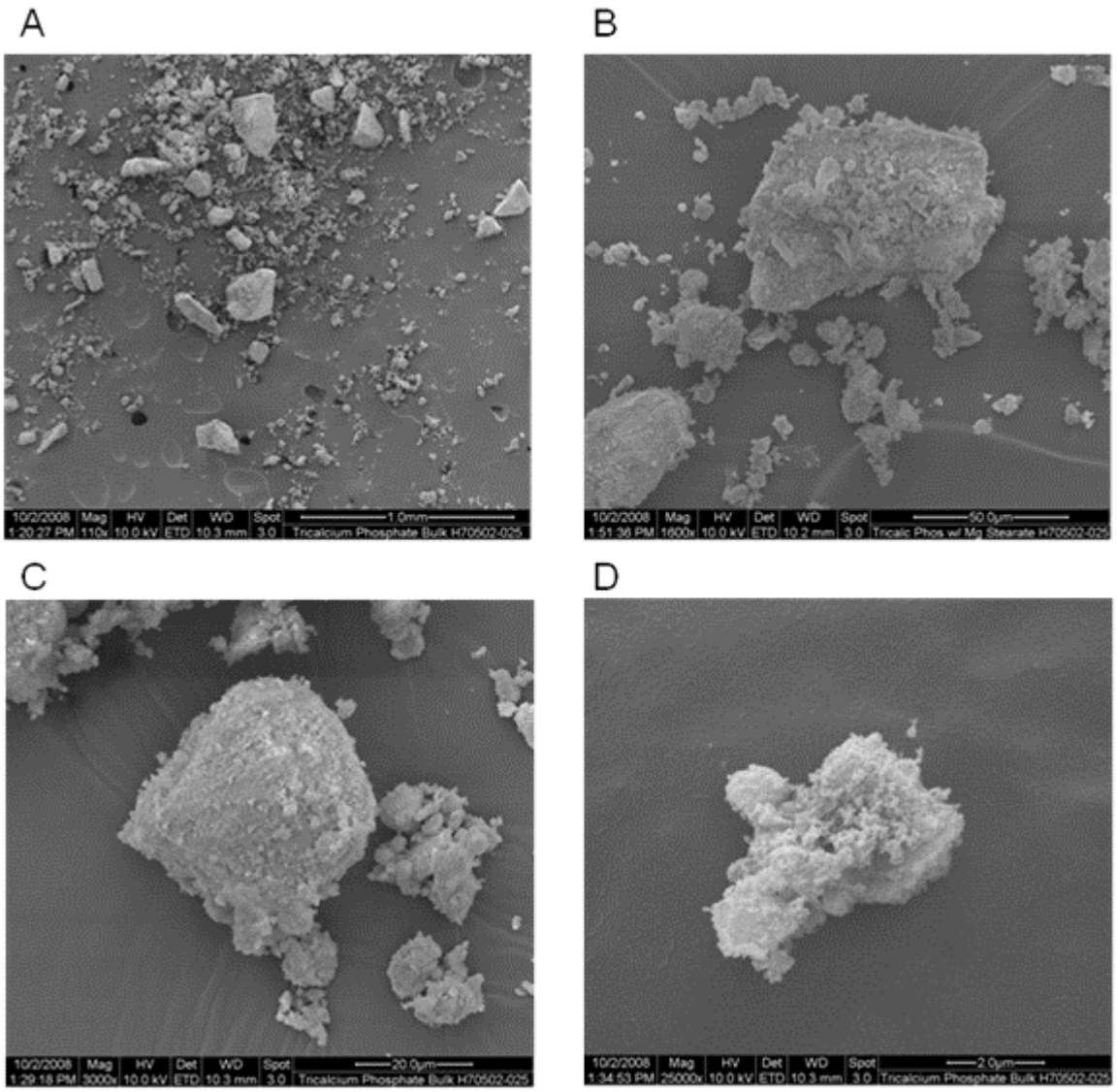

Figure 3-1. Scanning electron micrograph of hydroxyapatite. A – 110 x magnification, B – 1600 x magnification, C – 3000 x magnification, D – 25000 x magnification.

Other micromeritic properties are given in Table 3-1. The true, bulk and tapped density results show HA to be markedly more dense than most other commonly used pharmaceutical materials. Example true densities of other pharmaceutical materials are stearic acid 0.99 g cm^{-3}, sorbitol 1.48 g cm^{-3}, spray dried lactose 1.55 g cm^{-3} and microcrystalline cellulose PH101 1.56 g cm^{-3} [65]. The particle size distribution for HA is relatively wide but reproducible for the samples tested. Specific surface area results show the sample to have high surface area owing to the small irregular particles adhered to the surfaces of the larger particles.

Table 3-1. Micromeritic properties of hydroxyapatite. Mean ± SD.

Property		Result
True density (n=20) [g cm^{-3}]		2.906 ± 0.0008
Particle size (n=3) [μm]	d_{10}	35 ± 3.6
	d_{50}	275 ± 12.5
	d_{90}	530 ± 23.6
Specific surface area (n=3) [m^2/g]		59.2 ± 0.46
Bulk density (n=4) [g cm^{-3}]		0.78 ± 0.005
Tapped density (n=4) [g cm^{-3}]		1.13 ± 0.004

3.2.2 Moisture characterisation

Monolayer water coverage was calculated by two methods. Firstly, using the measured specific surface area of the HA sample [66], and secondly using moisture sorption isotherm data (Figure 3-2) fitted to the modified BET equation [53, 54]. The first approach gave a monolayer water coverage of 1.54 % *w/w* using a specific surface area of 59.2 m^2/g (Table 3-1), the mass of one water molecule (2.99 x 10^{-23} g) and the cross-sectional area of a water molecule, which must take into account the packing density between the water molecules and the hydroxyapatite surface. The cross sectional area for the adsorption of a water molecule into the surface of HA has previously been reported as 0.115 nm^2 [67]. The second method using the modified BET equation gave a monolayer water coverage of 1.06 % *w/w* (Figure 3-3).

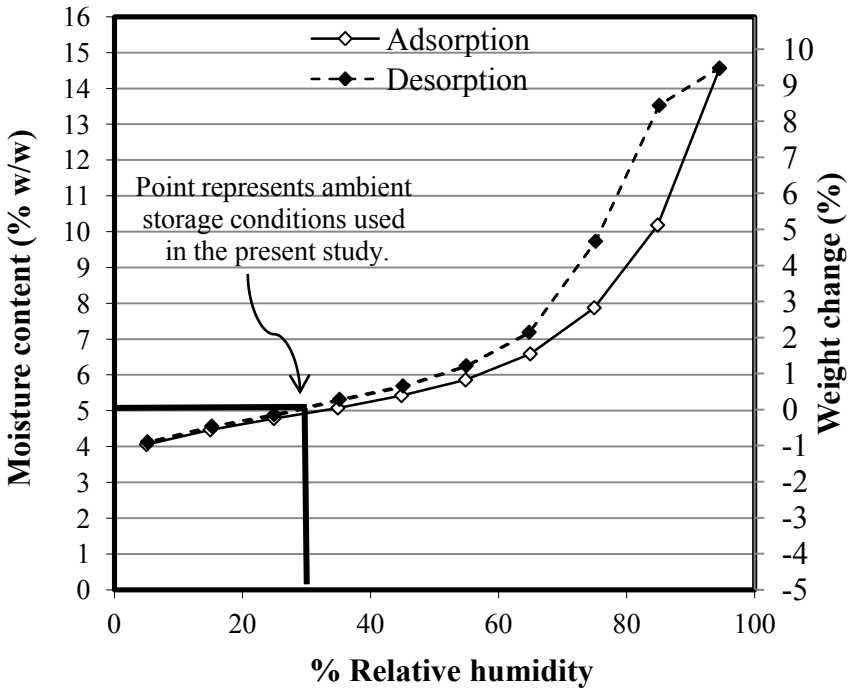

Figure 3-2. Moisture sorption isotherm for hydroxyapatite. Left y-axis presents total moisture content as determined by TGA at 450 °C and right y-axis represents weight change determined during moisture sorption analysis.

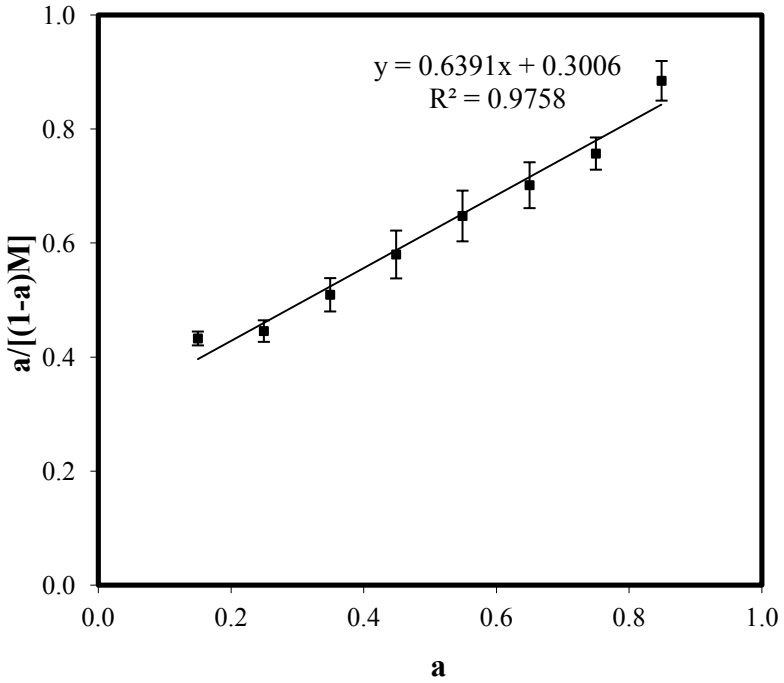

Figure 3-3. Modified BET plot of moisture sorption data for hydroxyapatite. Error bars represent 1 SD, n=3.

The monolayer coverage calculated by the modified BET method is lower than that calculated by the specific surface area approach. This is converse to findings reported for microcrystalline cellulose [6] where moisture penetrates the relatively porous particles, covering the surfaces of microfibrils and concentrates in amorphous regions, therefore the surface area approach gives a falsely low measure of monolayer coverage. In contrast HA has a less porous, crystalline structure with tightly bound moisture, which is only removed at elevated temperatures [67]. Therefore, at the 25 ˚C / 2 % RH conditions used for determination of the 'dry' state prior to generating the moisture sorption isotherms, it is hypothesised that some active sites are occupied with water molecules and are not available for further moisture sorption. Accordingly the modified BET approach is likely to underestimate the true monolayer coverage and the specific surface area approach might be anticipated to provide a more accurate determination.

The moisture content of HA was determined by TGA over the temperature range 25–450 °C. The total mass loss from HA stored at 20 °C / 30 % RH conditions was 5.26 % ± 0.04 % (Table 3-2).

Table 3-2. Moisture data for hydroxyapatite samples treated under different temperature conditions. Mean ± SD (n=2).

Preparation condition	Moisture content [%] (SD)	Number of water layers[a]
20 °C / 30 % RH	5.26 ± 0.04	2.53
100 °C re-equilibrated at 20 °C / 30 % RH	4.97 ± 0.03	2.39
60 °C	4.56 ± 0.07	2.19
100 °C	4.02 ± 0.01	1.93
325 °C	2.12 ± 0.01	1.38

[a] The number of water layers was calculated by dividing the moisture content for the sample by the monolayer water coverage of 1.54 % *w/w* obtained from the specific surface area method. The calculation assumes layers of water molecules pack with a face centred cubic structure [68] with a packing efficiency of 0.74 [69].

The TGA thermogram (Figure 3-4) shows three distinct stages of weight loss which can be explained by the loss of loosely bound, physisorbed and chemisorbed moisture [67] respectively. Approximately 0.70 % of loosely bound mono- and multi-layer water is lost in the temperature range 20–60 °C, approximately 0.54 % of physisorbed moisture

is lost between 60–100 °C, and approximately 1.90 % of chemisorbed moisture is lost between 100–325 °C. A moisture content of approximately 2.12 % remains in the samples when thermally treated at 325 °C.

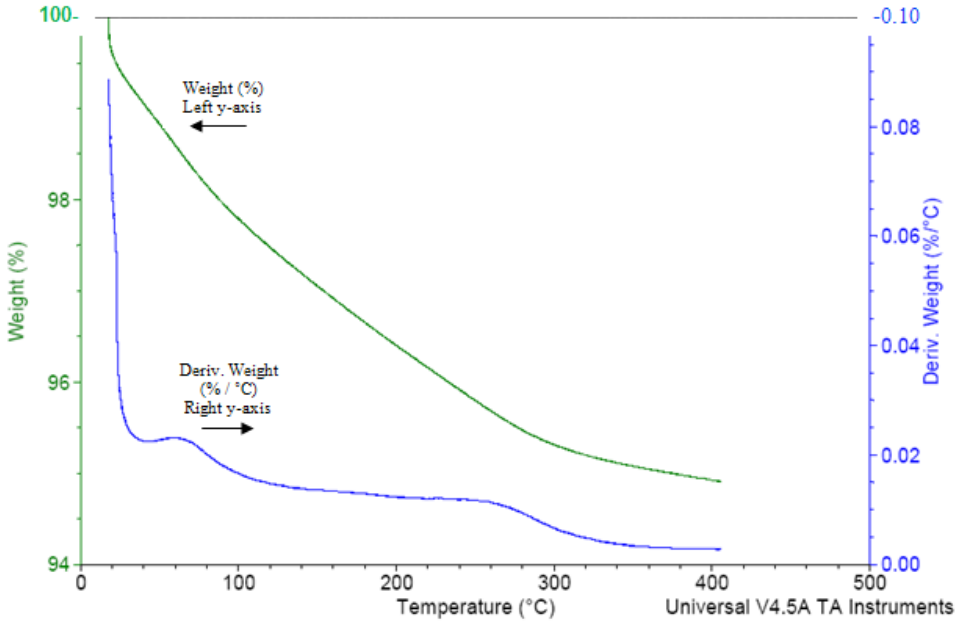

Figure 3-4. Example TGA thermogram for hydroxyapatite.

At ambient conditions the surface of HA particles is totally covered with water [70]. Rootare [67] reported that adsorbed mono- and multi-layer moisture were easily removed by lowering the relative vapor pressure of the water at the surface, i.e. decreasing RH. However, a layer of chemisorbed water remains on the HA surface which could only be removed when the sample was heated to ~300 °C and temperatures greater than 1000 °C were required to completely remove all chemisorbed water from the surface of HA, which includes water associated with the surface hydroxyl groups. For the present study a maximum drying temperature of 325 °C was used. Rootare [71] demonstrated that HA pore volume, porosity, bulk density, true density, surface area and pore diameter were unaffected at temperatures below 400 °C. However, above 400 °C surface area was reported to be reduced slightly and pore diameter increased, and above 600 °C significant changes in all properties were observed. Pontier [15] reported that HA heated at 720 °C for 1 h began to sinter and also displayed reduced compaction properties due to a marked decrease in specific surface area and an increase in

pycnometric density. As a result, the evaluation of HA with moisture content significantly below that achieved in this study (2.12 % *w/w* or 1.38 monolayers) is not possible by either relative humidity change or thermal treatment.

3.2.3 Powder compaction properties

Compaction of powders can be systematically evaluated based on tabletability (tensile strength as a function of compaction pressure), compressibility (porosity as a function compaction pressure) and compactibility (tensile strength as a function of porosity) [6]. This terminology was first defined by Joiris *et al* [72] for the compaction of orthorhombic paracetamol and has been used consistently in the literature since 1998 for describing the simultaneous relationship between compaction pressure, tensile strength and porosity [31, 60, 73-76].

3.2.3.1 Tabletability

Tabletability (the capacity of a powder material to be transformed into a tablet of specified strength under the effect of compaction pressure) is often found to be strain rate dependent for materials that undergo plastic deformation [7, 77-80] and hence it is considered an indirect relationship. However, it still provides a useful insight into the compaction process and the mechanical properties of a material [75] and is of practical importance in formulation and process development [76]. The tabletability of HA was found to be affected by increasing moisture content (Figure 3-5).

Under identical compaction conditions, the highest tensile strength for tablets at 2.12 % moisture content was more than two-fold of the highest tensile strength for tablets at 5.26 % moisture content. When compaction pressure was below approximately 200 MPa the effect of moisture on tabletability was minimal. At this lower compaction pressure volume reduction occurs predominantly by particle rearrangement, rather than plastic deformation, which is largely independent of moisture content. At compaction pressures between 200–400 MPa an increase in moisture content causes a decrease in tensile strength.

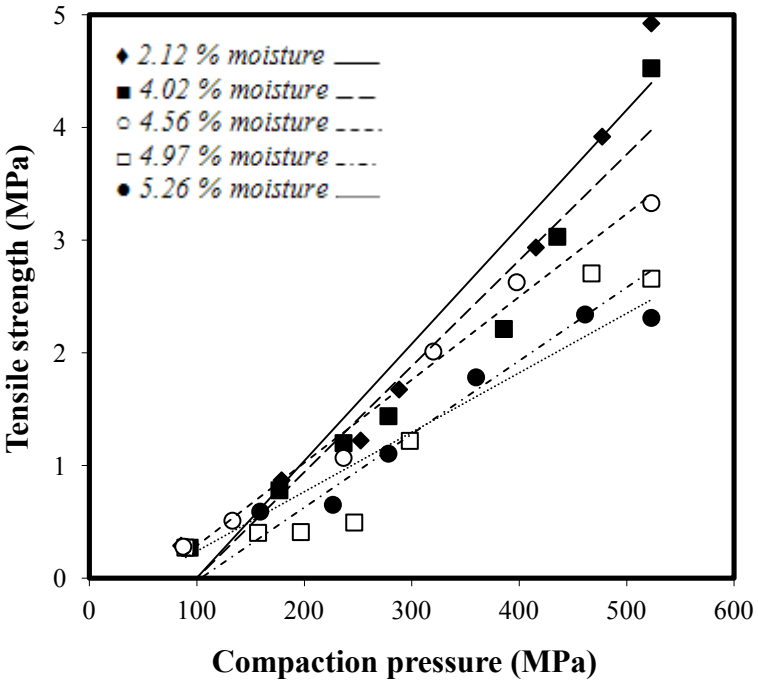

Figure 3-5. Tensile strength as a function of compaction pressure for hydroxyapatite tablets of different moisture content, n=10. R^2 >0.95 in all cases.

3.2.3.2 Compressibility

Compressibility is the ability of a material to undergo a reduction in volume as a result of an applied pressure [72] and since the compressibility of powders depends on moisture content, the same pressure may not result in the same tablet porosity. Porosity relates to the pore structure of a tablet and is an important factor in liquid penetration, and by consequence tablet disintegration and dissolution. For a given powder sample, a decreased tablet porosity results in an increased interparticulate bonding area and increased tensile strength. Compressibility plots of HA containing different amounts of moisture are presented in Figure 3-6. At a common compaction pressure the tablet porosity is reduced as moisture content is increased indicating that HA with greater moisture content is more compressible.

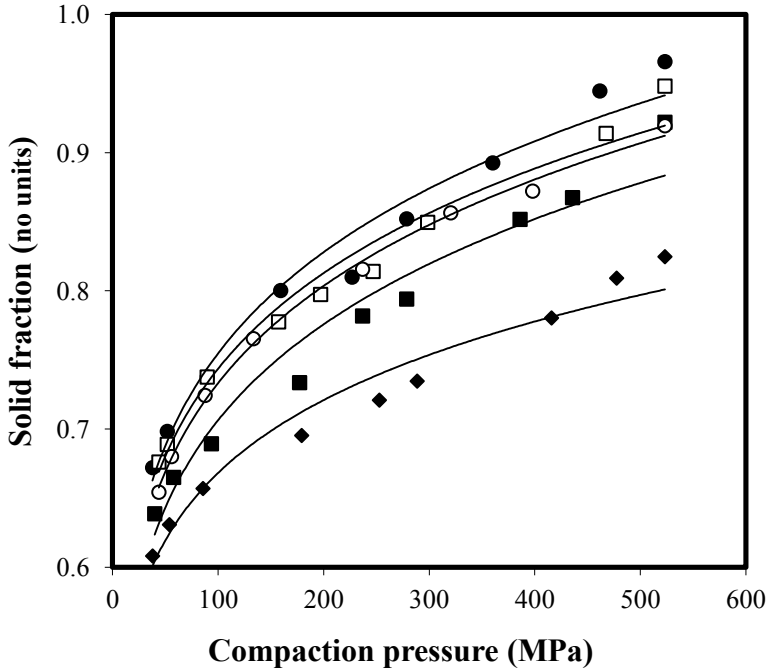

Figure 3-6. Tablet solid fraction as a function of compaction pressure for hydroxyapatite tablets of different moisture content, n=10. R^2 >0.95 in all cases. ♦ 2.12 % moisture, ■ 4.02 % moisture, ○ 4.56 % moisture, □ 4.97 % moisture, ● 5.26 % moisture.

The Walker equation [35] and Heckel equation [57, 58] have both been used to derive material compressibility constants. The Walker equation considers the course of volume reduction as a result of applied compaction pressure and is based on the assumption that the rate of change in volume is proportional to the applied pressure [56]. The compressibility coefficient, *w*, expresses the percentage change in volume which occurs when the pressure is increased by a factor of 10 and is considered a measure of the irreversible compressibility of the compact, with the greater the value of *w* the higher the compressibility of the material. The Heckel equation was derived assuming that particles undergo plastic deformation under pressure, whereby the volume reduction of the powder is assumed to obey first-order kinetics in which the pores constitute the disappearing "reactant" [57, 58]. During compaction, at low pressures, densification occurs through particle re-arrangement and slippage, resulting in a curved region in the plot. The linear portion of the plot that follows reflects densification through plastic deformation. The extent of density change is suggested to be proportional to the amount of permanent plastic deformation.

A thorough evaluation of the impact of HA moisture content on compressibility has not previously been reported. Previous studies [9, 49-51] have applied the Heckel equation to HA in order to characterise the compaction behaviour, however in each case the storage conditions for the HA prior to compaction were not reported and the mean yield pressure was not calculated from the Heckel plot over the entire compaction pressure range. Instead, the studies investigated the observed non-linearity of the Heckel plot. Carstensen and Hou [49] reported that the Heckel plot for HA is atypically non-linear when using the crystallographic density for HA of 3.10 g cm^{-3} as determined by helium pycnometry. It was hypothesised that part of the HA internal pore structure is occluded and therefore does not participate during the compaction process. Liquid pycnometry with methanol and water showed that HA had an average density of 1.92 g cm^{-3} and when this value was used the Heckel plot became linear [49]. When the same HA sample was placed in an ultrasonic bath the sample disintegrated, the supernatant became turbid and air was liberated. The measured density for this sonicated sample was 3.10 g cm^{-3} supporting the presence of occluded pores. Their presence was further investigated [50] by performing mercury porosimetry on HA tablets (500 mg weight, flat faced, 10 mm diameter) compressed over the force range 4.5–35.6 kN (57.3–453.27 MPa). The pore volume in the diameter range 0.5–2 μm was linearly reduced with increasing compaction pressure, however pores below 0.5 μm were not compressible over the conventional pressure range used in tablet compaction and should therefore not be considered part of the Heckel pore space. Consequently a true density, ρ_t, of 1.92 g cm^{-3} was used when calculating tablet porosity data [49-51] in the present study.

The compressibility coefficient and mean yield pressure were calculated as the gradient of the Walker plot (Figure 3-7) and the reciprocal of the gradient of the Heckel plot (Figure 3-8) respectively. The results are presented in Table 3-3.

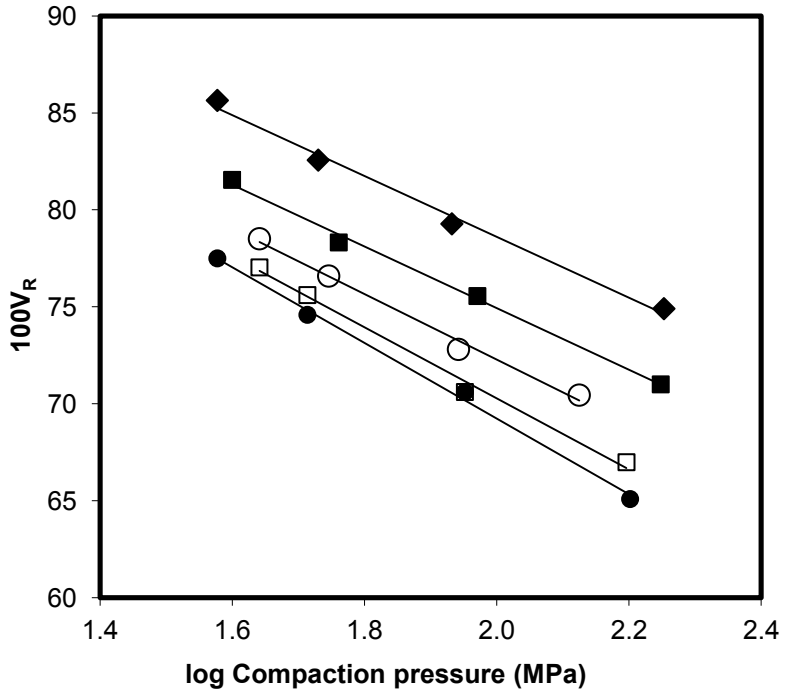

Figure 3-7. Walker plot (where V_R is the relative volume of the tablet compared to the tablet volume at zero porosity) for hydroxyapatite tablets of different moisture content. Walker equation applied to data in the compaction pressure range 37–133 MPa, n=10. R^2 >0.99 in all cases. ♦ 2.12 % moisture, ■ 4.02 % moisture, ○ 4.56 % moisture, □ 4.97 % moisture, ● 5.26 % moisture.

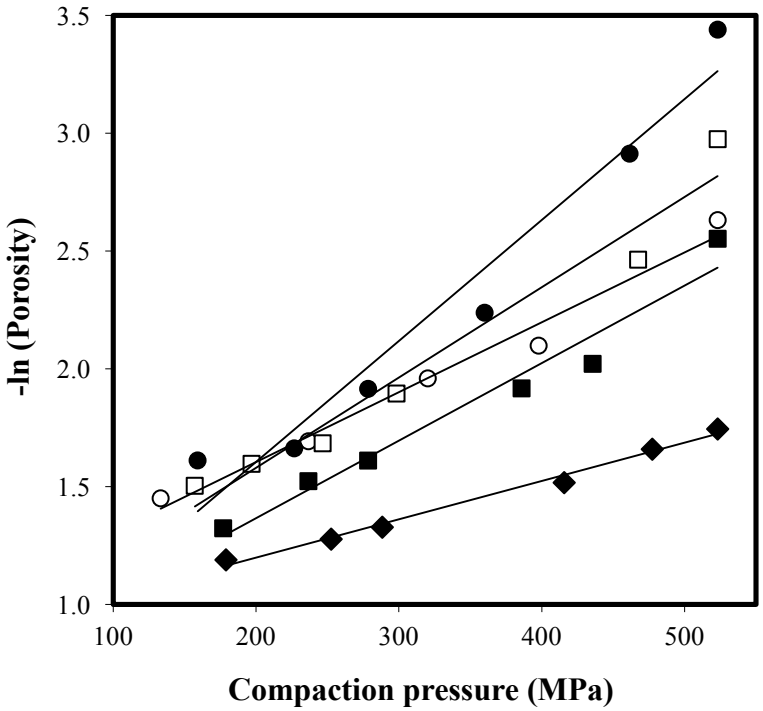

Figure 3-8. Heckel plot for hydroxyapatite tablets of different moisture content. Heckel equation applied to data in the compaction pressure range 133–523 MPa, n=10. R^2 >0.95 in all cases. ♦ 2.12 % moisture, ■ 4.02 % moisture, ○ 4.56 % moisture, □ 4.97 % moisture, ● 5.26 % moisture.

Table 3-3. Compressibility equation fit parameters for hydroxyapatite tablets of different moisture contents.

	Compressibility coefficient[a]		Mean yield pressure[b]	
Moisture content [%]	w [%]	R^2 [-]	P_y [MPa]	R^2 [-]
2.12	15.7	0.9926	625	0.9902
4.02	15.9	0.9957	303	0.9629
4.56	16.9	0.9922	333	0.9805
4.97	18.3	0.9932	263	0.9629
5.26	19.5	0.9967	196	0.9523

[a] Determined over the compaction pressure range 37–133 MPa.
[b] Determined over the compaction pressure range 133–523 MPa.

The mean yield pressure decreased and the compressibility coefficient increased as moisture content increased from 2.12 to 5.26 % supporting the observation that volume reduction of HA is facilitated by moisture. This effect has been widely reported in both polymeric materials, where the primary mechanism for increased plasticity is a decrease in glass transition temperature, [5, 6, 25, 26, 28-30, 81-84] and crystalline materials, where the presence of water is thought to weaken the strength of bonds between adjacent crystalline planes allowing material to slide under pressure [4, 31, 33, 34, 85].

While the Heckel equation provides a means for comparison of material compressibility its usefulness in generating a material constant has been criticised. It has been reported that the values obtained for mean yield pressures using the Heckel equation are dependent upon the dimensions of the punches and dies [86], the compaction pressure [62, 87], the strain rate [77, 88], the material true density value used [89] and the material particle size [7, 59]. Provided experimental conditions are maintained constant, as was the case in the present study, the derived value is useful for evaluating the directional effect of variables, however an absolute comparison of such values to other materials compressed under different conditions is not advised [87].

The Walker equation was introduced to the pharmaceutical research field in 1956 [90] for the investigation of magnesium carbonate compression. The compressibility coefficient, w, derived from the Walker equation has been shown to provide a more

reproducible and discriminatory compressibility constant [56, 87, 91] than the Heckel equation and therefore comparison of the compressibility coefficient between systems is possible. The compressibility coefficient results obtained for HA in the present study ranged from 15.7–19.5 as the moisture content increased over the range 2.12–5.26 %. When compared to values reported for a range of commonly used pharmaceutical materials (Table 3-4) the compressibility of HA is seen to be low, however can be enhanced slightly by increasing the moisture content.

Table 3-4. Summary of compressibility coefficient values for a range of pharmaceutical materials. [a] Reflects that data were not reported in the reference.

Material	Compressibility coefficient, *w*	Pressure range (MPa)	R^2	Ref.
Microcrystalline cellulose (Avicel® PH 102)	128.5	5–125	[a]	[87]
	125.0	5–100	[a]	[87]
	84	32–127	0.977	[92]
Microcrystalline cellulose (Avicel® PH 101)	114.6	5–100	[a]	[87]
	77	32–127	0.985	[92]
Microcrystalline cellulose (Avicel® PH 301)	96.8	5–100	[a]	[87]
	77	32–127	0.982	[92]
Microcrystalline cellulose (Avicel® PH 200)	77	32–127	0.957	[92]
Pre-gelatinised starch	64	32–127	0.979	[92]
Dicalcium phosphate dihydrate (Emcompress®)	58.5	5–105	[a]	[87]
	56.6	5–100	[a]	
Sorbitol	50.5	5–100	[a]	[87]
	48.7	5–105	[a]	
Corn starch	44.7	[a]	0.990	[93]
Sodium chloride	44.2	5–105	[a]	[87]
	43.5	5–100	[a]	
Lactose monohydrate	42.5	5–100	[a]	[87]
	26	32–255	0.985	[92]
	23.2	[a]	0.998	[93]
	16.1	[a]	0.989	[93]
Anhydrous lactose	31	32–255	0.998	[92]
Spray dried mannitol	30	32–255	0.995	[92]
Paracetamol 700-1000 µm	29.4	5–125	0.989	[91]
Paracetamol (as-received)	28.5	5–100	[a]	[87]
Paracetamol (as-received)	27.5	5–105	[a]	[87]
Paracetamol 500-650 µm	28.4	5–125	0.989	[91]
Paracetamol 300-450 µm	25.1	5–125	0.989	[91]
Paracetamol 150-250 µm	24.2	5–125	0.989	[91]
Isomalt (GalenIQ®)	29.1	[a]	0.997	[93]
α-indomethacin	26.3	0–104	0.990	[94]
Powdered mannitol	24	32–255	0.986	[92]
Dicalcium phosphate anhydrous (Bekapress®)	19.8	[a]	0.999	[93]
γ-indomethacin	19.1	0–104	0.990	[94]

3.2.3.3 Compactibility

Compactibility refers to the ability of a material to produce tablets with sufficient strength under the effect of densification [72]. When considering tablet tensile strength it is important to compare tablets at the same porosity in order to represent the same number of interparticulate contacts, and therefore comparable bonding contributions [74, 95]. This relationship has been shown to be independent of compression speed [75].

Compactibility was quantified using the Ryshkewitch-Duckworth equation [96, 97]:

$$\sigma_T = \sigma_{T_0} e^{-k\varepsilon} \qquad \textit{Equation 3-9}$$

where ε is the porosity of the compacts (no units), σ_{T_0} is the tensile strength of the sample at zero porosity (MPa), and k is a constant representing the bonding capacity (no units). A higher value of k corresponds to stronger bonding of primary particles [98, 99]. It has been demonstrated that the Ryshkewitch-Duckworth equation can usefully be employed to represent the variation of tensile strength with the porosity for a wide range of porous materials [75, 98, 100-102].

A common batch of HA was used in this study therefore the physical properties of each powder sample can be considered identical. The cross-sectional area of tablets of identical porosity is therefore expected to be similar for HA containing different amounts of moisture. The tablet tensile strength at a common porosity can therefore be used to evaluate the effect of moisture on bond strength. Compactibility plots of HA containing different amounts of moisture are presented in Figure 3-9.

At comparable tablet porosities the tablet tensile strength was reduced as moisture content increased. The tensile strength and porosity data for HA tablets with different moisture content were fitted according to Equation 3-9. By means of regression analysis, values of σ_{T_0} and k were obtained with correlation coefficients being greater than 0.95 in all cases (Table 3-5).

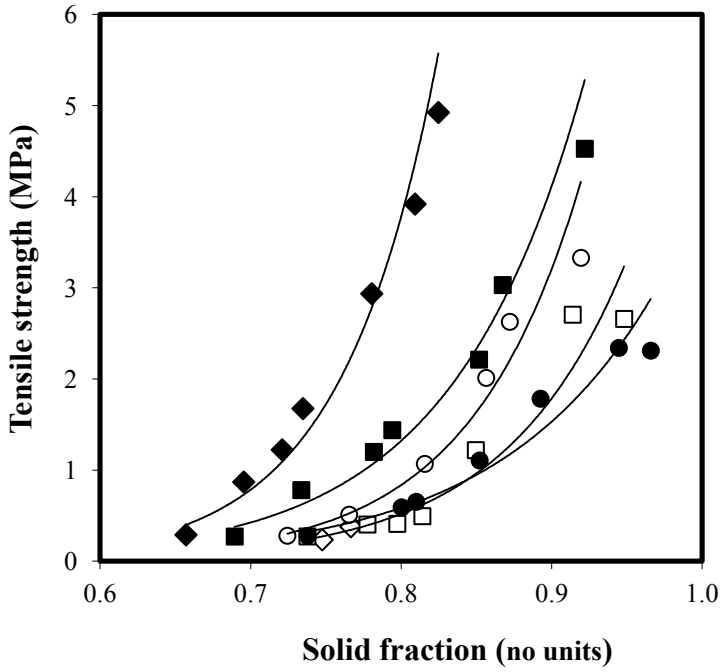

Figure 3-9. Tensile strength as a function of solid fraction for hydroxyapatite tablets of different moisture content;, n=10. R^2 >0.95 in all cases. ♦ 2.12 % moisture, ■ 4.02 % moisture, ○ 4.56 % moisture, □ 4.97 % moisture, ● 5.26 % moisture.

Table 3-5. Ryshkewitch-Duckworth equation fit parameters for hydroxyapatite tablets of different moisture contents.

Moisture content [%]	σ_{T_0} [MPa]	k [-]	R^2 [-]
2.12	67.09	15.72	0.9616
4.02	8.60	11.36	0.9566
4.56	13.82	13.45	0.9785
4.97	6.89	12.34	0.9515
5.26	4.41	9.60	0.9642

An increase in moisture generally results in a decrease in σ_{T_0} and k suggesting that moisture acts to reduce the strength of interparticulate bonds between HA particles. Although the mean yield pressure is also reduced and the compressibility coefficient is increased, the effect appears to be outweighed by the reduction in interparticulate bond strength. The bonding capacity obtained for HA in the present study decreased from 15.72–9.60 as the moisture content increased over the range 2.12–5.26 %. When compared to values reported for other pharmaceutical materials (Table 3-6) the

compactibility of HA is seen to be high. An increase in moisture content reduces the bonding capacity, however the relative bonding capacity remains high compared to the other materials shown.

Table 3-6. Summary of Ryshkewitch-Duckworth equation fit values for a range of pharmaceutical materials. [a] Reflects that data were not reported in the reference.

Material	k [-]	σ_{T_0} [MPa]	R^2	Ref.
Lactose monohydrate (Granulac® 140)	20.15	12.89	[a]	[103]
Poly(DL-lactic acid) compressed at 300 mm s^{-1}	10.31	10.3	0.994	[98]
Poly(DL-lactic acid) compressed at 30 mm s^{-1}	9.45	7.7	0.991	
Poly(DL-lactic acid) compressed at 3 mm s^{-1}	8.00	6.3	0.999	
Poly(DL-lactic acid) compressed at 0.033 mm s^{-1}	7.26	5.8	0.997	
Silicified microcrystalline cellulose (Prosolv®)	7.72	37.14	[a]	[103]
Silicified microcrystalline cellulose 90 (Prosolv® 90)	7.14	24.19	[a]	[103]
Amylodextrin stored at 7 % RH	7.33	34.96	0.965	[25]
Amylodextrin stored at 11.4 % RH	6.33	22.40	0.993	
Amylodextrin stored at 15.0 % RH	4.61	11.2	0.889	
Amylodextrin stored at 23.4 % RH	5.43	3.28	0.865	
Aspartame	6.31	5.2	0.953	[104]
Microcrystalline cellulose (Vivapur® 102)	5.95	21.11	[a]	[103]
γ-sorbitol <25 µm	5.20	9.1	[a]	[99]
γ-sorbitol 53 - 75 µm	6.94	8.6	[a]	
γ-sorbitol 75 - 106 µm	10.87	9.5	[a]	
γ-sorbitol 106 - 149 µm	7.74	12.2	[a]	
γ-sorbitol 212 - 300 µm	8.61	11.7	[a]	
γ-sorbitol 600 - 850 µm	8.95	12.0	[a]	

3.2.3.4 Elastic behaviour

An increase in moisture content caused an increase in the extent of elastic recovery ($p < 0.10$ Wilcoxon) and a decrease in Young's modulus of elasticity ($p < 0.10$ Wilcoxon) (Table 3-7). In parallel tablet tensile strength was decreased (Figure 3-6) with increasing moisture content; the effect being larger at increased compaction pressure.

Table 3-7. Elastic recovery and Young's modulus of elasticity of hydroxyapatite tablets with different moisture contents. Mean ± SD (n=3).

Moisture content [%]	Elastic Recovery [%] [a]	Young's Modulus [GPa] [b]
2.12	29.79 ± 1.09	0.89 ± 0.10
4.02	31.24 ± 0.82	0.89 ± 0.10
4.56	37.65 ± 0.49	0.73 ± 0.04
5.26	37.53 ± 0.40	0.63 ± 0.02

[a] At compaction pressure of 254.65 MPa. [b] At tablet solid fraction of 0.9.

During the compaction process a plateau region will exist where increased compaction pressure results in no further decrease in tablet porosity, and the energy supplied by compaction pressure above the plateau level will be stored as elastic energy. During unloading elastic recovery of the particles takes place resulting in breakage of bonds that were formed during compression [17]. It is also commonly stated that as compaction pressure and/or moisture content increase greater quantities of moisture can be forced out of the internal structure of the particles onto the surface. Here the moisture would act as a lubricant facilitating the movement of crystal planes within particles, and slipping of particles past each other and the die wall, contributing to increased elastic recovery and bond breakage.

The Young's modulus of elasticity is the ratio of the stress to the relative elongation (strain) and is a fundamental property of the material. It is hypothesised that at low moisture content a greater extent of hydrogen bonding can occur which increases particle attraction and bonding. At higher moisture content hydrogen bonding is compromised resulting in the lower Young's Modulus [47].

3.2.3.5 Relationship between bonding area and bond strength

As HA moisture content increased so the mean yield pressure decreased and compressibility coefficient increased. The increase in compressibility is seen in Figure 3-6 as lower tablet porosity at constant compaction pressure, and represents an increase in bonding area. If all other factors were constant this increased bonding area would represent a greater number of bonds per cross-sectional area and would be manifested as an increase in tensile strength. However, an increase in moisture affects also both the

strength of interparticulate bonds and the extent of the elastic behaviour of the compact. In the case of HA this effect on interparticulate bonds is negative, with the effect being more pronounced as moisture content increases. Likewise the contribution of elastic recovery is least at reduced moisture content due to minimal surface moisture being available for particle lubrication, however as moisture content increased the negative effect of elastic recovery contributed to the decrease in tablet tensile strength. As HA moisture content increases from 2.12 % to 5.26 % the tensile strength is steadily reduced when compared at both constant compaction pressure and constant tablet porosity. This suggests that the increase in bonding area as a result of increased moisture does not contribute significantly to tensile strength and that bond strength is dominant across the moisture content studied.

It is recognised that multiple material specific attributes such as deformation mechanism, solubility, surface chemistry, pore structure and surface area contribute to the relationship between moisture content and tablet tensile strength. In general the effect of moisture on tablet tensile strength is driven by two mechanisms; an increase in bonding area due to a decrease in mean yield pressure and increase in the compressibility coefficient, and a positive or negative effect on interparticulate bond strength. The relative balance of these effects yields a net increase or decrease in tablet tensile strength that is material dependent.

3.3 Conclusions

HA tablet tensile strength was shown to be predominantly determined by the strength of the interparticulate interactions, and that an increase in moisture content results in decreased tablet tensile strength. Moisture acted as a plasticiser during the compaction process, facilitating tablet porosity reduction at constant compaction pressure. However, an increase in moisture content reduced the tablet tensile strength at constant tablet porosity despite the increased bonding area. This was likely caused by the deleterious effect of adsorbed moisture on intermolecular bond strength and the increase in elastic behaviour due to the lubricating effects of moisture. The moisture sensitivity of a given material must therefore simultaneously consider the effect of adsorbed moisture on plasticity (compressibility) and interparticulate interactions (compactibility). The interplay between these factors will determine the effect of moisture on tablet tensile strength. The data presented clearly highlights the importance of controlling moisture content in hydroxyapatite when performing mechanical strength analyses. This knowledge is used in the present thesis when assessing the strength of both granule and tablet samples by ensuring that all samples are stored at the same temperature and humidity conditions before analysis.

3.4 References

[1] Carstensen, J.T., Effect of moisture on the stability of solid dosage forms, Drug Dev. Ind. Pharm., 14 (1988) 1927-1969.

[2] Shukla, A.J., Price, J.C., Effect of moisture content on compression properties of two dextrose-based directly compressible diluents, Pharm. Res., 8 (1991) 336-340.

[3] Coelho, M.C., Harnby, N., Moisture bonding in powders, Powder Technology, 20 (1978) 201-205.

[4] Nokhodchi, A., The effect of moisture content on the energies involved in the compaction of ibuprofen, Int. J. Pharm., 120 (1995) 13-20.

[5] Amidon, G.E., Houghton, M.E., The effect of moisture on the mechanical properties of microcrystalline cellulose, Pharm. Res., 12 (1995) 923-929.

[6] Sun, C.C., Mechanism of moisture induced variations in true density and compaction properties of microcrystalline cellulose, Int. J. Pharm., 346 (2008) 93-101.

[7] Roberts, R.J., Rowe, R.C., The effect of the relationship between punch velocity and particle size on the compaction behaviour of materials with varying deformation mechanisms, J. Pharm. Pharmacol., 38 (1986) 567-571.

[8] Patel, N.K., Patel, B.R., Plakogiannis, F.M., Reier, G.E., An evaluation of tricalcium phosphate excipients particularly using instrumented rotary and single station tablet presses, Drug Dev. Ind. Pharm., 13 (1987) 2693-2718.

[9] Carstensen, J.T., Ertell, K., Physical and chemical properties of calcium phosphates for solid state pharmaceutical formulations, Drug Dev. Ind. Pharm., 16 (1990) 1121-1133.

[10] Schmidt, P.C., Herzog, R., Calcium phosphates in pharmaceutical tableting, Pharmacy World & Science, 15 (1993) 105-115.

[11] Milev, A., Kannangara, G.S.K., Ben-Nissan, B., Morphological stability of hydroxyapatite precursor, Materials Letters, 57 (2003) 1960-1965.

[12] Teshima, K., Lee, S., Sakurai, M., Kameno, Y., Yubuta, K., Suzuki, T., Shishido, T., Endo, M., Oishi, S., Well-formed one-dimensional hydroxyapatite crystals grown by an environmentally friendly flux method, Cryst. Growth Des., 9 (2009) 2937-2940.

[13] Pontier, C., Champion, E., Vieana, M., Chulia, D., Bernache-Assollant, D., Use of cycles of compression to characterize the behaviour of apatic phosphate powders, J. Eur. Ceram. Soc., 22 (2002) 1205-1216.

[14] Muralithran, G., Ramesh, S., The effects of sintering temperature on the properties of hydroxyapatite, Ceramics International, 26 (2000) 221-230.

[15] Pontier, C., Viana, M., Champion, E., Chulia, D., Apatic calcium phosphates used in compression: rationalization of the end-use properties, Powder Technology, 130 (2003) 436-441.

[16] Nystrom, C., Alderborn, G., Duberg, M., Karehill, P., Bonding surface area and bonding mechanism – two important factors for the understanding of powder compactibility, Drug. Dev. Ind. Pharm., 19 (1993) 2143-2196.

[17] Adolfsson, A., Nystrom, C., Tablet strength, porosity, elasticity and solid state structure of tablets compressed at high loads, Int. J. Pharm., 132 (1996) 95-106.

[18] Adolfsson, A., Gustafsson, C., Nystrom, C., Use of tablet tensile strength adjusted for surface area and mean interparticulate distance to evaluate dominating bonding mechanism, Drug. Dev. Ind. Pharm., 25 (1999) 753-764.

[19] Rankell, A.S., Higuchi, T., Physics of tablet compression XV. Thermodynamic and kinetic aspects of adhesion under pressure, J. Pharm. Sci., 57 (1968) 574-577.

[20] Jayasinghe, S.S., Pilpel, N., Harwood, C.F., The effect of temperature and compression on the cohesive properties of particulate solids, Mater. Sci. Eng., 5 (1969/1970) 287-294.

[21] Adolfsson, A., Olsson, H., Nystrom, C., Effect of particle size and compaction load on interparticulate bonding structure for some pharmaceutical materials studied by compaction and strength characterization in butanol, Eur. J. Pharm. Biopharm., 44 (1997) 243-251.

[22] Hiestand, E.N., Principles, tenets and notions of tablet bonding and measurements of strength, Eur. J. Pharm. Biopharm., 44 (1997) 229-242.

[23] Olsson, H., Nystrom, C., Assessing tablet bond types from structural features that affect tablet tensile strength, Pharm. Res., 18 (2001) 203-210.

[24] Butt, H.-J., Makowski, M., Kappl, M., Ptak, A., On the adhesion between individual particles, KONA Powder and Particle Journal, 29 (2011) 53-66.

[25] Steendam, R., Frijlink, H.W., Lerk, C.F., Plasticisation of amylodextrin by moisture: Consequences for compaction behavior and tablet properties, Eur. J. Pharm. Sci., 14 (2001) 245-254.

[26] Pande, G.S., Shangraw, R.F., Characterization of β-cyclodextrin for direct compression tableting: II. The role of moisture in the compactibility of β-cyclodextrin, Int. J. Pharm., 124 (1995) 231-239.

[27] Alderborn, G., Sebhatu, T., Ahlneck, C., The effect of moisture content on the compression and bond-formation properties of amorphous lactose particles, Int. J. Pharm., 146 (1997) 101-114.

[28] Khan, F., Pilpel, N., Ingram, S., The effect of moisture on the density, compaction and tensile strength of microcrystalline cellulose, Powder Technology, 54 (1988) 161-164.

[29] Nokhodchi, A., The effect of moisture on the Heckel and energy analyses of hydroxypropylmethylcellulose 2208, J. Pharm. Pharmacol., 48 (1996) 1121-1127.

[30] Malamataris, S., Karidas, T., Effect of particle size and sorbed moisture on the tensile strength of some tableted hydroxypropyl-methylcellullose (HPMC) polymers, Int. J. Pharm., 104 (1994) 115-123.

[31] Malaj, L., Censi, R., Gashi, Z., Martino, P.D., Compression behavior of anhydrous and hydrate forms of sodium naproxen, Int. J. Pharm., 390 (2010) 142-149.

[32] Sun, C.C., Grant, D.J.W., Improved tableting properties of p-hydroxybenzoic acid by water of crystallization: a molecular insight, Pharm. Res., 21 (2004) 382-386.

[33] Garr, J.S.M., Rubinstein, M.H., The influence of moisture on consolidation and compaction properties of paracetamol, Int. J. Pharm., 81 (1992) 187-192.

[34] Armstrong, N.A., Patel, A., Jones, T.M., Relationship between porosity and water content of dicalcium phosphate tablets, Int. J. Pharm., 48 (1988) 173-177.

[35] Walker, E.E., The properties of powders VI: the compressibility of powders, Trans. Faraday Soc., 19 (1923) 73-82.

[36] Rumpf, H. The strength of granules and agglomerates in: Knepper W.A., (Eds.) *Agglomeration*, Interscience-Wiley, New York, 1962, pp. 379-418.

[37] Eaves, T., Jones, T.M., Effect of Moisture on Tensile Strength of Bulk Solids: I. Sodium Chloride and Effect of Particle Size, J. Pharm. Sci., 61 (1972) 256-261.

[38] Turner, G.A., Balasubramanian, M., Investigations of the contribution to the tensile strength of weak particulate masses, Powder Technology, 10 (1974) 121-127.

[39] Rees, J.E., Hersey, J.A., The strength of compacts containing moisture, Pharm. Acta Helv., 45 (1972) 235-243.

[40] Ahlneck, C., Alderborn, G., Moisture adsorption and tabletting. I. Effect on volume reduction properties and tablet strength for some crystalline materials, Int. J. Pharm., 54 (1989) 131-141.

[41] Armstrong, N.A., Patel, A., The compressional properties of dextrose monohydrate and anhydrous dextrose of varying water contents, Drug Dev. Ind. Pharm., 12 (1986) 1885-1901.

[42] Hermann, W., The effect of water vapour on the shear strength of briquettes, Powder Technology, 5 (1971/2) 25-30.

[43] Lordi, N., Shiromani, P., Use of sorption isotherms to study the effect of moisture on the hardness of aged compacts, Drug Dev. Ind. Pharm., 9 (1983) 1399-1416.

[44] Zografi, G., State of water associated with solids, Drug Dev. Ind. Pharm., 14 (1988) 1905-1926.

[45] Malamataris, S., Goidas, P., Dimitriou, A., Moisture sorption and tensile strength of some tableted direct compression excipients, Int. J. Pharm., 68 (1991) 51-60.

[46] Stubberud, L., Arwidsson, H.G., Larsson, A., Graffner, C., Water-solid interactions II. Effect of moisture sorption and glass transition temperature on compactibility of microcrystalline cellulose alone or in binary mixtures with polyvinyl pyrrolidone, Int. J. Pharm., 134 (1996) 79-88.

[47] Maarschalk, K.V.d.V., Vromans, H., Groenendijk, W., Bolhuis, G.K., Lerk, S.F., Effect of water on deformation and bonding of pregelatinized starch compacts, Eur. J. Pharm. Biopharm., 44 (1997) 253-260.

[48] Zografi, G., Kontny, M.J., Yang, A.Y.S., Brenner, G.S., Surface area and water vapor sorption of microcrystalline cellulose, Int. J. Pharm., 18 (1984) 99-116.

[49] Carstensen, J.T., Hou, X., Compressibility of Anhydrous Tricalcium Phosphate, J. Pharm. Sci., 74 (1985) 466-468.

[50] Cartsensen, J.T., Hou, X., The Athy-Heckel Equation Applied to Granular Agglomerates of Basic Tricalcium Phosphate, Powder Technology, 42 (1985) 153-157.

[51] Carstensen, J.T., Hou, X., Compression characteristics of basic tricalcium phosphate, Int. J. Pharm., 25 (1985) 207-215.

[52] Chowhan, Z.T., Amaro, A.A., The effect of low- and high-humidity aging on the hardness, disintegration time and dissolution rate of tribasic calcium phosphate-based tablets, Drug. Dev. Ind. Pharm., 5 (1979) 545-562.

[53] Constantino, H.R., Curley, J.G., Hsu, C.C., Determining the water sorption monolayer of lyophilized pharmaceutical proteins, J. Pharm. Sci., 86 (1997) 1390-1393.

[54] Kaleemullah, S., Kailappan, R., Monolayer moisture, free energy change and fractionation of bound water of red chillies, Journal of Stored Product Research, 43 (2007) 104-110.

[55] Fell, J.T., Newton, J.M., The tensile strength of lactose tablets, J. Pharm. Pharmacol., 20 (1968) 657-658.

[56] Ilic, I., Govedarica, B., Sibanc, R., Dreu, R., Srcic, S., Deformation properties of pharmaceutical excipients determined using an in-die and out-die method, Int. J. Pharm., 446 (2013) 6-15.

[57] Heckel, R.W., Density-pressure relationships in powder compaction, Trans. Metall. Soc. AIME, 221 (1961) 671-675.

[58] Heckel, R.W., An analysis of powder compaction phenomena, Trans. Metall. Soc AIME, 221 (1961) 1001-1008.

[59] Fell, J.T., Newton, J.M., Effect of particle size and speed of compaction on density changes in tablets of crystalline and spray-dried lactose, J. Pharm. Sci., 60 (1971) 1866-1869.

[60] Sun, C.C., Grant, D.J.W., Compaction properties of L-lysine salts, Pharm. Res., 18 (2001) 281-286.

[61] Armstrong, N.A., Haines, R.F., Elastic recovery and surface area changes in compacted powder systems, Powder Technology, 9 (1974) 287-290.

[62] Patel, S., Kaushal, A.M., Bansal, A.K., Mechanistic investigation on pressure dependency of Heckel parameter, Int. J. Pharm., 389 (2010) 66-73.

[63] Asmani, M., Kermel, C., Leriche, A., Ourak, M., Influence of porosity on Young's modulus and Poisson's ratio in alumina ceramics, J. Eur. Ceram. Soc., 21 (2001) 1081-1086.

[64] Jang, B., Matsubara, H., Influence of porosity on hardness and Young's modulus of nanoporous EB-PVD TBCs by nanoindentation, Material Letters, 59 (2005) 3462-3466.

[65] Hancock, B.C., Colvin, J.T., Mullarney, M.P., Zinchuk, A.V., The relative densities of pharmaceutical powders, blends, dry granulations, and immediate-release tablets, Pharmaceutical Technology, April (2003) 64-80.

[66] Markovic, M., Fowler, B.O., Tung, M.S., Preparation and Comprehensive Characterization of a Calcium Hydroxyapatite Reference Material, J. Res. Natl. Inst. Stand. Technol., 109 (2004) 553-568.

[67] Rootare, H.M., Craig, R.G., Vapor Phase Adsorption of Water on hydroxyapatite, J. Dent. Res., 56 (1977) 1437-1488.

[68] Sing, K.S.W., Reporting physisorption data for gas/solid systems with special reference to the determination of surface area and porosity, Pure and Applied Chemistry, 54 (1982) 2201-2218.

[69] Chung, Y.W. Introduction to Materials Science and Engineering. Boca Raton, Florida: CRC Press Taylor & Francis.

[70] Rootare, H.M., Craig, R.G., Free surface energy change for water adsorbed on hydroxyapatite, J. Dent. Res., 56 (1977) 744-747.

[71] Rootare, H.M., Craig, R.G., Characterization of the compaction and sintering of hydroxyapatite powders by mercury porosimetry, Powder Technology, 9 (1974) 199-211.

[72] Joiris, E., Martino, P.D., Berneron, C., Guyot-Hermann, A.M., Guyot, J.C., Compression behavior of orthorhombic paracetamol, Pharm. Res., 15 (1998) 1122-1130.

[73] Sun, C.C., Grant, D.J.W., Effects of initial particle size on the tableting properties of L-lysine monohydrochloride dihydrate powder, Int. J. Pharm., 215 (2001) 221-228.

[74] Sun, C.C., Grant, D.J.W., Influence of crystal structure on the tableting properties of sulfamerazine polymorphs, Pharm. Res., 18 (2001) 274-280.

[75] Tye, C.K., Sun, C.C., Amidon, G.E., Evaluation of the effects of tableting speed on the relationships between compaction pressure, tablet tensile strength, and tablet solid fraction, J. Pharm. Sci., 94 (2005) 465-472.

[76] Sun, C.C., Himmelspach, M.W., Reduced tabletability of roller compacted granules as a result of granule size enlargement, J. Pharm. Sci., 95 (2006) 200-206.

[77] Roberts, R.J., Rowe, R.C., The effect of punch velocity on the compaction of a variety of materials, J. Pharm. Pharmacol., 37 (1985) 377-384.

[78] Armstrong, N.A., Palfrey, L.P., The effect of machine speed on the consolidation of four directly compressibility tablet diluents, J. Pharm. Pharmacol., 41 (1989) 149-151.

[79] Ishino, R., Yoshino, H., Hirakawa, Y., Noda, K., Influence of tabletting speed on compactibility and compressibility of two direct compressible powders under high speed compression, Chem. Pharm. Bull., 38 (1990) 1987-1992.

[80] Ruegger, C.E., Celik, M., The effect of compression and decompression speed on the mechanical strength of compacts, Pharm. Dev. Technol., 5 (2000) 485-494.

[81] Oksanen, C.A., Zografi, G., The relationship between the glass transition temperature and water vapor absorption by poly(vinylpyrrolidone), Pharm. Res., 7 (1990) 654-657.

[82] Hancock, B.C., Zografi, G., The relationship between the glass transition temperature and the water content of amorphous pharmaceutical solids, Pharm. Res., 11 (1994) 471-477.

[83] Rees, J.E., Tsardaka, K.D., Some effects of moisture on the viscoelastic behaviour of modified starch during powder compaction, Eur. J. Pharm. Biopharm., 40 (1994) 193-197.

[84] Zografi, G., Kontny, M.J., The interaction of water with cellulose-starch-derived pharmaceutical excipients, Pharm. Res., 3 (1986) 187-194.

[85] Morris, K.R. Structural aspects of hydrates and solvates in: Brittain H.G., (Eds.) *Polymorphism in Pharmaceutical Solids*, Marcel Decker, New York, 1999, pp. 125-181.

[86] York, P., A consideration of experimental variables in the analysis of powder compaction behaviour, J. Pharm. Pharmacol., 31 (1979) 244-246.

[87] Sonnergaard, J.M., A critical evaluation of the Heckel equation, Int. J. Pharm., 193 (1999) 63-71.

[88] Roberts, R.J., Rowe, R.C., The compaction of pharmaceutical and other model materials - a pragmatic approach, Chem. Eng. Sci., 42 (1987) 903-911.

[89] Sonnergaard, J.M., Impact of particle density and initial volume on mathematical compression models, Eur. J. Pharm. Sci., 11 (2000) 307-315.

[90] Train, D., A investigation into the compaction of powders, J. Pharm. Pharmacol., 8 (1956) 745-761.

[91] Patel, S., Kaushal, A.M., Bansal, A.K., Effect of particle size and compression force on compaction behavior and derived mathematical parameters of compressibility, Pharm. Res., 24 (2007) 111-124.

[92] Aburub, A., Mishra, D., Buckner, I., Use of compaction energetics for understanding particle deformation mechanism, Pharm. Dev. Technol., 12 (2007) 405-414.

[93] Govedarica, B., Ilic, I., Sibanc, R., Dreu, R., Srcic, S., The use of single particle mechanical properties for predicting the compressibility of pharmaceutical materials, Powder Technology, 225 (2012) 43-51.

[94] Khomane, K.S., More, P.K., Raghavendra, G., Bansal, A.K., Molecular understanding of the compaction behaviour of indomethacin polymorphs, Molecular Pharmaceutics, 10 (2013) 631-639.

[95] Hiestand, E.N., Dispersion forces and plastic deformation in tablet bond, J. Pharm. Sci., 74 (1985) 768-770.

[96] Ryshkewitch, E., Compression strength of porous sintered alumina and zirconia, J. Am. Ceram. Soc., 36 (1953) 65-68.

[97] Duckworth, W., Discussion of Ryshkewitch paper, J. Am. Ceram. Soc., 36 (1953) 68.

[98] Steendam, R., Lerk, C.F., Poly(DL-lactic acid) as a direct compression excipient in controlled release tablets. Part I. Compaction behaviour and release characteristics of poly(DL-lactic acid) matrix tablets, Int. J. Pharm., 175 (1998) 33-46.

[99] Maarschalk, K.V.d.V., Zuurman, K., Vromans, H., Bolhuis, G.K., Lerk, C.F., Porosity expansion of tablets as a result of bonding and deformation of particulate solids, Int. J. Pharm., 140 (1996) 185-193.

[100] Wu, C.Y., Best, S.M., Bentham, A.C., Hancock, B.C., Bonfield, W., A simple predictive model for the tensile strength of binary tablets, Eur. J. Pharm. Sci., 25 (2005) 331-336.

[101] Barralet, J.E., Gaunt, T., Wright, A.J., Gibson, I.R., Knowles, J.C., Effect of porosity reduction by compaction on compressive strength and microstructure of calcium phosphate cement, J. Biomed. Mater. Res. Part B., 63 (2002) 1-9.

[102] Shin, H.S., Lee, S.K., Lee, B.K., Aggregate and necking force in Mn-Zn ferrite, Material Letters, 57 (2003) 1467-1470.

[103] Michrafy, A., Michrafy, M., Kadiri, M.S., Dodds, J.A., Predictions of tensile strength of binary tablets using linear and power law mixing rules, Int. J. Pharm., 333 (2007) 118-126.

[104] Sun, C.C., A material-sparing method for simultaneous determination of true density and powder compaction properties - Aspartame as an example, Int. J. Pharm., 326 (2006) 94-99.

CHAPTER FOUR: THE EFFECT OF LIQUID SATURATION AND BINDER LIQUID VISCOSITY ON A NOVEL REVERSE-PHASE WET GRANULATION PROCESS

4 Introduction

The aim of this study is to report on the development of a novel reverse-phase wet granulation process. Such a reverse-phase process involves the controlled addition of the powder formulation into the agitated binder liquid to create completely wetted powder particles which favour granule formation. Addition of further powder is proposed to reduce the liquid saturation of the granules, with the desired particle size being obtained through controlled breakage. This is in stark contrast to the conventional granulation approach where binder liquid is added to the dry powder. Addition of further binder liquid increases the liquid saturation of the granules and growth occurs through controlled coalescence. A number of advantages motivate the development of the reverse-phase process (Section 1.7). It is hypothesised that the reverse-phase granulation process can be controlled by a few simple variables; binder liquid quantity, binder liquid viscosity and impeller speed, to reach the desired granule properties without the risk of uncontrolled growth and batch rejection. Binder liquid quantity and binder liquid viscosity are the focus of this study.

Granule growth is favoured when granules deform upon collision through rearrangement of individual particles. The effect of binder liquid content is complex since it impacts interparticulate friction, as well as viscous and capillary forces, and it affects each of these differently. Increasing binder liquid content may reduce the contribution of interparticulate friction due to a lubrication effect [1]. In addition, granule deformation promotes movement of binder liquid from within the granule to the surface through intragranular capillaries [2]. An increased binder liquid content increases the contribution of viscous forces since there is more binder liquid present within and on the surfaces of granules. Capillary forces also increase up to an S_{max} of 1 [3, 4]. When interparticulate friction dominates, increasing binder liquid content generally increases the extent of consolidation. However, when viscous forces dominate increasing the amount of binder liquid may decrease the extent of consolidation. Discrete element modeling (DEM) simulations [5] have shown that at low collision velocity the majority of the collision energy is dissipated by viscous effects, since little interparticulate movement occurs. At higher collision velocities both viscous and frictional effects contribute significantly to energy dissipation. The relationship is further complicated when considering the effect of binder liquid viscosity. In

consolidation experiments it was found that increasing binder viscosity decreased the rate of consolidation and that the effects of liquid content and viscosity were intertwined. Increasing the amount of a binder with a low viscosity of 0.0011 Pa.s was found to increase the rate of consolidation due to increased lubrication, whereas increasing the amount of a binder with a high viscosity of 1.1 Pa.s decreased the rate of consolidation due to increased viscous forces [6, 7]. Iveson and Litster [7] warn that unless the relative magnitudes of the frictional, viscous and capillary forces are known it is impossible to predict the effect of changing binder content and viscosity, even qualitatively.

Ohno *et al* [8] considered the effect of increased binder amount on both the granule size and pore structure, and the subsequent relationship of these properties with drug dissolution rate of mefenamic acid in a formulation containing, lactose monohydrate, low-substituted hydroxypropyl cellulose, hydroxypropyl cellulose and microcrystalline cellulose. These workers used water as the binder and found that an increase in content from 30 to 50 % *w/w* resulted in a significant increase in the d_{50} particle size and a decrease in the d_{50} pore diameter determined. The overall effect was a corresponding decrease in the amount of mefenamic acid dissolved after 15 min. These data illustrate the importance of granulation binder amount on the size of the resultant granules as well as on the consolidation behaviour.

Accordingly, the aim of this study was to compare the effects of liquid saturation and binder liquid viscosity on the size and porosity of the granules prepared using the reverse-phase and conventional methods of granulation.

4.1 Materials and Methods

4.1.1 Materials

Hydroxyapatite (HA) (TRI-CAL WG^{TM}), poly (vinyl pyrrolidone) (PVP) (Plasdone K29/32) and Dry*Flo*® displacement media were obtained as detailed in Section 2.1.1.

4.1.2 Granulation process

Aqueous granulation binder liquid was prepared as described in Section 2.1.2.1. Binder liquid viscosity was varied by manipulating the concentration of PVP in water. Granules were prepared by the reverse-phase process (Section 2.1.2.1). Granules were also prepared by the conventional process where 600 g of dry HA powder was added to the granulator bowl and mixed for 30 s using an impeller speed of 400 rpm (3.14 m s^{-1}) and chopper speed of 1000 rpm (0.89 m s^{-1}). Following mixing the 10 or 20 % *w/w* PVP binder liquid was sprayed onto the moving powder bed through a 65° VeeJet nozzle (SS-650033, Spraying Systems, Wheaton, Illinois, USA) at 3 bar pressure. Wet massing was performed for 10 s following complete addition of the binder liquid. Separate experiments were performed employing 50, 100, 150, 200 and 250 cm^3 of 10 or 20 % *w/w* binder liquids. The resultant granules were dried as described in Section 2.1.2.1. A summary of the experimental conditions is presented in Table 4-1.

Table 4-1. Summary of experimental conditions in both granulation methodologies studying the effects of binder liquid viscosity and impeller speed.

Binder liquid composition	Binder liquid volume (cm^3)	Hydroxyapatite mass (g)	Impeller tip speed (m s^{-1})
10 % *w/w* PVP	50	600	3.14
	100		
	150		
	200		
	250		
20 % *w/w* PVP	50	600	3.14
	100		
	150		
	200		
	250		

4.1.3 Binder liquid characterisation

4.1.3.1 Surface tension

Surface tension (n=3) was determined using the Wilhelmy plate method (K100, Krüss GmbH, Hamburg, Germany) and an illustration of the technique is shown in Figure 4-1.

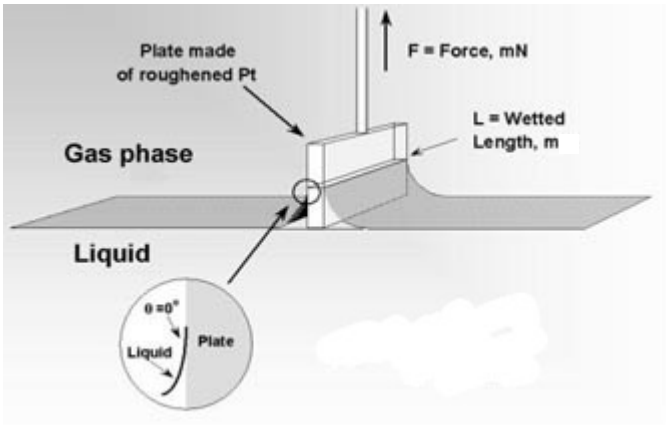

Figure 4-1. Illustration depicting surface tension measurement using the Wilhelmy plate method. Taken from http://www.kruss.de/en/theory/measurements/surface-tension/plate-method.html, last accessed 13 June 2013.

A liquid volume of approximately 25 cm^3 was added to the sample vessel. The temperature was between 24.97–25.60 °C for all measurements. The platinum plate (19.900 mm width, 10.000 mm height and 0.200 mm thickness) was thoroughly cleaned with water and heat treated with an oxyacetylene flame prior to use. The plate is assumed to be perfectly wetted such that the contact angle, θ, between the plate and the liquid sample is zero and therefore the term cos θ is taken to be 1. The probe was then attached to the instrument microbalance and lowered to a 2.00 mm immersion depth at which point measurements were recorded at approximately 12 s intervals over a 120 s period. Surface tension was calculated according to Equation 4-1.

$$\gamma = \frac{F}{L\cos\theta} \qquad \textit{Equation 4-1}$$

where γ is the surface tension of the liquid (mN m^{-1}), F is the force acting on the microbalance (mN), L is the wetted length (m) and θ is the contact angle between the liquid and the plate (°).

4.1.3.2 Density

Liquid density (n=3) was determined by weighing a known volume of binder liquid. A mechanical pipette was fitted with a 1 cm^3 plastic disposable tip and used to draw 1 cm^3 of liquid. The liquid was then dispensed into a tared container and the weight recorded to the nearest 0.001 g. The 1 cm^3 drawn volume was calibrated using purified water as a reference liquid.

4.1.3.3 Viscosity

Binder liquid viscosity (n=3) was determined in triplicate using a continuous shear rotational rheometer (AR2000, TA Instruments, New Castle, DE, USA) fitted with a 60 mm diameter cone (0:58:47 deg:min:sec) with 26 μm truncation gap. The inertia without cone fixture, with cone fixture and the zero gap distance between cone fixture and sample stage were calibrated prior to use. The cone and sample stage were cleaned with de-ionised water prior to each sample measurement. The sample stage was maintained at a temperature of 20 °C using a thermostatically controlled water jacket. Viscosity was determined over a shear rate range of 1–10000 s^{-1}. Measurements were recorded at 10 points per decade with equilibrium criteria of less than 3.0 % difference for 3 consecutive measurements or a maximum measurement time of 1 min.

4.1.3.4 Contact angle

The contact angle between the binder liquid and HA powder (n=3) was determined by sorption measurements using the Washburn equation [9]. A stainless steel fritted base sample holder fitted with a filter paper was packed with 3.5000 g of HA powder. The sample holder was manually tapped 100 times to present a consistently packed powder column before each measurement. Approximately 25 cm^3 of binder liquid sample was placed in the liquid sample vessel. The holder containing the HA sample was then attached to the instrument microbalance and lowered into the liquid. The mass increase as a function of time was recorded every 5 s over a period of 600 s. The gradient of the slope for data points between 400–600 s (R^2 >0.9999 in all cases) was processed by the instrument software to calculate the contact angle according to Equation 4-2:

$$m^2 = c\frac{\rho^2 \gamma \cos\theta}{\mu}T \qquad \textit{Equation 4-2}$$

where m is the mass of liquid in the capillary (g), c is a constant (m^{-5}), ρ is the liquid density (kg m^{-3}), γ is the liquid surface tension (N m^{-1}), θ is the contact angle (°) between the liquid sample and solid sample, μ is the liquid viscosity (Pa.s) and T is the time (s). The constant, c, was determined experimentally from capillary rise measurements using hexane as a completely wetting liquid [10].

4.1.4 Granule physical characterisation

4.1.4.1 Granule size

Granule size analysis (n=4) was performed as described in Section 2.1.2.3. The sieve analysis results led to characterisation of three granule classes; fine (corresponding to the sieve diameter of as-received HA and agglomerates ≤600 μm), intermediate (granules with sieve diameters between 600–2000 μm) and coarse (granules with sieve diameters between 2000–8000 μm). No granules >8000 μm, i.e. lumps, were formed.

4.1.4.2 Bulk and tapped density

Bulk and tapped densities (n=4) were measured as described in Section 2.1.2.4. The Carr's index of compressibility [11] was used to assess flowability and was calculated from the bulk and tapped density values as:

$$Carr's\ Index = 100 \times \frac{(\rho_{tap} - \rho_{bulk})}{\rho_{tap}} \qquad \textit{Equation 4-3}$$

A lower index defines a powder with greater flowability and can be related to the interparticulate friction and cohesiveness of the moving powder mass [12, 13]. Table 4-2 provides flow character descriptors for the Carr's index results [11].

Table 4-2. Carr's index scales of flowability

Compressibility Index (%)	Flow Character
≤ 10	Excellent
11-15	Good
16-20	Fair
21-25	Passable
26-31	Poor
32-37	Very poor
>38	Very. Very poor

4.1.4.3 Granule envelope density

Granule envelope density (n=4) was determined using the GeoPyc® apparatus described in Chapter 2. Dry*Flo*® displacement media (~2.5 cm^3) was added to the sample chamber (25.4 mm diameter) and five preparation cycles and 20 blank cycles were performed with a consolidation force of 51 N. A riffled sample (~4 g) was then added to the sample chamber and five preparation cycles and 20 measurement cycles were repeated using a consolidation force of 51 N. Envelope density was automatically calculated by the GeoPyc® software as described in Section 2.1.2.2 with the average of 20 measurement cycles being reported as the mean envelope density for the sample.

4.1.5 Statistical analysis

Statistical analysis to determine whether significant differences existed between sample means was performed as described in Section 2.1.2.8.

4.2 Results and Discussion

4.2.1 Binder liquid characterisation

The measured properties of 10 and 20 % *w/w* PVP aqueous binder liquid are shown in Table 4-3. Data for water is also shown for comparison purposes where the density and contact angle were determined experimentally and the viscosity and surface tension results were obtained from the literature [14]. An increase in PVP concentration from 10 to 20 % *w/w* resulted in an increase in density and viscosity and a decrease in surface tension and contact angle.

Table 4-3. Surface tension, density, viscosity and contact angle between binder liquid and hydroxyapatite powder values for water, 10 and 20 % w/w PVP solutions. Mean ± SD (n=3).

Property	Surface tension [mN m^{-1}]	Density [g cm^{-3}]	Viscosity [mPa.s]	Contact angle [°]
Water	72.80 (- -)	1.003 (± 0.008)	1.00 (- -)	61.9 (± 4.7)
10 % *w/w* PVP	59.86 (± 0.407)	1.022 (± 0.003)	6.86 [a] (± 0.307)	62.5 (± 5.9)
20 % *w/w* PVP	55.48 (± 0.917)	1.048 (± 0.002)	33.70 [a] (± 1.912)	51.0 (± 7.2)

[a] Reported at shear rate of 5012 s^{-1}.

4.2.1.1 Binder liquid surface tension and density

In the present study an increase in PVP concentration from 10 to 20 % *w/w* resulted in a decrease ($p < 0.10$ Wilcoxon) in surface tension and an increase ($p < 0.10$ Wilcoxon) in density (Table 4-3). These results are similar to those previously reported for aqueous PVP solutions, however the majority of previously reported data is for different viscosity grades of PVP as defined by the K value. The PVP grade used in the present study was PVP K29/32. When the concentration of PVP K10 was increased from 3 to 13 % *w/w* the surface tension decreased from 63.6 to 53.8 mN m^{-1} [15]. Similarly, when the concentration of PVP K25 was increased in 5 % increments from 0 to 25 % *w/w* the surface tension consistently decreased from 72.80 to 44.17 mN m^{-1} [16]. When the concentration of PVP (grade not specified) was increased from 2 to 5 % *w/w* the density

of the solution increased from 1.000 to 1.003 g cm^{-3} [17]. Similar density increases as a function of increasing polymer concentration have also been reported for HPMC [15] and sodium carboxymethylcellulose [17].

4.2.1.2 Binder liquid viscosity

The viscosity for each PVP binder liquid (Table 4-3) was reported as the mean of triplicate results generated at a shear rate of 5012 s^{-1}, which represents the approximate midpoint of the shear rate range studied. An increase in PVP concentration from 10 to 20 % *w/w* resulted in an increase ($p < 0.10$ Wilcoxon) in viscosity (Table 4-3). This is consistent with previously reported results for much higher levels of PVP K29/32 where the viscosity at 35.5, 50, 54.5 and 58.3 % *w/w* concentration, as calculated using the reported data, in an aqueous solution was 300, 4600, 12800 and 27900 mPa.s respectively [18]. Similarly, an increase in PVP K10 concentration in an aqueous solution from 3 to 13 % *w/w* increased the viscosity from 1.3 to 3.1 mPa.s [15].

Continuous shear viscosity data was generated in the present study over a shear rate range of 1–10000 s^{-1}. Figure 4-2 presents an example of the relationship between shear rate and shear stress for the 10 and 20 % *w/w* PVP binder liquids.

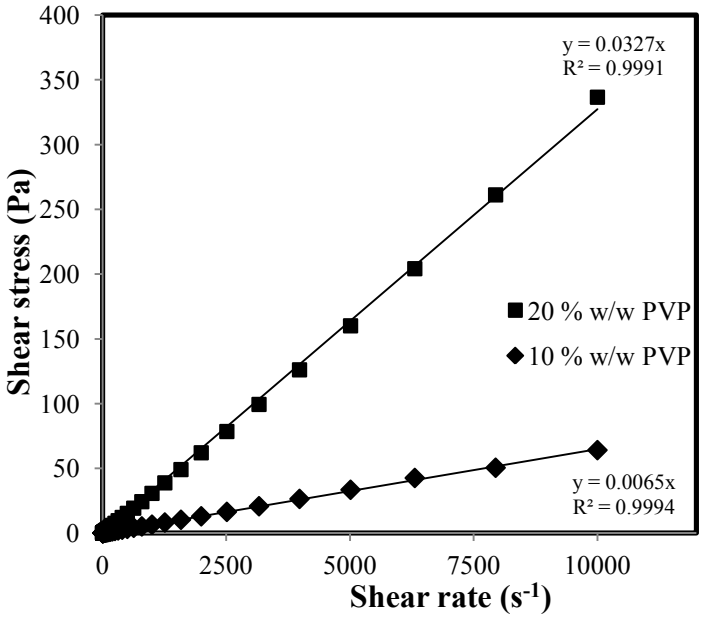

Figure 4-2. Example shear rate versus shear stress profile for 10 and 20 % w/w PVP aqueous solutions generated using a continuous shear rotational rheometer.

The analysis was conducted in triplicate for each binder liquid and the correlation coefficient (R^2) for a linear fit line was >0.9987 in all cases. These data support the conclusion that both 10 and 20 % *w/w* PVP binder liquids are Newtonian, i.e. viscosity is shear rate independent. The observed Newtonian behaviour is important since it is likely that a wide range of shear rates exist within the granulator. Newtonian behaviour allows the assumption that, provided the shear rates experienced within the granulator fall within the range studied, the contribution of viscous forces will be consistent regardless of flow patterns, impeller speed, etc. The use of a non-Newtonian binder could complicate evaluation of the granulation process since the viscous contributions from the binder liquid may be expected to vary with the experimental conditions used.

4.2.1.3 Contact angle

The contact angles between both the 10 and 20 % *w/w* PVP binder liquids and the HA powder were < 90 ° implying that the liquid wets the surface, which will favour binder liquid distribution [19]. No previous reports were found in the literature for the contact angle between PVP binder liquids and HA powder, however results have been reported for other materials using the same Washburn equation method used in the present study. A range of liquids and powders have been studied with liquids including water, paraffin oil, 3 and 13 % *w/w* aqueous PVP and 0.5, 1 and 1.5 % *w/w* aqueous HPMC solutions and ethylene glycol and powders including glass beads, aluminium oxide, zirconium dioxide, calcium carbonate and microcrystalline cellulose [9, 10, 15, 20]. These studies all reported the standard deviation for contact angle measurements in the range of 3-10 % demonstrating that the variability presented in Table 4-3 is similar to that previously reported by other workers using the same Washburn equation method.

4.2.2 Liquid saturation

Granule growth is influenced by the degree of pore saturation by binder liquid. Different binder volumes will result in different levels of granule pore saturation depending upon the formulation properties and process conditions. Therefore, liquid saturation, S_{max}, was used as a dimensionless measure of liquid content [21, 22]:

$$S_{max} = \frac{m\,\rho_s\,(1-\varepsilon_{min})}{\rho_l\,\varepsilon_{min}} \qquad \textit{Equation 4-4}$$

where m is the mass ratio of liquid to solid, ρ_s is the density of solid particles, ρ_l is the liquid density and ε_{min} is the minimum porosity the formulation reaches under given operating conditions. ε_{min} is a complex function of formulation properties and operating conditions [6, 7]. For low intensity drum granulation it has been suggested that ε_{min} could be estimated by measuring the in-process wet-tapped porosity of the formulation [21]. However, in high intensity granulators, such as the high shear mixer used in the present study, formulations are consolidated to a greater extent and ε_{min} cannot be predicted without performing actual experimental measurements of granule porosity [21]. The determination of granule porosity for use in the calculation of S_{max} has previously been measured by mercury porosimetry [23]. In the present study the granule envelope density was measured by a powder pycnometry method (GeoPyc®) based on the experimental procedure developed in Chapter 2 where the powder pycnometry and mercury porosimetry methods were compared. A calibration curve was constructed (Section 2.2.3) and used to correct appropriately the corresponding results. ε_{min} was then calculated by the following equation:

$$\varepsilon_{min} = 1 - \left(\frac{\rho_e}{\rho_g}\right) \qquad \textit{Equation 4-5}$$

Where ρ_e is the envelope density of the granule sample and ρ_g is the true density of the granule sample. The PVP true density of 1.18 g cm^{-3}, determined using the experimental method described in Section 3.1.2.1, and the previously reported HA true density value of 1.92 g cm^{-3} [24-26], were used. True density of the HA/PVP granules, ρ_g, is expressed as a function of the true densities of the constituent single component powders, ρ_1 and ρ_2, as follows:

$$\frac{1}{\rho_g} = \frac{n_1}{\rho_1} + \frac{n_2}{\rho_2} \qquad \textit{Equation 4-6}$$

where, n_1 and n_2 are the weight fractions of the constituent powders respectively. Such an approach assumes homogeneous mixing of the constituent powder components and representative sampling of the mixture.

S_{max} was directly proportional to binder liquid volume for each granulation process and binder viscosity (Figure 4-3) as would be predicted from Equation 4-4. An S_{max} of 1 theoretically indicates complete saturation of the pores in the powder bed, with no residual surface liquid present. S_{max} <1 would be a limiting growth condition due to the absence of free liquid and S_{max} >1 would initially promote rapid growth, potentially resulting in the formation of a slurry. Therefore a delicate balance exists between achieving sufficient growth and preventing uncontrolled growth, or slurry formation, which would result in an un-usable over-wet mass.

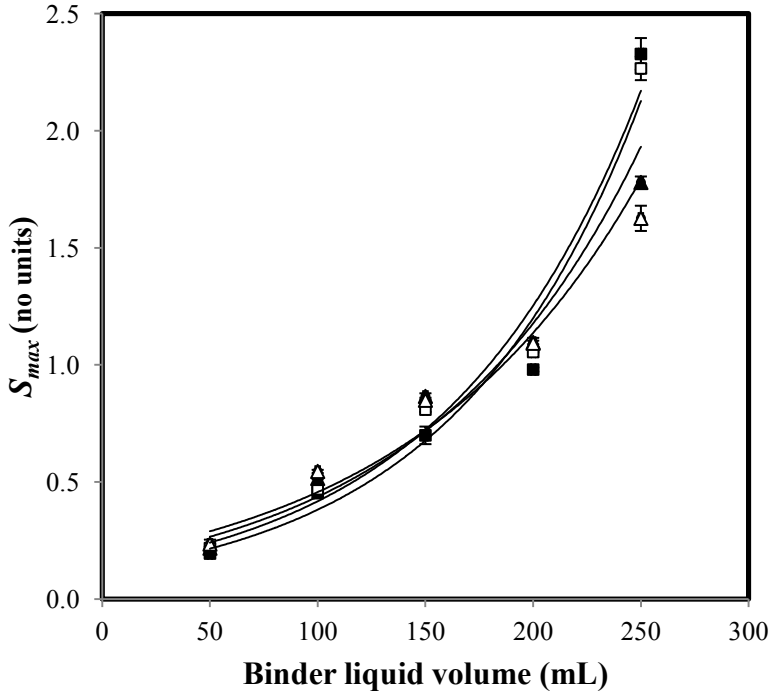

Figure 4-3. Hydroxyapatite granule liquid saturation, S_{max}, as a function of binder liquid volume. ■ 10 % w/w PVP by conventional granulation (R^2 0.9731), □ 20 % w/w PVP by conventional granulation (R^2 0.9780), ▲ 10 % w/w PVP by reverse-phase granulation (R^2 0.9553), Δ 20 % w/w PVP by reverse-phase granulation (R^2 0.9488). Error bars represent 1 SD, n=4.

In the 50–200 cm^3 binder liquid volume range all granulation processes displayed a steady increase in S_{max} to a maximum ~1, with the reverse-phase process resulting in granules with a higher S_{max} ($p < 0.05$ Wilcoxon) when compared to granules prepared using the conventional process. At the 250 cm^3 binder volume the granulation processes differ significantly with the conventional process exhibiting significantly greater ($p < 0.05$ Wilcoxon) S_{max} values which are approximately 30–40 % greater, than those of the reverse-phase process under identical processing conditions. These data indicate that

the conventional granules undergo greater consolidation, resulting in a lower ε_{min}, and are therefore more prone to uncontrolled growth at the elevated binder liquid volume. At all binder liquid volumes the PVP concentration did not have a significant effect on S_{max} ($p > 0.05$ Wilcoxon).

It would be assumed that the immersion mechanism of the reverse-phase process would result in a greater S_{max} than the conventional process, however these results indicate the opposite at the 250 cm^3 condition. One possible explanation is that the immersion of powder into the binder liquid during the reverse-phase process facilitates more complete wetting of capillaries within the HA particles, whereas the conventional granulation process has a lesser and more variable extent of capillary wetting. The plausibility of this capillary saturation theory is supported by results reported for the wet granulation of microcrystalline cellulose where the initial moisture content of microcrystalline cellulose was increased by exposing the material to elevated relative humidity conditions [27]. The microcrystalline cellulose was then wet granulated with a constant amount of binder liquid and the resultant granule size determined. It was found that an increase in microcrystalline cellulose moisture content resulted in a significant increase in granule size ($d_{50\%}$). This finding was attributed to the fact that as the initial moisture content of the microcrystalline cellulose was increased the interparticulate capillaries were filled with moisture to a greater degree. This resulted in increased binder liquid being present at the surface of the particles which facilitated coalescence and growth. If correct, this mechanism may support the reverse-phase process being less variable than the conventional granulation process since the extent of capillary wetting, and therefore S_{max}, would be expected to be more consistent.

4.2.3 Granule particle size distribution

Granule size distribution plots were constructed for both the conventional and reverse-phase granulation processes (Figure 4-4 and Figure 4-5 respectively). Data representing un-granulated HA (employed as received) were included (S_{max} = 0) to indicate the baseline particle size. The results show visually that binder viscosity had a minimal effect on the granule size distribution for both the conventional and reverse-phase granulation processes. Differences are however observed when comparing the conventional and reverse-phase processes. As S_{max} increases to ~1 the conventional

process shows a minimal change in the granule size distribution, with a small percentage of particles >425 μm being formed. A further increase in S_{max} resulted in a marked decrease in the percentage of particles <425 μm and a sharp increase in the proportion of granules >1000 μm. In contrast the reverse-phase granulation process shows a steady decrease in particles <425 μm and corresponding increase in granules of the size range 425–4750 μm as S_{max} increases over the range studied. These data indicate that granule size distribution may be simpler to control in the reverse-phase granulation process.

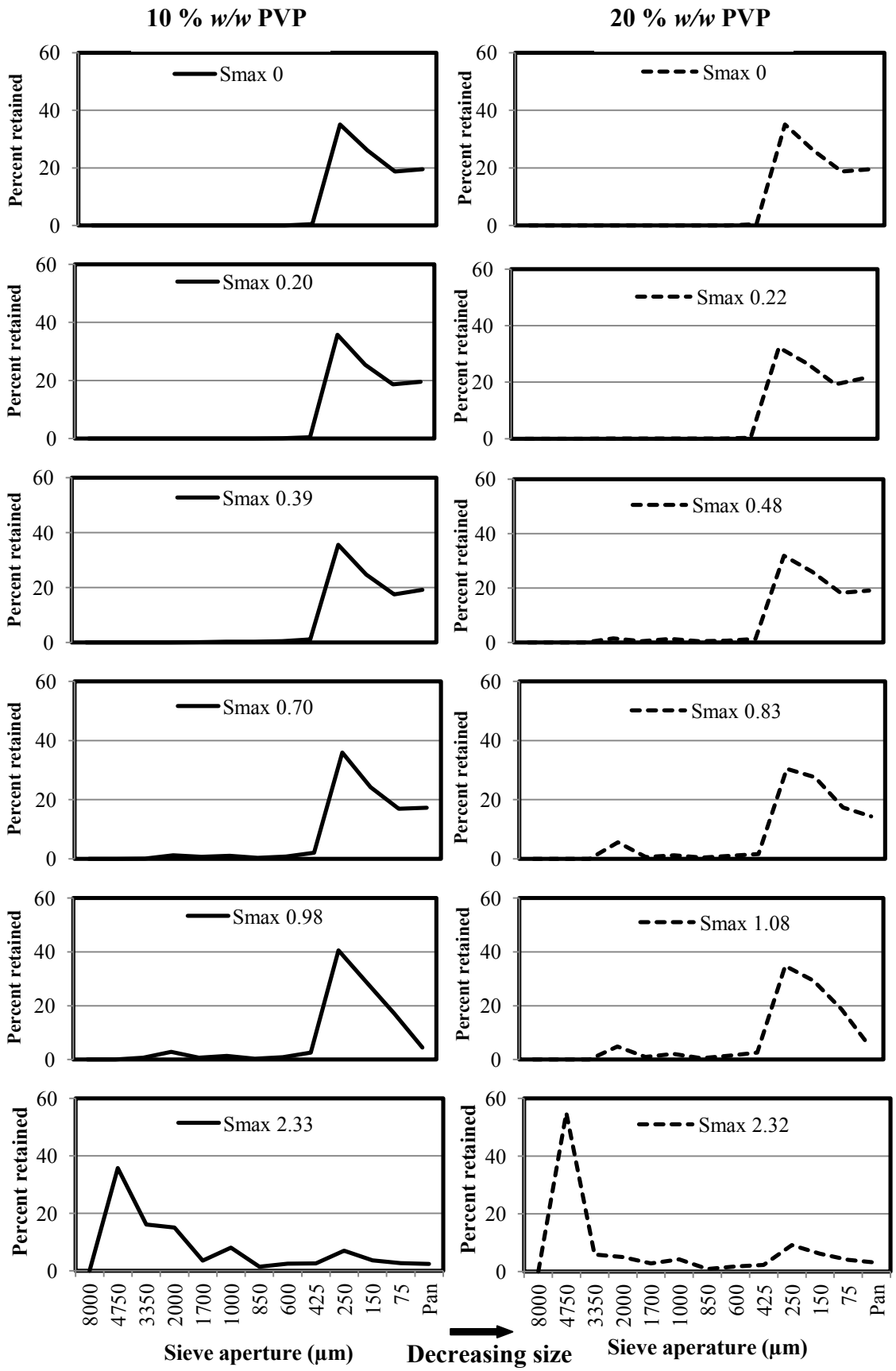

Figure 4-4. Size distribution for hydroxyapatite granules prepared using a conventional granulation process as a function of liquid saturation, S_{max}. Solid line represents 10 % w/w PVP binder, dashed line represents 20 % w/w PVP binder. Mean shown, n=4.

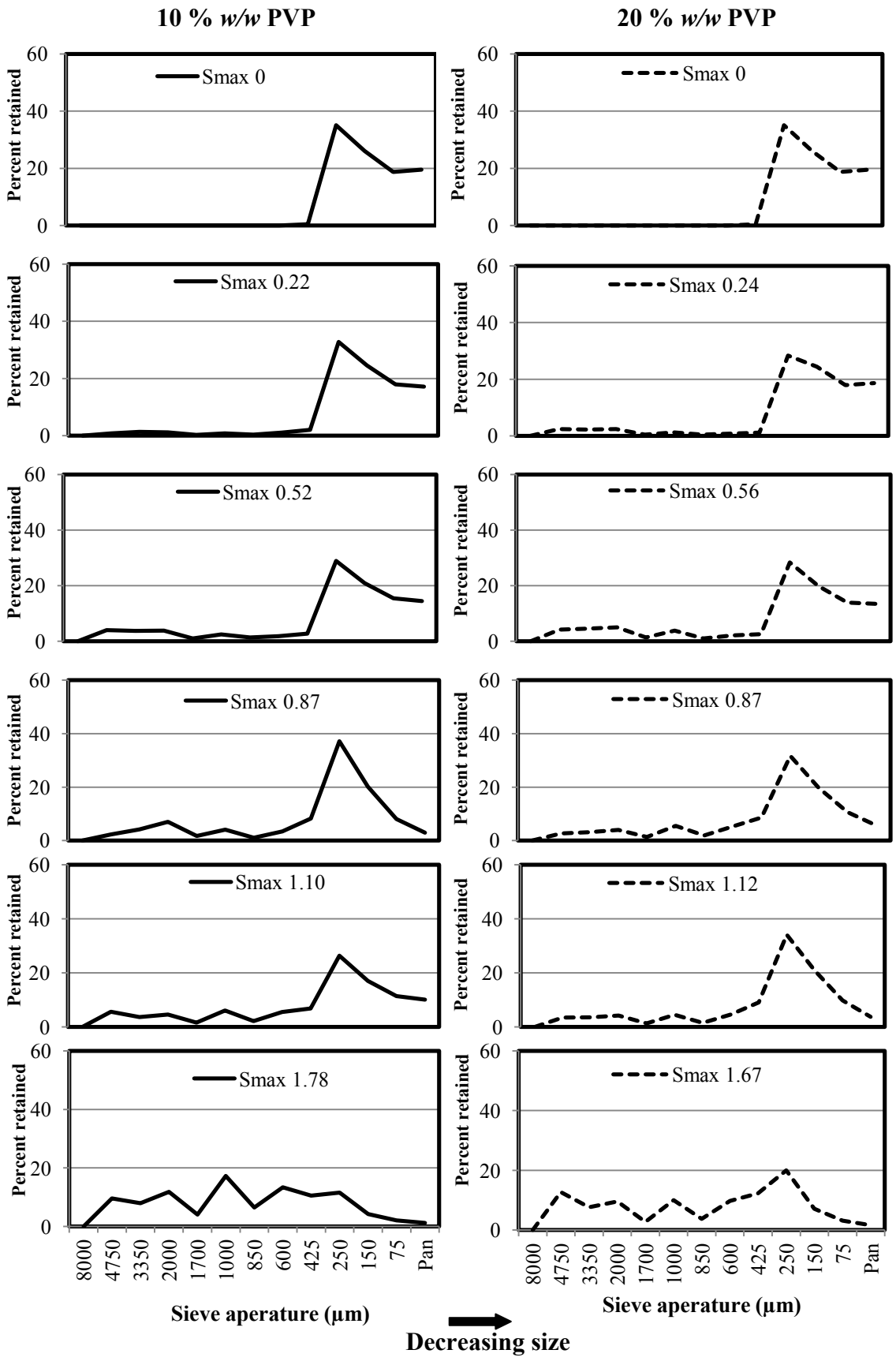

Figure 4-5. Size distribution for hydroxyapatite granules prepared using a reverse-phase granulation process as a function of liquid saturation, S_{max}. Solid line represents 10 % w/w PVP binder, dashed line represents 20 % w/w PVP binder. Mean shown, n=4.

When the size distribution is considered on a mass mean diameter basis (Figure 4-6) the conventional granulation process shows a statistically significant, but practically modest, increase with increasing S_{max} up to ~1.1 ($p < 0.05$ Wilcoxon), while being insensitive to PVP binder liquid concentration ($p > 0.05$ Wilcoxon). At S_{max} >1.1 rapid increase ($p < 0.05$ Wilcoxon) in the mass mean diameter is observed. This is consistent with an induction growth mechanism where a period of little or no growth is associated with strong, slowly consolidating granules that do not deform sufficiently during impact to form strong contact bonds [2, 28, 29]. A period of rapid growth then occurs when granules either consolidate sufficiently to squeeze binder liquid to their surface or, as in this case, additional binder liquid is added.

In contrast the reverse-phase process exhibits a gradual mass mean diameter increase ($p < 0.05$ Wilcoxon) with increasing S_{max} across the full range studied. The mass mean diameter of granules prepared using the reverse-phase process is also insensitive to PVP binder liquid concentration ($p > 0.05$ Wilcoxon). These results are consistent with steady growth behaviour. The reverse-phase granules start from a fully saturated state and are therefore likely to be more deformable which facilitates coalescence and growth. Provided that the bond is strong enough to resist granule breakage from the forces imparted within the granulator, the pair of granules will coalesce to form a new larger granule. This behaviour leads to a steady increase in granule size and is common in systems with coarse, narrowly-sized particles and low surface tension and/or low viscosity binders [4, 28, 30].

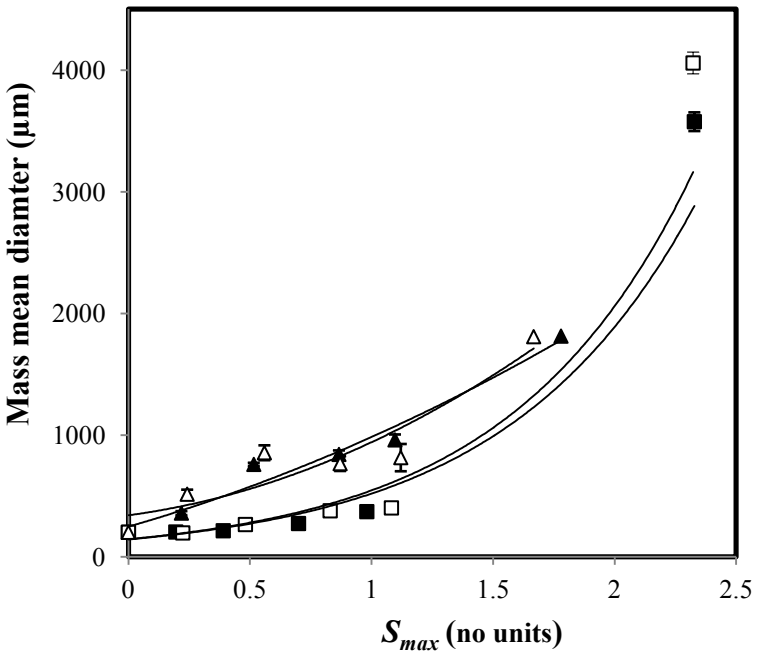

Figure 4-6. Hydroxyapatite granule mass mean diameter as a function of liquid saturation, S_{max}. ■ 10 % w/w PVP by conventional granulation, R^2 0.9447. □ 20 % w/w PVP by conventional granulation, R^2 0.9437. ▲ 10 % w/w PVP by reverse-phase granulation, R^2 0.9712. Δ 20 % w/w PVP by reverse-phase granulation, R^2 0.8850. Error bars represent 1 SD, n=4.

Analysis of the characteristic granule size fractions (Figure 4-7 – Figure 4-9) shows clear differences between the conventional and reverse-phase processes in each size category. Employing the conventional granulation process resulted in a greater percentage of particles being <600 µm than when the reverse-phase process was used, as S_{max} increases from 0 to ~1. At S_{max} values >1.1 the particles <600 µm are incorporated rapidly and to a similar extent for both processes. The proportion of granules with a particle size in the range 600–2000 µm increased approximately linearly over the entire S_{max} range for both granulation processes. The gradient of the growth slope for granules classified in the 600–2000 µm category is ~3–4 times greater for the reverse-phase process with values ~25–40 % compared to ~15% of the conventional granules. The conventional process shows only a low increase in the percentage of granules >2000 µm as S_{max} increases from 0 to ~1.1, at which point ~5 % of the granules are in this size range. An increase in S_{max} >1.1 resulted in much more rapid growth, with a marked increase in the mass of granules >2000 µm when the conventional granulation process was used reflecting the point at which induction growth is triggered. For the reverse-phase process a steady increase in the mass of

granules >2000 µm is observed as S_{max} increases across the entire range studied. For each specific process, there were minimal differences in particle size of the granules as a function of S_{max} when either 10 or 20 % *w/w* PVP binder liquids were utilised (Figure 4-7 – Figure 4-9).

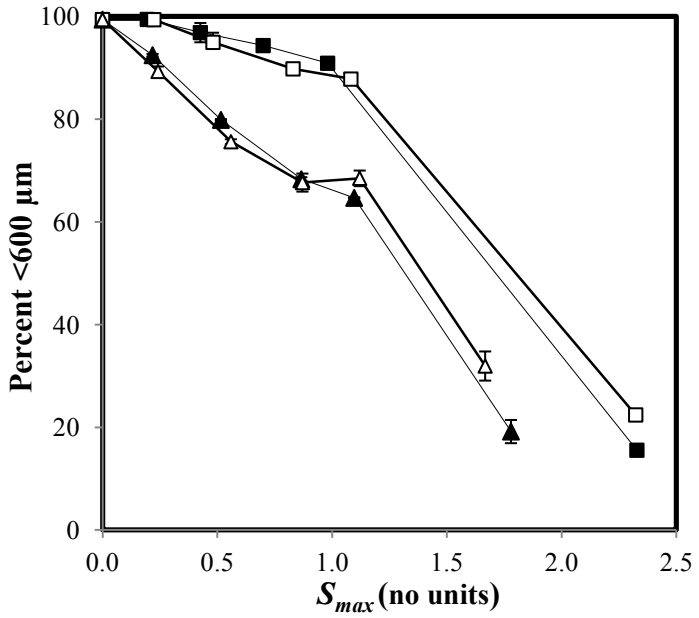

Figure 4-7. Percent of hydroxyapatite granules <600 µm as a function of liquid saturation, S_{max}. ■ 10 % w/w PVP by conventional granulation, □ 20 % w/w PVP by conventional granulation, ▲ 10 % w/w PVP by reverse-phase granulation, Δ 20 % w/w PVP by reverse-phase granulation. Error bars represent 1 SD, n=4.

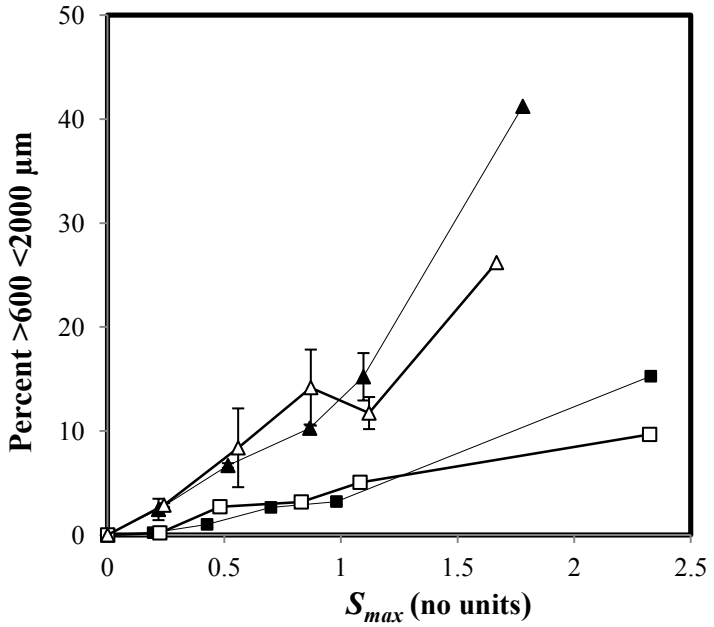

Figure 4-8. Percent of hydroxyapatite granules >600 µm and <2000 µm as a function of liquid saturation, S_{max}. ■ 10 % w/w PVP by conventional granulation, □ 20 % w/w PVP by conventional granulation, ▲ 10 % w/w PVP by reverse-phase granulation, Δ 20 % w/w PVP by reverse-phase granulation. Error bars represent 1 SD, n=4.

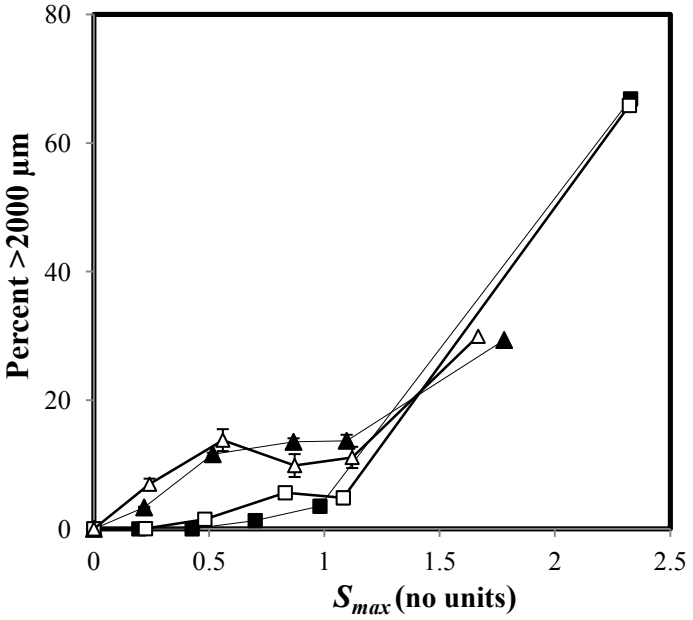

Figure 4-9. Percent of hydroxyapatite granules >2000 µm as a function of liquid saturation, S_{max}. ■ 10 % w/w PVP by conventional granulation, □ 20 % w/w PVP by conventional granulation, ▲ 10 % w/w PVP by reverse-phase granulation, Δ 20 % w/w PVP by reverse-phase granulation. Error bars represent 1 SD, n=4.

4.2.4 Bulk density, tapped density and Carr's index

Bulk density (Figure 4-10) increased as S_{max} increased to ~0.70–0.85 ($p < 0.05$ Wilcoxon). Above a S_{max} value of ~0.85 further increases in S_{max} resulted in a marked decrease in bulk density ($p < 0.05$ Wilcoxon). Tapped density (Figure 4-11) was unaffected as S_{max} increased to ~0.70–0.85 ($p > 0.05$ Wilcoxon). Above S_{max} of ~1 tapped density decreased markedly ($p < 0.05$ Wilcoxon). The Carr's index (Figure 4-12) decreased indicating an increase in the granule flowability for all granulation conditions as S_{max} increased to ~1 ($p < 0.05$ Wilcoxon). At S_{max} >1 a plateau ($p > 0.05$ Wilcoxon) in Carr's index was reached, with the values of the latter being between 13–19, which indicates fair to good flow properties [11]. The reverse-phase granulation process resulted in a lower Carr's index ($p < 0.05$ Wilcoxon) than when the conventional granulation process was employed whereas the PVP binder liquid concentration had no effect on Carr's index ($p > 0.05$ Wilcoxon).

The trends of these parameters can be explained in terms of the progression of the granulation process. As S_{max} increases from 0 to ~0.7–0.85 the granule size distribution broadens (Figure 4-4 and Figure 4-5), which increases the packing efficiency and hence the bulk density increases [31]. As S_{max} increases further above ~1 the proportion of particles <600 μm decrease markedly (Figure 4-7) and the proportion of granules >600 μm (Figure 4-8 and Figure 4-9) increased greatly. This reduced the packing efficiency creating a relatively open packing structure [32] and the bulk and tapped density decreased. A corresponding minimum in the Carr's index is obtained due to the decreased internal frictional properties of the granules [33].

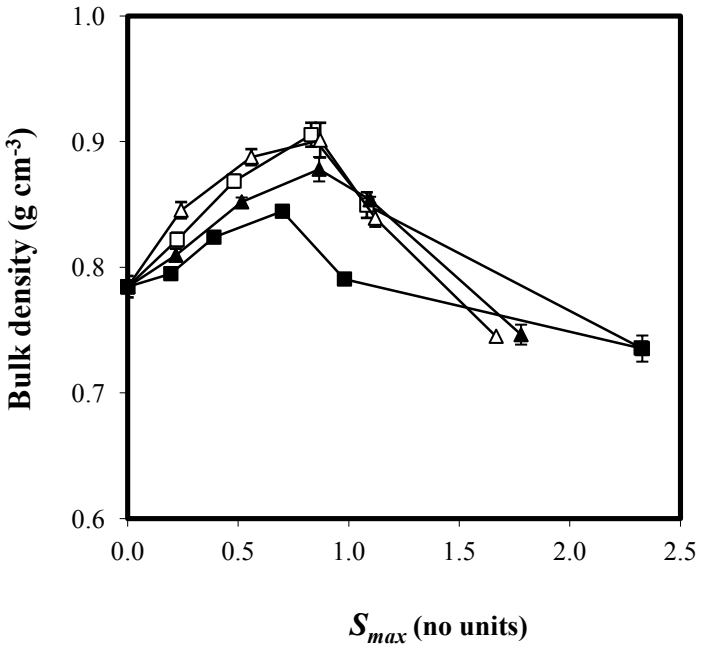

Figure 4-10. Hydroxyapatite granule bulk density as a function of liquid saturation, S_{max}. ■ 10 % w/w PVP by conventional granulation, □ 20 % w/w PVP by conventional granulation, ▲ 10 % w/w PVP by reverse-phase granulation, Δ 20 % w/w PVP by reverse-phase granulation. Error bars represent 1 SD, n=4.

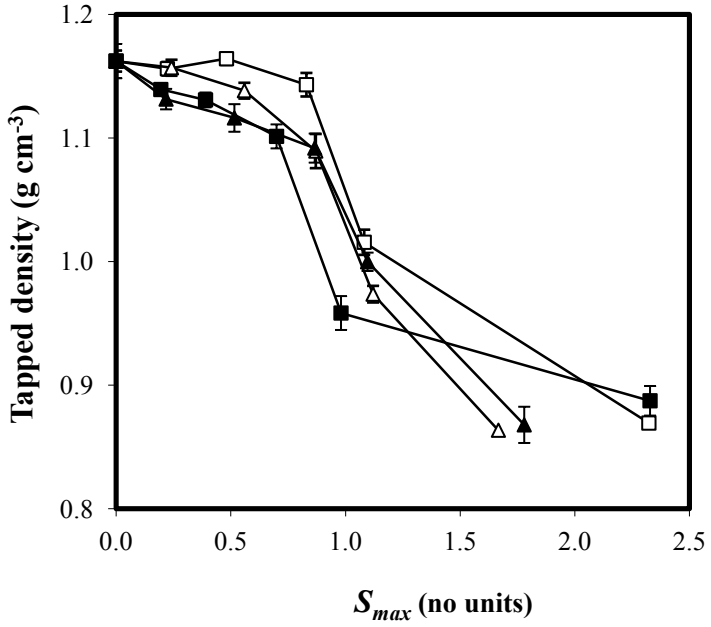

Figure 4-11. Hydroxyapatite granule tapped density as a function of liquid saturation, S_{max}. ■ 10 % w/w PVP by conventional granulation, □ 20 % w/w PVP by conventional granulation, ▲ 10 % w/w PVP by reverse-phase granulation, Δ 20 % w/w PVP by reverse-phase granulation. Error bars represent 1 SD, n=4.

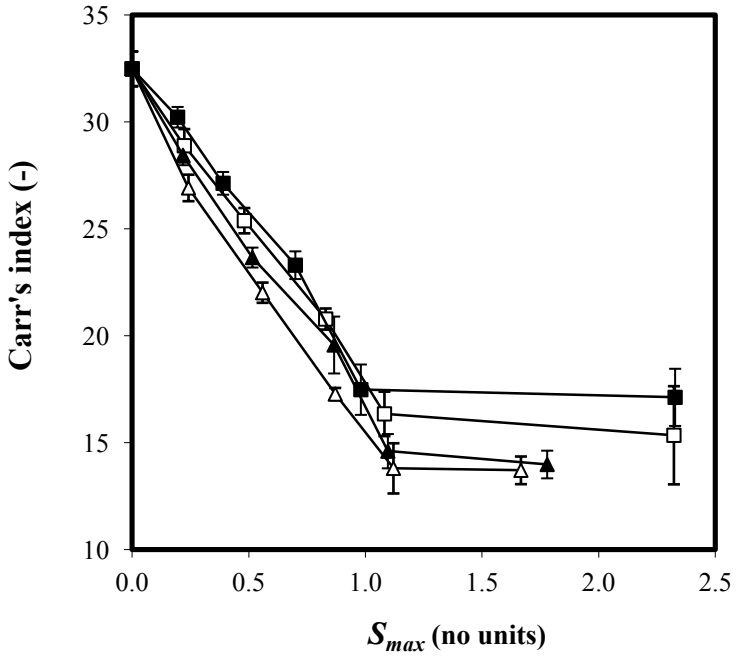

Figure 4-12. Hydroxyapatite granule Carr's index as a function of liquid saturation, S_{max}. ■ 10 % w/w PVP by conventional granulation, □ 20 % w/w PVP by conventional granulation, ▲ 10 % w/w PVP by reverse-phase granulation, Δ 20 % w/w PVP by reverse-phase granulation. Error bars represent 1 SD, n=4.

4.2.5 Intragranular porosity

Granule envelope density was measured using the GeoPyc® powder pycnometry apparatus and the results were corrected to approximate the mercury intrusion methodology using the linear regression calibration obtained as described in Section 2.2.3. Intragranular porosity was then calculated from the sample true and envelope densities (Equation 4-5). Intragranular porosity (Figure 4-13) decreased with increasing S_{max} for all granulation conditions.

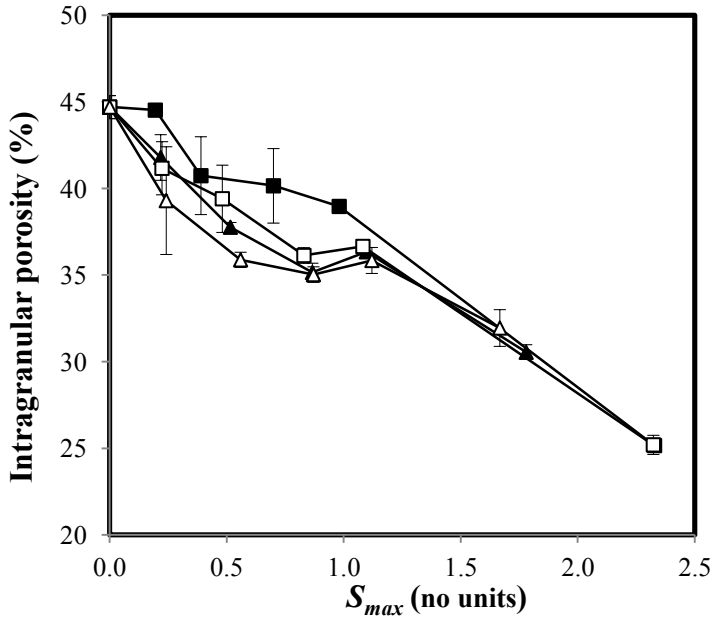

Figure 4-13. Hydroxyapatite granule porosity as a function of liquid saturation, S_{max}. ■ 10 % w/w PVP by conventional granulation, □ 20 % w/w PVP by conventional granulation, ▲ 10 % w/w PVP by reverse-phase granulation, Δ 20 % w/w PVP by reverse-phase granulation. Error bars represent 1 SD, n=4.

As S_{max} increased from 0 to 0.85 differences were observed between the conventional and reverse-phase granulation processes when considering the same binder liquid concentration. The reverse-phase process generated granules with lower intragranular porosity than the conventional process ($p < 0.05$ Wilcoxon), consistent with the greater granule growth seen for the reverse-phase process in this S_{max} range. At S_{max} >1 the differences in intragranular porosity become minimal with the maximum S_{max} achieved being ~2.3 for the conventional process and ~1.7 for the reverse-phase process. Both experiments were performed with 250 cm^3 of binder liquid. The difference in the S_{max}

achieved for this binder amount is explained by the intragranular porosity results; the conventional process consolidates to an intragranular porosity of ~25 % whereas the reverse-phase process consolidates to a higher intragranular porosity of ~30 %.

4.2.6 Effect of binder liquid viscosity

The results from this study show that the binder liquid viscosity has little to no effect on the physical properties of granules produced by both the reverse-phase and conventional granulation processes. Previous studies have reported on the effects of binder liquid properties on granules prepared using the conventional granulation process. Iveson *et al* [6] showed that there was an interaction between binder liquid content and viscosity. These researchers reported that an increase in content of a low viscosity binder (1 mPa.s) decreased the granule porosity, while an increase in content of a high viscosity binder (650 mPa.s) increased the granule porosity, yet an increase in content of intermediate viscosity binders (5.4 and 70 mPa.s) had minimal effect on porosity. These differences were attributed to the different relative contributions of interparticulate friction, viscous dissipation and capillary forces in resisting deformation. Johansen and Shaefer [34] reported that when using a lower binder viscosity of 66 mPa.s the granulation process proceeded by nucleation and coalescence mechanisms giving steady growth. However, when viscosity was increased above 760 mPa.s immersion of particles in the binder droplets dominated and growth proceeded by layering of particles on the surface of the agglomerates and granule growth was hindered.

In the present study the granule mass mean diameter increased (Figure 4-6) and granule porosity decreased (Figure 4-13) with increasing binder liquid content, with binder liquid viscosity having no effect ($p < 0.05$ Wilcoxon). The two binder liquid viscosities evaluated were 6.86 (10 % *w/w* PVP) and 33.70 mPa.s (20 % *w/w* PVP), both of which fall below the growth behaviour transition reported by Johansen and Shaefer [34] and within the intermediate viscosity range where Iveson *et al* [6] reported little effect on granule deformation. Considering these data one could suppose that the viscosity range evaluated in the present study was such that minimal differences existed in the contribution of the binder liquid viscosity on interparticulate friction, viscous dissipation and capillary forces resulting in the observed similarities in granule size and porosity.

4.2.7 Proposed reverse-phase granulation mechanism

Figure 4-14 shows the theoretical progression in S_{max} for both the conventional and reverse-phase granulation processes. The figure is based on 600 g of HA and 250 cm^3 of 10 % *w/w* PVP binder quantity being used in the granulation process. The x-axis represents the percentage of the formulation component added. For the conventional process the component added is the PVP binder liquid and the liquid:solid ratio is increased on the ordinate from 0–100 %, whereas for the reverse-phase process the component added is the HA powder and the liquid:solid ratio is decreased along the ordinates. The effect of three minimum porosity, ε_{min}, values considered representative of the granulation process were simulated in the figure; 25 %, 35 % and 45 %. For the purposes of this figure it is assumed that the ε_{min} reached is constant regardless of the amount of binder liquid added, however in reality an increase in binder liquid will change the consolidation behaviour of the granules and result in changes in ε_{min}, and therefore S_{max}, as the process proceeds.

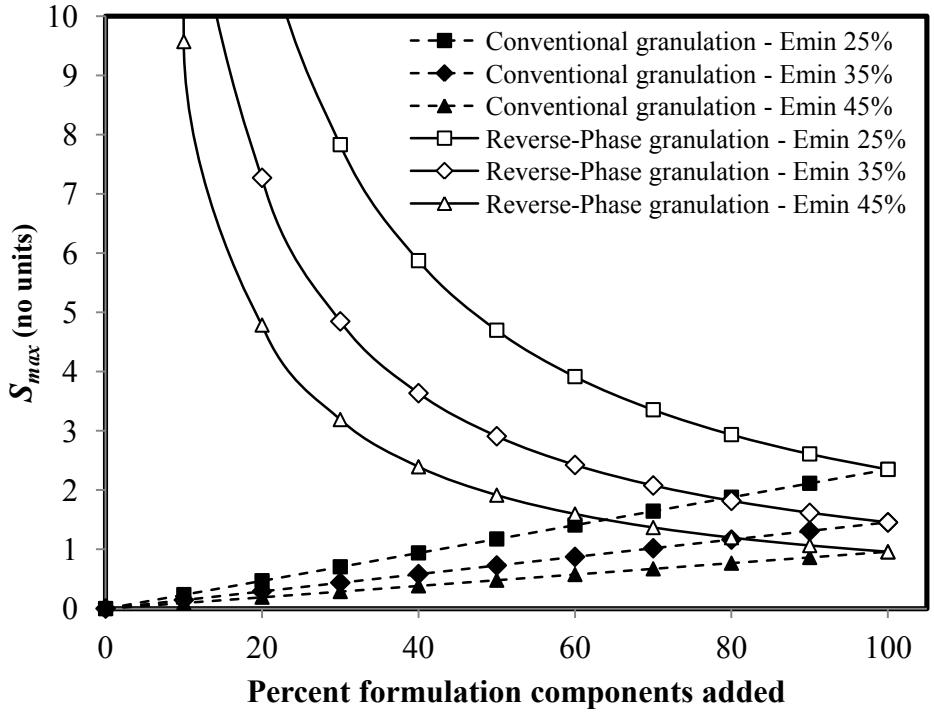

Figure 4-14. Plot of liquid saturation as a function of percent formulation components added showing the effect of different minimum intragranular porosity reached. For the conventional process the component added is 250 cm^3 10 % w/w PVP binder liquid. For the reverse-phase process the formulation component is 600 g hydroxyapatite powder.

The conventional granulation process undergoes a gradual linear increase in S_{max} as the binder liquid is added. In contrast the reverse-phase process undergoes a steep non-linear decrease in S_{max} as the HA powder is added. However, once all formulation components are added, i.e. 600 g HA and 250 cm^3 PVP binder liquid, both granulation processes reach identical S_{max} values provided that the same ε_{min} is achieved. As ε_{min} is decreased, i.e. granule consolidation occurs, the final S_{max} attained is increased. In the present study clear differences in intragranular porosity were observed at higher liquid:solid ratios, in particular the 250 cm^3 PVP:600 g HA experiments (Figure 4-3). In these cases the conventional granulation process reached a significantly lower intragranular porosity, and therefore greater S_{max}, than the reverse-phase process under identical conditions. This indicates that the method of granulation affected the consolidation behaviour of the granules and their subsequent performance. A proposed mechanism for the reverse-phase granulation process is presented in Figure 4-15.

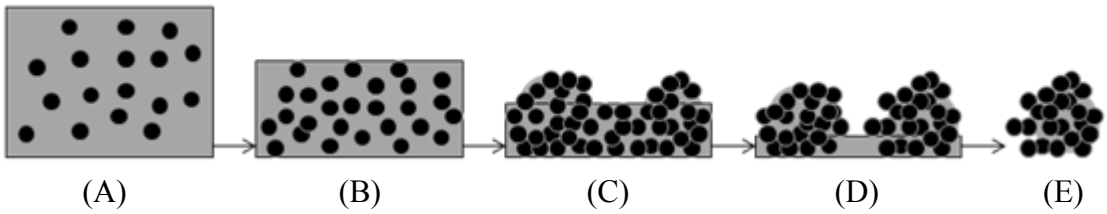

Figure 4-15. Proposed mechanism for the reverse-phase granulation process.

The proposed mechanism for granule growth in the reverse-phase process shows the state at the start of the process as a suspension of powder particles in binder liquid (Figure 4-15A). At this point only viscous and frictional forces act, which are insufficient to dissipate the collision energy of the impeller blade and particles rebound. The concentration of particles in the binder liquid is low such that the probability of a successful collision between two particles is low. As the process proceeds further dry powder is added and the suspension becomes more concentrated and binder is present within, around and between powder particles (Figure 4-15B). Further powder addition reaches a point where available binder liquid becomes limiting and powder begins to be deposited onto liquid saturated powder particles rather than directly into binder liquid (Figure 4-15C). Distribution of the binder liquid over the surfaces and within the dry powder is controlled by wet granule breakage and binder mechanical distribution by the impeller and chopper blades. At this point S_{max} is decreased significantly to a critical

point where capillary forces begin to act and granules begin to form (Figure 4-15D). At this stage equilibrium is reached between granule growth and breakage, the balance of which is determined by the collision energy provided by the impeller blade versus the strength of the wet granules (Figure 4-15E). This is the desired endpoint for both the reverse-phase and conventional granulation processes. Further addition of dry powder results in further decrease in S_{max} which eventually reaches a critical point below which further granule formation is limited.

4.3 Conclusions

The effects of S_{max} and binder liquid viscosity on a novel-reverse phase wet granulation process were investigated. The results were contrasted with those obtained using a conventional wet granulation process with the same formulation, equipment and process variables. Two important effects were reported. First, granule mass mean diameter increased with increasing S_{max} in all cases, with marked differences observed between the two processes. The conventional process exhibited induction growth behaviour, followed by uncontrolled growth at S_{max} >1.1. In contrast the reverse-phase process exhibited steady growth behaviour across the S_{max} range studied and uncontrolled growth was not observed. Second, intragranular porosity decreased with increasing S_{max}. In the S_{max} range ~0.2–1.0 use of the reverse-phase process resulted in lower intragranular porosity. At the highest binder volume studied, granules produced using the conventional process underwent a significantly greater decrease in intragranular porosity than those generated from the reverse-phase process. This resulted in a significant increase in S_{max}, which caused the observed uncontrolled growth for the conventional granulation process.

On the basis of these findings a growth mechanism for the reverse-phase wet granulation process was proposed. The process is depicted to proceed from a state where powder particles are suspended in binder liquid, with only viscous and frictional forces acting, and particles rebound upon collision. Further addition of dry powder increases the suspension concentration to a point where available binder liquid becomes limiting. Distribution of the binder liquid over the surfaces and within the dry powder is controlled by breakage and mechanical distribution. At this point S_{max} decreases significantly to a critical point where capillary forces begin to act and granules begin to form. At this stage equilibrium is reached between granule growth and breakage.

This study investigated the effect of binder liquid content and viscosity, while maintaining a constant impeller speed. However, impeller speed has been reported to have varying, and sometimes conflicting, effects on granule consolidation [35], growth [36] and breakage [37]. Since the mechanism for the reverse-phase granulation process has been shown to be sensitive to both granule consolidation and it is recommended that the effect of impeller speed be the focus of future study.

4.4 References

[1] Iveson, S.M., Beathe, J.A., Page, N.W., The dynamic strength of partially saturated powder compacts: the effect of liquid properties, Powder Technology, 127 (2002) 149-161.

[2] P.C. Kapur. Balling and Granulation *Advances in Chemical Engineering*, 1978, pp. 55-123.

[3] Rumpf, H. The strength of granules and agglomerates in: Knepper W.A., (Eds.) *Agglomeration*, Interscience-Wiley, New York, 1962, pp. 379-418.

[4] Newitt, D.M., Conway-Jones, J.M., A contribution to the theory and practice of granulation, Trans. I. Chem. Eng., 36 (1958) 422-430.

[5] Lian, G., Thornton, C., Adams, M.J., Discrete particle simulation of agglomerate impact coalescence, Chem. Eng. Sci., 53 (1998) 3381-3391.

[6] Iveson, S.M., Litster, J.D., Ennis, B.J., Fundamental studies of granule consolidation Part 1: Effects of binder content and binder viscosity, Powder Technology, 88 (1996) 15-20.

[7] Iveson, S.M., Litster, J.D., Fundamental studies of granule consolidation Part 2: Quantifying the effects of particle and binder properties, Powder Technology, 99 (1998) 243-250.

[8] Ohno, I., Hasegawa, S., Yada, S., Kusai, A., Moribe, K., Yamamoto, K., Importance of evaluating the consolidation of granules manufactured by high shear mixer, Int. J. Pharm, 338 (2007) 79-86.

[9] Nowak, E., Combes, G., Stitt, E.H., Pacek, A.W., A comparison of contact angle measurement techniques applied to highly porous catalyst supports, Powder Technology, 233 (2013) 52-64.

[10] Siebold, A., Walliser, A., Nardin, M., Oppliger, M., Schultz, J., Capillary rise for thermodynamic characterization of solid particle surfaces, Journal of Colloid and Interface Science, 186 (1997) 60-70.

[11] Carr, R.L., Evaluating flow properties of solids, Chem. Eng., 72 (1965) 163-168.

[12] Hausner, H.H., Friction conditions in a mass of metal powder, Int. J. Pow. Metal., 3 (1967) 7-13.

[13] Rastogi, S., Dhodapkar, S.V., Cabrejos, F., Baker, J., Weintraub, M., Klinzing, G.E., Wang, W.-C., Survey of characterisation techniques of dry ultrafine coals and their relationships to transport, handling and storage, Powder Technology, 74 (1993) 47-59.

[14] Haynes, W.M. CRC Handbook of Chemistry and Physics. 93rd, 2012-2013 ed.

[15] Chitu, T.M., Oulahna, D., Hemati, M., Wet granulation in laboratory scale high shear mixers: Effect of binder properties, Powder Technology, 206 (2011) 25-33.

[16] Kiekens, F., Zelko, R., Antal, I., Remon, J.P., Evaluation of substrate-binder interaction in a model granule system, Int. J. Pharm., 169 (1998) 175-182.

[17] Benali, M., Gerbaud, V., Hemati, M., Effect of operating conditions and physico-chemical properties on the wet granulation kinetics in a high shear mixer, Powder Technology, 190 (2009) 160-169.

[18] Vandendries, K., Vromans, H., Quantitative proof of liquid penetration-involved granule formation in a high shear mixer, Powder Technology, 189 (2009) 165-171.

[19] Hapgood, K.P., Litster, J.D., Biggs, S.R., Howes, T., Drop penetration time into porous powder beds, Journal of Colloid and Interface Science, 253 (2002) 353-366.

[20] Marston, J.O., Sprittles, J.E., Zhu, Y., Li, E.Q., Vakarelski, I.U., Thoroddsen, S.T., Drop spreading and penetration into pre-wetted powders, Powder Technology, 239 (2013) 128-136.

[21] Iveson, S.M., Litster, J.D., Growth regime map for liquid-bound granules, AIChE J., 44 (1998) 1510-1518.

[22] Kristensen, H.G., Holm, P., Schaefer, T., Mechanical properties of moist agglomerates in relation to granulation mechanisms: Part 1. Deformability of moist, densified agglomerates, Powder Technology, 44 (1985) 227-238.

[23] Iveson, S.M., Wauters, P.A.L., Forrest, S., Litster, J.D., Meesters, G.M.H., Scarlett, B., Growth regime map for liquid-bound granules: further development and experimental validation, Powder Technology, 117 (2001) 83-97.

[24] Carstensen, J.T., Hou, X., Compressibility of Anhydrous Tricalcium Phosphate, J. Pharm. Sci., 74 (1985) 466-468.

[25] Carstensen, J.T., Hou, X., Compression characteristics of basic tricalcium phosphate, Int. J. Pharm., 25 (1985) 207-215.

[26] Cartsensen, J.T., Hou, X., The Athy-Heckel Equation Applied to Granular Agglomerates of Basic Tricalcium Phosphate, Powder Technology, 42 (1985) 153-157.

[27] Shi, L., Feng, Y., Sun, C.C., Initial moisture content in raw material can profoundly influence high shear wet granulation process, Int. J. Pharm., 416 (2011) 43-48.

[28] Linkson, P.B., Glastonbury, J.R., Duffy, G.J., The mechanism of granule growth in wet pelletisation, Trans. I. Chem. Eng., 51 (1973) 251-257.

[29] Sastry, K.V., Panigraphy, S.C., Fuerstenau, D.W., Effect of wet grinding and dry grinding on the batch balling behaviour of particulate materials, Trans. Soc. Mining Engineers, 262 (1977) 325-331.

[30] Capes, C.E., Danckwerts, P.V., Granule formation by the agglomeration of damp powders: 1. The mechanism of granule growth, Trans. I. Chem. Eng., 43 (1965) 116-122.

[31] Furnas, C.C., Grading aggregates. I. Mathematical relations for beds of broken solids of maximum density, Ind. Eng. Chem., 23 (1931) 1052-1058.

[32] Orband, L.R., Geldart, D., The Use of an Antistatic Agent to Improve Powder Flowability, Particle Particle System Characterization, 12 (2005) 204-206.

[33] Chan, L.C.Y., Page, N.W., Particle fractal and load effects on internal friction in powders, Powder Technology, 90 (1997) 259-266.

[34] Johansen, A., Schaefer, T., Effects of interactions between powder particle size and binder viscosity on agglomerate growth mechanisms in a high shear mixer, Eur. J. Pharm. Sci., 12 (2001) 297-309.

[35] Saleh, K., Vialatte, L., Guigon, P., Wet granulation in a batch high shear mixer, Chem. Eng. Sci., 60 (2005) 3763-3775.

[36] Knight, P.C., Johansen, A., Kristensen, H.G., Schaefer, T., Seville, J.P.K., An investigation of the effects on agglomeration of changing the speed of a mechanical mixer, Powder Technology, 110 (2000) 204-209.

[37] Liu, L.X., Litster, J.D., Wet granule breakage in a breakage only high-shear mixer: Effect of formulation properties on breakage behaviour, Powder Technology, 189 (2009) 158-164.

CHAPTER FIVE: THE EFFECT OF IMPELLER SPEED AND BINDER LIQUID VISCOSITY ON A NOVEL REVERSE-PHASE WET GRANULATION PROCESS

5 Introduction

It is hypothesised that the reverse-phase granulation process can be controlled by a few simple variables, namely: binder liquid quantity, binder liquid viscosity and impeller speed (Section 1.7). The effects of binder liquid quantity and binder liquid viscosity at a constant impeller tip speed has been studied previously (Chapter 4). The use of the reverse-phase process was found to produce granules with a greater mass mean diameter and lower intragranular porosity when compared to those generated using the conventional granulation process under the same liquid saturation conditions. For both granulation processes the binder liquid viscosity was found to have no effect on granule mass mean diameter and intragranular porosity. The effect of impeller speeds on these relationships is of interest since this variable is known to impact granule consolidation [1], growth [2] and breakage [3]. Accordingly the effect of impeller speed and binder liquid viscosity upon granule properties provides the focus of the work described in this chapter.

An increase in impeller speed, when using the conventional granulation process, has been reported to increase granule consolidation and growth, but also increase granule breakage in high shear granulators, depending upon the formulation and process variables. Knight *et al* [2] found that as impeller speed in a high shear mixer increased there was an initial increase in granule size, followed by a subsequent reduction. At low impeller speeds the granules had high sphericity, while those at high impeller speeds had a more irregular shape, indicative of breakage phenomena. Saleh *et al* [1] studied the combined effects of liquid content and impeller speed on the granulation of alumina powder with aqueous PEG binders and reported that increasing liquid content and/or increasing impeller speed resulted in a decrease in granule porosity and an increase in pore saturation. The effect of impeller speed on granule size distribution of a gabapentin tablet formulation was found to be complex [4], due to the balance between the increase in growth but also the increase in breakage, making *a priori* prediction difficult without quantitative knowledge of the growth and breakage regimes.

Increasing impeller speed will increase the frequency and energy of impacts resulting in reduced granular porosity, and therefore increased liquid saturation [5-7]. An investigation of the breakage of glass ballotini and lactose particles found that the rate

of breakage was influenced by liquid saturation, binder liquid viscosity, binder liquid surface tension, and primary powder particle size [3]. The calculated Stokes deformation number, St_{def}, gave a good prediction of the breakage probability for each formulation and a boundary St_{def} value of 0.2 was proposed. The increase in impeller speed was thought to promote a shift from nucleation to steady or induction growth; and from steady growth to crumb behaviour. Such an observation could explain the apparently contrasting reports that increased impeller speed can both increase granule growth and increase granule breakage.

The breakage mechanism is considered very important in wet granulation processes as it is thought to influence, and potentially control, the final granule size distribution [3]. Iveson *et al* [8] discuss the relevance of granule consolidation in breakage, indicating that an increase in impeller speed will increase the collision velocity between granules. If the increase in collision energy is greater than the dissipation capacity of the system then colliding granules will rebound, which reduces the probability of granule coalescence and growth. Therefore the effect of impeller speed on granule consolidation, and porosity, should be considered along with the resultant granule particle size, in order to gain further insight into this phenomenon. Hoornaert *et al* [9] reported an increase in the rate of granule consolidation with increasing impeller speed, whereas in contrast Eliasen *et al* [10] reported a decrease in granule consolidation. The effects of impeller speed appear to depend upon the formulation and equipment variables selected and therefore warrant further study for the specific system in question.

Due to the fundamental differences between the reverse-phase and conventional granulation processes: i.e. the reverse-phase process starts from a condition characterised by a high S_{max} and the conventional process starts from a low S_{max} condition; it is proposed that an increase in impeller speed will have different effects. It is hypothesised that in the reverse-phase granulation process breakage of large moist agglomerates will control the final granule size, and that an increase in impeller speed will result in a greater extent of breakage and a reduced granule size. In contrast it may be suggested that use of the conventional granulation process will cause an increase in consolidation with increasing impeller speed, which might result in an increase in S_{max}, and a corresponding increase in granule size. There is the potential that for the

conventional process, at elevated impeller speed, the impact energy may not be able to be dissipated and granules may either rebound resulting in a minimal growth, or break resulting in a granule size decrease.

Given the possible differences in consolidation between the conventional and reverse-phase granules, the compaction properties of the latter may also be hypothesised to be different. A previous study by Carvajal and Macias [11] showed that as microcrystalline cellulose granule porosity decreased the granule strength increased according to an exponential relationship. They extended the finding by compressing the granules and showed that as the granule strength increased the tablet tensile strength decreased, again according to an exponential relationship. Based upon the proposed granulation mechanism for the reverse-phase process it is thought that the reverse-phase process may result in granules having a lower porosity, and therefore a greater strength, than granules produced using the conventional granulation process. The proposed less porous, stronger reverse-phase granules may therefore be expected to result in tablets with a lower tensile strength.

Accordingly, the aim of this study was to compare the effect of impeller speed and binder liquid viscosity on the physical and compaction properties of granules prepared using both the reverse-phase and conventional methods of granulation.

5.1 Materials and Methods

5.1.1 Materials

Hydroxyapatite (HA) (TRI-CAL WG^{TM}), poly (vinyl pyrrolidone) (PVP) (Plasdone K29/32) and Dry*Flo*® displacement media were obtained from the suppliers detailed in Section 2.1.1.

5.1.2 Granulation process

Aqueous granulation binder liquid was prepared as described in Section 2.1.2.1 and granules were prepared by both the novel reverse-phase described in Section 2.1.2.1 and the conventional granulation process described in Section 4.1.2. A summary of the experimental conditions is presented in Table 5-1.

Table 5-1. Summary of experimental conditions in both granulation methodologies studying the effects of binder liquid viscosity and impeller speed.

Binder liquid composition (% *w/w* PVP)	Binder liquid volume (cm^3)	Hydroxyapatite mass (g)	Impeller tip speed ($m\ s^{-1}$)
10	200	600	1.57 2.36 3.14 3.93 4.71
20	200	600	1.57 2.36 3.14 3.93 4.71

Binder liquid surface tension (Section 4.1.3.1), density (Section 4.1.3.2), viscosity (Section 4.1.3.3) and contact angle (Section 4.1.3.4) data used in this chapter are presented in Table 4-3. Granule size distribution (Section 2.1.2.3), bulk and tapped density (Section 2.1.2.4), Carr's index (Section 4.1.4.2), envelope density (Section 2.1.2.2) and intragranular porosity (Section 4.2.2) were determined as described previously.

5.1.3 Granule strength measurement

Granules prepared using the 20 % *w/w* PVP binder liquid, both the conventional and reverse-phase granulation processes, were sieved according to the method described in Section 4.1.4.1. Granules in the sieve fractions 425–600, 600–850, 850–1000, 1000–1700, 1700–2000 and 2000–3250 μm were retained and used for strength measurements. Granules were compressed individually (n=6) at a loading rate of 0.01 mm s^{-1} using a texture analyser (TA, Stable Micro Systems, Haslemere, UK) equipped with a 5 kg load cell and a 3 mm diameter stainless steel sample probe. The texture analyser load cell was calibrated prior to use using a 1 kg weight and the displacement transducer was calibrated prior to use by taking a zero distance reference measurement. The peak fracture force was determined for each granule tested as the first discontinuity in the force-displacement profile, which corresponded to the point where the granule cracked. The diameter of each granule was obtained from the force-displacement profile as the point at which the force increases above zero, i.e. the point at which the probe touches the granule. The granule fracture strength was calculated as [12]:

$$\sigma_g = \frac{4\ F_{\max}}{\pi\ D^2} \qquad \textit{Equation 5-1}$$

where σ_g is the granule fracture strength (MPa), F_{max} is the peak fracture force (N) and D is the granule diameter (mm). This equation assumes granules fracture in tension along a plane representing the initial diameter. All granules were monitored visually during fracture and measurements were rejected for any granules that were observed to slip, or crush, rather than undergo tensile failure.

5.1.4 Granule compaction

Granules from the retained sieve fractions in Section 5.1.3 were compressed into flat-faced compacts (n=6) weighing ~300 mg with a 10 mm diameter. The compaction was performed, as described in Section 3.1.10, with a compression force of 20 kN (250 MPa), tablet tensile strength was calculated as described in Section 3.1.6 and tablet porosity was calculated as described in Section 3.1.7. All granule samples and compacts were stored under monitored conditions (minimum and maximum values of 20–22 ºC

and 22–33 % RH) to ensure moisture was not a factor in the determination of mechanical strength based on the results presented in Chapter 3.

5.1.5 Statistical analysis

Statistical analysis to determine whether significant differences existed between sample means was performed as described in Section 2.1.2.8.

5.2 Results and Discussion

5.2.1 Liquid saturation and intragranular porosity

Liquid saturation was calculated as described in Section 4.2.2. The binder liquid volume was held constant at 200 cm^3 for all experiments based upon the results in Chapter 4 where an impeller speed of 400 rpm resulted in an S_{max} of ~1 for the conventional and reverse-phase granulation processes when either 10 or 20 % *w/w* PVP binder concentrations were used. S_{max} ~1 represents a theoretical threshold between nucleation and growth behaviour. An impeller speed range of 200–600 rpm was selected to generate granules with varying degrees of consolidation and S_{max} which would result in transitions in the growth behaviour, e.g. from nucleation at S_{max} <1 to growth at S_{max} >1. The variation in impeller speed also produced varying degrees of collision energy which was expected to promote transitions from growth to breakage behaviour.

According to Equation 4-3 S_{max} is inversely related to granule porosity. This relationship is evident in Figure 5-1 and Figure 5-2 which show the effect of impeller tip speed on intragranular porosity and S_{max} respectively.

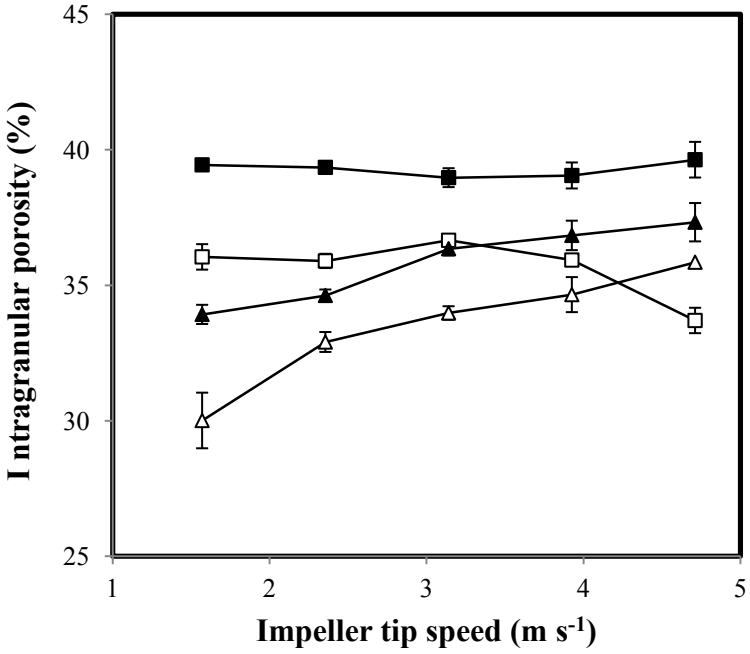

Figure 5-1. Hydroxyapatite granule porosity as a function of impeller tip speed. ■ 10 % w/w PVP by conventional granulation, □ 20 % w/w PVP by conventional granulation, ▲ 10 % w/w PVP by reverse-phase granulation, Δ 20 % w/w PVP by reverse-phase granulation. Error bars represent 1 SD, n=4.

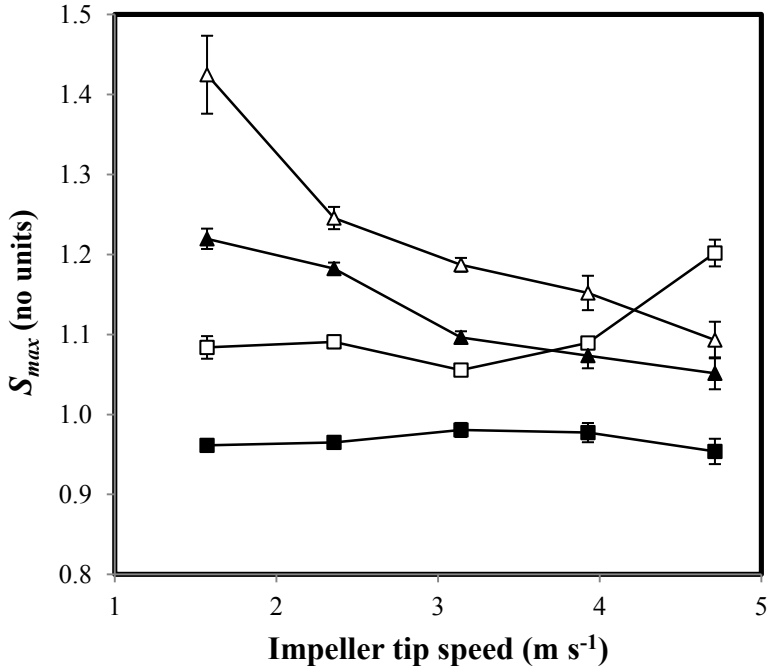

Figure 5-2. Hydroxyapatite granule liquid saturation, S_{max}, as a function of impeller tip speed. ■ 10 % w/w PVP by conventional granulation, □ 20 % w/w PVP by conventional granulation, ▲ 10 % w/w PVP by reverse-phase granulation, Δ 20 % w/w PVP by reverse-phase granulation. Error bars represent 1 SD, n=4.

For both the conventional and reverse-phase granulation processes the 20 % *w/w* PVP binder resulted in a lower intragranular porosity, therefore greater S_{max}, than the 10 % *w/w* PVP binder at the same impeller tip speed ($p < 0.05$ Wilcoxon). When the 10 % *w/w* PVP binder was used in the conventional process an increase in impeller tip speed had no effect on intragranular porosity and S_{max} ($p > 0.05$ Wilcoxon). The profile was similar when the 20 % *w/w* PVP binder was used with impeller tip speeds of 1.57–3.93 m s^{-1}. However, at increased impeller tip speeds of 3.93 and 4.71 m s^{-1} a reduction in intragranular porosity and increase in S_{max} occurred ($p < 0.05$ Wilcoxon). One possible explanation is that a critical collision velocity is reached above which appreciable granule consolidation takes place and liquid is squeezed from within the granule structure to the surface, consistent with the induction growth behaviour observed for the conventional granulation process at 3.14 m s^{-1} in Chapter 4.

The reverse-phase process produced an opposite trend. An increase in impeller tip speed increased intragranular porosity and reduced S_{max} ($p < 0.05$ Wilcoxon), indicating that the increased collision energy may not be dissipated by interparticulate friction, viscous or capillary forces within the granules. The excess energy is then dissipated as elastic

energy and the granules dilate or break. S_{max} is lower using the 10 % *w/w* PVP binder than when 20 % *w/w* was employed. It is likely that the 10 % *w/w* PVP may dissipate less energy through viscous forces, when compared to the use of 20 % *w/w* PVP binder, causing a more ready loss of elastic energy, and therefore increased granule dilation resulting in a decreased S_{max}.

The effect of S_{max} on granule mass mean diameter is presented in Figure 5-3. The data were obtained using both conventional and reverse-phase granulations processes, 10 and 20 % *w/w* PVP binder liquid concentrations and 1.57–4.71 m s^{-1} impeller tip speeds. Each granulation process and binder liquid concentration is described by a unique best fit relationship. The conventional process using 10 % *w/w* PVP produced minimal changes in S_{max} and granule mass mean diameter. All other granulation experiments showed a positive relationship between granule diameter and S_{max} indicating that by controlling the S_{max} of the granulation process the final granule mass mean diameter can be predicted.

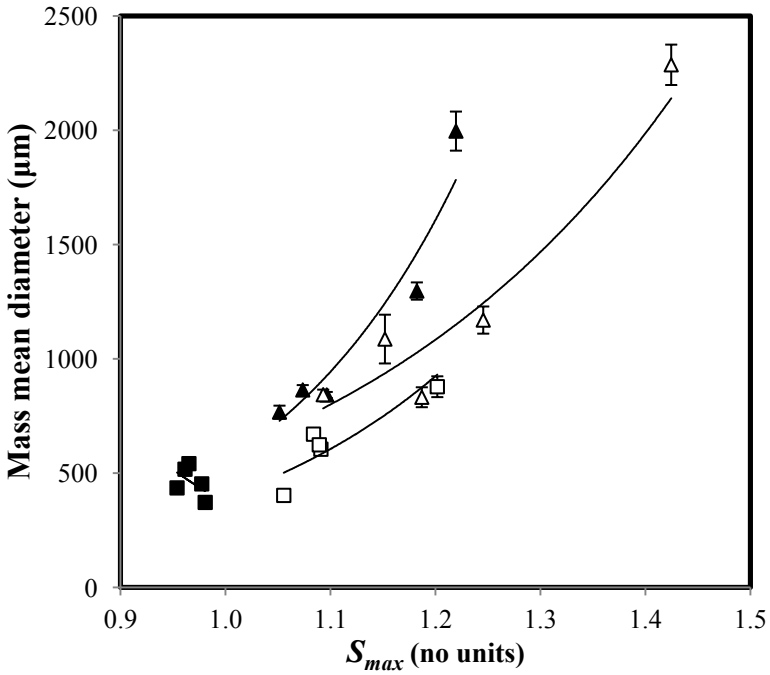

Figure 5-3. Hydroxyapatite granule mass mean diameter as a function of liquid saturation, S_{max}. ■ 10 % w/w PVP by conventional granulation, R^2 0.2448. □ 20 % w/w PVP by conventional granulation, R^2 0.7203. ▲ 10 % w/w PVP by reverse-phase granulation, R^2 0.9349. Δ 20 % w/w PVP by reverse-phase granulation, R^2 0.8727. Error bars represent 1 SD, n=4.

5.2.2 Granule particle size distribution

Granule size distribution plots were constructed for both the conventional and reverse-phase granulation processes at various impeller tip speeds (Figure 5-4 and Figure 5-5 respectively).

For the conventional process an impeller tip speed of 1.57 m s^{-1} resulted in a broad granule size distribution with the majority of particles in the 75–250 μm size range indicative of minimal granule growth. At impeller speeds of 2.36 m s^{-1} and 3.14 m s^{-1} there was a decrease in the percent of particles in the size range 1000–2000 μm and an increase in the percent of particles in the 75–425 μm indicating breakage occurred. As impeller tip speed increased further to 3.93 m s^{-1} and 4.71 m s^{-1} there was a small increase in the percent of particles in 2000–4750 μm size range indicating that the additional collision energy resulted in a small amount of granule consolidation and growth.

For the reverse-phase granulation process an impeller tip speed of 1.57 m s^{-1} resulted in a bimodal distribution with the primary mode centred around 4750 μm and the secondary mode centred around 250 μm. At impeller speeds of 2.36 m s^{-1} and 3.14 m s^{-1} there is a decrease in the percent of particles in the size range 3350–4750 μm and an increase in the percent of particles in the 75–425 μm indicating that marked breakage of the granules had occurred. As the impeller tip speed increased further to 3.93 m s^{-1} and 4.71 m s^{-1} there is minimal change in the granule size distribution. Binder viscosity appears to have a minimal effect on the granule size distribution for both the conventional and reverse-phase granulation process.

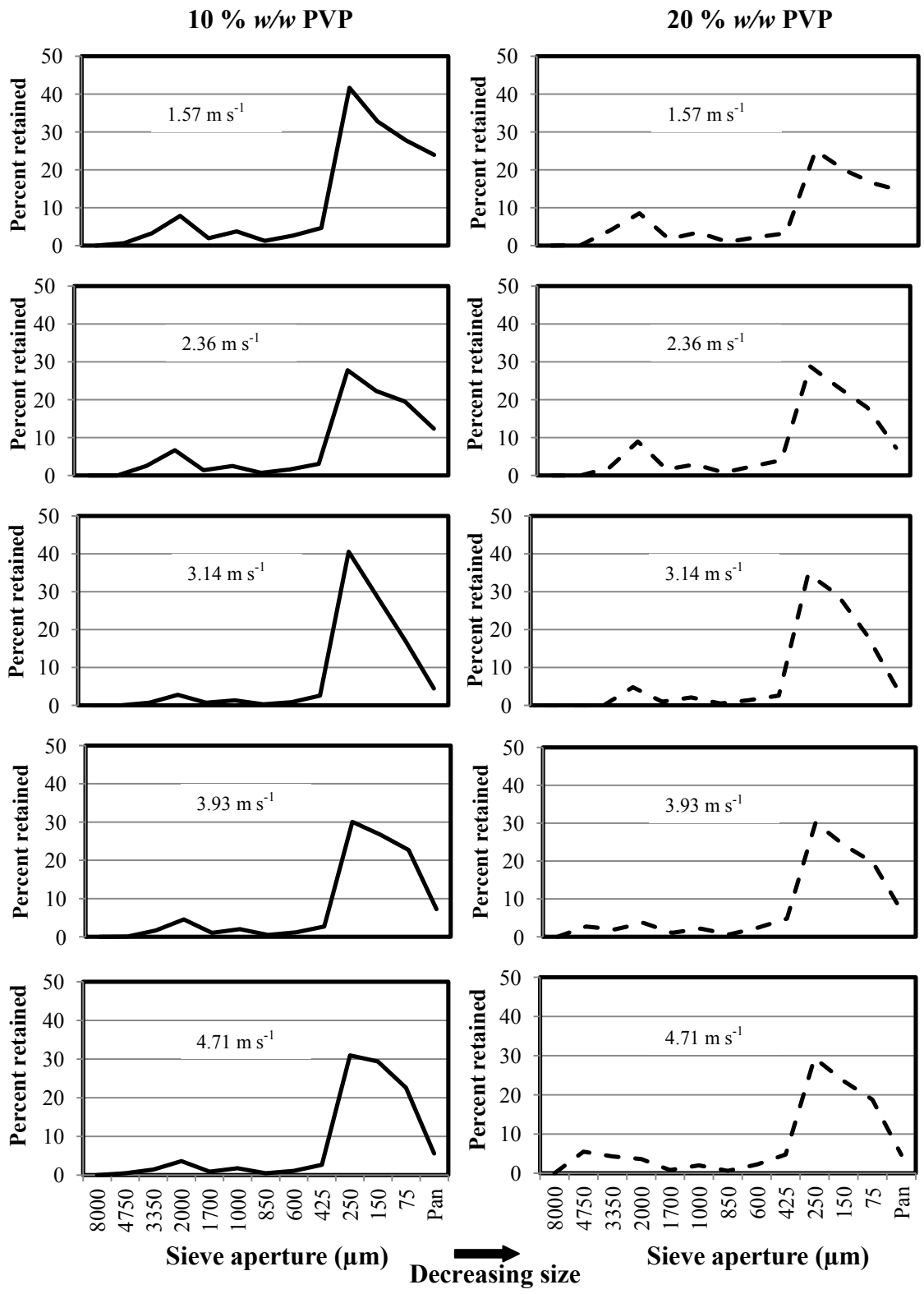

Figure 5-4. Size distribution for hydroxyapatite granules as a function of impeller tip speed. Granules were prepared using a conventional granulation process using 200 cm^3 binder liquid. Solid line represents 10 % w/w PVP binder, dashed line represents 20 % w/w PVP binder. Mean shown, n=4.

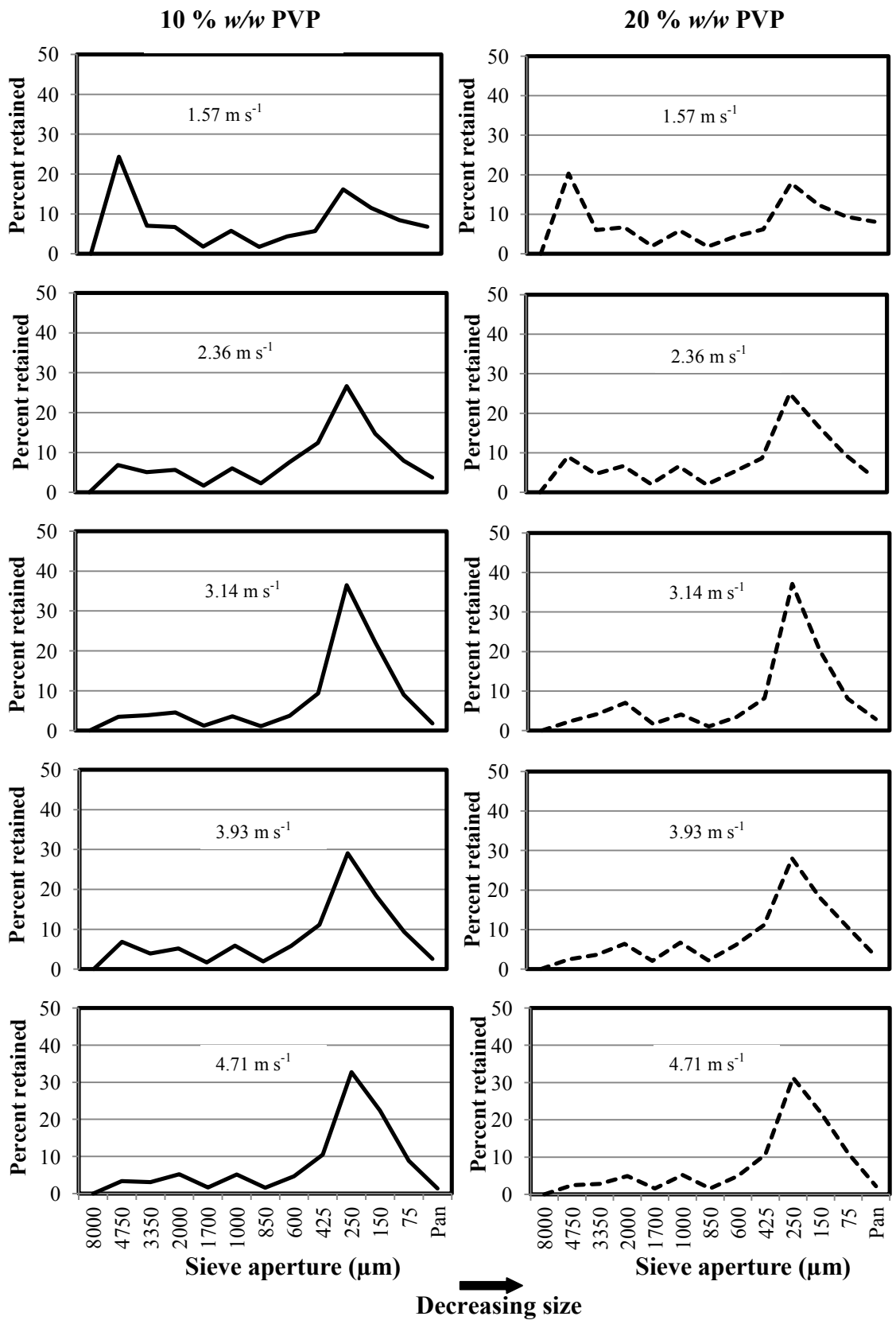

Figure 5-5. Size distribution for hydroxyapatite granules as a function of impeller tip speed. Granules were prepared using a reverse-phase granulation process using 200 cm^3 binder liquid. Solid line represents 10 % w/w PVP binder, dashed line represents 20 % w/w PVP binder. Mean shown, n=4.

When comparing the granule size distributions that were obtained using the conventional and reverse-phase processes clear differences were seen. The conventional process produced a greater proportion of granules with a small particle size (<600 μm) than the reverse-phase process at all impeller tip speeds. The proportion of granules in the intermediate size range (600–2000 μm) were approximately constant for all impeller tip speeds for both processes, however the reverse-phase produced ~10–15 % of the mass of particles in this category compared to ~3–6 % for the conventional process. The reverse-phase process generated a greater proportion of coarse granules (>2000 μm) at all impeller tip speeds than the conventional process. However, increasing the impeller tip speed reduced the total proportion of the coarse particles that were obtained using the reverse-phase process but increased when the conventional process was employed. To allow further analysis the effect of impeller tip speed on granule mass mean diameter was determined (Figure 5-6).

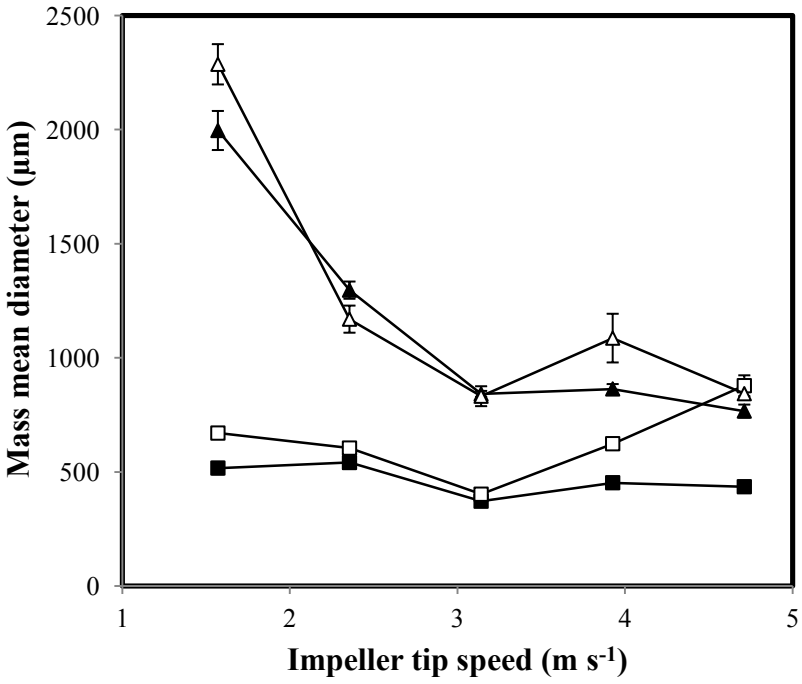

Figure 5-6. Hydroxyapatite granule mass mean diameter as a function of impeller tip speed. ■ 10 % w/w PVP by conventional granulation, □ 20 % w/w PVP by conventional granulation, ▲ 10 % w/w PVP by reverse-phase granulation, Δ 20 % w/w PVP by reverse-phase granulation. Error bars represent 1 SD, n=4.

The granule mass mean diameter obtained using the conventional process with 10 % *w/w* PVP binder concentration is insensitive to impeller tip speed (P >0.05 Wilcoxon). The conventional granulation incorporating 20 % *w/w* PVP binder produces granules

with a particle size which are decreased slightly ($p < 0.05$ Wilcoxon) as impeller tip speed increased from 1.57 to 3.14 m s^{-1}, however, at increased impeller tip speeds of 3.93 and 4.71 m s^{-1} the granule mass mean diameter increased ($p < 0.05$ Wilcoxon). This increase in granule mass mean diameter coincides with the increase in S_{max} shown in Figure 5-2. This behaviour for the conventional granulation process is consistent with the induction growth discussed previously in Section 4.2.3. At impeller tip speeds of 3.93 and 4.71 m s^{-1} the conventionally formed granules using 20 % *w/w* PVP likely undergo significant consolidation, and this forces liquid from within the granule structure to the surface. Such movement of fluid increases the S_{max} and facilitates coalescence and growth of the granules.

In contrast the use of the reverse-phase process resulted in a greater granule mass mean diameter than that obtained from the conventional process for all impeller tip speeds. The only exception to this observation was when conventional granulation was effected using 20 % *w/w* PVP and an impeller tip speed of 4.71 m s^{-1}, discussed above. A significant decrease ($P < 0.05$ Wilcoxon) in reverse-phase granule mass mean diameter occurs as impeller tip speed increased from 1.57 to 3.14 m s^{-1}. However, at even greater impeller tip speeds of 3.93 and 4.71 m s^{-1} a plateau ($p > 0.05$ Wilcoxon) occurred indicating a steady state between granule growth and breakage. The response of the reverse-phase process at the lower impeller speeds provides a useful means of process control; much more so than with the conventional granulation method if the objective is to produce granules with a pre-defined size.

These granule size distribution and mass mean diameter results can be explained if the concept of dimensionless spray flux [13] is considered, which quantifies the conditions in the nucleation zone of the granulator for a conventional granulation process as:

$$\Psi_a = \frac{3V}{2\, d_d\, v\, w_s} \qquad \textit{Equation 5-2}$$

where Ψ_a is the dimensionless spray flux, V is the liquid volumetric flow rate (m^3/s), d_d is the average droplet size (m), v is the powder surface velocity beneath the nozzle (m/s) and w_s is the width of the spray 90° perpendicular to the direction of powder flow (m).

The chances of a single droplet hitting the powder bed and being untouched by its nearest neighbor was modeled by Hapgood *et al* [14] as a Poisson distribution:

$$f_{(single\ drop)} = e^{-4\Psi_a} \qquad \textit{Equation 5-3}$$

For Ψ_a = 0.1, $f_{(single\ drop)}$ equals 0.67 which signifies a 67 % probability of a droplet hitting the powder bed and not overlapping another drop and a drop-controlled nucleation regime is likely. In contrast for Ψ_a = 1.0, $f_{(single\ drop)}$ equals 0.018, or a 1.8% chance of a droplet not overlapping another when it hits the powder bed and a mechanical distribution regime is likely. If Ψ_a is sufficiently large the surface of the powder bed will become over-wet and form large wet areas. The mechanical action of the granulator is then required to break up these wet areas and distribute the binder liquid. In this regime large granules from wet clumps are formed very early in the process resulting in a bimodal distribution [15, 16]. As the process progresses the larger granules consolidate and binder liquid is squeezed to their surfaces, which enables incorporation of fine un-granulated particles through a layering mechanism [17-19]. The ultimate size of the granules will then be determined by the breakage forces experienced in the granulator [20].

The reverse-phase process can be considered analogous to a situation where the Ψ_a is very large. The distribution of binder liquid, and the resultant granule size distribution, is therefore controlled by breakage of the large wet granules by impacts with the impeller. At lower impeller speeds granule breakage is less and large wet granules exist. This is seen as a bimodal distribution in Figure 5-5 for the 1.57 m s^{-1} experiment. As the impeller tip speed increased above 2.36 m s^{-1}, the degree of breakage and binder liquid distribution increased and the bimodal granules move to a uni-modal distribution of significantly lower mass mean diameter. This is consistent with the findings of van den Dries *et al* [21] where an increase in impeller speed improved granule homogeneity by increasing the extent of granule breakage.

An assessment of the granule size results for the reverse-phase process (Figure 5-5 and Figure 5-6) shows that breakage of large agglomerates appears to occur at an impeller speed between 1.57 and 2.36 m s^{-1}. This observation can be further explored by applying the work of Benali *et al* [22] who showed that the degree of mixing in a high

shear mixer depends on the competition between the gravitational force, F_g, and the centrifugal force, F_c , as shown in Equations 5-4 and 5-5:

$$F_{\mathrm{g}} = mg \qquad \textit{Equation 5-4}$$

$$F_{\mathrm{c}} = m\frac{(\pi N D_b)^2}{\left(\frac{D_b}{2}\right)} \qquad \textit{Equation 5-5}$$

where m is the wet powder mass, g is the acceleration due to gravity, N is the number of impeller rotations per unit time, and D_b is the diameter of the granulator bowl. The equilibrium between these forces occurs when a critical impeller tip speed, N_c, is reached:

$$N_c = \left(\frac{g}{2\pi^2 D_b}\right)^{1/2} \qquad \textit{Equation 5-6}$$

When calculated for the present reverse-phase granulation system a critical impeller tip speed of 1.82 m s^{-1} is obtained. In the present study only one impeller tip speed, 1.57 m s^{-1}, was below this critical value. At speeds below the critical value, gravitational forces dominate and mixing will be less efficient. In the case of the reverse-phase process the combination of poor mixing at this low impeller speed and high $\Psi_{a,}$ result in large over wet areas of the powder bed which cannot be dispersed mechanically and a bimodal particle size distribution results. As the impeller tip speed increased above the critical value the granule size progressed towards a uni-modal distribution indicating that improved mechanical dispersion occurred (Figure 5-5).

In contrast the conventional process operates at a much lower Ψ_a, therefore is closer to a drop-controlled regime and operating below the critical impeller speed does not impact the granule size distribution or mass mean diameter as shown by the plateau in granule mass mean diameter in Figure 5-6. The exception are the granules produced using the conventional process with 20 % *w/w* PVP binder which exhibited rapid induction growth at an impeller tip speed of 4.71 m s^{-1} as discussed in Section 5.2.1.

5.2.3 Modified capillary number

Granule consolidation and the resultant liquid bound granule strength is controlled by at least three forces: capillary forces, viscous forces and interparticulate friction [23]. In the current context interparticulate friction and viscous forces are dissipative in that they resist particle motion, whereas capillary forces are conservative in that they always act to pull particles together and therefore aid consolidation and resist dilation [23]. The effect of formulation variables, such as binder content and viscosity, and process variables, such as impeller speed, on the relative magnitude of these forces is complex to predict [24] and for this purpose a capillary number approach has been developed.

A viscous capillary number (Ca_{vis}) relating the ratio between viscous forces and static forces has been defined [5]:

$$Ca_{vis} = \frac{\mu v_o}{\gamma} \qquad \textit{Equation 5-7}$$

where, μ is the binder liquid viscosity (Pa.s), γ is the binder liquid surface tension (mN m^{-1}) and v_o is the speed of the particles (m s^{-1}). In a high shear mixer v_o may be approximated as equal to $\pi N D_b$, where N is the impeller speed and D_b is the granulator bowl diameter. It was found that if $Ca_{vis} < 10^{-3}$ viscous dissipation is negligible compared to capillary forces and that adhesion is the product of interfacial forces [5], whereas if Ca_{vis} is >1 viscous dissipation is dominant over capillary forces. Benali *et al* [22] later refined the approach and defined a modified capillary number (Ca^*) which takes a similar form but incorporates the work of adhesion of the binder liquid:

$$Ca^* = \frac{\mu v_o}{\omega} \qquad \textit{Equation 5-8}$$

where ω is the work of adhesion (N m^{-1}) equal to γ (1 + cosθ) and θ is the contact angle (°) of the binder liquid on the powder surface. In the latter study it was generalised that if $Ca^* < 1$ the interfacial forces are dominant and growth was not affected by binder viscosity and if $Ca^* > 1.62$ viscous forces dominate and control granule growth. Experimental data [22] suggests a Ca^* value of 0.80 represents the threshold between interfacial and viscous forces dominating, however as the next closest Ca^* values were

0.46 and 1.64 respectively the boundary value of 0.80 should be considered as approximate.

Figure 5-7 shows the relationship between *Ca** and the granule mass mean diameter for the data generated in the present study. An increasing *Ca** represents a decrease in the relative contribution of capillary forces and an increase in the viscous contributions of the binder liquid.

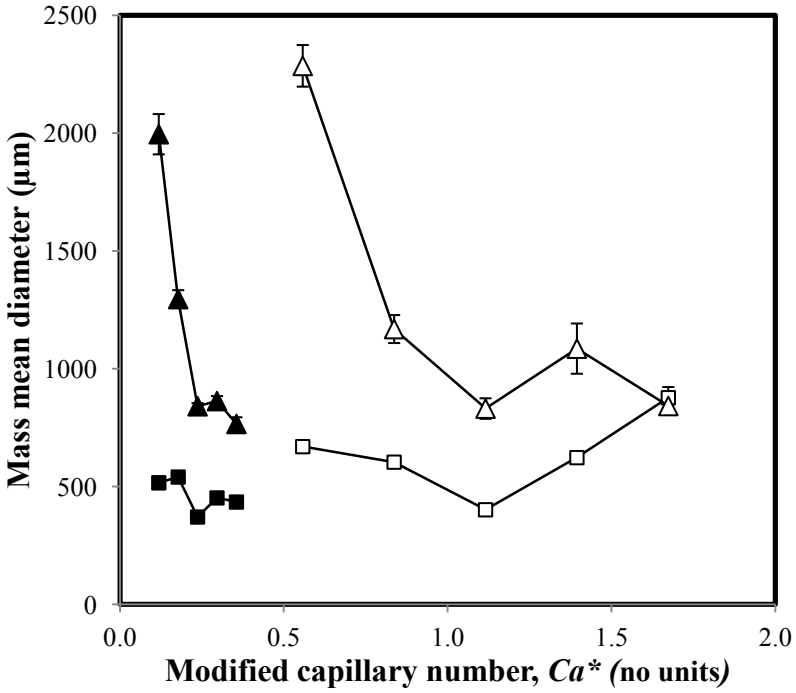

Figure 5-7. Hydroxyapatite granule mass mean diameter as a function of modified capillary number, Ca. ■ 10 % w/w PVP by conventional granulation, □ 20 % w/w PVP by conventional granulation, ▲ 10 % w/w PVP by reverse-phase granulation, Δ 20 % w/w PVP by reverse-phase granulation. Error bars represent 1 SD, n=4.*

The conventional granulation process produced granules with a mass mean diameter which was insensitive to *Ca** <0.8. At *Ca** >0.8, which only occurs for the 20 % *w/w* PVP, there is an increase in the mass mean diameter. This coincides with the decrease in intragranular porosity (Figure 5-1) and increase in S_{max} (Figure 5-2) observed for these experimental conditions, suggesting that an increase in the contribution of viscous forces facilitates granule consolidation and growth for the conventional granulation process.

For the reverse-phase process the granule mass mean diameter decreased as *Ca** increased to ~0.8, and at *Ca** >1.1 a plateau in granule mass mean diameter is reached. These data suggest that granule growth in the reverse-phase process may be driven by capillary forces consistent with the fact that the reverse-phase process facilitates a greater degree of capillary wetting of the particles that the conventional process. These findings are also in agreement with the proposed mechanism outlined in Section 4.2.7, where granule growth begins once S_{max} has decreased sufficiently such that capillary forces begin to contribute to wet granule strength.

The fact that the conventional granulation process appears to be driven by viscous forces, whereas the reverse-process appears to be driven by capillary forces, can be explained by the effect of viscosity on the time it takes binder liquid to penetrate into the granule pores. The penetration time is defined in Equation 5-9 [25]:

$$\tau_{CDA} = 1.37 \frac{V_d^{\frac{2}{3}}}{\left((1-\zeta)\varepsilon^*_{eff}\right)^2 R_{eff}} \frac{\mu}{\gamma \cos\theta} \qquad \textit{Equation 5-9}$$

where τ_{CDA} is the predicted drop penetration time, V_d is the drop volume, ζ is the proportion of the powder surface comprised of hydrophobic particles, ε^*_{eff} is the effective porosity of the powder bed, R_{eff} is the effective pore radius, μ is the binder viscosity, γ is the liquid surface tension and θ is the contact angle of the binder liquid on the powder bed.

During the conventional granulation process the penetration of liquid into particle or granule pores depends upon the liquid viscosity. Low viscosity liquids penetrate the granules faster than high viscosity liquids. An increase in impeller tip speed will increase the rate of consolidation and also increase the rate and extent of liquid penetration. Granule growth can only be expected once the granule pores have been saturated with liquid of sufficient viscous force to dissipate the collision energy. In the present study this occurs only for the 20 % *w/w* PVP at impeller tip speeds of 3.93 and 4.71 m s^{-1}.

In contrast the reverse-phase starts with complete saturation of the granule pores and therefore binder has already penetrated the pores and the concept of penetration time

has no meaning and effects of viscosity have little influence. Increases in impeller tip speed act to dilate the granule structure and act against capillary forces, therefore as *Ca** increases the mass mean diameter decreases. Above a critical point, at which viscous forces dominate and the contribution of capillary forces diminishes, there is little effect of *Ca** on mass mean diameter.

5.2.4 Bulk density, tapped density and Carr's index

Both bulk and tapped densities (Figure 5-8 and Figure 5-9) decreased marginally as impeller tip speed increased from 1.57 to 3.14 m s^{-1} ($p < 0.05$ Wilcoxon). A further increase in impeller tip speed to 3.93 m s^{-1} and 4.71 m s^{-1} result in both densities attaining plateau ($p > 0.05$ Wilcoxon), with the exception of the granules prepared using the 20 % *w/w* binder liquid and the conventional granulation, where bulk and tapped density increased ($p < 0.05$ Wilcoxon). An increase in impeller tip speed had no clear effect on Carr's index (Figure 5-10), however all granulation conditions resulted in granules with a Carr's index between 13–19 which indicates fair to good flow properties [26].

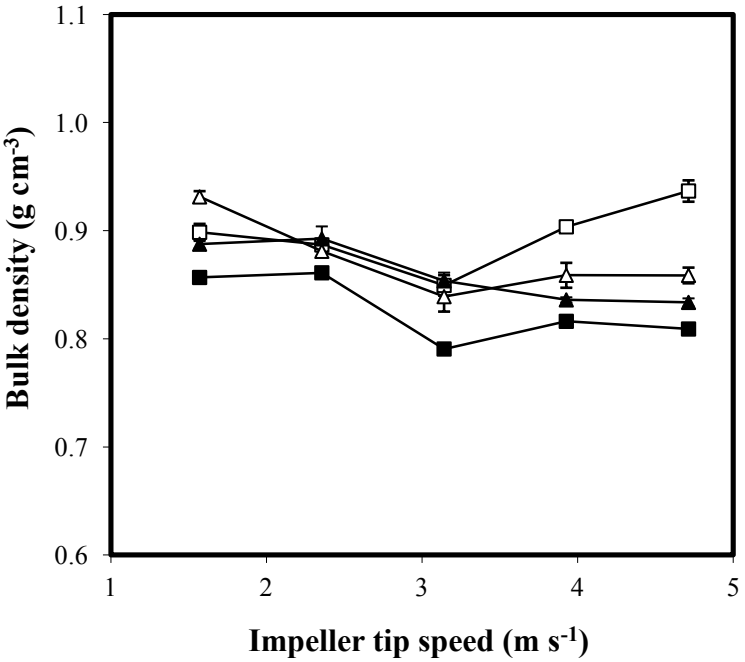

Figure 5-8. Hydroxyapatite granule bulk density as a function of impeller tip speed. ■ 10 % w/w PVP by conventional granulation, □ 20 % w/w PVP by conventional granulation, ▲ 10 % w/w PVP by reverse-phase granulation, Δ 20 % w/w PVP by reverse-phase granulation. Error bars represent 1 SD, n=4.

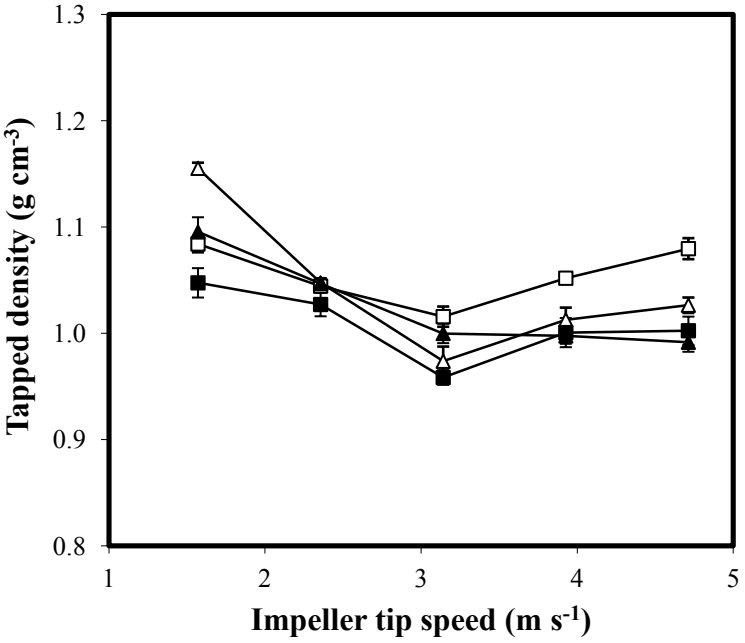

Figure 5-9. Hydroxyapatite granule tapped density as a function of impeller tip speed. ■ 10 % w/w PVP by conventional granulation, □ 20 % w/w PVP by conventional granulation, ▲ 10 % w/w PVP by reverse-phase granulation, Δ 20 % w/w PVP by reverse-phase granulation. Error bars represent 1 SD, n=4.

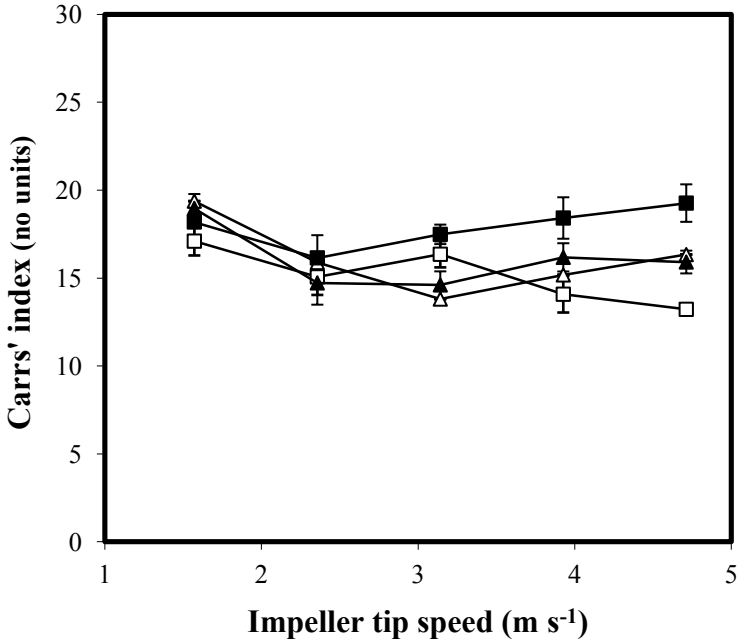

Figure 5-10. Hydroxyapatite granule Carr's index as a function of impeller tip speed. ■ 10 % w/w PVP by conventional granulation, □ 20 % w/w PVP by conventional granulation, ▲ 10 % w/w PVP by reverse-phase granulation, Δ 20 % w/w PVP by reverse-phase granulation. Error bars represent 1 SD, n=4.

5.2.5 Granule breaking strength

Granule size fractions with size cuts corresponding to 425–600, 600–850, 850–1000, 1000–1700, 1700–2000 and 2000–3250 μm were collected from both the conventional and reverse-phase granulation processes with impeller tip speeds of 1.57, 2.36, 3.14, 3.93 and 4.71 m s^{-1}. Individual granules were compressed using a texture analyser and the peak fracture force and granule diameter were used to calculate the granule strength. The results are presented in Figure 5-11 and Figure 5-12 for granules obtained using the conventional granulation process and Figure 5-13 and Figure 5-14 for those obtained using the reverse-phase granulation process. The mean granule strength results are presented as a function of impeller tip speed and then as a function of mean size fraction to allow visualisation of both effects.

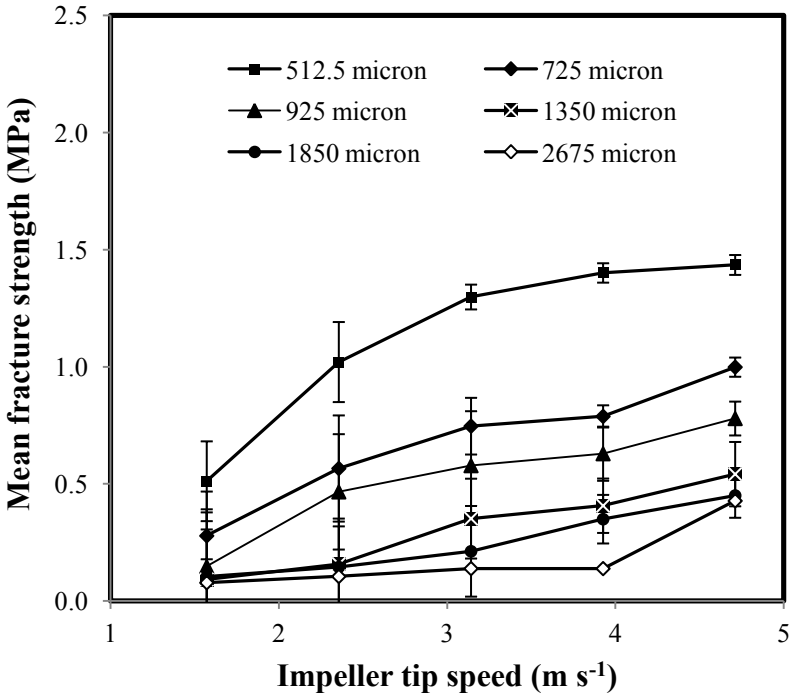

Figure 5-11. Hydroxyapatite mean granule fracture strength as a function of impeller tip speed for different granule size fractions. Granules were prepared using a conventional granulation process using 200 cm^3 of 20 % w/w PVP binder liquid. Error bars represent 1 SD, n=6.

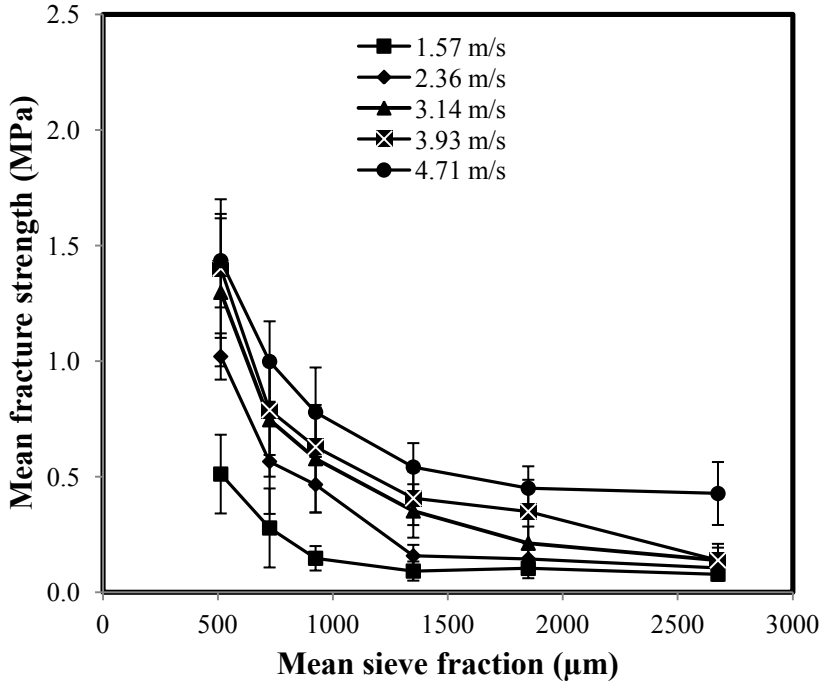

Figure 5-12. Hydroxyapatite granule mean fracture strength as a function of mean of granule size fraction. Granules were prepared using a conventional granulation process using 200 cm^3 of 20 % w/w PVP binder liquid at different impeller speeds. Error bars represent 1 SD, n=6.

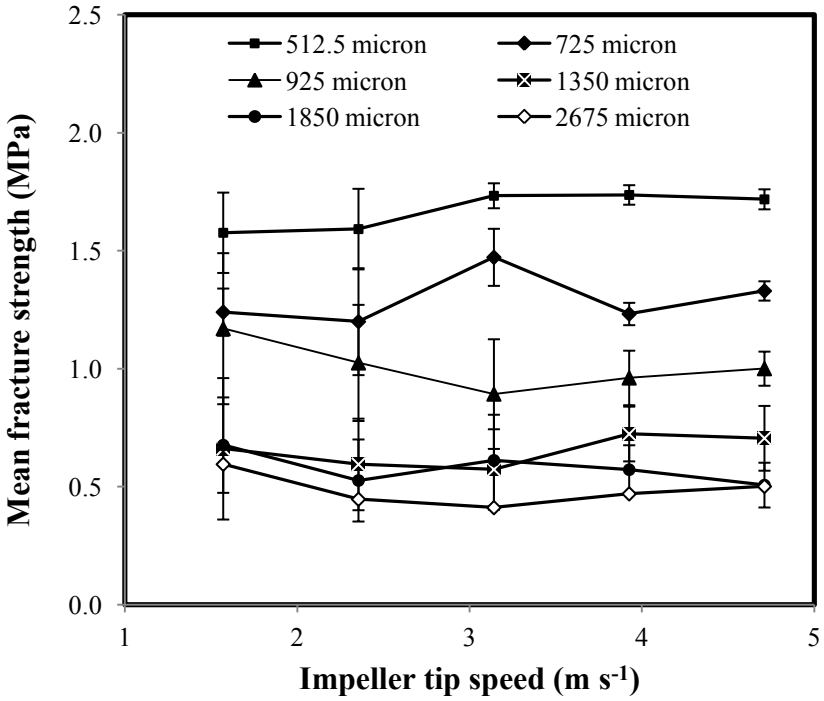

Figure 5-13. Hydroxyapatite mean granule fracture strength as a function of impeller tip speed for different granule size fractions. Granules were prepared using a reverse-phase granulation process using 200 cm^3 of 20 % w/w PVP binder liquid. Error bars represent 1 SD, n=6.

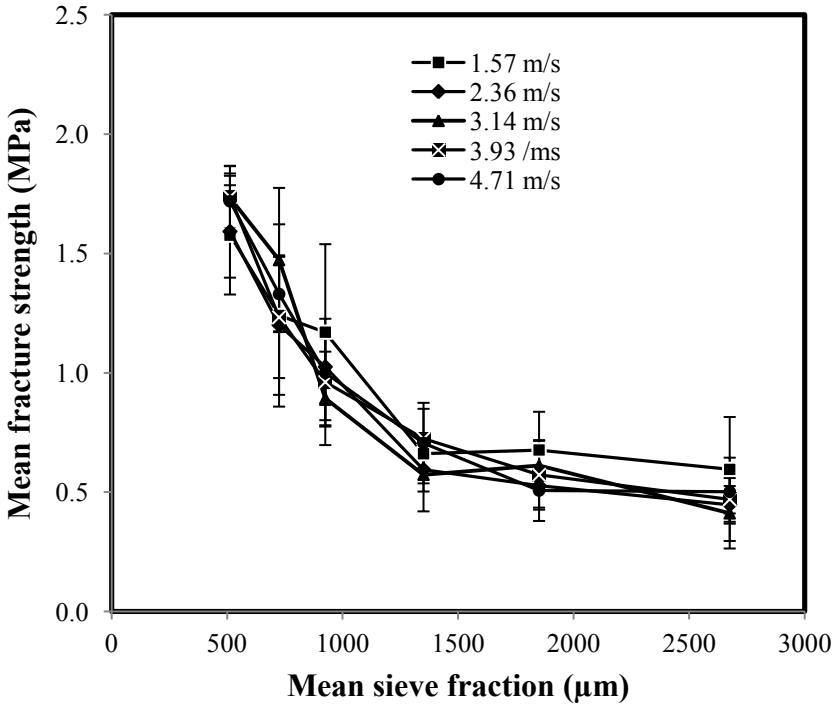

Figure 5-14. Hydroxyapatite mean granule fracture strength as a function of mean of granule size fraction. Granules were prepared using a reverse-phase granulation process using 200 cm^3 of 20 % w/w PVP binder liquid at different impeller speeds. Error bars represent 1 SD, n=6.

For the conventional granulation process an increase in the impeller tip speed from 1.57 to 4.71 m s^{-1} resulted in an increase in the mean granule strength ($p < 0.05$ ANOVA) for all granule size fractions (Figure 5-11) and as the granule size fraction increased from 425–600 to 2000–3350 µm the mean fracture strength decreased ($p < 0.05$ ANOVA) (Figure 5-12). For the reverse-phase process an increase in impeller tip speed had no effect ($p > 0.05$ ANOVA) on mean granule strength (Figure 5-13) whereas an increase in granule size fraction from 425–600 to 2000–3350 µm resulted in a decrease ($p < 0.05$ ANOVA) in the mean fracture strength (Figure 5-14). From these data two major observations are apparent. First, the mean fracture strength of granules from the conventional process is sensitive to impeller tip speed, while the reverse-phase granules are not. Second, for both granulation processes, as granule size fraction increases the mean fracture strength decreases. Each is discussed separately.

5.2.5.1 Effect of granulation process on mean granule fracture strength

Due to the limited quantity of granules in each size fraction porosity analysis (either by powder pycnometry or mercury porosimetry) was not possible. However, consideration of the Rumpf model for granule strength [27] can assist in understanding the differences in mean fracture strength obtained for granules produced using the conventional and reverse-phase granulation processes:

$$\sigma_d = \frac{1-\varepsilon}{\varepsilon}\frac{F}{D^2} \qquad \textit{Equation 5-10}$$

where σ_d is the dry granule strength (MPa), ε is the granule porosity (no units), F is the mean fracture force (N) and D is the diameter of the primary particles (mm).

The model predicts that as granule porosity decreases the granule strength increases for particles of a given size. Previously reported studies support this model. For example the relationship between the porosity and strength of microcrystalline cellulose granules, comprising 12 size fractions in the size range 53–1190 μm, has been modelled using the Rumpf equation [11]. Additionally, granulation of calcium carbonate with 65 % *w/w* aqueous PEG 4000 binder liquid at different impeller speeds showed that as the porosity of granules in the size fraction 500–600 μm decreased from 38.6 to 16.1 % the mean fracture force increased from 0.24 to 2.30 N [28]. Similarly, a second study employing the same formulation and granule size fraction produced with a higher range of impeller speeds showed that as the granule porosity decreased from approximately 38 to 28 % the mean fracture force increased from approximately 0.5 to 2.0 N [29].

In conventional granulation processes granule growth occurs by the formation of liquid bridges between particles. As particles collide with each other, the impeller and granulator bowl, they consolidate and decrease in porosity. When the impeller tip speed is increased the magnitude and frequency of the collisions increases and a greater degree of consolidation occurs. This increased consolidation results in the observed increase in dry granule strength [29]. In contrast the proposed mechanism for the reverse-phase granulation process (Figure 4-15) depicts granules with closely packed particles and fully saturated pores. As granules collide the probability of consolidation

is lower since the granules are already near their minimum porosity. An increase in impeller speed will increase the collision energy, however since the interparticulate distance is already smaller than that of the conventional process, relatively less consolidation will take place and granules will be at approximately their maximum strength. Consequently, the increase in impeller tip speed in the current study has no effect on mean fracture strength of granules prepared using the reverse-phase process. This explanation is further supported by the fact that granules prepared using the reverse-phase process have a greater mean fracture strength than the granules prepared using the conventional granulation process.

5.2.5.2 Effect of granule size fraction on mean granule fracture strength

In practice it is typically observed that large agglomerates are more prone to fracture, since larger agglomerates are comprised of a greater number of primary particles, therefore a greater number of contact points and flaws exist through which cracks can propagate and cause fracture [30]. When considering the smaller granule size there is a higher probability that an individual particle may be the same length as the diameter of the granules and be positioned in the same orientation as the applied stress. This results in measurement of the fracture strength of individual particles rather than the strength of solid bridges between particles which would be expected to be weaker. It should also be considered that in the dynamic situation of the granulation process larger agglomerates would also be expected to undergo increased breakage, since for a given impact force the larger the size of the agglomerate the greater the momentum and the larger the stress that will be exerted on a weak point into the microstructure, i.e. a flaw or crack [30].

5.2.6 Granule compaction properties

Flat-faced compacts of ~300 mg mass and 10 mm diameter were prepared using a compaction pressure of 250 MPa for granule size fractions of 425–600, 600–850, 850–1000, 1000–1700, 1700–2000 and 2000–3250 μm obtained using both the conventional and reverse-phase processes at impeller tip speeds of 1.57–4.71 m s^{-1}. Compact solid fraction, tensile strength and elastic recovery were calculated for each set of experimental conditions.

5.2.6.1 Effect of impeller tip speed on tablet tensile strength

A plot of tablet tensile strength as a function of granule mean fracture strength was constructed as presented in Figure 5-15. There is no correlation between mean granule fracture strength and the tablet tensile strength and the granulation process, impeller speed and granule size fraction have no effect ($p > 0.05$ ANOVA). This data rejects the original hypothesis which stated that an increase in granule strength may result in a decrease in the tablet tensile strength.

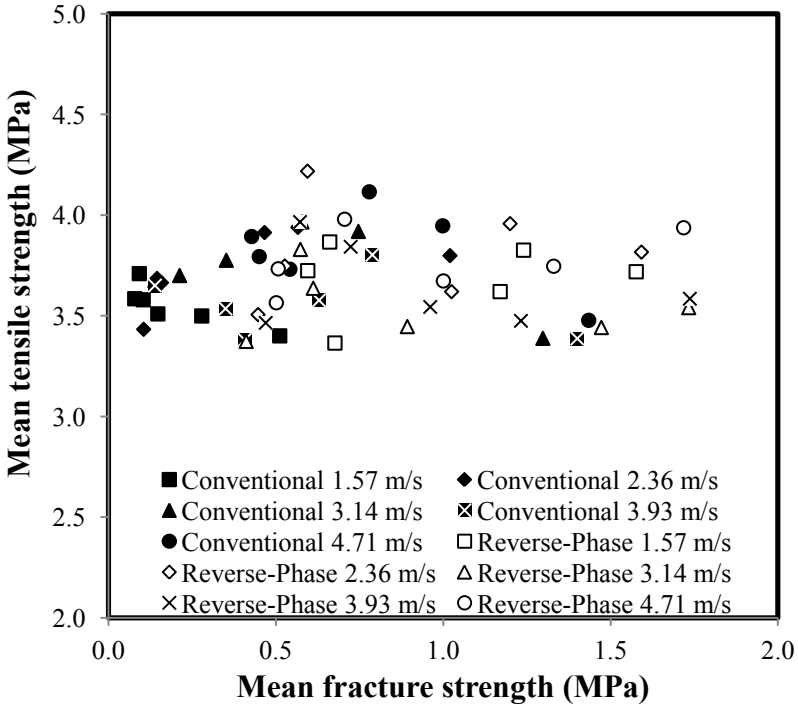

Figure 5-15. Mean tablet tensile strength as a function of hydroxyapatite granule mean fracture strength for different granule size fractions. Granules were prepared using both the conventional and reverse-phase granulation processes using 200 cm^3 of 20 % w/w PVP binder liquid at different impeller speeds, n=6.

The original hypothesis was based upon the findings of Carvajal and Macias [11] who reported that as the strength of microcrystalline cellulose granules increased over the range 0.69–54.49 MPa, the tensile strength of tablets compressed at a pressure of 700 MPa decreased from 6.77–0.23 MPa, according to an exponential relationship. In the present study the range of mean granule fracture strength (Section 5.2.5) was 0.079–1.737 MPa and granules were compressed at a compaction pressure of 250 MPa but showed no decrease in tablet tensile strength. The main differences between the studies

were the mean granule fracture strength and the compaction pressure evaluated with the microcrystalline cellulose granules having markedly greater strength and being compressed at a greater compaction pressure. In the microcrystalline cellulose example the granule strength was determined using the Kawakita equation where compaction data is used to calculate granule strength whereas the present study determined the granule strength by fracturing individual granules. The difference in methodology may have contributed to the observed differences in granule strength. Nevertheless, in the case of the microcrystalline cellulose granules the maximum granule strength evaluated was ~7.8 % of the maximum compaction pressure, whereas in the present study the maximum granule strength evaluated was ~0.69 % of the maximum compaction pressure. It is most likely that the granule strength differences observed in the present study were overwhelmed and masked as a consequence of the compaction pressure employed during tablet compaction. It should be noted that the 250 MPa which overwhelmed these differences is considered a typical tablet compaction pressure used in commercial pharmaceutical manufacturing operations indicating that the observed variations in HA granule fracture strength were of no practical significance to the compaction process.

The effect of impeller tip speed on the mean tablet tensile strength was evaluated for each granule size fraction obtained using both granulation processes. The results for the conventional process are presented in Figure 5-16 and for the reverse-phase process in Figure 5-17. Based on the fact that tablet tensile strength was not correlated with the granule fracture strength, and therefore granule porosity, the primary variable being evaluated in these figures is granule size fraction. The results show that no differences ($p > 0.05$ ANOVA) are observed as a result of the granulation process, impeller tip speed or granule size fraction. This is likely due to the fact that granules are a composite of HA primary particles held together primarily by PVP solid bridges. During compaction the granules will fragment into smaller particles, at relatively low compaction pressure, the size of which will be determined to a large extent by the particle size of the primary particles. These primary particles will then undergo plastic and elastic deformation at elevated compaction pressures. Since all granulation experiments used a common batch of HA it is expected that regardless of the size of the granule they will fragment into primary particles of approximately similar size with similar deformation properties.

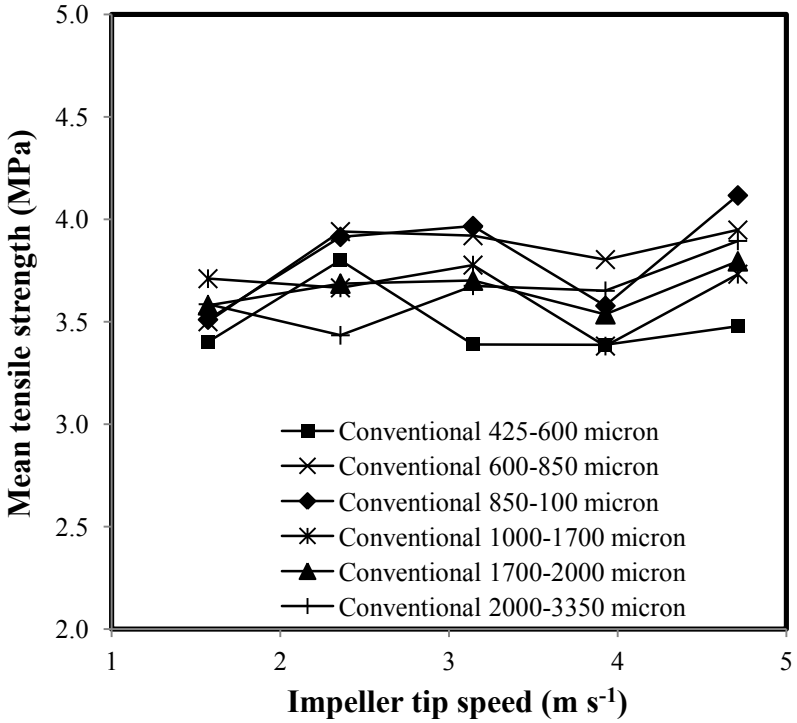

Figure 5-16. Mean hydroxyapatite tablet tensile strength as a function of impeller tip speed for different granule size fractions. Granules were prepared using a conventional granulation process using 200 cm^3 of 20 % w/w PVP binder liquid, n=6.

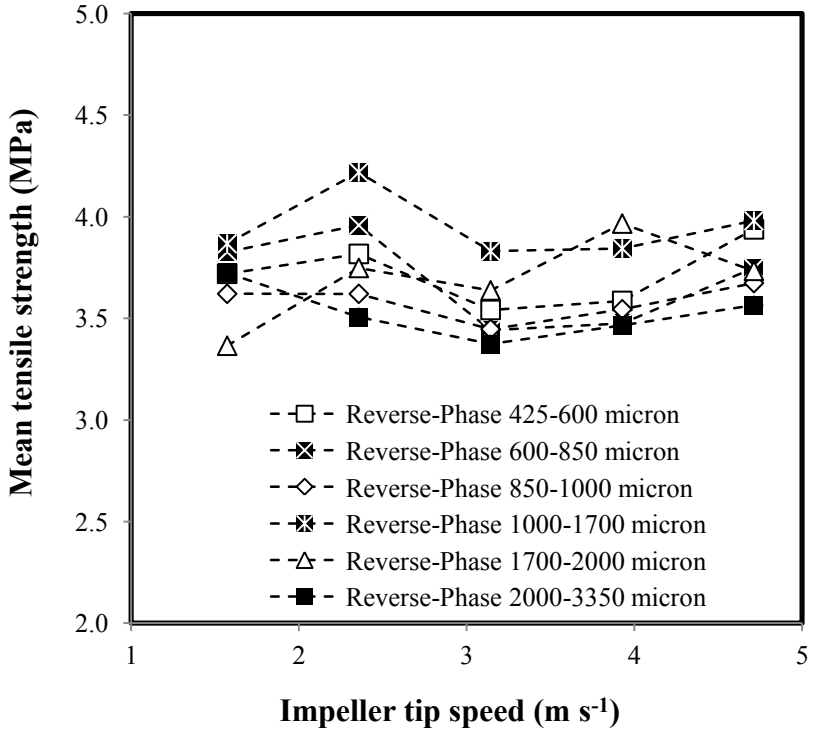

Figure 5-17. Mean hydroxyapatite tablet tensile strength as a function of impeller tip speed for different granule size fractions. Granules were prepared using a reverse-phase granulation process using 200 cm^3 of 20 % w/w PVP binder liquid, n=6.

As discussed in Section 3.2.3.3 the compactibility of HA tablets is well described by a plot of tablet solid fraction against tablet tensile strength. For the granules generated in this chapter the compactibility plot is presented in Figure 5-18.

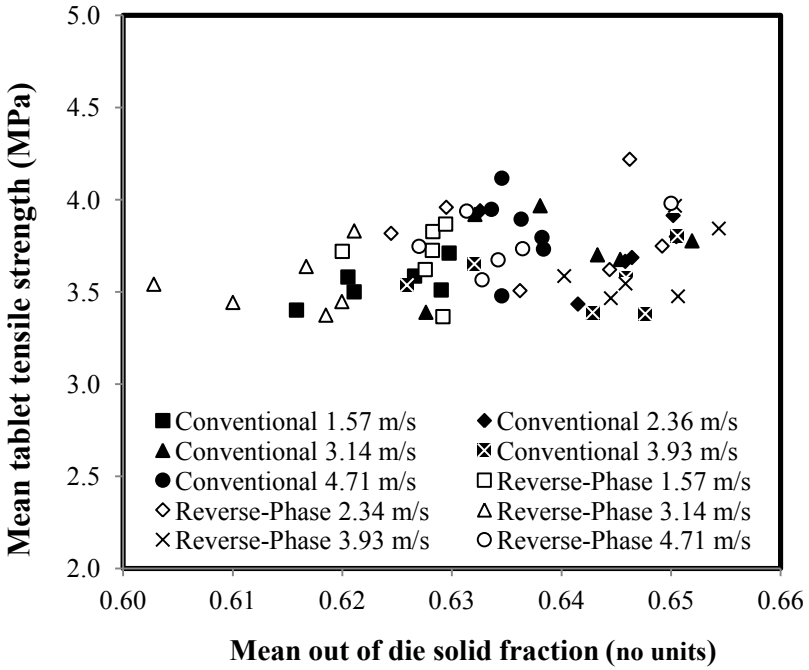

Figure 5-18. Compactibility plot showing tablet tensile strength as a function of out-of-die solid fraction for different hydroxyapatite granule size fractions. Granules were prepared using both the conventional and reverse-phase granulation processes using 200 cm^3 of 20 % w/w PVP binder liquid at different impeller speeds, n=6.

A relatively low out-of-die solid fraction was achieved due to the intermediate compaction pressure (250 MPa) used in this study. A narrow solid fraction range of 0.60–0.65 was obtained indicating that minimal differences in granule consolidation exist as a result of the granulation process used, the impeller tip speed or granule size fraction. Over the solid fraction range obtained there is no effect ($p > 0.05$ ANOVA) of the granulation process, impeller speed and granule size fraction.

5.2.6.2 Effect of impeller tip speed on elastic behaviour

During the compaction process a point exists where excess compaction pressure is stored as elastic energy and then released during unloading, resulting in the breakage of some bonds that were formed during compression [31]. The effect of impeller tip speed and granule size fraction on elastic recovery is shown for the conventional (Figure 5-19)

and reverse-phase (Figure 5-20) granulation processes. The results show that the elastic recovery is similar in all cases and that there is no effect ($p > 0.05$ ANOVA) of granulation process, impeller speed or granule size fraction.

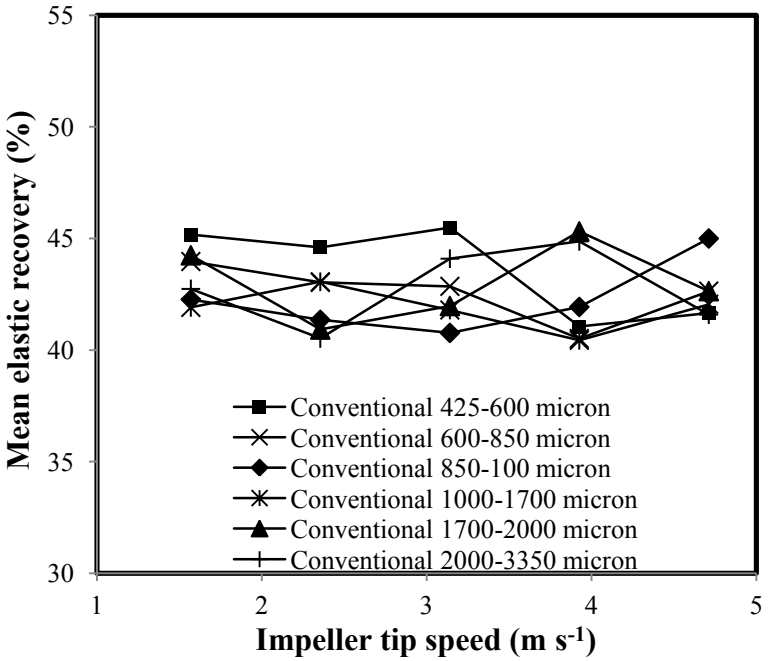

Figure 5-19. Elastic recovery as a function of impeller tip speed for different hydroxyapatite granule size fractions. Granules were prepared using a conventional granulation process using 200 cm^3 of 20 % w/w PVP binder liquid, n=6.

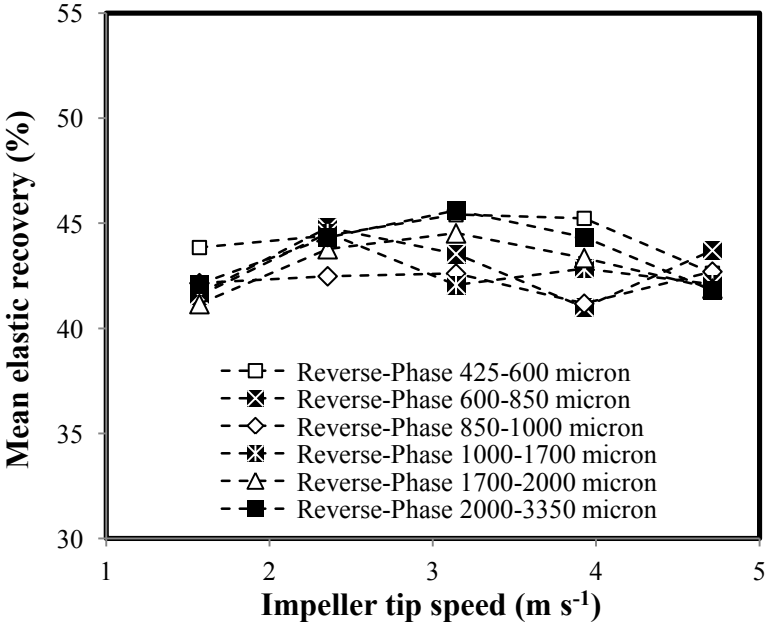

Figure 5-20. Elastic recovery as a function of impeller tip speed for different hydroxyapatite granule size fractions. Granules were prepared using a reverse-phase granulation process using 200 cm^3 of 20 % w/w PVP binder liquid, n=6.

The consolidation behaviour was found to be similar for different granule size fractions from the conventional and reverse-phase processes over a range of impeller tip speeds. The granule fracture strength was not correlated to tablet solid fraction, tablet tensile strength or elastic recovery. These findings are likely to be due to two factors.

First, the mean fracture strength of the granules is orders of magnitude weaker than the compaction pressure used in the tablet compaction. While the differences in granule strength between the reverse-phase and conventional granulation processes were significant, these differences were overwhelmed and masked as a consequence of the high pressures used during tablet compaction Second, tablet tensile strength is considered to be primarily determined by the bonding force between powder particles and the area over which these bonding forces act [32]. For all experiments a similar solid fraction was achieved meaning a constant bonding area existed. Also, the formulation and moisture content were maintained constant for all experiments meaning constant interparticulate bond strength existed. Consequently, tablet tensile strength and elastic behaviour were not affected by an increase in granule mean fracture strength. However, the increased granule strength resulting from the reverse-phase process will likely confer some advantages of improved robustness to handling, decreased friability and decreased segregation potential in a commercial manufacturing setting.

5.3 Conclusions

Impeller tip speed had significantly different effects on the granules produced by conventional and reverse-phase granulation processes. For the conventional granulation process an increase in impeller speed initially has minimal effect on granule size distribution. However, a further increase in impeller tip speed results in granule consolidation and an increase in granule size, consistent with an induction growth regime where binder liquid is squeezed to the surface of the granules facilitating coalescence and growth. Granule growth in the conventional process appears to be driven by viscous forces based upon analysis of the calculated modified capillary number. In contrast when the reverse-phase process was used, an increase in impeller speed resulted in increased granule breakage. This was postulated to be due to the fact that the granulation process begins with fully saturated pores. Under these conditions further consolidation of granules at increased impeller tip speeds is limited and rebound or breakage occurs. Granule growth in the reverse-phase process appears to be driven by capillary forces which is consistent with the mechanism proposed in Section 4.2.7.

In the reverse-phase process a critical impeller speed, represented by the equilibrium between centrifugal and gravitational forces, appears to represent the point above which breakage of large wet agglomerates and mechanical dispersion of binder liquid take place. The conventional process appears to be difficult to control due to variations in granule consolidation, which depends upon experimental variables. These variations mean impeller tip speed can both decrease and increase granule size. In contrast the reverse-phase process appears to offer simple control over granule porosity and size through manipulation of the impeller speed.

The compaction properties of the resultant granules were unaffected by the method of granulation (conventional and reverse-phase), impeller tip speed and granule size fraction. The similar performance between the conventional and reverse-phase granulation processes indicates that while mechanistic differences exist in the formation of the granules, which results in granule-scale porosity and strength differences, the granule compaction properties at pharmaceutically relevant pressures are unaffected.
Granule consolidation and growth behaviour in the reverse-phase process has been shown to be primarily controlled by the degree of liquid saturation (Chapter 4) and

impeller speed (Chapter 5). A growth regime map has been proposed for the conventional process, where granule growth behaviour is a function of only liquid saturation and the Stokes deformation number [7, 8]. The model is considered useful in that it ties easily measureable material properties (e.g. binder viscosity, wet granule strength, granule density and size) to operating conditions such as particle collision velocity or shear rate [33]. It is therefore recommended that a similar growth regime map be developed for the reverse-phase granulation process.

5.4 References

[1] Saleh, K., Vialatte, L., Guigon, P., Wet granulation in a batch high shear mixer, Chem. Eng. Sci., 60 (2005) 3763-3775.

[2] Knight, P.C., Johansen, A., Kristensen, H.G., Schaefer, T., Seville, J.P.K., An investigation of the effects on agglomeration of changing the speed of a mechanical mixer, Powder Technology, 110 (2000) 204-209.

[3] Liu, L.X., Litster, J.D., Wet granule breakage in a breakage only high-shear mixer: Effect of formulation properties on breakage behaviour, Powder Technology, 189 (2009) 158-164.

[4] Litster, J.D., Kayrak-Talay, D., *A priori* performance prediction in pharmaceutical wet granulation: Testing the applicability of the nucleation regime map to a formulation with a broad size distribution and dry binder addition, Int. J. Pharm., 418 (2011) 254-264.

[5] Ennis, B.J., Tardos, G.I., Pfeffer, R., A microlevel-based characterization of granulation phenomena, Powder Technology, 65 (1991) 257-264.

[6] Ouchiyama, N., Tanaka, T., Stochastic model for compaction of pellets in granulation, Ind. Eng. Chem. Fundam., 19 (1980) 555-264.

[7] Iveson, S.M., Litster, J.D., Growth regime map for liquid-bound granules, AIChE J., 44 (1998) 1510-1518.

[8] Iveson, S.M., Wauters, P.A.L., Forrest, S., Litster, J.D., Meesters, G.M.H., Scarlett, B., Growth regime map for liquid-bound granules: further development and experimental validation, Powder Technology, 117 (2001) 83-97.

[9] Hoornaert, F., Wauters, P., Meesters, G., Pratsinis, S., Scarlett, B., Agglomeration behaviour of powders in a lodige mixer granulator, Powder Technology, 96 (1998) 116-128.

[10] Eliasen, H., Schaefer, T., Kristensen, H., Effects of binder rheology on melt agglomeration in a high shear mixer, Int. J. Pharm., 176 (1998) 73-83.

[11] Carvajal, M.T., Macias, K.A., The influence of granule density on granule strength and resulting compact strength, Chem. Eng. Sci., 72 (2012) 205-213.

[12] Adams, M.J., Agglomerate strength measurement using a uniaxial confined compression test, Powder Technology, 78 (1994) 5-13.

[13] Litster, J.D., Hapgood, K.P., Michaels, J.N., Sims, A., Roberts, M., Kameneni, S.K., Hsu, T., Liquid distribution in wet granulation: dimensionless spray flux, Powder Technology, 114 (2001) 29-32.

[14] Hapgood, K.P., Litster, J.D., Smith, R., Nucleation regime map for liquid bound granules, AIChE J., 49 (2003) 350-361.

[15] Scott, A.C., Hounslow, M.J., Instone, T., Direct evidence of heterogeneity during high-shear granulation, Powder Technology, 113 (2000) 205-213.

[16] Holm, P., Jungerson, O., Schaefer, T., Kristensen, H.G., Granulation in High Speed Mixers Part I: Effects of process variables during kneading, Pharm. Ind., 45 (1983) 806-811.

[17] Tardos, G.I., Khan, M.I., Mort, P.R., Critical parameters and limiting conditions in binder granulation of fine powers, Powder Technology, 94 (1997) 245-258.

[18] Hounslow, M., Pearson, J., Instone, T., Tracer studies of high-shear granulation: II. Population balance modelling, AIChE J., 47 (2001) 1984-1998.

[19] Litster, J.D., Waters, A., Influence of the material properties of iron ore sinter feed on granulation effectiveness, Powder Technology, 55 (1988) 141-151.

[20] Litster, J.D., Ramachandran, R., Poon, J., Sanders, C., Glaser, T., Immauel, C., III, F.D., Stepanek, F., Wang, F., Cameron, I., Experimental studies on distributions of granule size, binder content and porosity in batch drum granulation: Inferences on process modelling requirements and process sensitivities, Powder Technology, 188 (2008) 89-101.

[21] vandenDries, K., deVegt, O.M., Girard, V., Vromans, H., Granule breakage phenomena in a high shear mixer; influence of process and formulation variables and consequences on granule homogeneity, Powder Technology, 133 (2003) 228-236.

[22] Benali, M., Gerbaud, V., Hemati, M., Effect of operating conditions and physico-chemical properties on the wet granulation kinetics in a high shear mixer, Powder Technology, 190 (2009) 160-169.

[23] Iveson, S.M., Beathe, J.A., Page, N.W., The dynamic strength of partially saturated powder compacts: the effect of liquid properties, Powder Technology, 127 (2002) 149-161.

[24] Iveson, S.M., Litster, J.D., Fundamental studies of granule consolidation Part 2: Quantifying the effects of particle and binder properties, Powder Technology, 99 (1998) 243-250.

[25] Hapgood, K.P., Nguyen, T., Shen, W., Drop penetration time in heterogeneous powder beds, Chem. Eng. Sci., 64 (2009) 5210-5221.

[26] Carr, R.L., Evaluating flow properties of solids, Chem. Eng., 72 (1965) 163-168.

[27] Rumpf, H. The strength of granules and agglomerates in: Knepper W.A., (Eds.) *Agglomeration*, Interscience-Wiley, New York, 1962, pp. 379-418.

[28] Ghadiri, M., Rahmanian, N., Jia, X., Stepanek, F., Characterisation of granule structure and strength made in a high shear granulator, Powder Technology, 192 (2009) 184-194.

[29] Ghadiri, M., Rahmanian, N., Naji, A., Effects of process parameters on granule properties produced in a high shear granulator, Chemical Engineering Research and Design, 89 (2011) 512-518.

[30] Mort, P.R., Scale-up of binder agglomeration processes, Powder Technology, 150 (2005) 86-103.

[31] Adolfsson, A., Nystrom, C., Tablet strength, porosity, elasticity and solid state structure of tablets compressed at high loads, Int. J. Pharm., 132 (1996) 95-106.

[32] Nystrom, C., Alderborn, G., Duberg, M., Karehill, P., Bonding surface area and bonding mechanism – two important factors for the understanding of powder compactibility, Drug. Dev. Ind. Pharm., 19 (1993) 2143-2196.

[33] Mort, P.R., Scale-up and control of binder agglomeration processes - Flow and stress fields, Powder Technology, 189 (2009) 313-317.

CHAPTER SIX: DEVELOPMENT OF A GROWTH REGIME MAP FOR A NOVEL REVERSE-PHASE WET GRANULATION PROCESS

6 Introduction

The growth regime map for conventionally formed liquid bound granules (Figure 1-5) depicts the regime that a given granulation process will operate within to be a function of granule liquid saturation, S_{max}, and Stokes deformation number, St_{def} [1, 2]. Several general themes are immediately identified from the growth regime map. An increase in binder liquid amount will increase the liquid saturation and move the system from dry to nucleation to induction or steady growth, and potentially the slurry condition. An increase in impeller speed or binder viscosity will increase the St_{def}, and potentially S_{max}, and therefore move the system from nucleation or induction to steady growth to the crumb or slurry regimes.

The regime map boundaries are not "validated", however some experimental data have been reported previously. The boundary between nucleation and steady or induction growth behaviour depends upon the binder amount required to reach critical pore saturation and the consolidation behaviour of the wet granules. Published results suggest at S_{max} <0.7 insufficient liquid is present to achieve coalescence and only nuclei form [3]. An S_{max} between 0.8–0.9 % generally results in a steady growth regime [2, 4, 5]. Whereas, induction growth systems are those which are so strong they do not deform sufficiently to coalesce without the presence of free liquid at the granule surfaces, i.e. S_{max} >100 %. The boundary between steady growth and induction growth has been reported in the range of St_{def} 0.001–0.003 [2]. Since an increase in the liquid saturation reduces the induction time it stands to reason that at high liquid saturations the difference between steady growth and induction growth disappears and both systems exhibit fast steady growth. The boundary between steady and crumb growth has been reported as St_{def} of 0.1 [2] and ~0.2 [6].

Since the reverse-phase granulation process has been shown to be primarily controlled by the degree of liquid saturation (Chapter 4) and impeller speed (Chapter 5), there is a reasonable likelihood that the growth regime map should be able to describe the growth regimes for reverse-phase process. The aim of this chapter was therefore to develop such a growth regime map for the novel reverse-phase granulation process.

6.1 Method

The results for binder liquid characteristics and granule physical properties reported in Chapters 4 and 5 are combined in this chapter and used in the calculation of S_{max} and St_{def}. Binder liquid viscosity (Section 4.1.3.3), density (Section 4.1.3.2), surface tension (Section 4.1.3.1) and contact angle (Section 4.1.3.4) data used in this chapter are presented in Table 4-3. Granule size distribution (Section 2.1.2.3), envelope density (Section 2.1.2.2) and intragranular porosity (Section 4.2.2) were determined as described previously and presented in Chapters 4 and 5.

6.1.1 Measurement of powder surface velocity

In the present study the surface velocity of the powder bed was used as a surrogate for the representative collision velocity experienced between two particles in the granulator. Surface velocity was measured using a high-speed camera (TroubleShooter TS1000ME, Fastec Imaging, San Diego, USA) fitted with a wide angle lens. The high-speed camera was mounted on a tripod such that the camera was facing directly downwards and focussing on the granulation process through a safety interlocked Perspex^{TM} cover. Two 1000 W halogen spotlights were used to illuminate the focal area. Video footage of the powder bed was recorded at 500 frames s^{-1} during the 10 s wet massing period of each experiment. The diameter of the granulator bowl (12.00 cm) was used as a reference feature to calibrate the distance measurements.

The video footage was downloaded and analysed manually using MiDAS 4.0 Express software. During playback a clear feature in the wet granule bed (n=6) was identified (e.g. crack in the powder bed, large granule, etc) and followed using the frame-by-frame scrolling feature for a linear distance between 1.8–7.6 cm. The start and end frame numbers were recorded and the duration that the feature was tracked was calculated by the number of frames between point 1 and point 2 divided by the frame speed (500 frames s^{-1}). The linear distance between point 1 and point 2 determined by the software is shorter than the actual arc distance travelled by the feature. The arc distance was calculated using the approach reported by Hapgood *et al* [7], as depicted in Figure 6-1, which assumes the path travelled by the feature follows the curvature of a circle.

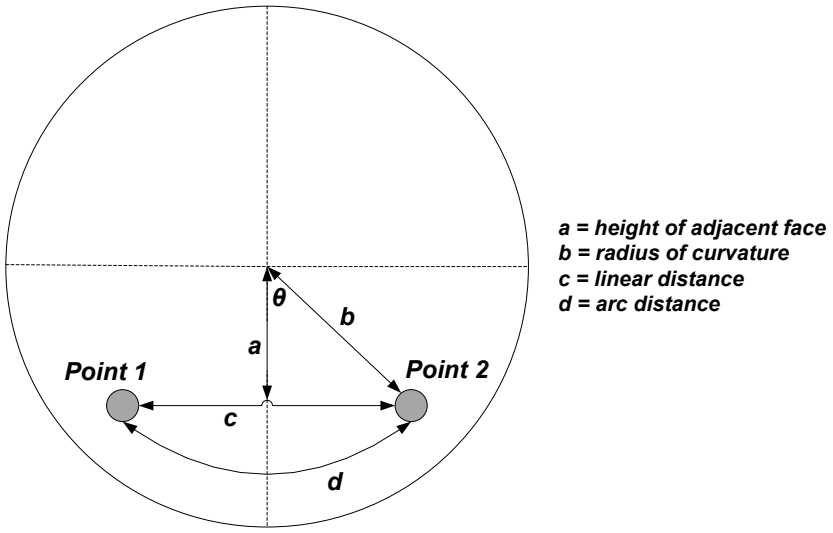

Figure 6-1. Diagram of powder feature movement in the granulator bowl from a top-down view. Adapted from [7].

The linear distance travelled is shown as straight line *c* and the distance actually travelled by the feature is shown as arc line *d*. The distance *a* was measured using the MiDAS 4.0 Express software at the midpoint between point 1 and point 2. The actual distance travelled by the feature was calculated using the radius of curvature, *b*:

$$b = \sqrt{(a^2 + \frac{c^2}{2})} \qquad \textit{Equation 6-1}$$

The angle of the triangle, θ, was calculated by:

$$\theta = sin^{-1}\left(\frac{\left(\frac{c}{2}\right)}{b}\right) \qquad \textit{Equation 6-2}$$

The distance travelled by the granule is the circumference of the arc, *d*, and is calculated as:

$$d = \frac{2\theta \times \pi \times b}{180} \qquad \textit{Equation 6-3}$$

The powder surface velocity was then calculated by dividing the arc distance, *d,* by the duration that the feature was tracked.

6.1.2 Wet granule strength

An additive model, derived by Liu and Litster [8], which considers both the capillary strength and dynamic strength of the liquid bridges was used to calculate granule strength, σ, in the wet state:

$$\sigma = S_{max}\left[6\frac{1-\varepsilon}{\varepsilon}\frac{\gamma cos\theta}{d_p} + \frac{9}{8}\frac{(1-\varepsilon)^2}{\varepsilon^2}\frac{9\pi\mu v_p}{16 d_{3,2}}\right] \qquad \textit{Equation 6-4}$$

where S_{max} is the liquid saturation (no units), ε is the granule porosity (no units), d_p is the particle size of the primary particles (μm), γ is the liquid surface tension (mN m^{-1}), θ is the liquid-solid contact angle (°), μ is the liquid viscosity (Pa.s) and v_p is the relative velocity of particles (m s^{-1}) within the granule, which is taken as the impeller tip speed and $d_{3,2}$ is the surface mean particle size of the primary particles.

6.1.3 Stokes deformation number

The Stokes deformation number, St_{def}, is the ratio of the impact kinetic energy of the wet granules just before collision to the characteristic work done in a collision to plastically deform the granules [2, 6]. St_{def} gives a manner in which the relationship between formulation properties, binder liquid properties and operating conditions can be described.

$$St_{def} = \frac{\rho_g v_c^2}{2\sigma} \qquad \textit{Equation 6-5}$$

where ρ_g is the granule's density, v_c is the representative collision velocity, and σ is the wet granule strength. A smaller Stokes St_{def} implies that significant energy is dissipated in deforming the granule during a collision and granule coalescence is favoured.

6.1.4 Statistical analysis

Statistical analysis to determine whether significant differences existed between sample means was performed as described in Section 2.1.2.8.

6.2 Results and Discussion

In order to calculate Stokes deformation number one must obtain suitable measurements of both the representative collision velocity and the wet granule strength. Each is discussed.

6.2.1 Representative collision velocity

The term for the representative collision velocity, v_c, in Equation 6-5 has been reported to be 15–20 % of the impeller tip speed and investigators have used this fixed value assumption in the calculation of St_{def} [8, 9]. The accuracy of this estimate has received little attention, though Cavinato *et al* [10] pointed to it as a source of error in their calculation of St_{def}. Consequently the present study sought to either validate the 15–20 % of tip speed approach or determine a more appropriate method. Powder surface velocity was selected as a practical in-process measurement to consider. Powder surface velocity has previously been found to be affected by impeller speed, mixer scale, fill level and extent of granulation [11]. In the current study the effect of liquid saturation, binder liquid viscosity, impeller tip speed and the type of granulation process (conventional and reverse-phase) on surface velocity was studied.

The surface velocity of the granule bed (Figure 6-2) increased with increasing S_{max} ($p < 0.05$ ANOVA) to a critical point, and then decreased significantly ($p < 0.05$ ANOVA). The inclusion of 20 % *w/w* PVP binder within the granule mixture resulted in a greater surface velocity than when 10 % *w/w* PVP binder was included, reflecting a difference in cohesion between particles attributable to the increased binder concentration. The critical S_{max} is ~0.8 for the conventional process whilst this was ~1 for reverse-phase process. Below this critical S_{max} the granule mixture prepared using the reverse-phase process has a greater surface velocity than the conventional process when comparable amounts of binder liquid were incorporated ($p < 0.05$ ANOVA). Above the critical S_{max} the surface velocity decreased significantly for both granulation processes ($p < 0.05$ ANOVA). At this point, rather than moving as a powder bed with consistent speed, large granules and over wet areas were observed to exhibit start/stop behaviour as they rolled over the top of the impeller blade. This suggests that determination of surface velocity could provide a potential in-process measurement to determine granulation

end-point. In the case of the conventional process it is noted that for S_{max} ~1 the surface velocity began to decrease before a rapid granule growth was observed. This suggests that the surface velocity may decrease before, rather than at the point of rapid growth, and therefore be an early indicator of excess surface liquid before rapid coalescence and growth occur.

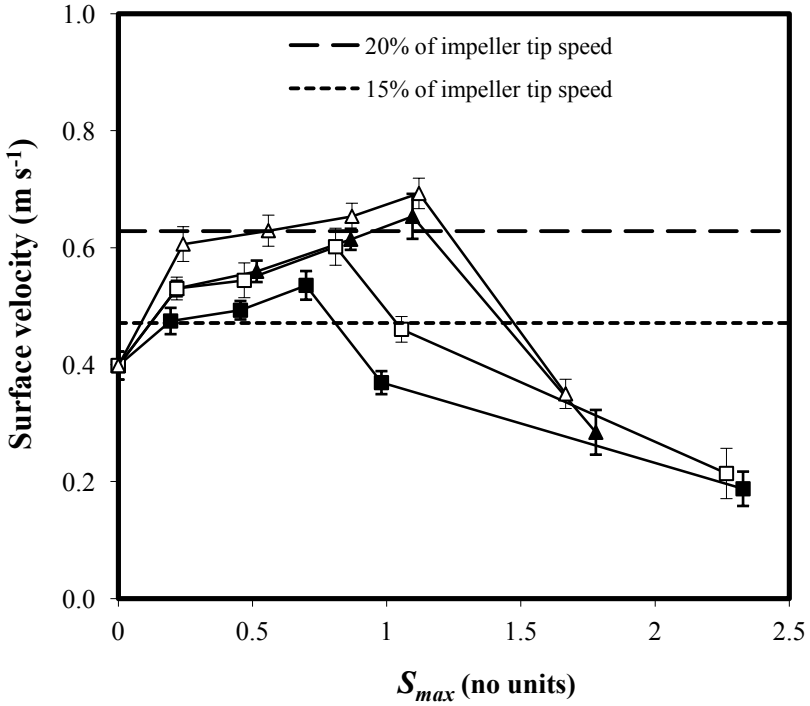

Figure 6-2. Hydroxyapatite wet granule surface velocity as a function of liquid saturation, S_{max}, at 3.14 m s^{-1} impeller tip speed. ■ 10 % w/w PVP by conventional granulation, □ 20 % w/w PVP by conventional granulation, ▲ 10 % w/w PVP by reverse-phase granulation, Δ 20 % w/w PVP by reverse-phase granulation. Error bars represent 1 SD, n=6.

The observed differences in critical S_{max} between the reverse-phase and conventional granulation processes are potentially due to a greater involvement of liquid filled capillaries in the reverse-phase process, which was proposed initially in Section 4.2.2. The immersion mechanism of the reverse-phase process is likely to result in a greater degree of binder liquid present in the capillaries of the HA particles and granules than in the conventional process where less complete wetting of capillaries is likely. This effect means that at the same S_{max} the granules prepared by the conventional process will have a greater amount of binder liquid present at their surface and will experience rapid coalescence and growth, and therefore decreased surface velocity, at a lower S_{max} than granules prepared by the reverse-phase process. This proposal is further supported when

one considers that theoretically an S_{max} of 1 represents the point at which all pores within the particles and granules are filled with binder liquid and liquid will be available at the particle surfaces to facilitate coalescence and growth, which is then seen as a reduction in the surface velocity. According to this theory, and the preceding discussion, it would be predicted that the conventional granules, where incomplete wetting of intraparticulate capillaries occurs, would reach a point where surface liquid is present at $S_{max} < 1$ and surface velocity decreases. In contrast it would be predicted that the reverse-phase process, where more complete wetting of intraparticulate capillaries occurs, would reach a point where surface liquid is present only at $S_{max} \sim 1$ and surface velocity decreases. The data presented are in good agreement with the proposed explanation.

The surface velocity of the granule bed (Figure 6-3) remained relatively constant as impeller tip speed increased, with some statistically significant ($p < 0.05$ ANOVA) differences between means but no consistent theme in increase or decrease occurred. The granule mixture prepared using the reverse-phase process had a greater surface velocity than that prepared using the conventional process at all impeller tip speeds ($p < 0.05$ ANOVA). For all data points the inclusion of 20 % *w/w* PVP binder was found to produce a granular mixture with a greater surface velocity than that produced using 10 % *w/w* PVP binder ($p < 0.05$ ANOVA). This finding can be explained by the greater viscous forces acting between particles produced using the higher concentration of binder, creating a more cohesive granule bed than when the lower concentration was employed, which facilitates mass movement. Granules prepared with lower viscosity binder have weaker liquid bridges acting between particles and are more likely to move past each other and the equipment surfaces when impacted by the impeller blade, resulting in a lower surface velocity. Such reasoning accounts for the strategy of measuring increasing impeller torque, or power consumption, as particle size increases during the granulation process, to determine the suitable endpoint [12].

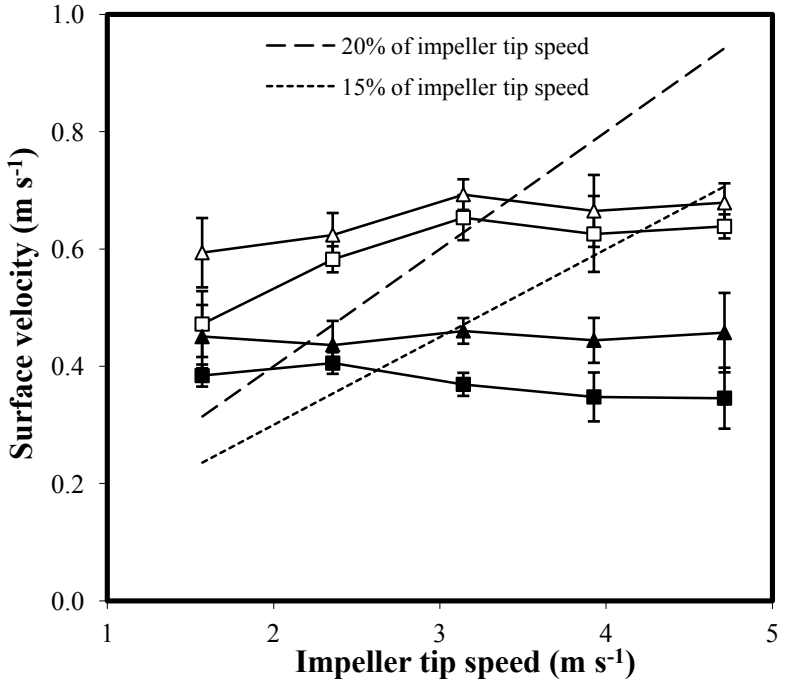

Figure 6-3. Hydroxyapatite wet granule surface velocity as a function of impeller tip speed using 200 cm^3 binder liquid. ■ 10 % w/w PVP by conventional granulation, □ 20 % w/w PVP by conventional granulation, ▲ 10 % w/w PVP by reverse-phase granulation, Δ 20 % w/w PVP by reverse-phase granulation. Error bars represent 1 SD, n=6.

Figure 6-2 and Figure 6-3 show dashed lines representing the fixed 15 and 20 % of impeller tip speed approaches which have previously been employed to estimate the representative collision velocity [8-10]. When considering the effect of S_{max} the powder surface velocity varied between 5.98–20.81 % of the impeller tip speed; however in all cases the impeller tip speed was held constant at 3.14 m s^{-1}. When considering the effect of impeller tip speed the surface velocity varied between 9.71–37.80 % of the impeller tip speed. These data indicate that the collision velocity will change significantly depending on the binder liquid amount, binder liquid viscosity, and consolidation properties of the granules. As such, the assumption of a fixed representative collision velocity is considered flawed and so in an attempt to represent the dynamic nature of the representative collision velocity the surface velocity measurements determined in this study have been used in the calculation of St_{def}. It is recognised that a velocity gradient is likely to exist both from the center of the granulator bowl to the outside (though likely relatively small in the present case where the radius is 6 cm) and from the base of the granulator bowl to the powder surface. Therefore the surface velocity measurements presented likely represent a minimum collision velocity experienced. The

magnitude of this gradient could be further investigated by loading the granulator bowl with a varying mass of powder and performing surface velocity measurements.

6.2.2 Wet granule strength

Figure 6-4 shows the calculated wet granule strength as a function of S_{max}. Wet granule strength increased for all conditions as S_{max} increased as would be predicted by Equation 6-4. A single best fit curve adequately describes the relationship between S_{max} and wet granule strength for each binder liquid concentration, regardless of whether the reverse-phase or conventional granulation processes are used.

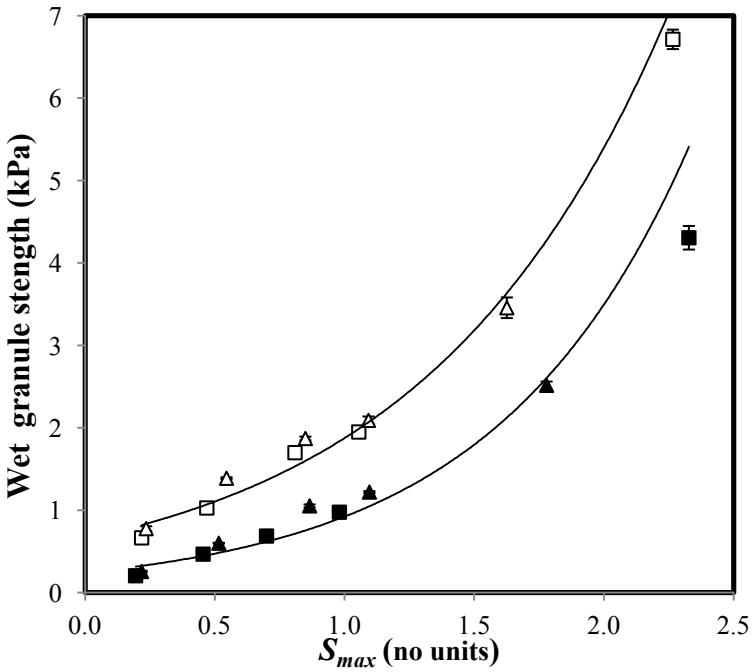

Figure 6-4. Calculated hydroxyapatite wet granule strength as a function of liquid saturation, S_{max}. ■ 10 % w/w PVP by conventional granulation, □ 20 % w/w PVP by conventional granulation, ▲ 10 % w/w PVP by reverse-phase granulation, Δ 20 % w/w PVP by reverse-phase granulation. R^2 0.9401 for 10 % w/w PVP, R^2 0.9705 for 20 % w/w PVP. Error bars represent 1 SD, n=4.

Figure 6-5 shows the effect of impeller tip speed on the calculated wet granule strength. The conventional process calculated wet granule strength differs depending upon the viscosity of the binder liquid that is incorporated. When the 10 % *w/w* PVP binder liquid was included the impeller tip speed had no effect ($p > 0.05$ Wilcoxon) on wet granule strength, whereas incorporation of 20 % *w/w* PVP binder liquid induced an

increase ($p < 0.05$ Wilcoxon) across the entire impeller speed range. These results confirm the behaviour represented in Figure 5-2, where a marked increase in S_{max} was found to occur as a result of the increased consolidation. The reverse-phase granulation for the 10 % *w/w* PVP binder liquid shows a slight decrease ($p < 0.05$ Wilcoxon) in wet granule strength as impeller tip speed increased, while the 20 % *w/w* PVP binder resulted in an initial decrease ($p < 0.05$ Wilcoxon) in wet granule strength as impeller speed increased from 1.57 to 3.14 m s^{-1} followed by a plateau ($p > 0.05$ Wilcoxon) as the impeller speed was increased further to 4.71 m s^{-1}. The relationship between impeller speed and wet granule strength is similar to the relationship between impeller speed and granule mass mean diameter shown in Figure 5-6 indicating that the wet granule strength may be a good predictor of the final granule size.

.

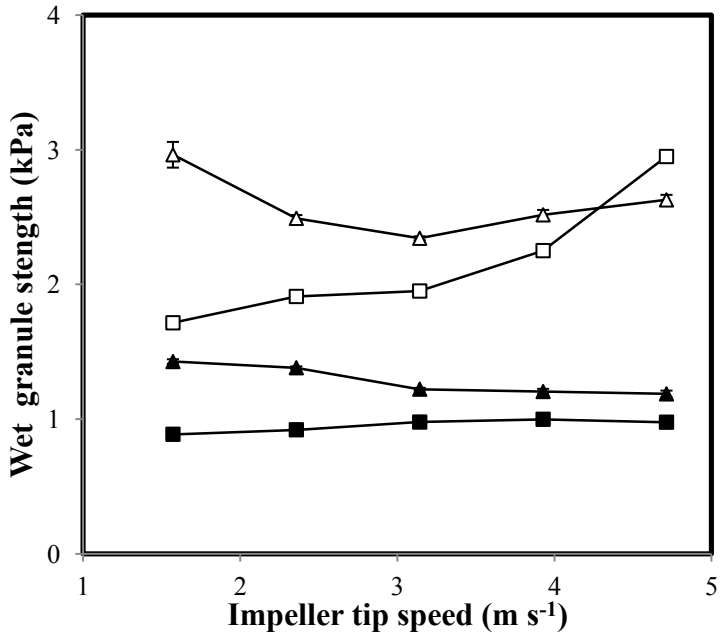

Figure 6-5. Hydroxyapatite wet granule strength as a function of impeller tip speed ■ 10 % w/w PVP by conventional granulation, □ 20 % w/w PVP by conventional granulation, ▲ 10 % w/w PVP by reverse-phase granulation, Δ 20 % w/w PVP by reverse-phase granulation. Error bars represent 1 SD, n=4.

6.2.3 Relationship between St_{def} and process parameters

Granule size and porosity are important granule parameters in relation to product quality and both of these factors are fixed by the rate and extent of various macroscopic growth mechanisms in the granulation process. St_{def} decreased as S_{max} increased (Figure 6-6). As St_{def} increases the system is capable of dissipating less collision energy and this

creates a condition where excess energy may be dissipated as elastic energy resulting in dilation of the granule structure. In the present study a decrease in St_{def} was induced by an increase in the amount of binder liquid added (Figure 6-6). An increase in the amount of binder liquid can cause an increased dissipation of collision energy by viscous forces, however this will also decrease the contributions of interparticulate friction forces through lubrication of particle-particle contacts, and decrease capillary forces when S_{max} is > 1.0.

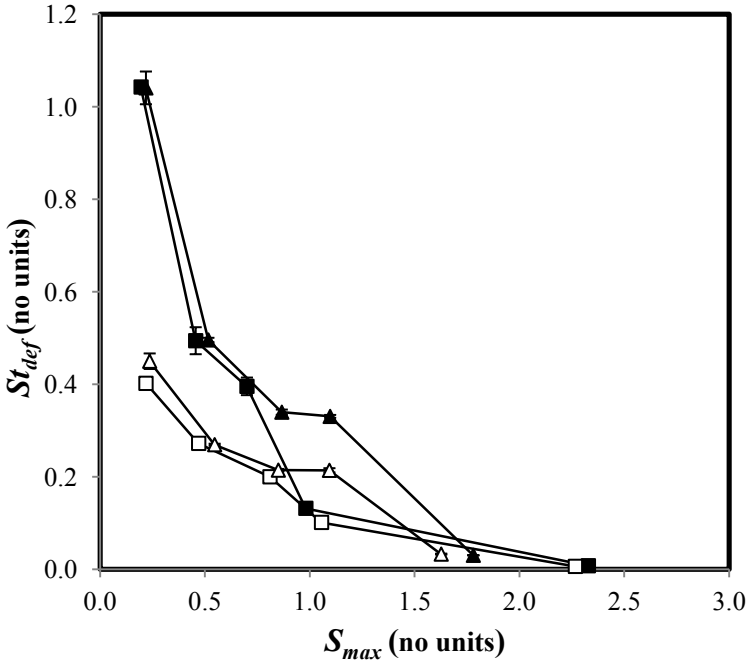

Figure 6-6. St_{def} as a function of S_{max} for hydroxyapatite granules using an impeller tip speed of 3.14 m s^{-1}. ■ 10 % w/w PVP by conventional granulation, □ 20 % w/w PVP by conventional granulation, ▲ 10 % w/w PVP by reverse-phase granulation, Δ 20 % w/w PVP by reverse-phase granulation. Error bars represent 1 SD, n=4.

The effect of impeller tip speed on St_{def} is shown in Figure 6-7. The granulation process plays a significant role in determining the St_{def}. For the conventional process an increase in impeller tip speed resulted in a decrease ($p < 0.05$ Wilcoxon) in the St_{def} of the granule mixture. However, for the reverse-phase process an increase in impeller tip speed to 3.14 m s^{-1} resulted in a large initial increase ($p < 0.05$ Wilcoxon) in St_{def}, followed by a plateau ($p > 0.05$ Wilcoxon) as impeller tip speed increased further. Based on these data it would be expected that the conventional granule size would be relatively insensitive to St_{def}, however the reverse-phase granule size would be expected to be reduced as impeller tip speed increased to 3.14 m s^{-1}, followed by a subsequent plateau.

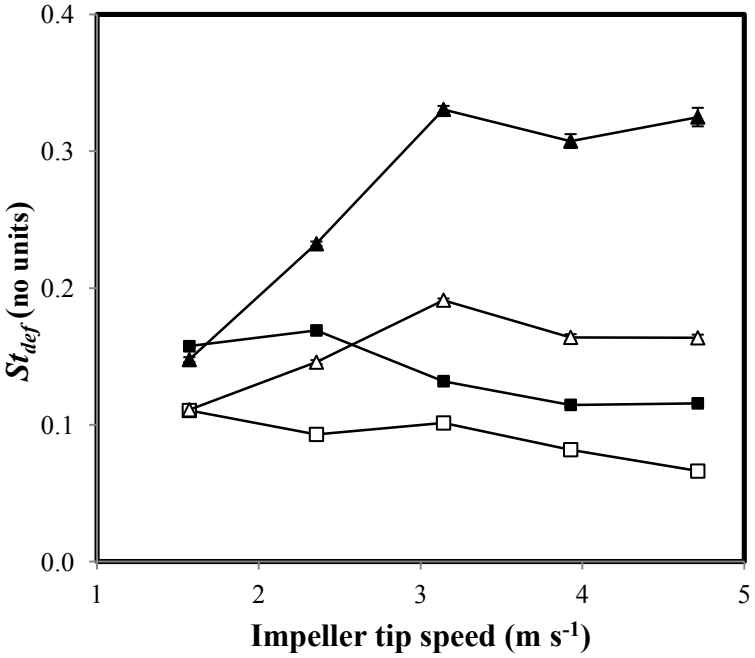

Figure 6-7. Stokes deformation number, St_{def}, as a function of impeller tip speed for hydroxyapatite granules. ■ 10 % w/w PVP by conventional granulation, □ 20 % w/w PVP by conventional granulation, ▲ 10 % w/w PVP by reverse-phase granulation, Δ 20 % w/w PVP by reverse-phase granulation. Error bars represent 1 SD, n=4.

6.2.4 Relationship between St_{def} and mass mean diameter

Figure 6-8 presents the relationship between St_{def} and granule mass mean diameter. The data include all results from the conventional and reverse-phase processes spanning S_{max} values between 0.20–2.33, impeller tip speeds between 1.57–4.71 m s^{-1}, containing either 10 or 20 % *w/w* PVP binder concentrations.

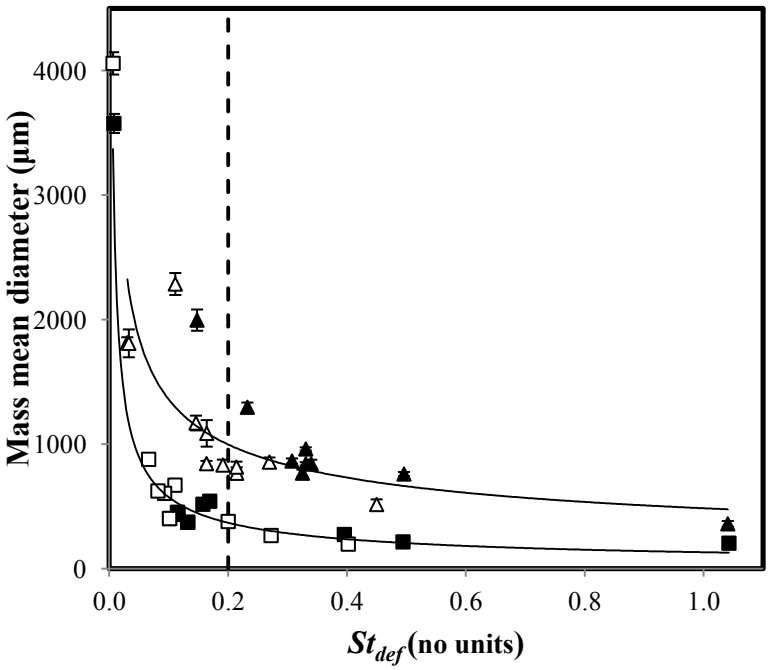

Figure 6-8. Hydroxyapatite granule mass mean diameter as a function of Stokes deformation number, St_{def}. ■ 10 % w/w PVP by conventional granulation, □ 20 % w/w PVP by conventional granulation, ▲ 10 % w/w PVP by reverse-phase granulation, Δ 20 % w/w PVP by reverse-phase granulation. Conventional process R^2 0.9204, Reverse-Phase process R^2 0.7340. Error bars within points represent 1 SD, n=4.

The granule mass mean diameter decreased with increasing St_{def} for all the sets of conditions studied. As St_{def} increases the probability of granule coalescence reduces which is clearly seen from the data as a reduction in the granule mass mean diameter, with St_{def} values >~0.2 appearing to represent a boundary above which granule breakage has occurred. The conventional and reverse-phase granulation processes show a similar profile, however distinctly different granule mass mean diameters are obtained for the same St_{def} values obtained using the two different processes. This indicates that the reverse-phase process is capable of dissipating a greater amount of collision energy than the conventional process. This is potentially due to the granulation mechanisms that have been proposed. The reverse-phase process begins from a fully saturated state meaning that the system is likely more deformable than the conventional process. St_{def} appears to be a good predictor of granule mass mean diameter over a wide range of process conditions, and is capable of differentiating between the conventional and reverse-phase granulation processes.

6.2.5 Relationship between St_{def} and intragranular porosity

Figure 6-9 presents the relationship between St_{def} and intragranular porosity. The data comprise all results from the conventional and reverse-phase processes spanning an S_{max} range of 0.20–2.33, impeller tip speeds of 1.57–4.71 m s^{-1}, including either 10 or 20 % *w/w* PVP binder concentrations.

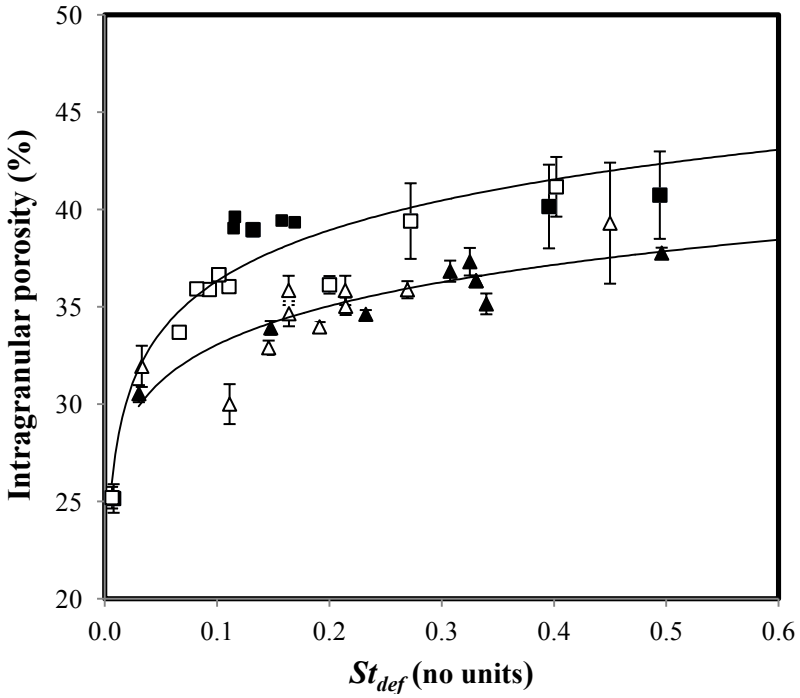

Figure 6-9. Hydroxyapatite granule porosity as a function of Stokes deformation number, St_{def}. ■ 10 % w/w PVP by conventional granulation, □ 20 % w/w PVP by conventional granulation, ▲ 10 % w/w PVP by reverse-phase granulation, Δ 20 % w/w PVP by reverse-phase granulation. Conventional process R^2 0.9099, Reverse-Phase process R^2 0.7808. Error bars represent 1 SD, n=4.

Intragranular porosity increased as St_{def} increased. As St_{def} increased the system is capable of dissipating less collision energy. Excess energy may be dissipated as elastic energy, increasing the probability that granules will rebound when they collide resulting in dilation or breakage of the granule structure. This is clearly seen from the data as an increase in the intragranular porosity with increasing St_{def}. The conventional and reverse-phase granulation processes show similar profiles, however the reverse-phase granulation process produces granules with a lower intragranular porosity than the conventional granulation process at the same St_{def} values. This supports the hypothesis that the mechanism of reverse-phase process results in a greater capillary saturation

which can dissipate a greater amount of collision energy than the conventional process and resist granule rebound. The model appears to be a good predictor of intragranular porosity over a wide range of process conditions, and is also capable of identifying differences between granules produced by the two granulation processes.

6.2.6 Proposed growth regime map

Based upon the granule consolidation and growth behaviour presented in Chapters 4 and 5, and the relationship between liquid saturation, S_{max}, and Stokes deformation number, St_{def}, a growth regime map is proposed for the reverse-phase granulation process (Figure 6-10). Data for the conventional granulation process has also been included in the growth regime map to allow comparison between the granules produced using the two different granulation processes.

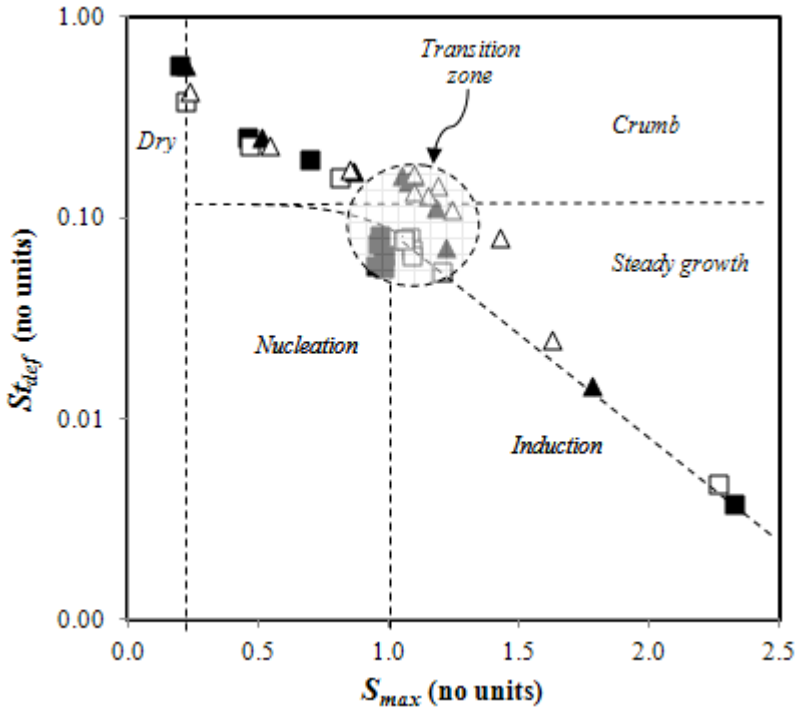

Figure 6-10. Proposed growth regime map for hydroxyapatite/poly (vinyl pyrollidone) granules, n=4. Error bars not shown. ■ 10 % w/w PVP by conventional granulation, □ 20 % w/w PVP by conventional granulation, ▲ 10 % w/w PVP by reverse-phase granulation, Δ 20 % w/w PVP by reverse-phase granulation.

When considering the granulation processes the data points move progressively from the dry region, through the nucleation and/or crumb regions, and finally into the steady or induction growth regimes as S_{max} increases. It is noted that the data points associated with changes in impeller tip speeds in the range 1.57–4.71 m s^{-1} are all positioned at the confluence between nucleation and induction growth and that changes in S_{max} over the range 0.2–2.33 have a much greater influence on the location within the growth regime map. The following data support the assignment of the approximate regime map boundaries in Figure 6-10.

6.2.6.1 Dry and nucleation regime boundary

The dry region is characterised by granule sizes similar to those of the un-granulated material, i.e. S_{max} of 0 with all particles <425μm. For the conventional process S_{max} of 0.20–0.22 resulted in dry material, whilst S_{max} of 0.39 and 0.44 (Figure 4-4) resulted in nucleation. An S_{max} of 0.22–0.24 for the reverse-phase process (Figure 4-5) resulted in a slight increase in the percent of particles greater than 425 μm. The dry to nucleation regime boundary was therefore proposed to be approximately 0.22.

6.2.6.2 Nucleation and growth regime boundary

The nucleation region is characterised by particles with size greater than the un-granulated material, but a period where only nuclei are formed and little granule growth takes place. Traditionally S_{max} values >1 are considered necessary to result in available binder liquid at the surface of the granules which allows coalescence and granule growth. For the conventional granulation process there was a negligible change in granule mass mean diameter for S_{max} between 0.95–0.98 (Figure 5-3) indicative of nucleation behaviour. For S_{max} values >1.05 obtained using the reverse-phase process, and 1.08 for the conventional granulation process, resulted in a transition from nucleation behaviour to granule growth (Figure 5-3). The nucleation to growth regime boundary was therefore proposed to occur when $S_{max} = 1$ (Figure 6-10).

6.2.6.3 Induction growth and steady growth boundary

The steady growth and induction regions are differentiated by the degree of granule size increase. An induction granulation system can appear to be operating in the nucleation regime, where little to no granule growth occurs, until a critical point is reached when induction behaviour is triggered and rapid granule growth takes place. In contrast for steady growth behaviour significant granule growth is seen as S_{max} increases or St_{def} decreases.

The reverse-phase process exhibited steady growth behaviour (Figure 4-6) as S_{max} increased from 0–1.78, whereas, in contrast under these conditions the conventional process exhibited induction growth. In particular for the 200 cm^3 20 % *w/w* PVP conventional process an impeller tip speed between 1.57–3.14 m s^{-1} yielded little granule growth, however an increase to 3.93 and 4.71 m s^{-1} resulted in significant reduction in intragranular porosity (Figure 5-1), an increase in S_{max} (Figure 5-2) and resultant granule growth (Figure 5-3). Process conditions where S_{max} >1 and St_{def} <0.08 appear to represent the point at which sufficient granule consolidation occurs to facilitate induction growth. As S_{max} increases the critical St_{def} required to cause consolidation and movement of binder liquid to the granule surfaces reduces. Therefore a negative sloping boundary between steady and induction growth exists (Figure 6-10), however it is difficult to definitively state the slope of this boundary without additional data.

6.2.6.4 Growth and crumb regime boundary

The crumb region is determined by the minimum wet granule strength required to withstand the breakage forces experienced in the granulator. In the present studies St_{def} >0.2 represents a condition where a significant reduction in granule mass mean diameter is observed (Figure 6-8) and is therefore proposed to represent the crumb regime boundary.

6.2.7 Discussion of the growth regime map

It is noted that in some cases the St_{def} values in the present study differ greatly from those reported previously. For instance the boundary between steady growth and induction in the present study was found to be St_{def} ~0.08, however has previously been reported to be St_{def} 0.001–0.003 [2]. This is not uncommon with regards to boundary conditions, for example the boundary between steady growth and crumb was found to be St_{def} ~0.2 in the present study but has been reported to be anywhere between St_{def} 0.01 [13], 0.04 [1] and 0.2 [6].

Several phenomena have been suggested to explain such deviations. Formulation constituents can dissolve in the binder liquid thereby causing the actual viscosity to differ from that experimentally determined for the binder alone; the value of which is subsequently used to calculate granule strength (Equation 6-4) [10, 14]. Moreover, errors in the estimation of the representative collision velocity, as acknowledged in the present study, can magnify discrepancies greatly since St_{def} is proportional to the representative collision velocity squared [2, 10].

In many cases interparticulate frictional forces and cohesive forces are neglected in the determination of wet granule strength [14]. In general the equations used to calculate wet granule strength effectively take into account strength differences due to viscosity, particle size, packing density, and velocity changes, however they do not account for changes in primary particle shape or granule saturation [3], which have been shown to be significant factors in determining the strength of wet agglomerates [15]. As a result direct measurements of granule yield strength have been pursued. Iveson *et al* [2] studied wet granule yield strength by direct measurement at strain rates of 0.015 mm s^{-1}. However, these researchers concluded that these strain rates were too low to be representative of those experienced during high speed impacts and that at such low strain rates dynamic effects and viscous dissipation may not be activated, resulting in an artificially high estimate of the St_{def}.

*S*ubsequently dynamic yield strength measurements have been performed using a specialised high-speed hydraulic load frame capable of reaching speeds up to 15 cm s^{-1} [16]. At these increased speeds it was found that the yield strength of granules was

strain rate dependent and that the ranking of yield strength for granules prepared with different viscosity binders varied with strain rate. However, this strain rate is still significantly less than the impeller tip speeds of 1.57–4.71 m s^{-1} used in the present study, and impact velocities up to 10 m s^{-1} [9, 17] which have been suggested to be present in some high shear granulators. In reality, granules will experience a distribution of shear and impact stresses, and the distribution will typically depend upon the flow pattern in the given granulator [18], therefore any *ex granulator* measurements will only be an estimate of the true forces experienced in the granulator. Positron Emission Particle Tracking (PEPT) has been employed recently for real time measurement of particle motion inside granulators, however this equipment is highly specialised and not widely available [19].

Given these experimental variations it is noted that a very tight window exists at the confluence between nucleation, steady and induction growth behaviour. In the context of the present study a transition zone has been proposed where the dominant growth behaviour cannot be elucidated completely, however such a zone should be considered a "knife edge" where subtle uncontrolled changes in material properties, or operating conditions, can result in a variety of growth scenarios. Based on the current variation in reported St_{def} across multiple formulations, granulation equipment and operating conditions, and the need to incorporate a transition zone into the map for the present study, the current proposed regime map boundaries conditions are considered tentative and specific to the system studied. Iveson *et al* [2] acknowledged that the regime boundaries are likely to depend on other factors not incorporated into the growth regime map, such as binder liquid viscosity; and that a fully general regime map, yet to be elucidated, will require at least three dimensions. As such it is concluded that the regime map is a useful tool for comparing the behaviour of similar materials and binder liquids in the same granulator, however comparisons across different formulations and granule blends incorporating binder liquids with large differences in viscosity or different granulators are likely to prove difficult. This is a clear opportunity for future study.

6.3 Conclusion

Granule surface velocity was shown to be a suitable method to estimate the representative collision velocity in the granulator and demonstrated that the assumption of a fixed representative collision velocity is flawed. This method was also sensitive to rapid increases in granule size and has the potential to be used in the future as a granulation process endpoint indicator.

Stokes deformation number, St_{def}, was shown to be a good predictor of both granule resultant mass mean diameter and intragranular porosity over a wide range of process conditions. The data presented support the hypothesis that the reverse-phase granulation process results in a greater degree of granule consolidation than that produced using the conventional granulation process. As a result reverse-phase granules have a greater amount of surface liquid present which can dissipate collision energy and resist granule rebound resulting in the greater granule growth observed. St_{def} was capable of differentiating these differences in granulation process. These results were used to construct a growth regime map to describe the wet granulation growth mechanisms which were observed. The growth regime map considered both the dimensionless St_{def} and S_{max} parameters. The regime map was able to differentiate between the dry, nucleation, steady and induction growth regimes. However, significant differences were observed between the boundary values in the present study and those previously reported. As a result it is concluded that although the growth regime map might be considered a useful tool for comparing the behaviour of similar formulations within the same granulator, it is unlikely that it can be applied numerically to other formulations or granulators.

At this stage the feasibility of the reverse-phase granulation process has been established, a mechanism for granule consolidation and growth has been proposed and the effect of major variables established according to the proposed growth regime map. Additionally, the hypothesis that the compaction properties of reverse-phase granules would be inferior to conventional granules was rejected. It is therefore recommended that further work be performed to address the concern that the reverse-phase granulation process may result in a greater rate or extent of drug solid state transformation, due to the immersion mechanism of powder into the binder liquid.

6.4 References

[1] Iveson, S.M., Litster, J.D., Growth regime map for liquid-bound granules, AIChE J., 44 (1998) 1510-1518.

[2] Iveson, S.M., Wauters, P.A.L., Forrest, S., Litster, J.D., Meesters, G.M.H., Scarlett, B., Growth regime map for liquid-bound granules: further development and experimental validation, Powder Technology, 117 (2001) 83-97.

[3] Kayrak-Talay, D., Dale, S., Wassgren, C., Litster, J., Quality by design for wet granulation in pharmaceutical processing: Assessing models for *a priori* design and scaling, Powder Technology, 240 (2013) 7-18.

[4] Butensky, M., Hyman, D., Rotary drum granulation. An experimental study of the factors affecting granule size, Ind. Eng. Chem. Fundam., 10 (1971) 212-219.

[5] Sherington, P.J., The granulation of sand as an aid to understanding fertilizer granulation, Chem. Eng., July/August (1968) 201-215.

[6] Tardos, G.I., Khan, M.I., Mort, P.R., Critical parameters and limiting conditions in binder granulation of fine powers, Powder Technology, 94 (1997) 245-258.

[7] Hapgood, K.P., Amelia, R., Zaman, M.B., Merrett, B.K., Leslie, P., Improving liquid distribution by reducing dimensionless spray flux in wet granulation - A pharmaceutical manufacturing case study, Chem. Eng. J., 164 (2010) 340-349.

[8] Liu, L.X., Litster, J.D., Wet granule breakage in a breakage only high-shear mixer: Effect of formulation properties on breakage behaviour, Powder Technology, 189 (2009) 158-164.

[9] Knight, P.C., Seville, J.P.K., Wellm, A.B., Instone, T., Prediction of impeller torque in high shear powder mixers, Chem. Eng. Sci., 56 (2001) 4457-4471.

[10] Cavinato, M., Franceschinis, E., Cavallari, S., Realdon, N., Santomaso, A., Relationship between particle shape and some process variables in high shear wet granulation using binders of different viscosity, Chem. Eng. J., 164 (2010) 292-298.

[11] Plank, R., Diehl, B., Grinstead, H., Zega, J., Quantifying liquid coverage and powder flux in high-shear granulators, Powder Technology, 134 (2003) 223-234.

[12] Bouwman, A.M., Henstra, M.J., Hegge, J.J.M.E., Zhang, Z., Ingram, A., Seville, J.P.K., Frijlink, H.W., The relation between granule size, granule stickiness, and torque in the high-shear granulation process, Pharm. Res., 22 (2005) 270-275.

[13] vandenDries, K., deVegt, O.M., Girard, V., Vromans, H., Granule breakage phenomena in a high shear mixer; influence of process and formulation variables and consequences on granule homogeneity, Powder Technology, 133 (2003) 228-236.

[14] Bouwman, A.M., Visser, M.R., Meesters, G.M.H., Frijlink, H.W., The use of Stokes deformation number as a predictive tool for material exchange behaviour of

granules in the 'equilibrium' phase in high shear granulation, Int. J. Pharm., 318 (2006) 78-85.

[15] Iveson, S., Page, N., Dynamic strength of liquid-bound granular materials; The effect of particle size and shape, Powder Technology, 152 (2005) 79-89.

[16] Iveson, S.M., Page, N.W., Litster, J.D., The importance of wet-powder dynamic mechanical properties in understanding granulation, Powder Technology, 130 (2003) 97-101.

[17] Iveson, S.M., Beathe, J.A., Page, N.W., The dynamic strength of partially saturated powder compacts: the effect of liquid properties, Powder Technology, 127 (2002) 149-161.

[18] Mort, P.R., Scale-up of binder agglomeration processes, Powder Technology, 150 (2005) 86-103.

[19] Hassanpour, A., Kwan, C.C., Ng, B.H., Rahmanian, N., Ding, Y.L., Antony, S.J., Jia, X.D., Ghadiri, M., Effect of granulation scale-up on the strength of granules, Powder Technology, 189 (2009) 304-312.

CHAPTER SEVEN: *IN-SITU* MONITORING OF ANHYDROUS THEOPHYLLINE HYDRATION USING RAMAN SPECTROSCOPY: A COMPARISON BETWEEN THE CONVENTIONAL AND REVERSE-PHASE GRANULATION PROCESSES

7 Introduction

The feasibility of the reverse-phase granulation process has been established by work presented in the preceding chapters. The influence of binder liquid amount, binder liquid viscosity and impeller speed on the resultant granule size and porosity were compared to the conventional granulation process and certain advantages of the reverse-phase granulation process were highlighted. As described in Section 1.7 two potentially negative consequences of the reverse-phase approach were identified; the potential for the resultant granules to possess inferior compaction properties and the potential for a higher rate or greater extent of formation of a different solid state form of the drug due to increased drug dissolution in the binder liquid. The former was examined in previous chapters, where it was shown that granules prepared by the reverse-phase and conventional processes had equivalent compaction properties. Therefore, the aim of the current study was to compare the rate and extent of the solid state transformation of a model drug during the reverse-phase and conventional granulation processes. Theophylline was selected as the model drug owing to the fact that the molecule undergoes a well characterised transformation from the anhydrous form to the monohydrate form during wet granulation processing [1-4]. In-situ Raman spectroscopy has been successfully applied to monitor the formation of theophylline monohydrate during wet granulation [2, 5] and accordingly this technique was selected as a means for investigating any potential differences between the conventional and reverse-phase granulation processes. The incorporation of different polymers into the binder liquid has previously been reported to inhibit or slow solid state transformations during wet granulation processing [6]. Therefore this variable was also studied in order to establish whether this inhibition can be leveraged to mitigate any differences in theophylline hydration observed between the two granulation processes.

7.1 Theoretical and experimental considerations

7.1.1 Polymorphism and pseudopolymorphism

Polymorphism describes the ability of a solid-state crystalline material to exist in different lattice structures and/or different molecular conformations without undergoing changes in chemical composition [7]. Figure 7-1 presents an example of the different solid forms in which a drug substance could exist. When solvent molecules are incorporated into the crystal lattice in a stoichiometric or non-stoichiometric manner, the resulting structure is designated a solvate, or pseudopolymorph [8]. When the solvent in question is water the pseudopolymorph is referred to as a hydrate [7]. When the material lacks a crystal lattice structure and is random in terms of both molecular packing and conformation it is referred to as amorphous [9]. Polymorphism and hydration of drugs is a common occurrence and it is estimated that 80–90 % of organic compounds are capable of existing in at least two polymorphic forms [10] and that approximately 30 % of pharmaceutical compounds can exist as hydrates [8].

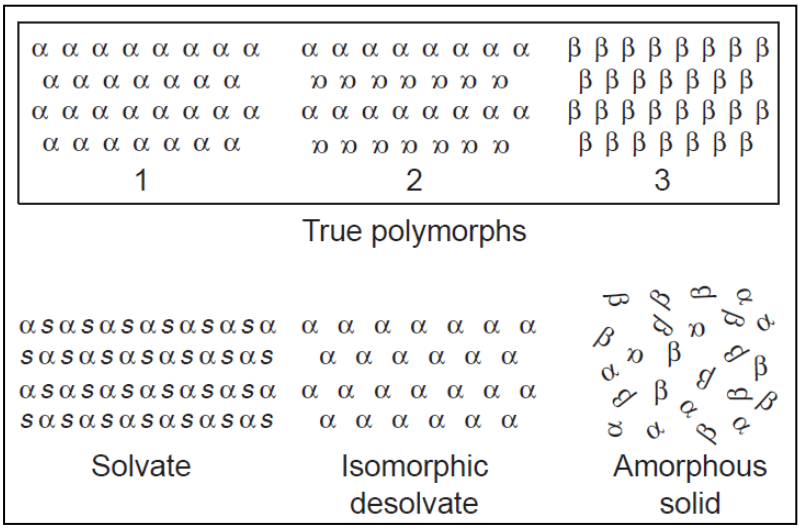

Figure 7-1. Representation of different solid forms of a drug substance. Drug molecules are represented by (α) and (β) and solvent molecules by (s). Adapted from [9].

Such solid-state transformations can be induced by the process conditions used to manufacture a pharmaceutical dosage form. In particular aqueous wet granulation processes are often considered a high risk for solid-state transformations due to the mechanical and thermal stresses involved and the exposure to water [11-13]. The thermodynamic stability of a given solid-state form is determined by Gibbs' free

energy. When considering the relative stability of solid-state forms of the material the difference in the Gibbs' free energy is decisive and is defined as [14]:

$$\Delta G = \Delta H - T \cdot \Delta S \qquad \textit{Equation 7-1}$$

where G is the Gibbs' free energy, H is the enthalpy which represents the total energy of a given phase, T is the absolute temperature of the system and S is the entropy which is defined as zero for a completely pure crystalline solid at absolute temperature of zero. A plot of Gibbs' free energy versus temperature is typically used to characterise solid-state systems. The solid-state form with the lowest Gibbs' free energy at a given temperature is the thermodynamically stable form and the difference in Gibbs' free energy between the current state and the thermodynamically most stable state will determine the relative stability of that solid-state form. Often a form other than the thermodynamically stable form may be isolated as a result of kinetic trapping of a metastable form in a local energy minimum (Figure 7-2).

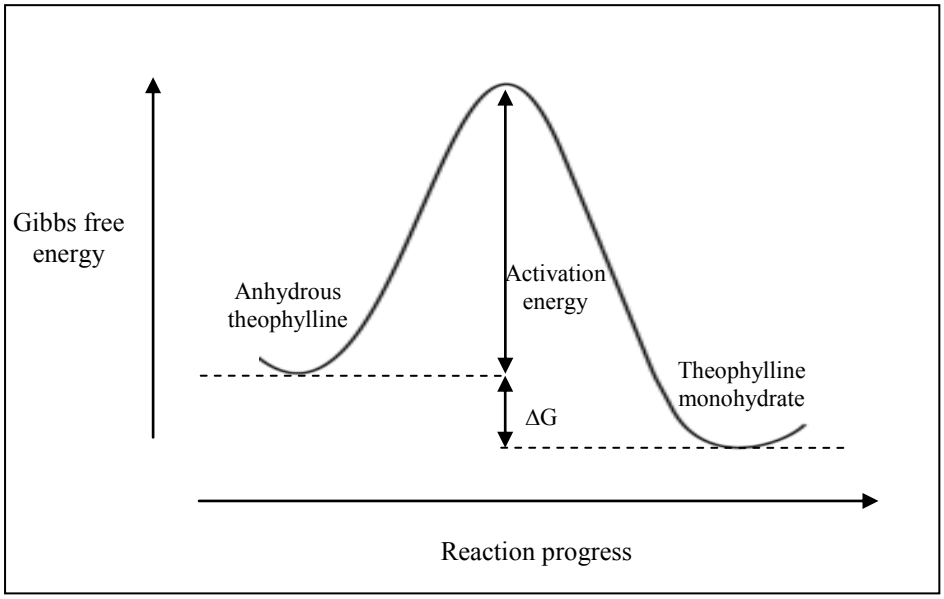

Figure 7-2. Illustration depicting kinetic trapping of metastable anhydrous theophylline relative to the thermodynamically stable theophylline monohydrate.

Over time a metastable form will transform into the thermodynamically stable form with the rate being dependent upon the Gibbs' free energy difference, the magnitude of the activation energy and other factors such as temperature, pressure and moisture.

Consequently an understanding of the multiple solid-state forms that a drug can exist in and the conditions under which they can transform between one another is critical to the successful formulation of a stable drug product.

The physical properties of the drug can be significantly different between solid-state forms. For example monoclinic paracetamol is poorly compressible and has to be co-processed with carefully selected excipients such as gelatine, PVP and starch to form a directly compressible material, however the orthorhombic form is readily compressible without further modification [15]. Similarly, Form I carbamazepine and γ-sulfanilamide have significantly lower Young's modulus of elasticity and yield stress than their corresponding Form III and β- polymorphs [16]. However, of utmost importance are differences in aqueous solubility between solid-state forms, which can result in differences in drug bioavailability, efficacy and toxicity [17]. Thermodynamically, only the polymorph with the lowest Gibbs' free energy at a given temperature and pressure is stable under those conditions and is characterised by the lowest solubility [7]. Typically, a solid having a higher Gibbs' free energy (i.e. a less stable polymorph) will dissolve faster since the release of a greater amount of stored free energy will increase the solubility and hence be the driving force for dissolution [18]. Generally the more thermodynamically stable polymorph is more chemically stable over the intended shelf life of the drug and this has been attributed to the higher crystal packing density and optimised orientation of molecules in the lattice structure [18]. Despite these considerations there may be occasions where a logical reason exists to formulate a drug product with the metastable polymorph, for instance with the intention of conferring increased solubility, dissolution rate and bioavailability. In these instances, the formulation strategy must ensure that the rate of conversion of the metastable form to more thermodynamically favoured forms is controlled.

7.1.2 Theophylline as a model drug

Theophylline is a natural derivative of xanthine, found mainly in tea, which has been widely used for the treatment of chronic obstructive pulmonary disease and bronchial asthma [19]. It is well known to undergo a solvent-mediated phase transformation from the anhydrate to the monohydrate during wet granulation [1-4] and was therefore

selected as a model drug in the present study. The chemical structure of anhydrous theophylline and theophylline monohydrate are shown in Figure 7-3.

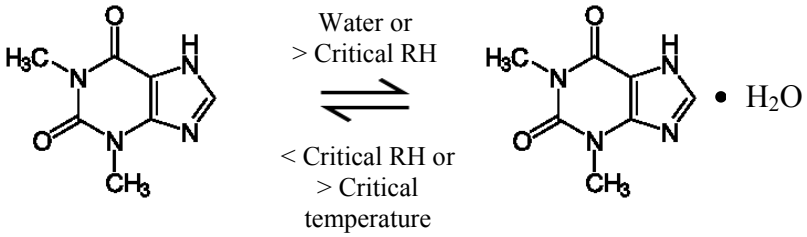

Figure 7-3. Chemical structures of anhydrous theophylline and theophylline monohydrate.

Theophylline is known to exist as a monohydrate crystal and four anhydrous forms (Form I, II, III and IV). In the context of aqueous wet granulation the anhydrous Form II and monohydrate are the two forms of practical interest. The monohydrate has been shown to dehydrate to produce anhydrous Form II, which is the most prevalent form and has long been considered the only stable form at room temperature [20, 21]. Anhydrous Form I is the thermodynamically stable form at elevated temperature and has been formed by evaporating a saturated water or methanol solution of theophylline at temperatures between 95–117 °C [22-24]. Form III is a highly metastable form which readily converts to Form II during storage [25, 26]. Form III has only been observed as an intermediate during dehydration of the monohydrate under low pressure or high temperature conditions [25, 27] and has not been observed during hydration of the anhydrous Form II [28]. Form IV was recently presented as the most thermodynamically stable anhydrous form and is produced as a result of a slow, solvent-mediated transformation over a period of 2–30 days depending upon the solvent system used [29].

The aqueous solubility of anhydrous theophylline and theophylline monohydrate at 25 °C have been reported as 12.3 mg cm^{-3} [2] and 5.96 mg cm^{-3} [30] respectively. Erratic dissolution performance has been reported for anhydrous theophylline tablets stored at high relative humidity [31, 32] or prepared by a wet granulation process [33]. In each of these cases the erratic dissolution performance was attributed to transformation of the anhydrous form to the monohydrate form, which has a slower dissolution rate [34].

The mechanism of theophylline hydration in an aqueous environment has been previously investigated [1, 30]. The monohydrate form heterogeneously nucleates from the surface of anhydrous theophylline crystals via a surface solution mediated transformation [1, 35] to form a channel hydrate [36] with a needle-like habit [3]. The transformation can also occur in the solid state under appropriate temperature and humidity conditions. Contact mode atomic force microscopy has been used to demonstrate that when exposed to elevated relative humidity the surface of anhydrous theophylline crystals exhibits enhanced mobility due to the formation of surface solution [35]. The critical water activity for the transformation has been reported as 0.62 [35], 0.64 [20], 0.65–0.70 [29] and 0.79 [37] at 25–30 °C. Dehydration of theophylline monohydrate to the anhydrous form has also been investigated. A critical water activity between 0.20–0.30 has been reported [37] for theophylline monohydrate dehydration.

7.1.3 Solid state transformation characterisation methods

A wide variety of characterisation methods are available to study drug hydrates, including X-ray diffraction, thermogravimetry, differential scanning calorimetry and hot stage microscopy. However, each of these methods involves removal of samples, a preparation step followed by an analysis off-line. More recently vibrational spectroscopy techniques using Near-Infra Red (NIR) and Raman methodology have been developed, which allow *in situ* measurements to be performed while minimising process disturbances and eliminating artefacts associated with sample preparation [2]. For a vibration to be NIR active the molecule generally possesses a strong dipole moment, whereas for a vibration to be Raman active the molecule is generally polarisable such that an induced dipole exists.

Differences in the hydrogen bonding network between anhydrous theophylline and theophylline monohydrate result in structural differences which have a direct effect on the position and intensity of bands in vibrational spectra [37]. NIR has two main drawbacks when analysing the hydration of anhydrous theophylline. Firstly, the bands in NIR spectra consist of overtones and combinations of fundamental molecular vibrations and thus cannot be specifically assigned [38]. Secondly, the differences between the anhydrous theophylline and theophylline monohydrate NIR spectra are overwhelmed by the presence of water, thus it is not possible to easily follow the

transformation [2]. Water has a σ-bonded electronic structure with a strong dipole moment, hence the vibrations are infrared active, however the electrons are not easily polarised and therefore dipole induction is difficult and Raman scattering is weak and spectral interference from water is low [39]. Raman spectroscopy can therefore be readily used to reveal changes in vibrations of drug molecules during hydrate formation [3] and was selected for this study.

The use of Raman spectroscopy has been reported for the study of a range of pharmaceutical dosage forms. Examples include the analysis of illicit drugs on the surface of paper currency [40], determination of a polymorphic form of tetracaine in bioadhesive transdermal patches [41], quantification of bucindolol within gel capsules which were inside blister packs [42] and the identification of single tyrosine moiety in 5 μm spray dried respirable powder containing a mixture of calcitonin and mannitol [43]. Raman spectroscopy has also been used to establish the degree of indomethacin crystallinity in tablets [44], the quantification of both captopril and prednisolone content in the same tablet [45] and the quantification of the mass [46] and thickness [47] of coating applied to tablets.

7.1.4 Raman spectroscopy theory

The Raman effect occurs when a photon from an excitation source (laser) interacts with the electron cloud of a molecule to excite it from a ground state to a virtual energy state. When the photon is emitted from the molecule it can have a different vibrational state resulting in a shift from the excitation frequency. If a sample is irradiated with monochromatic electromagnetic radiation (ν_o) the majority of the radiation is scattered elastically (Rayleigh scatter) and the frequency of the scattered light is the same as the incident beam. However a small fraction of the radiation, in the order 10^{-8} [48], is scattered inelastically (Raman scatter) with a smaller (Stokes radiation) or higher (anti-Stokes radiation) frequency than the incident beam ($\nu_o \pm \nu_m$). These differences in the frequency are called Raman shifts. At room temperature Stokes radiation predominantly occurs, and at higher temperatures (e.g. 500 °C) anti-Stokes radiation occurs since molecules are already at a higher vibrational state [48]. Figure 7-4 depicts the differences between Rayleigh scattering, Stokes radiation and anti-Stokes radiation in relation to excitations associated with IR, NIR and fluorescence.

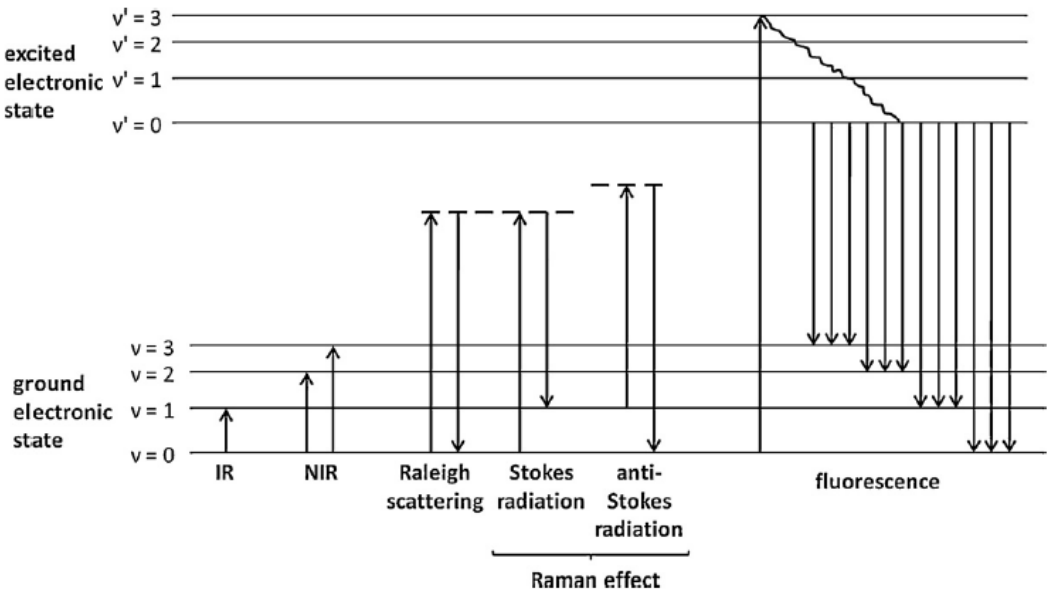

Figure 7-4. Illustration showing the relative energetic states associated with IR, NIR, Raman and fluorescence excitations. Taken from [48].

A Raman spectrum displays the frequency difference between the excitation source and the scattered radiation, expressed as wavenumber ($\Delta\nu$ cm^{-1}), versus the intensity of the scattered radiation [48]. Raman scattering relies upon: (1) the creation of an induced dipole (polarisation) in the molecule; (2) the modification of the dipole by molecular vibration; (3) subsequent scattering of a photon from the modified oscillating dipole [49]. This has important implications for analysing pharmaceutical formulations. Drug molecules frequently contain aromatic conjugated π-bonding systems which show strong Raman transitions, whereas excipients tend to be σ-bonded systems and are therefore weaker Raman scatterers [50]. Raman spectroscopy can therefore often be employed to monitor solid-state transformations of drugs without significant interference from excipient components within the formulation.

Since Raman scattering generates weak signals, with intensity inversely proportional to the fourth power of the wavelength of the radiation, the use of high-frequency excitation sources favours detection of Raman scattering [49]. However, decreasing the wavelength of the radiation may cause sample fluorescence. Fluorescence occurs when a photon from the laser source excites molecules in the sample to an electronically excited state, and then vibrational relaxation results in a photon of longer wavelength being emitted [50]. Fluorescence is typically several orders of magnitude stronger than Raman scattering and therefore typically obscures Raman bands [51]. For

pharmaceutical applications wavelengths of 785 nm and 1064 nm have been extensively used since these wavelengths are generally too low to electronically excite molecules in a sample and therefore fluorescence is typically avoided [50].

7.1.5 Sampling errors in Raman spectroscopy

The problem of ensuring representative sampling is one factor that can limit the precision of the quantitative Raman spectroscopic analysis of powders [52]. In particular the size of the powder particles relative to the probing laser spot size is important. If the spot size is smaller, or similar to, the size of an individual particle there is a high probability that only a single component might be detected in a mixture and therefore a false representation of the final mixture can be obtained. If the spot size is many times larger than the individual particles then the spectrum recorded is an average of many particles giving an improved overall indication of the composition. This effect has been clearly demonstrated with 50:50 % (*w/w*) mannitol polymorph samples which were sieved to give two sets. Smaller particles <125 μm gave a result of 49.0 ± 1.5 % whereas larger particles of 125–500 μm gave a result of 54.2 ± 16.1 % [53].

Static, or single point, measurements have also been cited as a source of sampling error [54-56] since the sample size, in terms of the number of particles analysed, is very low. One method used to improve the precision is to move the sample, while under the laser beam, to obtain an averaged representative spectrum [45, 57]. This effect was illustrated in the quantification of ambroxol content (8–16 %) in ambroxol/lactose tablets where the variability in the method was over 3-times lower (1.04 to 0.3 %) when the tablets were rotated compared to when they were stationary [58]. Another option is to move the position of the laser on the sample. Line focus is where mirrors are used to alter the points where the laser is focussed on the sample. Alternatively a mirror can be mounted on a rotating spindle, at a small angle to the rotation axis, to follow an elliptical path on the surface of the sample [59]. Grid sampling, where a small laser spot size is focussed over a number of grid locations on the sample by a motorised analyser, is another method that can be used for automated mapping to obtain a representative measurement [60]. For acetaminophen tablets changing the analysis method from spot (50 μm diameter) to line focus, and then to line focus with sample rotation, reduced the standard deviation of a standard signal from 13.0 % to 6.0 % to 1.5 % respectively [61]. In the

case of *in-situ* monitoring of wet granulation processes representative sampling is built into the process since the rotational movement of the impeller passes the sample under the laser focal area with high frequency.

Another option to reduce sampling error is to probe larger areas of the sample, rather than points or lines, since this maximises the number of particles examined. Wide area illumination is one solution where the laser is focussed from a fibre optic bundle with long focal length and large spot size. A wide area illumination optic has been employed to study poly (vinyl pyrrolidone) content in eyewash solutions contained in low-density polyethylene bottles where it was reported that the standard deviation between samples was 3.2 % using the wide area illumination approach compared to 32.5 % with a standard configuration [62].

7.1.6 *In-situ* monitoring of wet granulation processes

In-situ monitoring of drug hydration during wet granulation processes has been reported for a range of drugs including theophylline [2, 3, 63], caffeine [3, 63], carbamazepine, nitrofurantoin and sulfaguanidine [63]. Wet granulation processes represent a unique sampling challenge, when compared to liquid or powder samples, since the sample itself is prone to adhering to the sampling probe which can result in repeated sampling of the same portion of material. When using a stainless steel immersion Raman probe to study the effect of impeller speed on the *in-situ* hydration of anhydrous theophylline it was reported that probe design and placement in the granulator bowl were critical to ensure representative sampling and prevent sticking of the granulation material to the probe [2]. The authors recommended the use of non-contact optics for interfacing Raman spectroscopy to wet granulation processes. A commercially available non-contact wide area illumination optic is the P^hAT probe (Kaiser Optical Systems Inc., Ann Arbor, Michigan, USA). The performance of the P^hAT probe has been compared against two smaller laser spot sizes, one a contact probe and one a non-contact probe, for the monitoring of anhydrous theophylline hydration during a wet granulation process [5]. The variability between measurements decreased as spot size diameter increased from a 60 μm immersion probe to a 150 μm non-contact probe to a 3 mm P^hAT probe with an RSD of 31 %, 12 % and 10 % respectively.

In light of the discussion in this and preceding sections the following sampling methodology was selected to monitor the transformation of anhydrous theophylline during wet granulation experiments. *In-situ* sampling of the wet granulation was selected to eliminate artefacts associated with sample preparation. *In-situ* sampling in the wet granulation process ensures a continual movement of sample under the laser which favours representative sampling. A laser with 785 nm wavelength was selected to minimise the potential for sample fluorescence. A non-contact Raman probe was selected to eliminate the potential for the wet granules to stick to the probe. A wide area illumination probe was selected to increase the probed volume of the sample relative to the particle size of the individual components.

7.1.7 Inhibition of solid-state transformations using polymer additives

The transformation of theophylline from the anhydrous form to the monohydrate has been shown to be solvent-mediated and to involve three processes [2, 63]; (1) dissolution of the less stable phase; (2) nucleation of the more stable phase; (3) growth of the more stable phase. The first stage involves the dissolution of the anhydrous form which leads to supersaturation of the liquid with respect to the monohydrate form and provides the thermodynamic driving force for crystallisation. The second stage involves the nucleation of the monohydrate form on the surface of anhydrous crystals. The third stage is the growth of the monohydrate form which will deplete the solution concentration resulting in further dissolution of the anhydrous form. The monohydrate form will continue to grow until all of the anhydrous form has dissolved and the concentration of drug in solution reaches the solubility of the monohydrate form. For a substance to change the kinetics of the hydration transformation it must affect one or more of these three stages.

The transformation kinetics of anhydrous theophylline was studied by monitoring a suspension of 20 g water and 1 g anhydrous theophylline [63] where no relationship was found between the transformation kinetics and drug solubility or intrinsic dissolution rate. In fact, anhydrous theophylline was predicted to dissolve to a concentration equivalent to the solubility of the anhydrous form in less than one minute (based upon the intrinsic dissolution rate of the anhydrous drug and its initial surface area) leading to the conclusion that dissolution of anhydrous theophylline was not the

rate limiting step in the transformation. This is further supported by the solubility and intrinsic dissolution rate of both anhydrous theophylline and theophylline monohydrate which were reported to be the same in PVP and HPMC solutions (10 % *w/w* polymer:drug) as in water [6]. Therefore for a polymer to influence the transformation kinetics of anhydrous theophylline it must affect either the nucleation or growth stages.

Classical nucleation theory describes homogenous nucleation, however this is unlikely to occur in the high-shear wet granulation system due to the potential for secondary nucleation on foreign surfaces created by the shear generated within the granulator [6]. The crystallisation of theophylline monohydrate has in fact been shown to occur heterogeneously on the surface of the anhydrous theophylline crystals [1]. If nucleation of the monohydrate is inhibited then crystal growth cannot occur and inhibition of crystal growth only becomes important if seed crystals are present. The presence of 5 % *w/w* of theophylline monohydrate seed crystals has been reported to have no effect, indicating that transformation to the hydrate is not nucleation rate limited [2]. However, conflicting findings have been reported where seeding with 10 % *w/w* hydrate crystals increased the hydration rate by bypassing the nucleation stage [35]. These same investigators also reported that grinding of the anhydrous starting material increased the hydration rate due to increased surface dislocation which facilitated dissolution, and also generated increased nucleation sites. The reported inhibitory effect of polymer additives is therefore likely to be as a result of a combination of altered nucleation and growth kinetics.

Poly (acrylic acid) (PAA), HPMC, HPC and PVP have all been reported to have different levels of inhibition on the hydration of caffeine, carbamazepine and sulfaguanidine [64]. No single polymer resulted in complete inhibition of the drug hydration, however based upon the chemical structures of the drugs and polymers studied it was proposed that a specific hydrogen bonding interaction between the polymer and the crystal surface of the drug may be responsible for the inhibition [64]. PVP has been reported to inhibit the growth of sulfathiazole crystals through adsorption to the surface of the crystal and subsequent formation of a net-like structure [65]. Additionally, PVP has been reported to inhibit the crystallisation of amorphous indomethacin due to hydrogen bonds formed between the hydroxyl groups of the indomethacin and the carbonyl groups of the PVP [66]. Similarly, HPMC has been

suggested to inhibit the hydration of carbamazepine through hydrogen bonding of the oxygen and hydroxyl groups on the cellulose ring of HPMC and the amine and carbonyl groups of the carbamazepine molecule [67]. It has been hypothesised that a greater amount of hydrogen bonding between the polymer and the crystal surface results in greater adsorption of the polymer to the crystal surface and therefore a greater degree of inhibition [68].

An alternative mechanism has also been proposed to account for the inhibition of theophylline hydration by PVP, where it was speculated that hygroscopic excipients may act as desiccants that competitively sorb available moisture [69]. A similar proposal was put forward for the highly hygroscopic silicified microcrystalline cellulose which inhibited theophylline hydration at low moisture contents, but became saturated at high moisture contents when the retarding effect ceased [70]. Moreover these latter researchers reported that the non-hygroscopic and highly soluble α-lactose promoted theophylline hydration possibly due to the sugar increasing the number of secondary nucleation sites. However, Taylor *et al* [71] have challenged the 'desiccant mechanism' for open systems where there is a constant supply of moisture in spite of their own findings indicating that although PVP became saturated with moisture within a few hours, theophylline hydration was still delayed for days. It was suggested that since only a small portion of the theophylline is in solution at a given time the PVP to theophylline ratio will be high, and combined with the high viscosity of the system, a saturated solution of PVP is able to retard hydration, though an exact mechanism was not proposed. A separate study considered the effect of several grades of several excipients, including PVP, MCC, HPMC, HPC, PEG, PAA and methyl cellulose, on the hydration rate of anhydrous theophylline [6]. It was found that excipients which retarded hydration in slurry experiments also retarded hydration in granulation experiments. Additionally, no difference in retarding effect was observed when the excipient was either dissolved in the water, or added dry as a mixture with the drug during the granulation process, suggesting that the 'desiccant mechanism' may not adequately explain the inhibitory effect.

SEM and optical microscopy images have been used to further elucidate the inhibition mechanism. In the presence of inhibitory excipients the morphology of the theophylline monohydrate was altered [6], since although nucleation was still observed to occur at

the surfaces of the anhydrous crystal, there appeared to be fewer nucleation sites than with excipients that did not inhibit hydration. It was proposed that inhibitory polymers adsorbed to the fast-growing surfaces of the hydrate crystal retarding the overall growth rate. The morphology changed from needle-like in the absence of polymer to polygon-like when hydration was inhibited.

7.1.8 Hypothesis

Two hypotheses are put forth for the present study. First, in the conventional granulation process there is an onset period at the beginning of the process where little or no solid-state transformation occurs [5]. The onset time can determine whether the transformation occurs within a timeframe which may be of practical concern. For example, a drug which undergoes hydration during a wet granulation process with an onset time in the order of days may not necessarily present a concern as the granules may be dried below some critical water activity as part of normal processing in a much shorter time frame. In contrast an onset time in the order of minutes will almost certainly be of practical concern during the granulation process and will need to be addressed as part of process development. The efficiency of liquid distribution has been shown to determine the onset time with a linear relationship between impeller speed and onset time being reported for the hydration of anhydrous theophylline in a conventional granulation process [5]. In the reverse-phase process, where the drug is immersed in the binder liquid, the distribution time is predicted to be much shorter. It is hypothesised that the reverse-phase process will therefore have a faster onset time than the conventional granulation process. Therefore, the extent of transformation is predicted to be the same for the two granulation processes provided the formulation components and binder liquid amount are held constant and the process is continued to equilibrium. It is acknowledged that under normal operation the granulation process is unlikely to proceed to thermodynamic equilibrium and differences in the extent of hydration may exist.

Second, it is hypothesised that the incorporation of polymer additives into the binder liquid will inhibit the theophylline transformation [64]. It is proposed that this inhibition can be leveraged to mitigate the faster onset time expected in the reverse-phase process. Water is proposed to represent the worst case from a hydration perspective whereas the

addition of both PVP and HPMC has been reported to have an inhibitory effect on drug hydration [6].

Accordingly the aim of this study was to use *in-situ* Raman spectroscopy to compare the rate and extent of hydration of anhydrous theophylline during the reverse-phase and conventional granulation processes, while evaluating whether manipulation of the binder liquid composition might be used to control the transformation profile.

7.2 Materials and Methods

Hydroxyapatite (HA) (TRI-CAL WG™) and poly (vinyl pyrrolidone) (PVP) (Plasdone K29/32) were obtained from the suppliers detailed in Section 2.1.1. Hydroxypropyl methlycellulose (HPMC) (HPMC-5, Methocel™ grade 40-100) was obtained from Dow Chemical Company, Plaquemine, Louisiana, USA. Anhydrous theophylline (CAS Number 58-55-9) was obtained from Sigma-Aldrich, St. Louis, Missouri, USA.

To ensure the purchased theophylline was 100 % anhydrous the material was stored in a drying oven at 100 °C for 7 d prior to use [2, 72]. Theophylline monohydrate was prepared by placing a thin layer of anhydrous theophylline on a Petri™ dish and storing over water in a sealed desiccator for 7 d at room temperature [2, 6]. This approach minimises any particle size differences between the anhydrous and monohydrate samples. Samples were confirmed to be anhydrous and monohydrate material by thermogravimetric analysis (TGA) and differential scanning calorimetry (DSC) and were further characterized using SEM, laser light scattering and Raman spectroscopy as described immediately below.

7.2.1 Thermal behaviour

Thermal behaviour was determined by TGA and DSC (TGA Q500 / DSC Q1000, TA Instruments, New Castle, Delaware USA). Samples (~5 mg) were placed in open standard aluminium pans (n=3) and heated from 25 to 300 ºC at a rate of 10 °C min^{-1}. For the TGA analysis the weight change of the sample and the first derivative of weight change were collected as a function of temperature. For the DSC the heat flow between the sample and the instrument was collected as a function of temperature.

7.2.2 Scanning electron microscopy

SEM images were captured as described in Section 2.1.2.6.

7.2.3 Particle size analysis

Particle size (n=3) was measured by a wet dispersion laser light scattering method using a Hydro 2000S (Malvern, Worcestershire, UK). Samples were dispersed in a hexane/0.1

% polysorbate 80 dispersant using a sonic bath. The pre-prepared suspension was then added to a hexane/0.1 % polysorbate 80 solution and size analysis performed with a final obscuration range of 16–21 % being attained. Data were analysed using the general purpose Fraunhofer diffraction model.

7.2.4 Raman spectroscopy calibration model

Anhydrous theophylline and theophylline monohydrate were mixed in 10 % *w/w* increments to produce 1 g blended samples. All concentrations were prepared in triplicate and placed into a sealed glass sample vial. Each sample bottle was then opened in turn and placed into a static testing assembly with the Raman probe mounted vertically above the sample vial. Raman spectra were collected in triplicate for each sample using an RXN2-785 Raman spectrometer (Kaiser Optical Systems Inc., Ann Arbor, Michigan, USA) equipped with a P^{h}AT probe. A 10–400 mW diode laser at 784.8 nm was used for excitation and Raman spectra were obtained over a range of 1890–150 cm^{-1}. Each spectrum was composed of four scans with an exposure length of 1000 ms per scan.

iC Raman^{TM} software (version 4.1; Mettler-Toledo, Columbus, Ohio, USA) was used to control the Raman spectrometer. Raman spectra from the iC Raman^{TM} software were exported to MATLAB® (Natick, Massachusetts, USA) as .spc format files (Thermo Galactic, Salem, New Hampshire, USA) where they were baseline corrected and then exported to Microsoft® Excel (Microsoft Corporation, Redmond, Washington, USA) for analysis and graph plotting. The resultant Raman spectra were randomly divided into a calibration set and an independent test such that a linear plot of the actual versus predicted values could be constructed allowing the predictive capability of the model to be tested.

7.2.5 Wet granulation

Aqueous granulation binder liquid was prepared by mixing water with either 10 % *w/w* PVP or 5 % *w/w* HPMC. Following dissolution of the PVP or HPMC, the solution was held without agitation for at least 12 h to allow deaeration. Water alone was also used as a binder liquid. Granulation experiments were conducted in a 1-L high shear granulator

(P1-6, Diosna Dierks & Sohne GmbH, Osnabruck, Germany) as shown in Figure 2-1. Granules were prepared by both a conventional granulation process and the novel reverse-phase granulation process as described below. For each granulation experiment *in-situ* Raman spectra were collected for the duration of the granulation experiments. The tip of the Raman P^hAT probe was placed ~5 cm from the powder surface and the position was held constant for all studies using a fixed clamp stand. Raman spectra were obtained as described in Section 7.2.4 every 10 s over the duration of the experiments. Each granulation experiment was performed in triplicate to assess the variability associated with the *in-situ* Raman monitoring technique.

For the conventional granulation process the 450 g of dry HA powder and 150 g anhydrous theophylline powder were added to the granulator bowl and mixed for 30 s using an impeller speed of 400 rpm (3.14 m s^{-1} tip speed) and chopper speed of 1000 rpm (0.89 m s^{-1} tip speed). Following mixing 200 cm^3 binder liquid (either water, 10 % *w/w* aqueous PVP or 5 % *w/w* aqueous HPMC) was sprayed onto the moving powder bed through a 65° VeeJet nozzle (SS-650033, Spraying Systems, Wheaton, Illinois, USA) at 3 bar pressure. Separate experiments were performed in triplicate using each binder liquid. Impeller speed was maintained constant at 400 rpm (3.14 m s^{-1}) and chopper speed was maintained constant at 0.89 m s^{-1} (1000 rpm) for all experiments. Wet massing was performed for 10 s following complete addition of the binder liquid.

For the reverse-phase granulation process the total volume of 200 cm^3 binder liquid (either water, 10 % *w/w* aqueous PVP or 5 % *w/w* aqueous HPMC) was added directly to the granulator bowl. The binder liquid was mixed for 30 s with an impeller speed of 400 rpm (3.14 m s^{-1}) and chopper speed of 1000 rpm (0.89 m s^{-1}). A preblended mixture of 450 g of dry HA powder and 150 g anhydrous theophylline was added to the moving liquid using a vibratory feeder at a feed rate of approximately 5 g s^{-1} (Syntron F-T0, FMC Technologies Inc., Tupelo, MS, USA). Impeller and chopper speeds were maintained constant at 400 rpm (3.14 m s^{-1}) and 1000 rpm (0.89 m s^{-1}) respectively for all experiments. Wet massing was performed for 10 s following complete addition of the powder.

For both granulation processes the resultant granules were dried as a thin layer in a hot air convection oven (Lindberg/Blue, SPX Thermal Solutions, Rochester, New York,

USA) at 60 ºC for 24 h. A summary of the granulation experimental conditions is presented in Table 7-1.

Table 7-1. Summary of conditions in both granulation methodologies for the in-situ Raman monitoring of theophylline hydration.

Binder liquid (cm^3)	Binder liquid composition	Hydroxyapatite mass (g)	Anhydrous theophylline mass (g)	Impeller tip speed ($m\ s^{-1}$)
200	Water 10 % *w/w* PVP 5 % *w/w* HPMC	450	150	3.14

7.2.6 Statistical analysis

Statistical analysis to determine whether significant differences existed between sample means was performed as described in Section 2.1.2.8.

7.3 Results and Discussion

7.3.1 Thermal behaviour

Thermal behaviour of the anhydrous theophylline and theophylline monohydrate samples was determined by TGA and DSC over the temperature range of 25–300 °C. Representative thermograms for anhydrous theophylline and theophylline monohydrate are shown in Figure 7-5 and Figure 7-6 respectively.

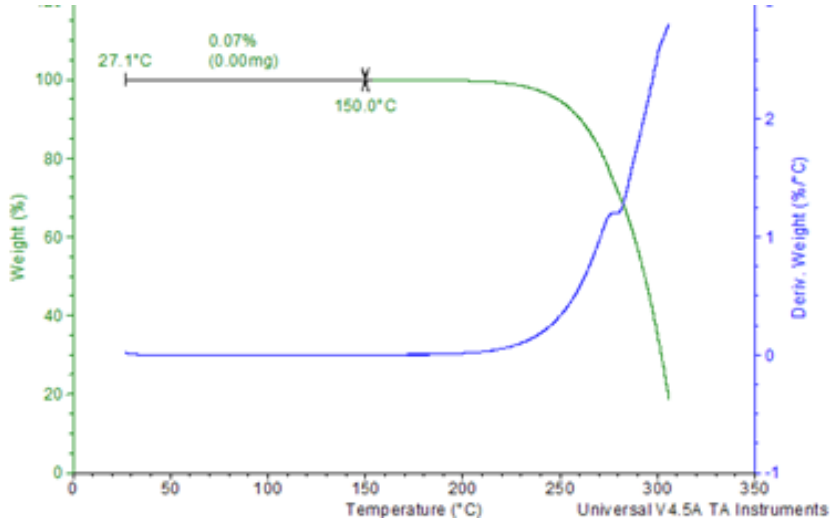

Figure 7-5. An example thermogram obtained for anhydrous theophylline heated from 0–300 °C at a rate of 10 °C min^{-1}.

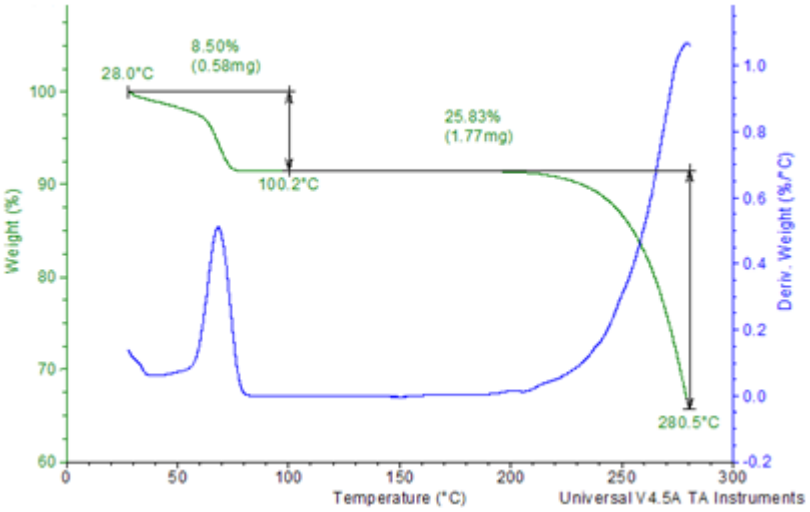

Figure 7-6. An example thermogram obtained for theophylline monohydrate heated from 0–300 °C at a rate of 10 °C min^{-1}.

The anhydrous theophylline thermogram (Figure 7-5) shows negligible mass loss up to a temperature of 150 °C whereas the theophylline monohydrate thermogram (Figure 7-6) shows a mass loss of ~8.5 % up to a temperature of 100 °C. A summary of the total moisture loss across the temperature range are shown in Table 7-2. The results are in agreement with previously reported values for the anhydrous and monohydrate forms of 0 % and 9 % *w/w* [4] respectively.

Table 7-2. Moisture loss for anhydrous theophylline and theophylline monohydrate samples when heated from 0–100 °C (n=3).

Sample	Moisture content [%] (SD)
Anhydrous theophylline	0.05 (± 0.03)
Theophylline monohydrate	8.56 (± 0.13)

Representative DSC profiles for anhydrous theophylline and theophylline monohydrate are shown in Figure 7-7 and Figure 7-8 respectively.

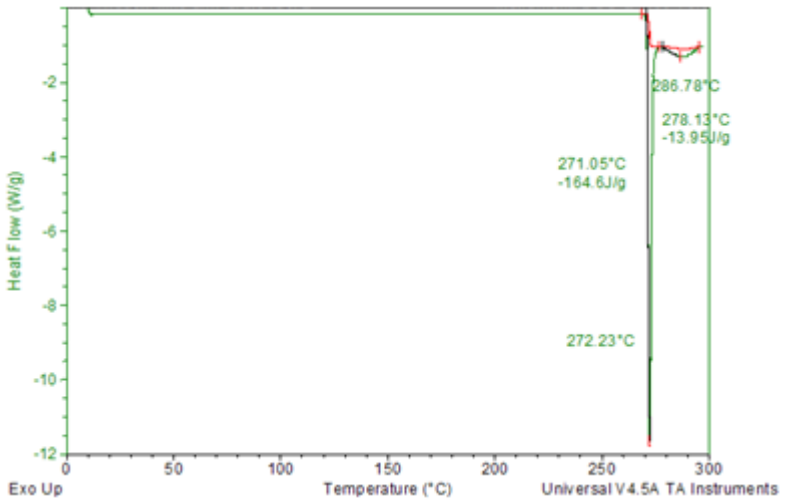

Figure 7-7. An example DSC profile obtained for anhydrous theophylline heated from 0–300 °C at a rate of 10 °C min^{-1}.

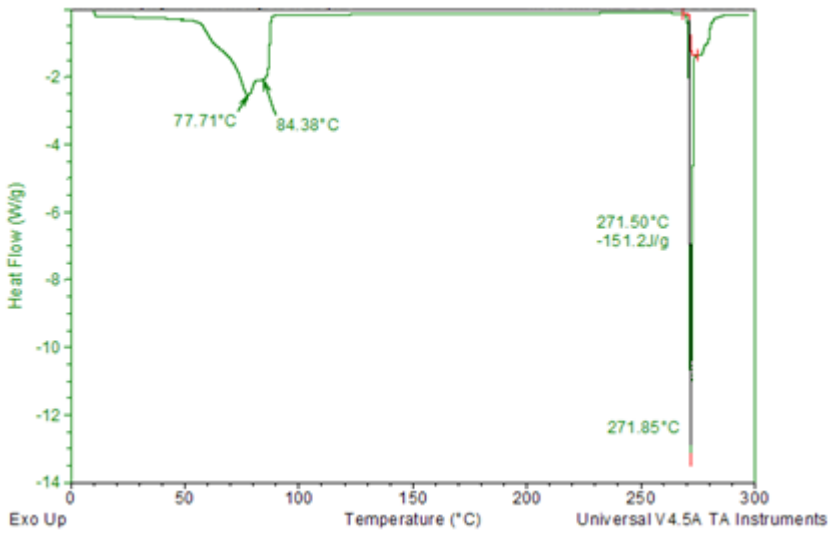

Figure 7-8. An example DSC profile obtained for theophylline monohydrate heated from 0–300 °C at a rate of 10 °C min^{-1}.

The DSC profile produced for anhydrous theophylline (Figure 7-7) shows an endotherm associated with melt/decomposition of the material at ~272 °C [29]. The DSC profile obtained for theophylline monohydrate (Figure 7-8) shows merged endotherms in the range ~60–90 °C associated with dehydration of theophylline monohydrate to the anhydrous form [29], and a second endotherm associated with melt/decomposition of the anhydrate at ~272 °C [29]. The latter endotherm was at a comparable temperature to that obtained in the DSC profile for anhydrous theophylline.

7.3.2 Scanning electron micrographs

Images of anhydrous theophylline and theophylline monohydrate samples were taken by scanning electron microscopy and representative micrographs are shown in Figure 7-9 and Figure 7-10 respectively.

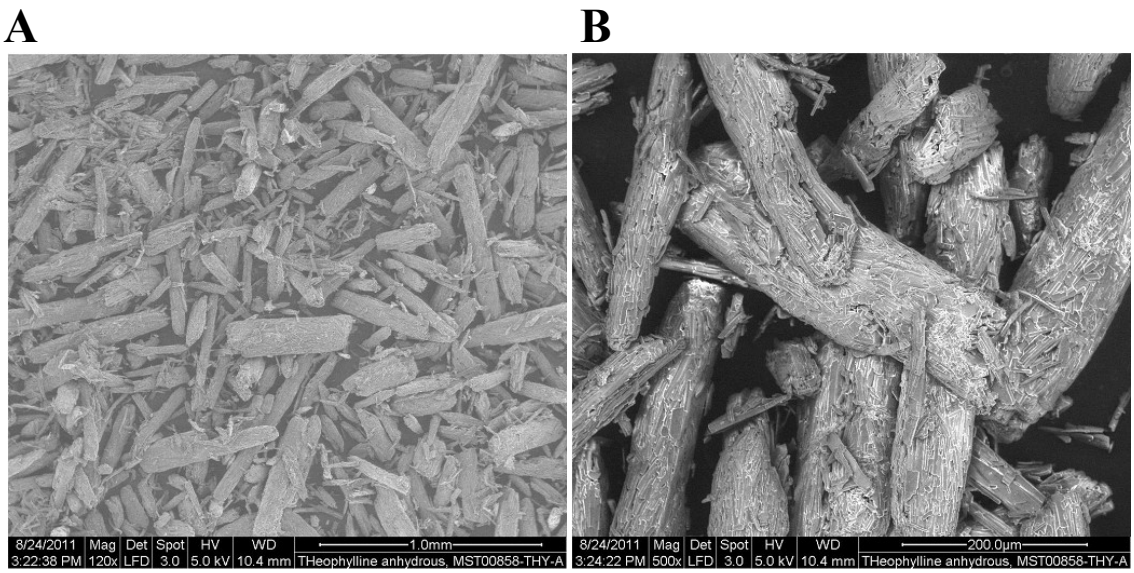

Figure 7-9. Representative anhydrous theophylline scanning electron micrographs. A – 130 x magnification, B – 500 x magnification.

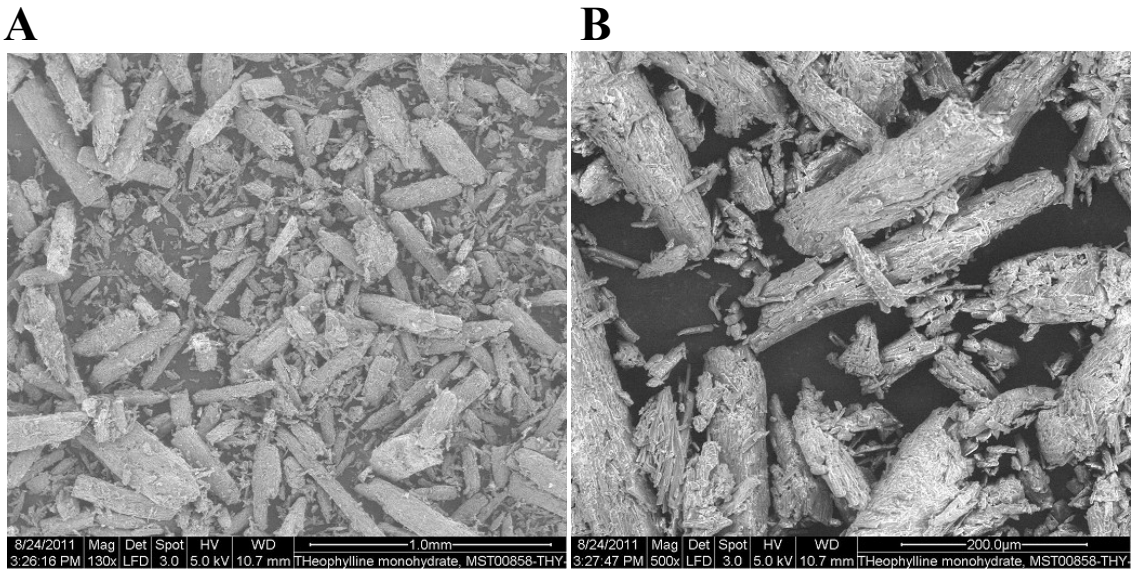

Figure 7-10. Representative theophylline monohydrate scanning electron micrographs. A – 130 x magnification, B – 500 x magnification.

The scanning electron micrographs show that both anhydrous theophylline and theophylline monohydrate crystals exhibit characteristic needle morphology [3]. Little difference is noted between the physical shape and structure of the anhydrous theophylline and theophylline monohydrate crystals indicating that the method of hydration did not markedly affect the particle morphology of the samples used for the calibration model.

7.3.3 Particle size distribution

The particle size distribution and volume undersize data of the anhydrous theophylline and theophylline monohydrate samples are shown in Figure 7-11. These data show that the method of hydration employed did not influence the particle size distribution of the samples used for the calibration model.

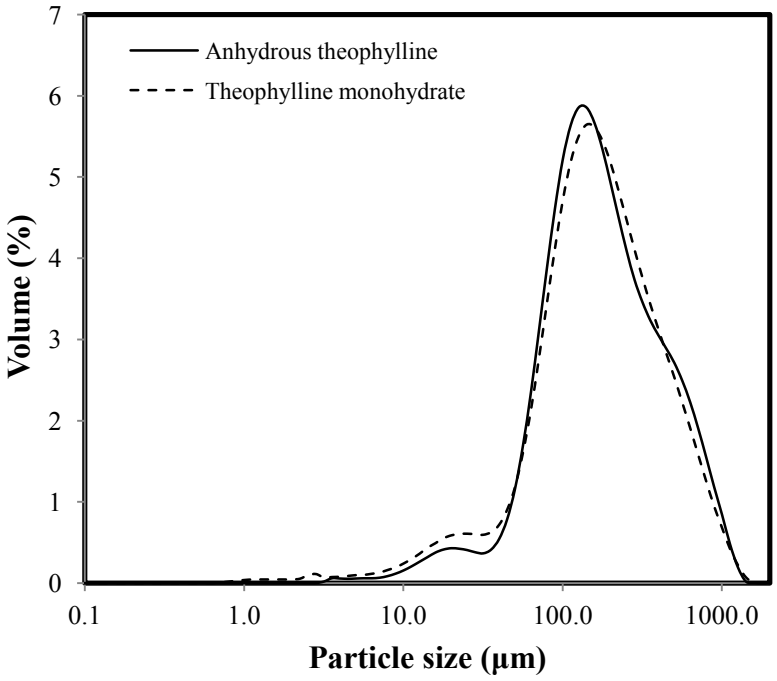

Figure 7-11. Particle size distribution plot for anhydrous theophylline and theophylline monohydrate calibration samples. Mean of n=3, error bars not shown as they obscure the data.

7.3.4 Calibration model

The intensity of the observed Raman signal can alter because of small changes in instrument and sample preparation parameters (e.g. laser power, sampling position relative to focus of the laser, etc) and as a result absolute Raman intensity is rarely used for quantitative analysis. This challenge was addressed in the present study by measuring the height of bands of interest in the sample relative to the height of other bands in the sample, since the intensity of each will increase or decrease in concert if experimental conditions change. Similar univariate calibration models based upon Raman peak height ratios have been reported for monitoring solid state transformations

of carbamazepine [73], L-glutamic acid [74], flufenamic acid [75] and risedronate sodium [76].

Figure 7-12 shows the complete Raman spectra of 100 % anhydrous theophylline, 100 % theophylline monohydrate and the difference in spectral intensity between the two. Clear differences are observed indicating that Raman spectroscopy can be used to monitor the transformation of anhydrous theophylline into theophylline monohydrate.

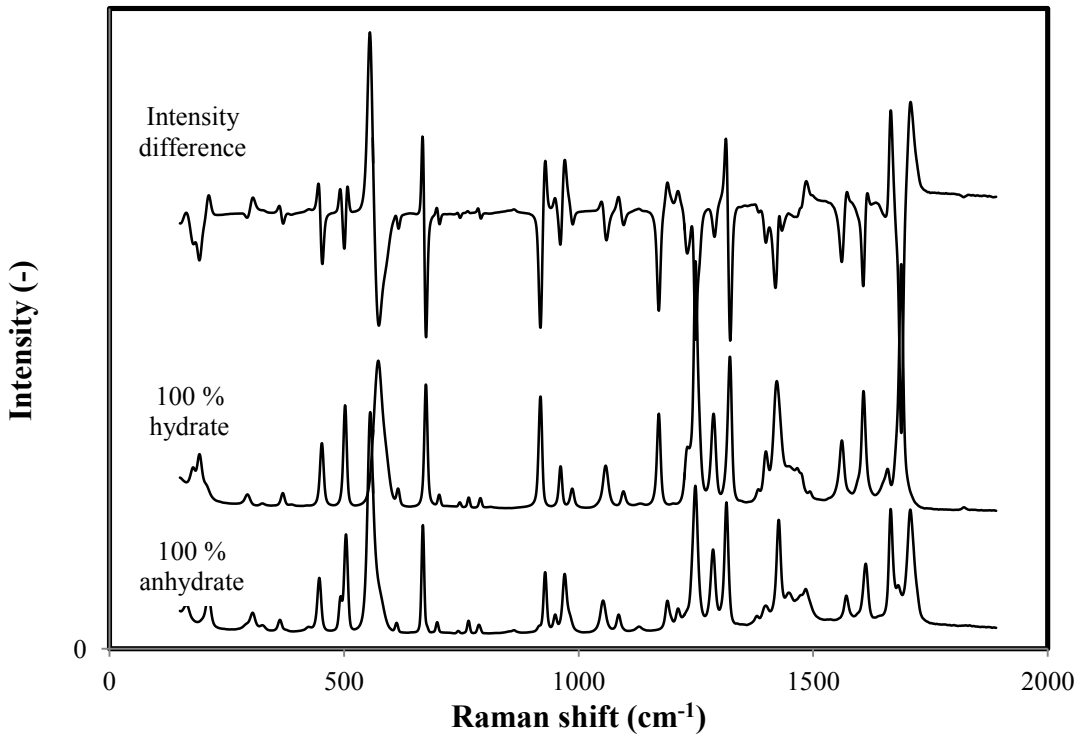

Figure 7-12. Raman spectrum of 0 % and 100 % w/w theophylline monohydrate, also showing the intensity difference between the two forms over the 0 – 2000 cm^{-1} range.

Two peaks in anhydrous theophylline at 1665 and 1707 cm^{-1} are replaced with a single peak in theophylline monohydrate at 1688 cm^{-1}, both associated with the C=O vibrations in the theophylline molecule [2, 3] The use of these peaks to monitor the transformation has been reported previously [2, 35] and this approach was therefore selected in the present study to construct a univariate calibration model. Figure 7-13 shows the 1640–1740 cm^{-1} spectral region of interest. Figure 7-14 shows the 1640–1740 cm^{-1} spectral region for 100 % anhydrous theophylline and 100 % theophylline monohydrate along with the Raman spectra for HA, PVP and HPMC. It is evident that there is no significant interference from the excipients in this spectral region, therefore

the changes in peak height ratios should feasibly be converted to percent theophylline monohydrate using appropriate calibration data.

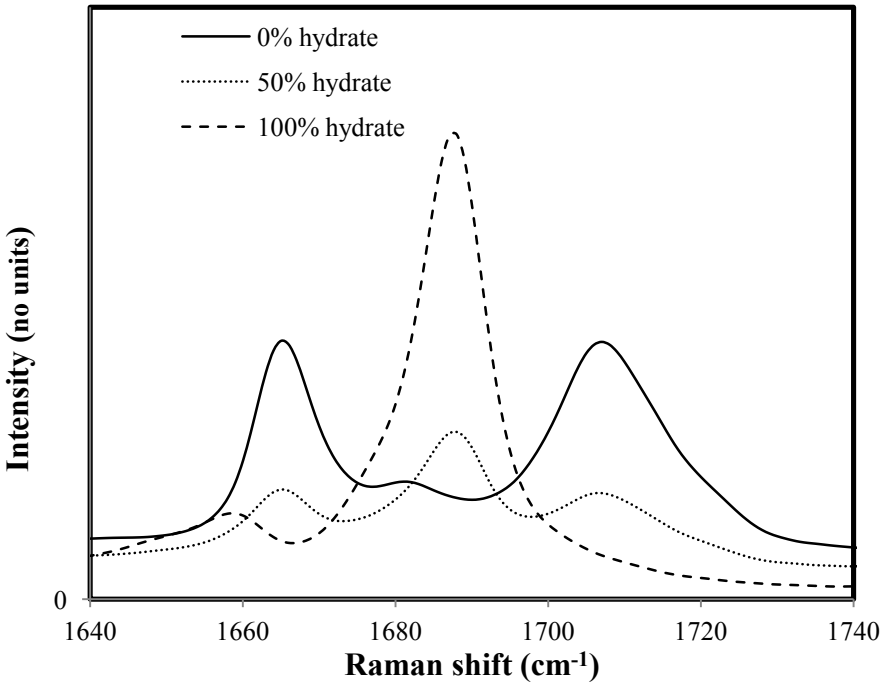

Figure 7-13. Raman spectrum of 0 % (i.e. 100 % w/w anhydrous theophylline), 50 % and 100 % w/w theophylline monohydrate showing the 1640–1740 cm^{-1} calibration range.

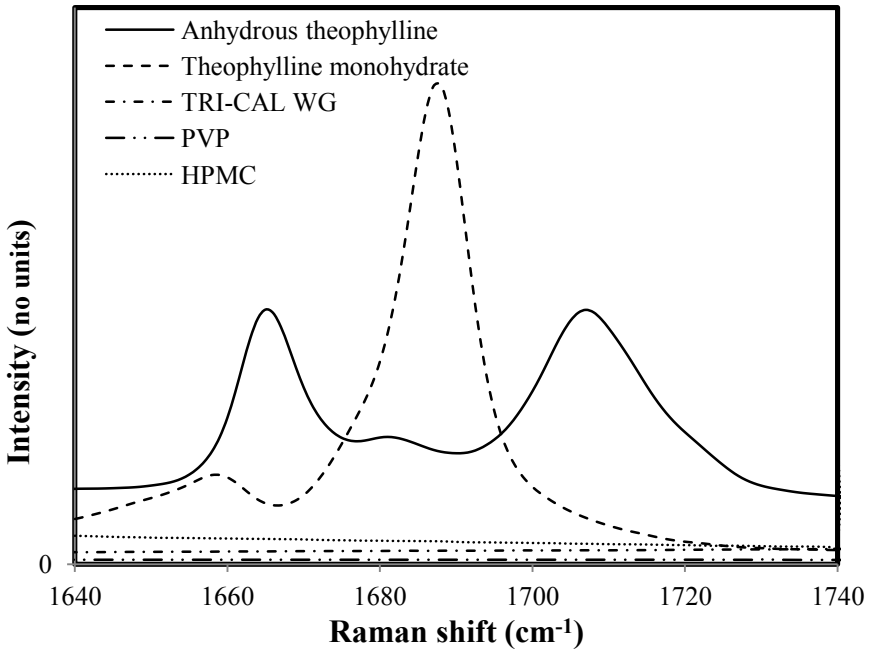

Figure 7-14. Raman spectrum for anhydrous theophylline, theophylline monohydrate, hydroxyapatite, poly (vinyl pyrollidone) and hydroxypropyl methylcellulose showing the 1640–1740 cm^{-1} calibration range.

The samples prepared in Section 7.2.4 were analysed using the Raman spectrometer and a univariate calibration model for the quantification of theophylline monohydrate was constructed. The data were well described with an exponential best fit curve (R^2 of 0.9895) (Figure 7-15). The calibration model was used to predict the theophylline monohydrate content in the independent test set. The actual versus predicted plot using the calibration model is shown in Figure 7-16. An R^2 of 0.9903 was obtained indicating that the Raman spectroscopy model can adequately discriminate between the anhydrous and monohydrate forms of theophylline over the entire concentration range.

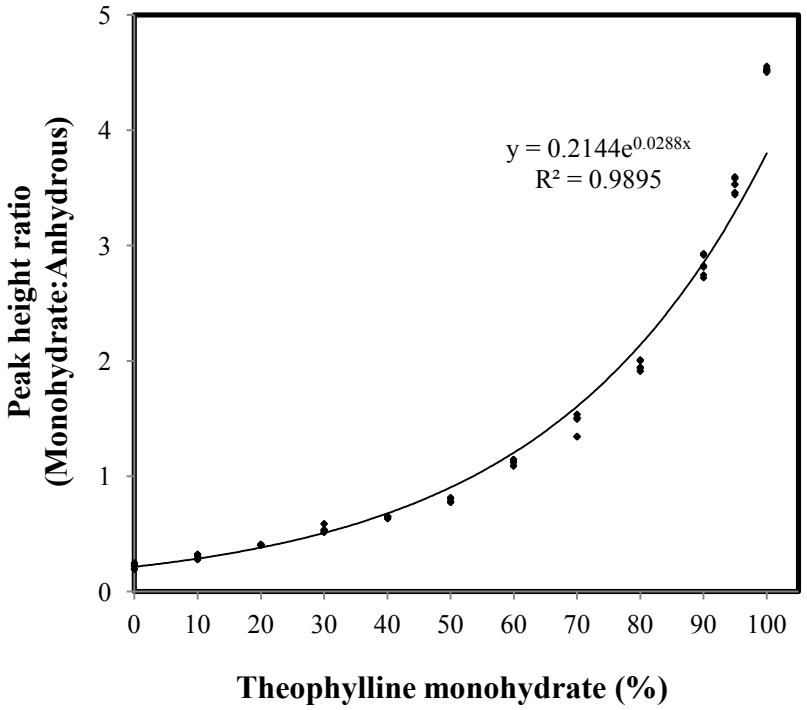

Figure 7-15. Calibration plot for Raman spectroscopy peak height ratios of theophylline monohydrate at 1688 cm^{-1} and anhydrous theophylline at 1665 and 1707 cm^{-1}. Data points correspond to individual sample measurements, (n=9).

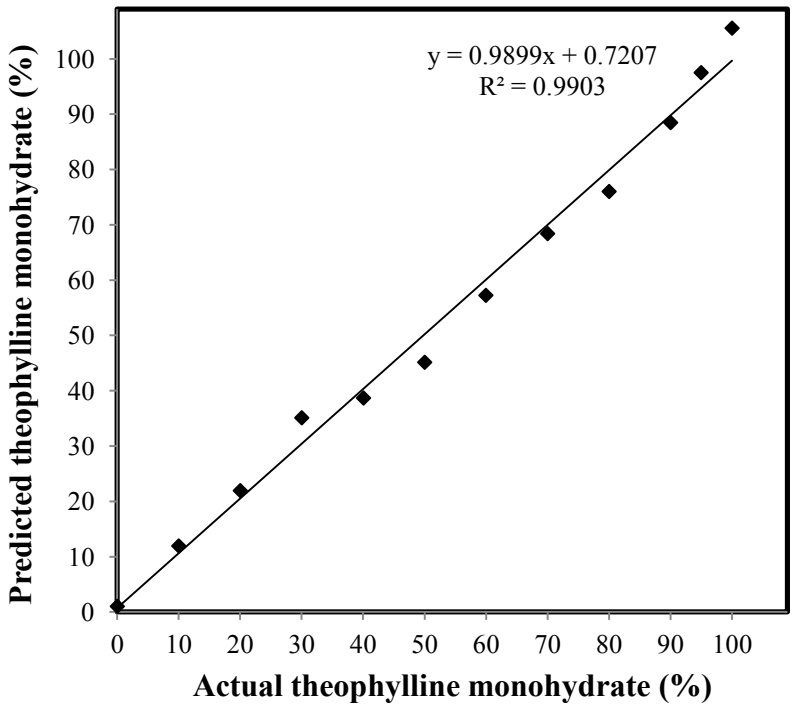

Figure 7-16. Actual versus predicted plot for theophylline monohydrate univariate calibration model.

7.3.5 Effect of granulation process on theophylline hydration

The transformation profiles which compare the appearance of theophylline monohydrate for the reverse-phase and conventional granulation processes are presented separately for each binder liquid composition (water in Figure 7-17, 10 % *w/w* PVP in Figure 7-18 and 5 % *w/w* HPMC in Figure 7-19) to allow direct comparison of the two different granulation processes. Error bars are not presented in the figures since they obscure the data, however in all cases the 1 SD error bars overlap for the conventional and reverse-phase processes at all time points.

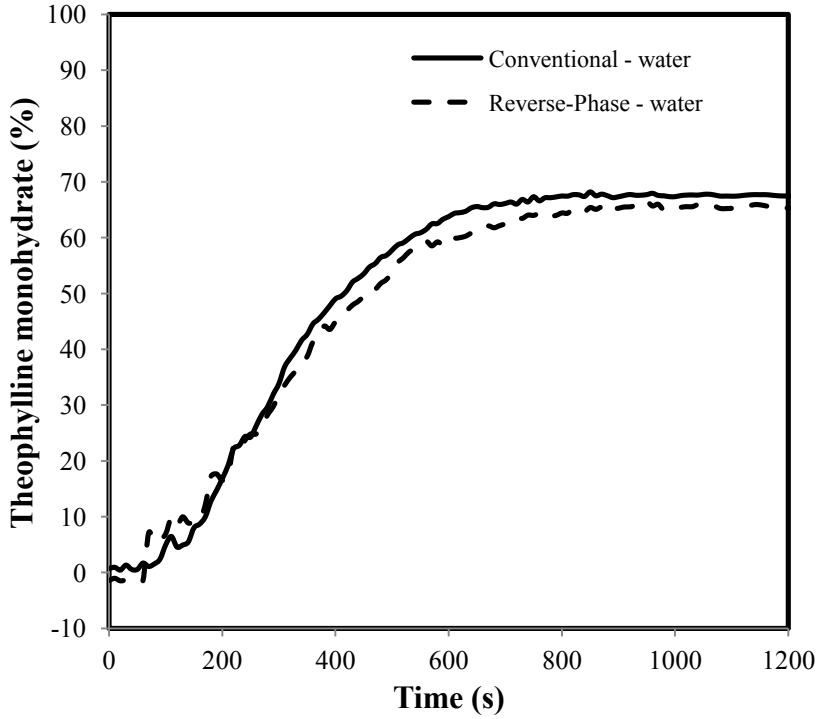

Figure 7-17. Plot of theophylline transformation profile using water as the binder liquid. Mean line displayed (n=3).Error bars not shown.

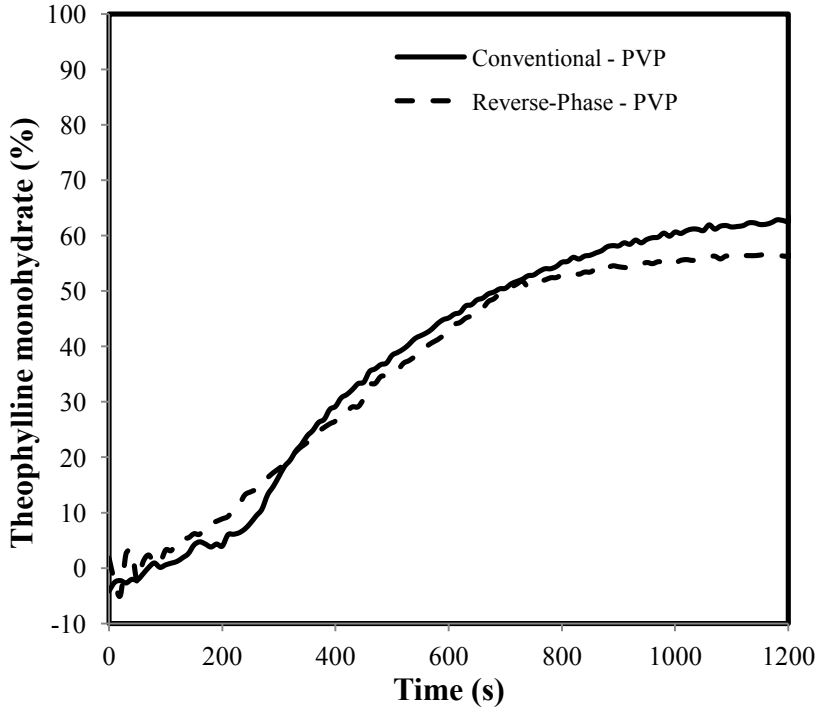

Figure 7-18. Plot of theophylline transformation profile using 10 % w/w PVP as the binder liquid. Mean line displayed (n=3). Error bars not shown.

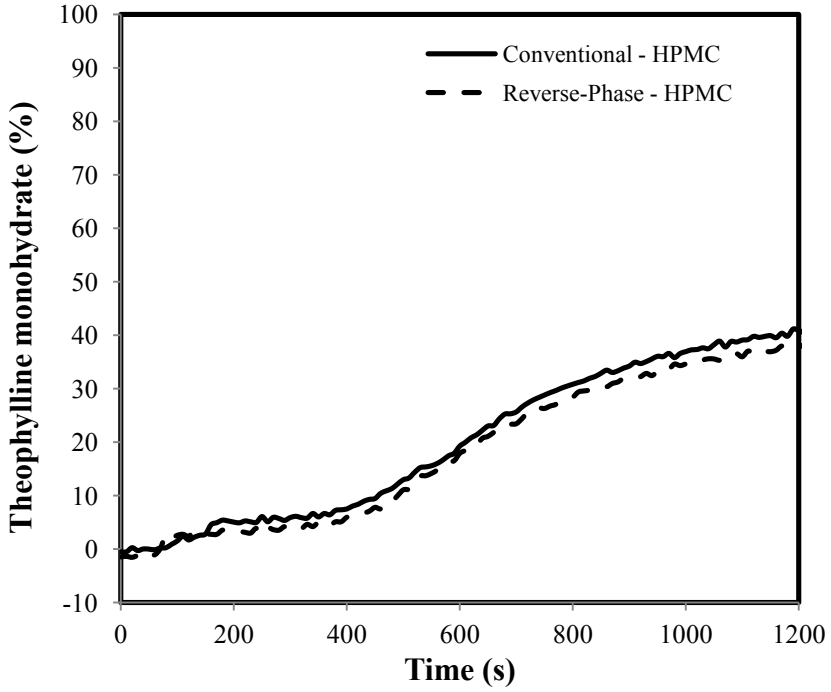

Figure 7-19. Plot of theophylline transformation profile using 5 % w/w HPMC as the binder liquid. Mean line displayed (n=3). Error bars not shown.

All transformation profiles are characterised by an onset period where little, or no, transformation was observed following the addition of binder liquid (at time zero). The onset period (defined presently as the duration taken to reach 5 % hydration) is associated with water distribution, wetting of theophylline and the initial dissolution stage [6] which is facilitated by an increase in impeller speed [2]. The onset period was followed by transformation of the anhydrous form to the monohydrate, where a steeper slope indicates a faster transformation rate. As the granulation process progressed the rate of hydration slowed in all cases with water reaching a relative plateau, however both the PVP and HPMC experiments did not reach equilibrium during the duration of the studies.

The onset time (t_{onset}), the duration to reach 35 % theophylline hydration ($t_{35\%}$) and the maximum theophylline monohydrate content reached (h_{max}) are summarised in Figure 7-20. No differences ($p > 0.10$ Wilcoxon) are observed between the granulation processes for the t_{onset}, $t_{35\%}$ or $h_{max.}$ These data indicate that the reverse-phase process does not result in an increase in the rate or extent of theophylline hydration when compared to the conventional granulation process.

The similarity in t_{onset} between the reverse-phase and conventional granulation processes does not support the hypothesis that the reverse-phase process has a faster onset time. This is likely explained by the fact that the transformation proceeds by a surface-mediated solution mechanism where monohydrate molecules heterogeneously nucleate on the surface of the anhydrous crystals. Nucleation of the monohydrate occurs once the liquid is supersaturated with respect to the monohydrate. According to Noyes-Whitney dissolution theory [77] a diffusion layer exists at the surface of the anhydrous theophylline crystal. In the very early stages of the reverse-phase granulation process the excess of binder liquid will represent sink conditions and diffusion of the dissolved theophylline will be possible which may in theory prolong the onset time. Given an aqueous solubility of theophylline monohydrate of 5.96 mg cm^{-3}, binder liquid volume of 200 cm^3 and an addition of a 25 % *w/w* anhydrous theophylline powder blend at a rate of 5 g s^{-1} a sufficient quantity of anhydrous theophylline will be added in <1 s to saturate the liquid with respect to the monohydrate. When considering the conventional granulation process an excess of anhydrous theophylline is present with respect to the sprayed binder liquid volume for the entirety of the process and saturation is possible from the initiation of the process.

Both processes reach a point where saturation of the liquid with respect to the monohydrate is possible in <1 s compared to onset times between 70–400 s depending upon the binder liquid composition. Therefore, other factors such as wetting of the anhydrous theophylline with binder liquid, dissolution of the anhydrous theophylline and nucleation of the monohydrate on the surfaces of the anhydrous theophylline crystals are likely contribute to the onset time. Since common batches of anhydrous theophylline and binder liquid were used in the present study the wetting properties, particle size distribution and surface area can be assumed to be constant. Therefore, the wetting rate, dissolution rate and nucleation rate are likely to be similar for the reverse-phase and conventional processes resulting in the observed similarity in onset time.

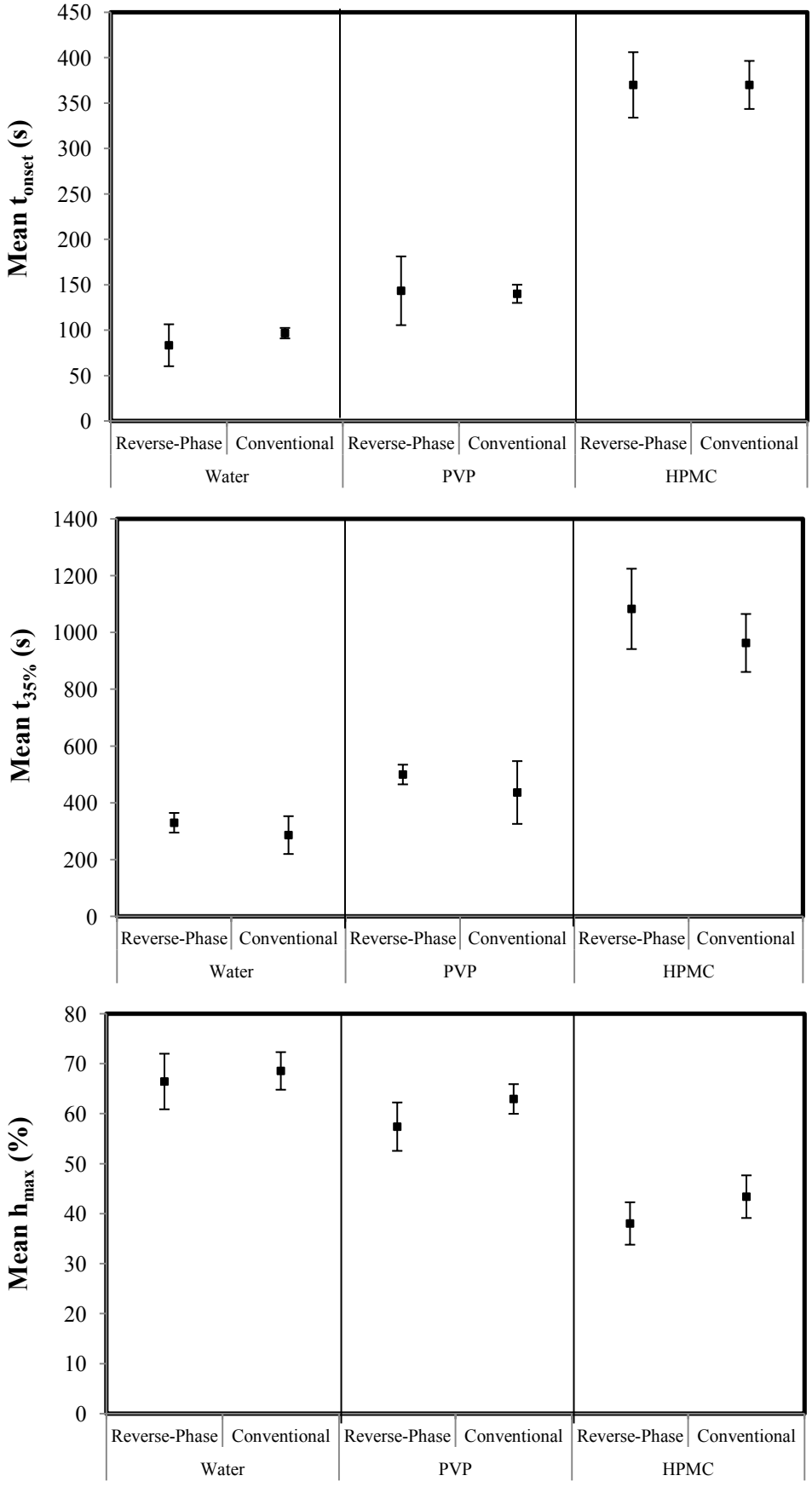

Figure 7-20. Plots of theophylline hydration parameters as a function of granulation process and binder liquid composition. Error bars represent 1 SD, n=3.

A surface mediated transformation using water as the binder liquid would be predicted to proceed until the saturation of the liquid equals the solubility of theophylline monohydrate (5.96 mg cm^{-3}). The present study employed 200 cm^3 of binder liquid meaning 1.19 % of theophylline would be predicted to remain in solution if the granulation process was continued to a point of equilibrium, i.e. a hydration extent of 98.81 %. In all cases however, an approximate plateau in hydration was reached at a point well below 100 % hydration. A number of factors may account for this observation.

First, an excess of anhydrous theophylline exists with respect to the quantity of binder liquid in both the conventional and reverse-phase granulation processes. The anhydrous theophylline present may act as seed crystals and promote crystallisation of the anhydrous form from the saturated solution rather than the monohydrate. This would contribute to a decreased extent of hydration. A similar effect has been reported during crystallisation studies of the Form I and Form II crystals of paracetamol from acetic acid solutions. When using an excess of acetic acid Form II is produced with ~95 % yield, however when using a saturated acetic acid solution where undissolved paracetamol Form I crystals were present Form I is produced with 100 % yield [78].

Second, crystallisation of theophylline monohydrate has been shown to occur through an epitaxial heterogeneous nucleation on the surface of the anhydrous theophylline crystal. This mechanism has been shown to hinder dissolution at the anhydrous crystal surface since a layer of the thermodynamically stable monohydrate is formed [1] which acts to inhibit the transformation. Finally, the use of high power lasers can result in sample heating due to absorption of radiation over time [48]. Dehydration of easily dehydrating materials has also been reported with the use of lasers [79]. Both of these observations could result in a conversion of the theophylline monohydrate back to the anhydrous form during the granulation process. However, since the rotational nature of the granulation process continually recycles fresh material through the laser this mechanism is thought unlikely. The probed volume using the 3 mm spot size has been estimated as 14.1 μL [5], whilst the wet granule volume will be ~250 cm^3 assuming a density of 1.74 g cm^{-3}. The probed volume would therefore represent approximately 0.056 % of the total granulation volume suggesting that the probability of the same

portion of material experiencing localised heating, evaporation and transformation back to the anhydrate is likely to be remote.

The resultant granules from each experiment were dried in a convection oven for 24 h at 60 °C (Section 7.2.5). Following drying, triplicate samples of ~1 g were analysed, each in triplicate, using a static Raman spectrometry method (Section 7.2.4) to quantify the theophylline monohydrate content. The theophylline monohydrate content results for each of the granulation experimental conditions are summarised in Table 7-3. In all cases theophylline monohydrate formed during the granulation process was transformed back to anhydrous theophylline with the granulation process and binder liquid composition having no significant effect (ANOVA $p > 0.05$). The transformation from the theophylline monohydrate to anhydrous theophylline as a result of heating is consistent with previously reported findings where the stepwise dehydration of theophylline monohydrate was monitored by NIR spectroscopy and it was reported that fluid bed drying at temperatures below 40 °C resulted in the evaporation of free water, while drying above 40 °C caused dehydration of the lattice-bound water [80]. The fact that between 5.7–6.6 % of theophylline monohydrate remained in the present experiments after 24 h of drying at 60 °C is likely explained by the fact that the drying temperature used was slightly below the previously reported dehydration transition temperatures of 63.4 ± 0.4 °C [81] and 63.8 ± 1.3 °C [82].

Table 7-3. Summary of theophylline monohydrate content in granules dried for 24 h at 60 °C. Mean ± SD (n=27).

Granulation process	Binder liquid composition	Theophylline monohydrate content (%)
Conventional	Water	6.6 ± 0.59
	10 % w/w PVP	6.4 ± 0.46
	5 % w/w HPMC	6.4 ± 0.63
Reverse-Phase	Water	6.6 ± 1.42
	10 % w/w PVP	5.7 ± 1.25
	5 % w/w HPMC	6.2 ± 0.84

7.3.6 Effect of binder liquid composition on theophylline hydration

The transformation profiles comparing the binder liquid composition are presented for the conventional (Figure 7-21) and reverse-phase (Figure 7-22) granulation processes separately to allow direct comparison of the binder liquid composition effects (re-plots of data shown in Figure 7-17 –Figure 7-20).

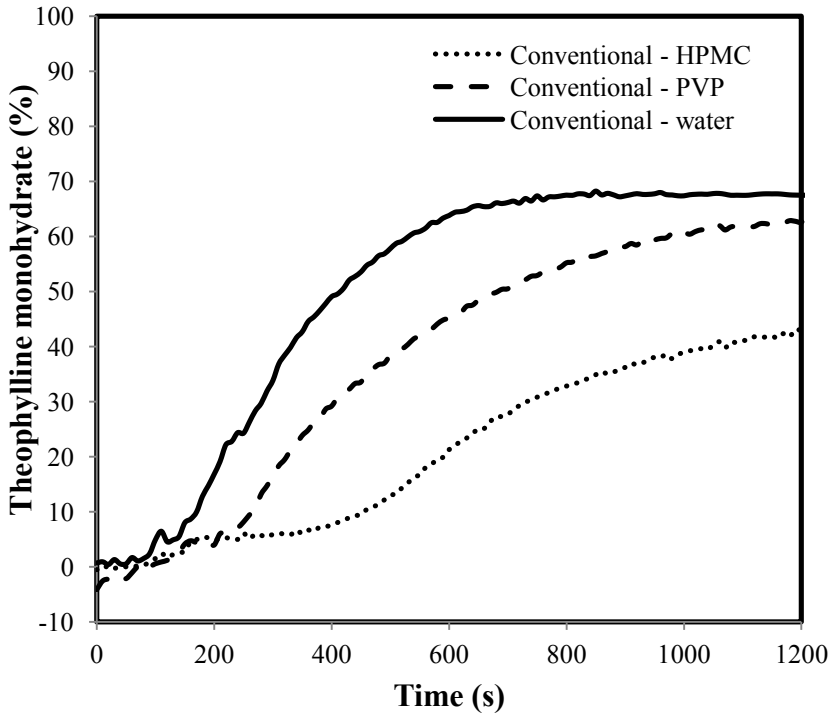

Figure 7-21. The effects of binder liquid composition on the percentage transformation of theophylline from the anhydrous form to the monohydrate expressed as a function of time, as generated using the conventional granulation process. Mean line displayed (n=3). Error bars not shown.

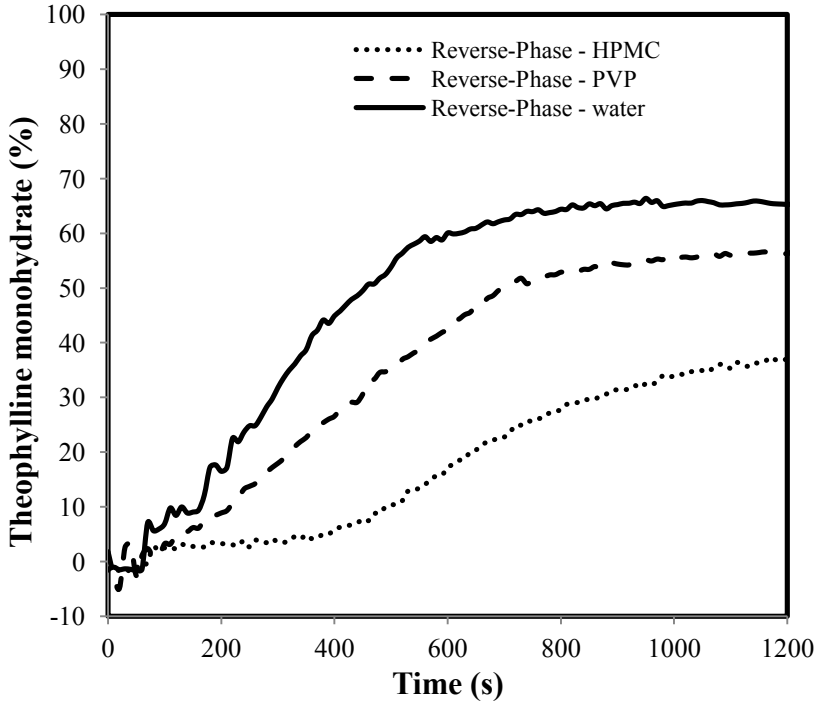

Figure 7-22. The effects of binder liquid composition on the percentage transformation of theophylline from the anhydrous form to the monohydrate expressed as a function of time, as generated using the reverse-phase granulation process. Mean line displayed (n=3). Error bars not shown.

Differences are observed when comparing the effects of the different binder liquids (Figure 7-20, Figure 7-21 and Figure 7-22). When considering t_{onset} and $t_{35\%}$ differences are observed between each of the binder liquids ($p < 0.10$ Wilcoxon). In the case of h_{max}, water and 10 % *w/w* PVP are similar ($p > 0.10$ Wilcoxon), however 5 % *w/w* HPMC results in a significantly lower result ($p < 0.10$ Wilcoxon). The use of water resulted in the fastest t_{onset}, $t_{35\%}$ and greatest h_{max}, whilst when 10 % *w/w* PVP was incorporated then an intermediate performance was obtained whereas replacement with 5 % *w/w* HPMC provided the slowest t_{onset}, $t_{35\%}$ and lowest h_{max}. These results are consistent with the rank order reported previously for the effect of water, PVP and HPMC on theophylline hydration where it was postulated that the more hydrophilic the polymer the greater the inhibitory effect on the transformation [6].

The role of hydrogen bonding in inhibiting solid-state transformations has been suggested to be of importance in a number of previous studies [65-68] but detailed mechanistic explanations are still lacking. The inference that hydrogen bonding is important is based upon the nature of the chemical structures of theophylline, PVP and HPMC. In the anhydrous theophylline molecule (Figure 7-23a) there is an excess of

hydrogen bond acceptors since there are two acidic hydrogen bond donors (the imidazole NH and =CH groups) and three acceptors (the two coordinate imidazole N and two carbonyl O atoms, both of which can accept two hydrogen bonds). The two hydrogen bond donors interact with two of the acceptors to form hydrogen bonded bilayers in anhydrous theophylline, with this structural arrangement forming crystals with a high aspect ratio with the third hydrogen bond acceptor being exposed on the largest face of the crystal [83]. In the case of theophylline monohydrate the water molecule satisfies the deficiency of hydrogen bond donors and a corrugated packing structure results such that =CH and CH_3 groups are exposed [83] and hydrogen bond acceptor sites are inaccessible.

It has been suggested that interactions between the drug and polymer additives lowers the nucleation barrier and promotes crystallisation of the thermodynamically less stable form [28]. In the context of the present study it is proposed that hydrogen bond donors present in the polymer interact with the exposed hydrogen bond acceptors of the theophylline molecule acting to reduce the free energy of the system and promote crystallisation of the metastable anhydrous form. The exposed hydrogen bond donor groups on the polymer can be considered to act as a template for selective growth of the metastable anhydrous form [83]. In this sense the hydrogen bonds donors present in water molecules and the dissolved polymer compete for the exposed hydrogen bond acceptor sites of the theophylline molecule. One can therefore rationalise that a polymer which acts as a stronger, or orientationally favoured, hydrogen bond donor than water will have an inhibitory effect on hydration. This description explains the observed similarities in h_{max} between water and 10 % *w/w* PVP conditions. PVP has two hydrogen bond acceptor sites but no donor sites (Figure 7-23b) and therefore does not compete with water molecules for the hydrogen bond acceptor sites on the anhydrous theophylline. As a result the extent of hydration is similar between water and PVP.

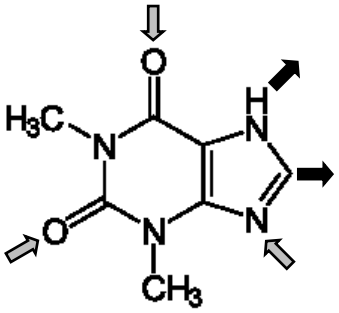

(a) Anhydrous theophylline.

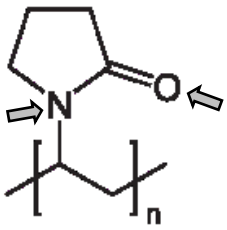

(b) Poly (vinyl pyrrolidone).

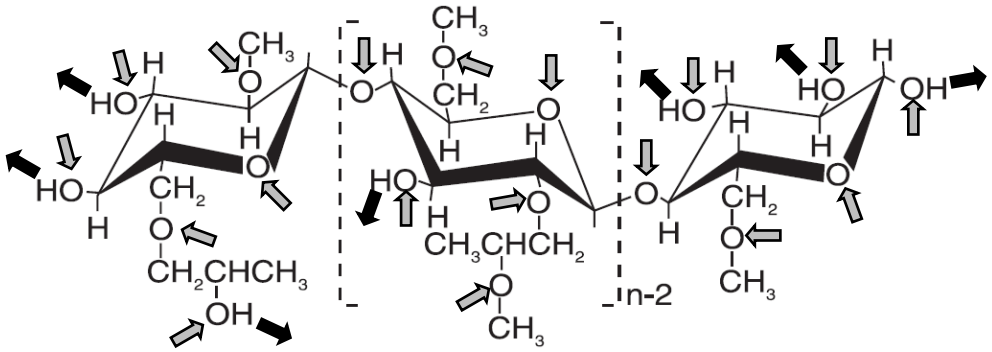

(c) Hydroxypropyl methylcellulose.

Figure 7-23. Chemical structures of (a) anhydrous theophylline, (b) PVP and (c) HPMC showing hydrogen bond donor sites as black arrows and acceptor sites as grey arrows.

This description however does not explain the observed differences in t_{onset}, and $t_{35\%}$ between the water and 10 % *w/w* PVP experiments. Based on the preceding argument PVP should not compete with water for the acceptor sites and should therefore have no inhibitory effect. Since the extent of hydration (h_{max}) is similar for both conditions it is proposed that PVP has a physical effect on the rate of hydration rather than a chemical effect. First, PVP can form hydrogen bonds with water molecules thereby restricting the availability of free water molecules to participate in the hydration. Second, it is feasible that the increase in viscosity caused by the addition of PVP slows the migration and orientation of water molecules [71]. The viscosity of water is 1 mPa.s whereas the

viscosity of 10 % *w/w* PVP is 6.86 mPa.s (Section 4.2.1). The increased viscosity of the PVP liquid binder likely contributed to a reduced rate at which hydrogen bonds are formed with the exposed acceptor sites on the theophylline molecule. By the same mechanism the viscosity of the PVP can also reduce the diffusivity of the solute molecules which will also act to slow the hydration rate. This hypothesis could be explored using a range of aqueous PVP solutions of varying concentration such that the hydrogen bond donor contribution is held constant but the viscosity is varied.

In contrast to PVP, the HPMC polymer molecule (Figure 7-23c) has three potential donor sites associated with the three ether groups, though the exact number of donor sites depends upon the nature of the ether substitutions since only hydrogen or hydroxypropyl groups will act as donors and the methyl substitution will be inactive. HPMC therefore competes with water molecules for the acceptor sites on the theophylline molecule and acts to inhibit transformation to the monohydrate. This mechanism does have the potential for HPMC to form a protective boundary at the face of the anhydrous crystal where the interior of the HPMC will form hydrogen bonds with the anhydrous crystal and the exterior will form hydrogen bonds with water molecules.

It is noted that the inhibition by HPMC is partial. Two mechanisms are proposed. Firstly, HPMC is a variable hydrogen bond donor, depending upon the exact ether substitution groups present, which will result in a variable degree of competition with water molecules for acceptor sites on the theophylline molecule and consequently some degree of hydration will occur. Secondly, HPMC is a long chain polymer that is many times larger than water and theophylline molecules. Optimised organisation of a hydrogen bond network between HPMC molecules and theophylline molecules is likely to be sterically hindered such that space exists for water molecules to also interact and form the monohydrate.

As with PVP it is noted that the rate of the transformation is also slowed by the use of HPMC. While the viscosity mechanism discussed earlier is likely to contribute to this slower rate so will the proposed hydrogen bonding mechanism. The discussion presented here thus far has considered only the largest face of the anhydrous theophylline crystal, where the available hydrogen bond acceptor carbonyl group is located. The other faces of the crystal which do not have an exposed acceptor site will

not be subject to the polymer inhibition mechanism and dissolution and subsequent nucleation of the monohydrate form will proceed uninhibited on these faces. In the case of anhydrous theophylline these faces represent a smaller fraction of the surface area and therefore the rate of hydration is slowed.

Given sufficient time, a complete transformation to the monohydrate will likely occur if one assumes that the theophylline-HPMC hydrogen bonded species is not more thermodynamically stable than the theophylline monohydrate solid state. However, in the present experiment complete hydration was not observed owing to the duration of the granulation experiment. The decreased transformation rate resulted in a decreased extent of hydration at the termination of the 20 min experiment relative to water and PVP. In light of this it should be considered that the concept of inhibiting theophylline hydration is relative to the duration that the molecules are exposed to a condition greater than the critical water activity, Therefore, the use of an optimised polymer binder might slow the rate of theophylline transformation such that negligible transformation occurs before drying of the granules and accordingly, it can be considered to have inhibited the transformation for the duration of the granulation process. This approach would obviously require extensive process development to understand the impact of variables such as temperature changes during the course of the granulation process and the effect of dissolution of other components of the formulation.

The findings reported herein provide further insight into the inhibition of anhydrous theophylline transformation. While complete inhibition of the transformation was not achieved it was possible to demonstrate a degree of inhibition using HPMC. Based upon the discussion presented one can postulate that improved inhibition may be possible with a polymer, or other similar additive, which: 1) acts as a stronger hydrogen bond donor than HPMC and/or 2) is less sterically hindered than HPMC such that favoured hydrogen bond orientation with the exposed hydrogen bond acceptor on the surface of anhydrous theophylline is possible. It would also be of interest to study the effect of the viscosity/concentration of such an additive to determine whether a physical slowing of the transit of water molecules to the crystal surface could negate a potentially slower orientation of the additive to form hydrogen bonds.

7.4 Conclusion

In situ Raman spectroscopy was used to monitor the hydration of theophylline during both the conventional and reverse-phase granulation processes. The effect of using water, 10 % *w/w* PVP or 5 % *w/w* HPMC binder liquid composition was also evaluated. The conventional and reverse-phase granulation processes were similar in terms of the onset time, duration to reach 35 % hydration and the maximum hydration extent reached indicating that the differences in the granulation mechanism do not increase the risk of a solid-state transformation for anhydrous theophylline. When considering the effect of binder liquid composition on the rate of hydration the following rank order was established for hydration rate parameters (t_{onset} and $t_{35\%}$): water > 10 % *w/w* PVP > 5 % *w/w* HPMC. The decreased rate of hydration in the presence of either of the two polymers was proposed to be primarily due to viscous forces in the case of PVP and competition for hydrogen bond sites in the case of HPMC. In terms of the maximum hydration extent reached (h_{max}) water and 10 % *w/w* PVP performed similarly, however 5 % *w/w* HPMC resulted in a significantly lower hydration extent. The decreased extent of hydration associated with HPMC, and relative lack of effect associated with PVP, was in agreement with the theory that for the polymer binder to have an inhibitory effect on the extent of theophylline transformation it must act as a hydrogen bond donor to compete with water for the excess acceptor sites present on the theophylline molecule.

7.5 References

[1] Rodriguez-Hornedo, N., Lechuga-Ballesteros, D., Wu, H.J., Phase-transition and heterogeneous epitaxial nucleation of hydrated and anydrous theophylline crystals, Int. J. Pharm., 85 (1992) 149-162.

[2] Wikstrom, H., Marsac, P., Taylor, L., In-line monitoring of hydrate formation during wet granulation using Raman spectroscopy, J. Pharm. Sci., 94 (2005) 209-219.

[3] Jorgensen, A., Rantanen, J., Karjalainen, M., Khriachtchev, L., Rasanen, E., Yliruusi, J., Hydrate formation during wet granulation studied by spectroscopic methods and multivariate analysis, Pharm. Res., 19(9) (2002) 1285-1291.

[4] Debnath, S., Suryanarayanan, R., Influence of processing-induced phase transformations on the dissolution of theophylline tablets, AAPS Pharm. Sci. Tech., 5 (2003) 1-11.

[5] Wikstrom, H., Lewis, I.R., Taylor, L.S., Comparison of sampling techniques for in-line monitoring using Raman spectroscopy, Appl. Spectrosc., 59 (2005) 934-941.

[6] Wikstrom, H., Carroll, W.J., Taylor, L.S., Manipulating Theophylline Monohydrate Formation During High-Shear Wet Granulation Through Improved Understanding of the Role of Pharmaceutical Excipients, Pharm. Res., 25 (2008) 923-935.

[7] Rades, T., Heinz, A., Strachan, C.J., Gordon, K.C., Analysis of solid-state transformations of pharmaceutical compounds using vibrational spectroscopy, J. Pharm. Pharmacol., 61 (2009) 971-988.

[8] Morris, K.R. Structural aspects of hydrates and solvates in: Brittain H.G., (Eds.) *Polymorphism in Pharmaceutical Solids*, Marcel Decker, New York, 1999, pp. 125-181.

[9] Yu, L., Reutzel, S.M., Stephenson, G.A., Physical characterization of polymorphic drugs: an integrated characterization strategy, Pharmaceutical Science & Technology Today, 1 (1998) 118-127.

[10] Stahly, G., Diversity in single- and multiple-component crystals. The search for and prevalence of polymorphs and cocrystals, Cryst. Growth Des., 7 (2007) 1007-1026.

[11] Zhang, G.X., Law, D., Schmidt, E.A., Qiu, Y.H., Phase transformation considerations during process development and maufacture or solid dosage forms, Adv. Drug Deliv. Rev., 56 (2004) 371-290.

[12] Morris, K.R., Characterization of humidity-dependent changes in crystal properties of a new HMG-CoA reductase inhibitor in support of dosage form development, Int. J. Pharm., 108 (1994) 195-206.

[13] Bauer-Brandl, A., Polymorphic transitions of cimetidine during manufacture of solid dosage forms, Int. J. Pharm., 149 (1996) 195-206.

[14] Grant, D.J.W. Theory and Origin of Polymorphism in: Brittain H.G., (Eds.) *Polymorphism in pharmaceutical solids*, Informa Healthcare, New York, 2007, pp. 1-34.

[15] DiMartino, P., Guyot-Hermann, A.M., Conflant, P., Drache, M., Guyot, J.C., Compression behavior of orthorhombic paracetamol, Int. J. Pharm., 128 (1996) 1122-1130.

[16] Roberts, R.J., Rowe, R.C., Influence of polymorphism on the Young's modulus and yield stress of carbamazepine, sulfathiazole and salfanilamide, Int. J. Pharm., 129 (1996) 79-94.

[17] Lu, G.W., Hawley, M., Smith, M., Geiger, B.M., Pfund, W., Characterization of a novel polymeric form of celecoxib, J. Pharm. Sci., 95 (2006) 305-317.

[18] Saifee, M., Inamdar, N., Dhamecha, D.L., Rathi, A.A., Drug Polymorphism: A Review, International Journal of Health Research, 2 (2009) 291-306.

[19] Sun, C., Zhou, D., Grant, D., Young, V.G., Theophylline monohydrate, Acta Cryst., 58 (2002) 368-370.

[20] Ticehurst, M.D., Storey, R.A., Watt, C., Application of slurry bridging experiments at controlled water activities to predict the solid-state conversion between anhydrous and hydrated forms using theophylline as a model drug, Int. J. Pharm., 247 (2002) 1-10.

[21] Zhu, H., Yuen, C., Grant, D.J.W., Influence of water activity in organic solvent + water mixtures on the nature of crystallizing drug phase. 1. Theophylline, Int.J. Pharm., 135 (1996) 151-160.

[22] Suzuki, E., Shimomura, K., Sekiguchi, K., Thermochemical study of theophylline and its hydrate, Chem. Pharm. Bull., 37 (1989) 493-497.

[23] Legendre, B., Randzio, S.L., Transiometric analysis of solid II/solid I transition in anhydrous theophylline, Int. J. Pharm., 343 (2007) 41-47.

[24] Otsuka, M., Kaneniwa, N., Kawakami, K., Umezawa, O., Effect of surface characteristics of theophylline anhydrate powder on hygroscopic stability, J. Pharm. Pharmacol., 42 (1990) 606-610.

[25] Matsuo, K., Matsuoka, M., Kinetics of humidity driven solid-state polymorphic transition of theophylline tablets, Journal of Chemical Engineering of Japan, 40 (2007) 541-549.

[26] Brittain, H.G., Grant, D.J.W., Crystalline solids, Adv. Drug. Deliv. Rev., 48 (2001) 3-26.

[27] Nunes, C., Mahendrasingam, A., Suryanarayanan, R., Investigation of the multi-step dehydration reaction of theophylline monohydrate using 2-dimensional powder X-ray diffractometry, Pharm. Res., 23 (2006) 2393-2404.

[28] Phadnis, N.V., Suryanarayanan, R., Polymorphism in anhydrous theophylline - implications on the dissolution rate of theophylline tablets, J. Pharm. Sci., 86 (1997) 1256-1663.

[29] Seton, L., Khamar, D., Bradshaw, I.J., Hutcheon, G.A., Solid State Forms of Theophylline: Presenting a New Anhydrous Polymorph, Crystal Growth & Design, 10 (2010) 3879-3886.

[30] Rodriguez-Hornedo, N., Wu, H.J., Crystal-growth kinetics of theophylline monohydrate, Pharm. Res., 8 (1991) 643-648.

[31] Ando, H., Ohwaki, T., Ishii, M., Watanabe, S., Myake, Y., Crystallization of theophylline tablets, Int. J. Pharm., 34 (1986) 153-156.

[32] Herman, J., Visavarungroj, N., Remon, J.P., Instability of drug release from anhydrous theophylline-microcrystalline cellulose formulations, Int. J. Pharm., 55 (1989) 143-146.

[33] Herman, J., Remon, J.P., Visavarungroj, N., Schwartz, J.B., Klinger, G.H., Formation of theophylline monohydrate during pelletisation of microcrystalline cellulose-anhydrous theophylline blends, Int. J. Pharm., 42 (1988) 15-18.

[34] Shefter, E., Higuchi, T., Dissolution behavior of crystalline solvated and nonsolvated forms of some pharmaceuticals, J. Pharm. Sci., 52 (1963) 781-791.

[35] Chen, D., Haugstad, G., Li, Z.J., Suryanarayanan, R., Water Sorption Induced Transformations in Crystalline Solid Surfaces: Characterization by Atomic Force Microscopy, J. Pharm. Sci., 99 (2010) 4032-4041.

[36] Sutor, D.J., The structures of the pyrimidines and purines. VI. The crystal structure of theophylline, Acta Crystallography, 11 (1958) 83-87.

[37] Amado, A.M., Nolasco, M.M., Ribiero-Claro, P.J.A., Probing Pseudopolymorphic Transitions in Pharmaceutical Solids using Raman Spectroscopy: Hydration and Dehydration of Theophylline, J. Pharm. Sci., 96 (2007) 1366-1379.

[38] Rades, T., Aaltonen, J., Gordon, K.C., Strachan, C.J., Perspectives in the use of spectroscopy to characterise pharmaceutical solids, Int. J. Pharm., 364 (2008) 159-169.

[39] McGoverin, C.M., Gordon, K.C., Raman mapping of pharmaceuticals, Int.J. Pharm., 417 (2011) 151-162.

[40] Noonan, K.Y., Beshire, M., Darnell, J., Frederick, K.A., Qualitative and quantitative analysis of illicit drug mixtures on paper currency using Raman spectroscopy, Applied Spectroscopy, 59 (2005) 1493-1497.

[41] Dennis, A.C., McGarvey, J.J., Woolfson, A.D., McCafferty, D.F., Moss, G.P., A Raman spectroscopic investigation of bioadhesive Tetracaine local anaesthetic formulations, Int. J. Pharm., 279 (2004) 43-50.

[42] Niemczyk, T.M., Delgado-Lopez, M.M., Allen, F.S., Quantitative determination of bucindolol concentration in intact gel capsules using Raman spectroscopy, Anal. Chem., 70 (1998) 2762-2765.

[43] Vehring, R., Red-excitation dispersive Raman spectroscopy is a suitable technique for solid-state analysis of respirable pharmaceutical powders, Applied Spectroscopy, 59 (2005) 286-292.

[44] Okumura, T., Otsuka, M., Evaluation of the microcrystallinity of a drug substance, indomethacin, in a pharmaceutical model tablet by chemometric FT-Raman spectroscopy, Pharm. Res., 22 (2005) 1350-1357.

[45] Mazurek, S., Szostak, R., Quantitative determination of captopril and prednisolone in tablets by FT-Raman spectroscopy, J. Pharm. Biomed. Anal., 40 (2006) 1225-1230.

[46] Romero-Torres, S., Perez-Ramos, J.D., Morris, K.R., Grant, E.R., Raman spectroscopic measurement of tablet-to-tablet coating variability, J. Pharm. Biomed. Anal., 38 (2005) 270-274.

[47] Romero-Torres, S., Perez-Ramos, J.D., Morris, K.R., Grant, E.R., Raman spectroscopy for tablet coating thickness quantification and coating characterization in the presence of strong fluorescent interface, J. Pharm. Biomed. Anal., 41 (2006) 811-819.

[48] DeBeer, T., Burggraeve, A., Fonteyne, M., Saerens, L., Remon, J.P., Vervaet, C., Near infrared and Raman spectroscopy for the in-process monitoring of pharmaceutical production processes, Int. J. Pharm., 417 (2011) 32-47.

[49] Long, D.A. The Raman Effect: A Unified Treatment of the Theory of Raman Scattering by Molecules. London: John Wiley & Sons Ltd 2002.

[50] McGoverin, C.M., Rades, T., Gordon, K.C., Recent Pharmaceutical Applications of Raman and Terahertz Spectroscopies, J. Pharm. Sci., 97 (2008) 4598-4621.

[51] Fevotte, G., In situ Raman spectroscopy for in-line control of pharmaceutical crystallization and solids elaboration processes: A review, Trans IChemE, Part A, 85 (2007) 906-920.

[52] Taylor, L.S., Zografi, G., The quantitative analysis of crystallinity using FT-Raman Spectroscopy, Pharm. Res., 15 (1998) 755-761.

[53] Roberts, S.N.C., Williams, A.C., Grimsey, I.M., Booth, S.W., Quantitative analysis of mannitol polymorphs by FT-Raman spectroscopy, J. Pharm. Biomed. Anal., 28 (2002) 1135-1147.

[54] Auer, M.E., Griesser, U.J., Swatzki, J., Qualitative and quantitative study of polymorphic forms in drug formulations by near infrared FT-Raman spectroscopy, J. Mol. Struct., 661-662 (2003) 307-317.

[55] Skoulika, S.G., Georgiou, C.A., Rapid, noninvasive quantitative determination of acyclovir in pharmaceutical solid dosage forms through their poly(vinyl chloride) blister package by solid-state fourier transform Raman spectroscopy, Applied Spectroscopy, 57 (2003) 407-412.

[56] Williams, A.C., Cooper, V.B., Thomas, L., Griffith, L.J., Petts, C.R., Booth, S.W., Evaluation of drug physical form during granulation, Int. J. Pharm., 275 (2004) 29-39.

[57] Szostak, R., Mazurek, S., FT-Raman quantitative determination of ambroxol in tablets, J. Mol.Struct., 704 (2004) 229-233.

[58] Hwang, M.S., Cho, S., Chung, H., Woo, Y.A., Nondestructive determination of the ambroxol content of tablets by Raman spectroscopy, J. Pharm. Biomed. Anal., 38 (2005) 210-215.

[59] Bell, S.E.J., Bourguignon, E.S.O., Dennis, A.C., Fields, J.A., McGarvey, J.J., Seddon, K.R., Identification of dyes on ancient Chinese papers samples using the subtracted shifted Raman spectroscopy method, Anal. Chem., 72 (2000) 234-239.

[60] Lin, W.-Q., Yang, J.-H., Ozaki, Y., Shen, G.-L., Yu, R.-Q., Characterisation of Chloramphenicol Palmitate drug polymorphs by Raman mapping with multivariate image segmentation using a spatial directed agglomeration clustering method, Anal. Chem., 78 (2006) 6003-6011.

[61] McCreery, R.L. Raman Spectroscopy for Chemical Analysis. New York: Wiley-Interscience 2000.

[62] Kim, M., Chung, H., Woo, Y., Kemper, M.S., A new non-invasive, quantitative Raman technique for the determination of an active ingredient in pharmaceutical liquids by direct measurement through a plastic bottle, Anal. Chim. Acta, 587 (2007) 200-207.

[63] Taylor, L.S., Wikstrom, H., Rantanen, J., Gift, A.D., Toward an Understanding of the Factors Influencing Anhydrate-to-Hydrate Transformation Kinetics in Aqueous Environments, Crystal Growth and Design, 8 (2008) 2684-2693.

[64] Taylor, L.S., Gift, A.D., Luner, P.E., Leudeman, L., Influence of Polymeric Excipients on Crystal Hydrate Formation Kinetics in Aqueous Slurries, J. Pharm. Sci., 97 (2008) 5198-5211.

[65] Simonelli, A.P., Mehta, S.C., Higuchi, W.I., Inhibition of sulfathiazole crystal growth by polyvinylpyrrolidone, J. Pharm. Sci., 59 (1970) 633-638.

[66] Hedoux, A., Guinet, Y., Descamps, M., The contribution of Raman spectroscopy to the analysis of phase transformations in pharmaceutical compounds, Int. J. Pharm., 417 (2011) 17-31.

[67] Katzhendler, I., Azoury, R., Friedman, M., Crystalline properties of carbamazepine in sustained release hydrophilic matrix tablets based on hydroxypropyl methylcellulose, J. Control. Release, 54 (1998) 69-85.

[68] Tian, F., Saville, D.J., Gordon, K.C., Strachan, C.J., Zeitler, J.A., Sandler, N., Rades, T., The influence of various excipients on the conversion kinetics of carbamazepine polymorphs in aqueous suspension, J. Pharm. Pharmacol., 59 (2007) 193-201.

[69] Kesaven, J.G., Peck, G.E., Solid-state stability of theophylline ahydrous in theophylline anhydrous-polyvinylpyrrolidone physical mixtures, Drug Dev. Ind. Pharm., 22 (1996) 189-199.

[70] Airaksinen, S., Luukkonen, P., Jorgensen, A., Karjalainen, M., Rantanen, J., Yliruusi, J., Effects of Excipients on Hydrate Formation in Wet Massess Containing Theophylline, J. Pharm. Sci., 92 (2003) 516-528.

[71] Taylor, L.S., Salameh, A.K., Physical stability of crystal hydrates and their anhydrates in the presence of excipients, J. Pharm. Sci., 95 (2006) 446-461.

[72] Wikberg, M., Alderborn, G., Compression characteristics of granulated materials. IV. The effect of granule porosity on the fragmentation propensity and the compactibility of some granulations., Int. J. Pharm., 69 (1991) 239-253.

[73] O'Brien, L.E., Use of in situ FT-Raman spectroscopy to study the kinetics of the transformation of carbamazepine polymorphs, J. Pharm. Biomed. Anal., 36 (2004) 335-340.

[74] Ono, T., terHorst, J.H., Jansens, P.J., Quantitative measurement of the polymorpic transformation of L-glutamic acid using in-situ Raman spectroscopy, Crystal Growth and Design, 4 (2004) 465-469.

[75] Hu, Y.R., Liang, J.K., Myerson, A.S., Taylor, L.S., Crystallization monitoring by Raman spectroscopy: Simultaneous measurement of desupersaturation profile and polymorphic form in flufenamic acid systems, Ind. Eng. Chem. Res., 44 (2005) 1233-1240.

[76] Hausman, D.S., Cambron, R.T., Sakr, A., Application of on-line Raman spectroscopy for characterizing relationships between drug hydration state and tablet physical stability, Int. J. Pharm., 299 (2005) 19-33.

[77] Noyes, A.A., Whitney, W.R., The rate of solution of solid substances in their own solutions, J. Am. Chem. Soc., 19 (1897) 930-934.

[78] Wilson, C.C., Thomas, L.H., Wales, C., Zhou, L., Paracetamol Form II: An Elusive Polymorph through Facile Multicomponent Crystallization Routes, Crystal Growth & Design, 11 (2011) 1450-1452.

[79] Taylor, L.S., Langkilde, F.W., Evaluation of solid-state forms present in tablets by Raman spectroscopy, J. Pharm. Sci., 89 (2000) 1342-1353.

[80] Rasanen, E., Rantanen, J., Mannermaa, J.-P., Yliruusi, J., Vuorela, H., Dehydration studies using a novel microchamber microscale fluid bed dryer with in-line near-infrared measurement, J. Pharm. Sci., 92 (2003) 2074-2081.

[81] Wikstrom, H., Kakidas, C., Taylor, L.S., Determination of hydrate transition temperature using transformation kinetics obtained by Raman spectroscopy, J. pharm. Biomed. Anal., 49 (2009) 247-252.

[82] Fokkens, J.G., VanAnslsfoort, J.G.M., DeBlaey, C.J., DeKruif, C.G., Wilting, J., A thermodynamic study of the solubility of theophylline and its hydrate, Int. J. Pharm., 14 (1983) 79-93.

[83] Cox, J.R., Dabros, M., Shaffer, J.A., Thalladi, V.R., Selective crystal growth of the Anhydrous and Monohydrate Forms of Theophylline on Self-Assembled Monolayers, Drug Crystal Growth, 119 (2007) 2034-2037.

CHAPTER EIGHT: GENERAL DISCUSSION

8 General discussion

8.1 Motivations for the present study

As discussed in Chapter 1 wet granulation is a common agglomeration technique used in the manufacture of tablets to enhance the flow, homogeneity and compaction properties of the powder blend and a large body of literature exists in the field in support of these conferred advantages. The first reports on the topic date back to 1958 [1], and since this time the state of thinking has gradually progressed from viewing the technology as an art form to treating it as a science and engineering based phenomena where outcomes can be predicted based upon control of formulation and process variables.

During this transition in thinking many researchers have highlighted the relative risks of uncontrolled granule growth associated with the conventional granulation approach, in particular, the need for tight control over binder liquid addition has been emphasised [2, 3]. Most recently this has taken the form of the nucleation regime map [4], which considers the binder liquid addition conditions [5] and the time taken for the binder liquid to penetrate the powder [6, 7]. Both of these approaches are predicated on the fact that, by design, the conventional granulation process proceeds in the direction of increased liquid saturation [8, 9], through addition of a binder liquid to a moving powder bed, and therefore progresses in a direction that increases the risk of uncontrolled granule growth.

While the practical benefits of quantifying liquid coverage relative to powder flux have been acknowledged [10] a number of concerns have been raised with the dimensionless spray flux and nucleation regime map approaches, and the questionable assumption that granules are optimally formed by a drop controlled nucleation process. Practical limitations in achieving a drop controlled nucleation regime during scale up to commercial scales have been highlighted, such as the need to either decrease volumetric binder liquid flow rate or increase impeller tip speed, both of which have significant effects on granule consolidation and growth, or the need to install an impractical number of spray nozzles into the granulator to achieve the required dimensionless spray flux [10].

Some authors have even argued that binder liquid addition conditions are not critical [11] and that granule growth is mainly affected by the binder liquid amount and the mixing conditions which subsequently break the initial nuclei and distribute the binder liquid by mechanical dispersion [3, 12, 13]. These arguments led to the conception of the reverse-phase granulation process, where the powder formulation is added to the agitated binder liquid to create saturated moist granules, which undergo breakage during the course of the process allowing binder liquid to be dispersed throughout the powder by mechanical distribution. Advantages of the reverse-phase process include elimination of process variables associated with binder liquid dimensionless spray flux, since the process would follow an immersion mechanism, and the fact that as the reverse-phase process progresses the liquid saturation decreases, thus moving away from potential over-wetting, uncontrolled growth and batch loss.

8.2 Overview of thesis findings

It was hypothesised that for the reverse-phase granulation process control of a few simple variables (binder quantity, binder viscosity and impeller speed) might be sufficient to form granules with the desired properties whilst eliminating the risk of uncontrolled growth and batch rejection. Achieving this goal would represent significant advantages over the conventional granulation process, however, two potentially negative consequences of the reverse-phase approach were acknowledged; the potential for the resultant granules to have inferior compaction properties and the potential for the increased rate or extent of formation of a different solid state form of the drug due to increased drug dissolution in the binder liquid.

The consolidation behaviour, and therefore density and porosity, of granules produced by a given granulation system determines to a large extent the growth and breakage behaviour, therefore understanding this behaviour is fundamental to characterising the reverse-phase wet granulation process. First powder pycnometry was evaluated as an alternative method for the measurement of granule envelope density since it offers safety, cost and cycle time advantages over the traditionally used mercury porosimetry method (Chapter 2). Since such a powder pycnometry method had been shown previously to be robust for envelope density measurement of larger solids [14, 15] and had also been applied to pharmaceutical granules <5 mm diameter [16-19] it was

considered a promising technique. However, evaluation of the appropriateness of the method for the latter smaller size granules, and the experimental procedure, had not been previously reported and concerns existed as to whether the packing behaviour between the displacement media and the sample particles of a similar size would be a significant limitation in the method [20].

It was demonstrated here that the proposed limitations in the powder pycnometry method for granules with a narrow size fractions did exist when considering samples prepared with narrow size fractions with a sieve diameter <1850 μm. The limitation was proposed to be related to the decrease in packing density between the displacement media and the granules as the size difference between the two decreased. However, it was demonstrated that when using the un-sieved polydisperse granule samples the limitations were mitigated and the method could be calibrated against the reference mercury porosimetry method with a linear regression fit (R^2) of 0.9029. These findings are of particular significance for two reasons. First, the results call into question the granule porosity data for granules of small and narrow size fractions reported in previous studies [16-19]. Second, the results support the use of the method for polydisperse granule samples, such as those used in the present studies, which allows a much faster, cheaper and safer approach to gain further insight into the consolidation mechanisms during wet granulation processes.

The ultimate goal of the wet granulation process is to form granules of the desired properties that can be formed into tablets. In order to achieve this a drying step must be performed to reduce the moisture content of the wet granules to a desired endpoint, after which they will likely be stored under some range of temperature and humidity conditions, before being compressed. Few studies dealing with the compaction properties of HA have previously been reported, while the effects of moisture have received even less attention, and both were therefore studied (Chapter 3). When compared to other pharmaceutical materials, HA was shown to have a low compressibility and high compactibility, while moisture affected both differently. An increase in moisture had a plasticising effect thereby increasing the compressibility, but also acted to reduce the strength of interparticulate bonds resulting in reduced compactibility, with the net effect of these interactions being a reduction in the tablet tensile strength. This finding was particularly important in the present study since it led

to the need to ensure HA samples were stored under known and monitored relative humidity conditions prior to performing mechanical properties tests such as HA granule strength (Section 5.1.3) and HA granule compaction and tensile strength testing (Section 5.1.4).

As stated previously, it was hypothesised that the reverse-phase process could be controlled by understanding the effects of binder liquid content (liquid saturation), binder liquid viscosity and impeller speed on the granule size and porosity. Evaluation of these variables was performed in two parts. First, the effects of liquid saturation and binder liquid concentration were studied (Chapter 4) and second, the effects of impeller speed and binder liquid concentration were studied (Chapter 5) with both studies comparing the properties of the granules obtained from the reverse-phase process to those produced by the conventional process. The findings from these studies support the original hypothesis that the reverse-phase process is a feasible option to form pharmaceutical granules equivalent, if not superior, to the conventional granulation process. The main mechanism for granule formation in the reverse-phase process was shown to be breakage of large saturated agglomerates, with binder liquid being dispersed throughout the powder formulation by mechanical distribution. This finding is in agreement with previous findings [3, 12, 13] and indicates that the assumption that the granulation process must proceed under a drop controlled nucleation regime [4] to achieve tight control over granule size is not universally true.

The granule size resulting from the reverse-phase process appeared to be predominantly influenced by capillary forces whereas the granule size from the conventional process was influenced by viscous forces. These observations are likely to be associated with the immersion mechanism of the reverse-phase process which was proposed to allow more complete and consistent wetting of intraparticulate capillaries of the HA powder particles. The conventional process was thought to reach a less complete and variable degree of capillary wetting which was dependent upon factors including process duration, particle size and pore structure, which would result in variable quantities of binder liquid being present on the surface of the granules. This difference is likely to have contributed to the reverse-phase process being less sensitive to extremes of binder liquid content leading to more predictable and controllable granule size and porosity.

This effect was most easily seen as induction growth behaviour for the conventional process versus steady growth behaviour in the reverse-phase process.

A key implication of these findings is that the nucleation regime map, while conceptually interesting, fails to be practically relevant. One probable reason for this is that the nucleation regime map was constructed using a regime separated approach, i.e. nucleation only, where binder liquid were sprayed in very small quantities (i.e. very low liquid saturation) onto static powder beds [4]. Such powder beds were never passed under the spray zone again and were never subjected to any impact forces associated with the movement of an impeller. The powders were then dried and the resultant nuclei recovered and characterised. Practically speaking this does not represent the actual conditions taking place in a wet granulator where the liquid saturation is much higher, the powder frequently passes through the spray zone where it is re-wetted, while also being subjected to forces associated with impact with other granules, the impeller blade and the granulator bowl.

One readily identifiable failure of the nucleation regime map is that it does not consider liquid saturation. As an example one could operate in the drop controlled nucleation regime but simply add sufficient binder liquid to achieve a liquid saturation >1, and regardless of whether individual nuclei were initially formed a multi-modal particle size distribution, or state of uncontrolled growth, will likely result. Additionally, the nucleation regime map depicts the regime as being dependent upon the drop penetration time, where this parameter is presented as being constant for a given formulation, depending upon various physicochemical properties of the powder and liquid. However, it has been shown that the moisture content of the powder bed affects the drop penetration time with pre-wetted powders always having faster penetration times than dry powders [21]. Consequently, it is likely that the nucleation regime map boundaries, which were based upon the behaviour of dry powders having relatively longer drop penetration times, are likely much broader and forgiving when considering the pre-wetted powders that are present in an actual granulation process.

From a practical standpoint the consolidation and growth of granules formed by the reverse-phase process were described by their degree of liquid saturation (Chapter 4), while the breakage of the reverse-phase granules was described by the Stokes

deformation number (Chapter 5). These findings support the initial hypothesis that the reverse-phase process could be controlled by manipulating the binder liquid content and impeller speed. However, it was concluded that the binder liquid viscosity, which was initially hypothesised to be an important variable in the control of the reverse-phase process, had negligible effect over the range studied. This is thought to be due to the fact that while the viscosity range studied was practically relevant for commercial formulations it was narrow (6.86–33.70 mPa.s) compared to previously reported studies (e.g. 1–650 mPa.s) which were consulted when forming the original hypothesis. The lack of effect of binder liquid viscosity allowed the general simplification that the reverse-phase process was dependent upon two main variables: liquid saturation and Stokes deformation number, and could therefore be summarised by applying the growth regime map which was initially developed for the conventional granulation process (Chapter 6).

The growth regime map provided a useful directional tool to aid formulation and process development and essentially showed two simple relationships. First, an increase in binder liquid content results in a shift from dry powder, to nucleation, to growth, to slurry regimes. Second, an increase in impeller speed results in a shift from growth to breakage. These observations could potentially be predicted without the application of the growth regime map since the HA formulation used in these studies is practically insoluble in water and can therefore be treated as a constant during the granulation process. In contrast previously reported growth regime maps for conventional granulation studies employed powders that were soluble, to some extent, in the binder liquid. The solubility gives rise to a dynamic situation where powder dissolution can change multiple variables such as the viscosity of the binder liquid, the surface area of the powder and the relative ratio of solid to liquid, all of which will create a much more complex growth regime map.

While the results presented highlight both the feasibility and advantages of the reverse-phase granulation process, two potentially negative consequences associated with the approach were addressed: first, the potential for the resultant granules to have inferior compaction properties and second, the potential for the increased rate or extent of formation of a different solid state form of the drug due to increased drug dissolution in the binder liquid. Nevertheless, the compaction properties of granules prepared using

the reverse-phase process were shown to be similar to those prepared using the conventional granulation process (Chapter 5). While although the reverse-phase process did result in granules of greater strength than the conventional process, the typical compaction pressures used to form tablets were orders of magnitude greater resulting in the differences being overwhelmed.

Moreover, when comparing the reverse-phase and conventional granulation processes no differences were observed in the rate or extent of hydration of the model drug anhydrous theophylline (Chapter 7). The latter results demonstrate that the immersion mechanism and elevated liquid saturation associated with the early stages of the reverse-phase process are not necessarily a cause for concern with respect to solid state transformations of the drug, though this should be evaluated on a case by case basis. The study was focussed on comparing the differences in the rate and extent of anhydrous theophylline between the two granulation processes, with the hypothesis that the reverse-phase process would result in a faster rate and greater extent of hydration. Based upon this hypothesis different polymer compositions were selected to demonstrate the feasibility of inhibiting the greater rate and extent of hydration in the reverse-phase process.

This initial hypothesis was proven incorrect and therefore the focus on using different polymers as a method to mitigate the differences between the two processes was less relevant. However, it was found that by changing the polymer composition of the binder liquid the rate and extent of anhydrous theophylline hydration could be partially inhibited to the same extent regardless of the granulation process employed. Two mechanisms for the inhibition were proposed. First, an increase in viscosity of the binder liquid may slow the dissolution of anhydrous drug by reducing the diffusivity of the solute, and the same mechanism may also slow the diffusion and incorporation of water molecules into the theophylline molecular structure. Second, when considering a polymer with an epitaxial match to the metastable drug crystals, i.e. complimentary spatial orientation of hydrogen donor/receptor groups between the polymer and drug, it is proposed that the polymer competes with water molecules for the available hydrogen bond acceptor sites of the anhydrous theophylline thus inhibiting the hydration.

The hydration of theophylline was the focus of this study, however further research comparing the solid state transformation of a range of drugs during the reverse-phase and conventional granulation processes is recommended. A number of suitable model drugs have previously been reported to undergo both hydrate and polymorphic transformations during wet granulation processing. The transformations of anhydrous caffeine to the 4/5 hydrate, anhydrous sulfaguanidine to the monohydrate and anhydrous carbamazepine to the dihydrate have all been monitored using Raman spectroscopy [22]. Additionally, the polymorphic transformation of flufenamic acid form I to form III has been monitored using *in-situ* X-ray powder diffraction during wet granulation with an ethanol binder liquid [23].

8.3 Future studies

The results and discussion presented in this thesis clearly illustrate both the feasibility and advantages of the reverse-phase granulation approach and further research is warranted in this field. Two main themes are proposed for future study. First, in the current thesis HA was used as the model powder owing to its practical insolubility in water. The applicability of the reverse-phase granulation approach to other material types of varying aqueous solubility should be evaluated. Second, the reverse-phase process research in this thesis was conducted at the 600 g scale in a 1 L granulator. Industrially wet granulation processes are often conducted on the 200–400 kg scale in 600–1200 L granulators [24]. The scale up of the process is therefore an obvious area for future study. Both proposed research areas are discussed further below.

8.3.1 Application to other material types

As mentioned above HA was selected due to its practical insolubility in water so that dissolution of formulation components as the process proceeded was not a complicating factor. The strength of liquid bridges between two particles is determined solely by the contributions of the quantity and composition of the binder liquid employed. A second consideration was that since a negligible quantity of material would be dissolved during the course of the process there would be negligible crystallisation of dissolved HA during the drying step.

However, multiple excipients are typically employed in an industrial wet granulation process and would typically include the drug, diluent, binder, disintegrant and surfactant. The formulation in this thesis included HA as a diluent and PVP as a binder liquid. While insoluble diluents are a common choice so too are soluble diluents such as lactose and hygroscopic diluents such as microcrystalline cellulose. The drug itself can also present unique physical properties to be considered [25]. Consideration of these more complex formulation variables means that future research should seek to evaluate the applicability of soluble and hygroscopic excipients to the reverse-phase granulation process.

Some results have been reported for the effect of soluble excipients on the conventional granulation process. Dissolution of soluble excipients decreases the quantity of binder liquid required since the surface area of the solid phase is reduced and the volume of the liquid phase is increased. For a granulation conducted where the lactose diluent was partially soluble in the water binder liquid a liquid saturation between 0.3–0.6 was required to achieve growth [26]. However when experiments were carried out using a polyethylene glycol (PEG) binder solution, in which the lactose was not soluble, rapid growth by coalescence required liquid saturations in the markedly higher range of 80–90 % [27].

These findings indicate the basic effect of using a soluble excipient. However, the effect has two significant implications in the reverse-phase process. First, since the process begins in a saturated condition it would postulated that a slurry of dissolved excipient may result is a very viscous paste that may be difficult to distribute mechanically throughout the remainder of the formulation resulting in a broad size distribution. The effect of impeller tip speed on the distribution of the paste would require comprehensive study.

Second, the dissolution of the soluble excipient will occur dynamically during the course of the granulation process. The rate and extent of this dissolution process will vary with the surface area of the particular batch of excipient and the temperature reached in the granulator. These factors are likely to vary from batch to batch and therefore one would expect the rate and extent of excipient dissolution to be variable from batch to batch. This has the effect of varying the quantity, viscosity and surface

tension of the binder liquid and particle size of the excipient from batch to batch. As a result characterisation of the granulation process using dimensionless groups such as liquid saturation and Stokes deformation number which rely upon these parameters becomes tenuous. One mitigation strategy that should be evaluated would be to saturate the binder liquid with the soluble excipient and to use a temperature controlled granulation process. This approach will decrease variability in the extent of excipient dissolution and allow the use of previously established dimensionless groups. Interestingly, these challenges are the same as those commonly encountered today with the conventional granulation process, however little literature exists examining these considerations.

Fewer studies have specifically studied the effect of using hygroscopic excipients in wet granulation processes. However one report for the wet granulation of microcrystalline cellulose particles with varying moisture content provides some basis for discussion [28]. When the initial moisture content of microcrystalline cellulose was increased there was an increase in the resultant granule size, even though a constant quantity of binder liquid was employed, which was attributed to the fact that capillary wetting plays a significant role in determining the quantity of moisture available for granule coalescence. In the context of the reverse-phase process this is not an insurmountable challenge, however sufficient processing time will likely be necessary in order to allow consistent capillary wetting otherwise variable quantities of binder liquid might be present at the surface of the particles and variability in granule size would result.

8.3.2 Scale up of the reverse-phase process

The basis for a process scale up approach should consider geometric, kinematic and dynamic similarity [29]. Geometric similarity implies two granulators have the same ratio of linear dimensions. Kinematic similarity implies the ratio of forces between two corresponding points in a granulator is similar. Dynamic similarity implies that all of the dimensionless numbers necessary to describe the process have the same numerical value. Since dimensionless numbers are independent of scale they can be used for scale up of granulation processes.

Scale up of conventional granulation processes has been investigated previously and a number of dimensionless techniques have been reported, including the Newton number, Froude number and Reynolds number [30]. In each approach the fill number, defined as the ratio powder fill height to granulator bowl diameter, is maintained constant for any scale up attempt. The Newton number relates the drag force acting on a unit area of the impeller and the inertial stress and is a measure of the power required to overcome friction [30]. The Reynolds number relates the inertial force to the viscous force [31]. The Froude number relates the centrifugal force to the gravitational force per unit area acting on the material [32]. It has been noted that the Froude number does not contain any terms describing the wet mass and therefore is best considered to describe scale up of the granulator than the process itself [11]. None of these approaches has been shown to be universal and often empirical scaling factors are incorporated into models to suit specific formulations and equipment sets. More recently calibrated test particles have been used in order to maintain a constant shear stress during scale up where a constant granule size distribution, strength and porosity have been achieved when moving from geometrically similar 2 L to 7 L to 25 L granulators [33, 34].

Industrial scale up of wet granulation processes presents many challenges. A number of different granulator models exist of differing size, design, geometry and material of construction. For example, two common industrial scale 600 L granulators are the PMA Fielder and the Collette Gral. The Glatt Powrex has a bottom mounted impeller whereas the Collette Gral has a top mounted impeller fitted to a shaft which penetrates the granule mass. As a result of fundamental differences such as this then geometric and kinematic similarities are unlikely to exist between different equipment vendors. Even when considering the same equipment vendor difficulty can be experienced. For example the Collete Gral 10 L, 75 L and 300 L granulators have been shown to be geometrically different [32]. When considering the same equipment vendor it is also necessary to understand the effect of different granulator bowl material of construction and impeller blade design. When comparing stainless steel and PTFE lined granulator bowls significant differences in flow patterns, adhesion of wet material to the walls and moisture distribution have been shown indicating the resistance between the formulation and the particular material of construction of the granulator bowl must be considered [35]. With respect to impeller design the scale-up of an MCC based wet granulation process in PMA Fielder 6 L, 25 L, 65 L, 150 L and 300 L granulators

demonstrated that maintaining a constant Froude number was only relevant when impellers with similar blade angle were used at the same tip speed [36]. The impeller shape is also important in determining the compressive and shearing forces exerted on the wet mass [37].

As presented in Chapter 6 the dimensionless groups of liquid saturation and Stokes deformation number were shown to be good predictors of the mass mean diameter and porosity of granules produced by the reverse-phase. Directionally the growth regime map has also been demonstrated to characterise the reverse-phase granulation process. During scale up to larger granulators it is expected that the wet granules will experience different forces than at the small scale resulting in different rates and extents of granule consolidation. Since both liquid saturation and Stokes deformation number consider the granule porosity and impact stress a logical hypothesis would be that a scale up approach might be employed where binder liquid volume and impeller tip speed are adjusted such that liquid saturation and Stokes deformation number are held constant to yield granules of similar size and porosity.

This hypothesis has been tested for a conventional granulation process scaling from a 10 L to a 75 L granulator [38]. While the authors predicted no change in the growth regime as a result of maintaining a constant liquid saturation and Stokes deformation number they observed marked differences in particle size distribution and lump formation. This was attributed to an approximate doubling of the dimensionless spray flux upon scale up which resulted from the attempt to maintain a constant liquid addition time but inadvertently increased the liquid addition rate. This resulted in a non-homogenous liquid distribution and demonstrated the importance of dimensionless spray flux in conventional granulation processes. As presented in Section 1.7 a motivating factor in the reverse-phase granulation process is the elimination of sensitivity to liquid addition variables where the process is intentionally designed to distribute binder liquid throughout the powder. As a result it could be predicted that scale up of the reverse-phase process using a constant liquid saturation and Stokes deformation number approach may be more robust than for the conventional granulation process.

Another option for efficient process scale-up is to leverage continuous granulation processing options such as twin screw extruders/granulators. Advantages of this equipment type include equipment design flexibility, short residence time, wide range of throughputs and intimate mixing of formulation ingredients [39, 40]. The batch size of twin screw granulated material is determined by the time the equipment operates [41]. Small scale process optimisation and scale-up to large scale commercial production can therefore be performed in the same granulator minimising scale-up challenges, improving process reproducibility and equipment investment costs [39]. Twin screw granulators have another major advantage of being regime-separated [42] where wetting and nucleation can be physically separated from consolidation and growth. Such a granulator design can provide a greater opportunity for controlling granule properties such as size and density [43, 44] when compared to the batch based wet granulation process where the rate processes typically occur spontaneously.

8.3.3 Conclusion

The recent industry trends towards implementation of Quality by Design [45-47] and Process Analytical Technology [48] bring with them increased regulatory and scientific expectations. These expectations are likely to sustain recent advances in continuous granulation processing since this technology allows the granulation process to be characterised, understood, scaled-up and controlled in a fashion that is not practically achievable today using batch high shear granulators. It is the author's assertion that in an environment where process control and understanding is paramount the reverse-phase granulation process should be considered as a viable and robust option when compared to the conventional granulation process. This is owing to the simplicity of the granule growth mechanism involved in the reverse-phase process and ease with which the resultant granule properties can be controlled.

8.4 References

[1] Newitt, D.M., Conway-Jones, J.M., A contribution to the theory and practice of granulation, Trans. I. Chem. Eng., 36 (1958) 422-430.

[2] Scott, A.C., Hounslow, M.J., Instone, T., Direct evidence of heterogeneity during high-shear granulation, Powder Technology, 113 (2000) 205-213.

[3] Holm, P., Jungerson, O., Schaefer, T., Kristensen, H.G., Granulation in High Speed Mixers Part I: Effects of process variables during kneading, Pharm. Ind., 45 (1983) 806-811.

[4] Hapgood, K.P., Litster, J.D., Smith, R., Nucleation regime map for liquid bound granules, AIChE J., 49 (2003) 350-361.

[5] Litster, J.D., Hapgood, K.P., Michaels, J.N., Sims, A., Roberts, M., Kameneni, S.K., Hsu, T., Liquid distribution in wet granulation: dimensionless spray flux, Powder Technology, 114 (2001) 29-32.

[6] Hapgood, K.P., Litster, J.D., Biggs, S.R., Howes, T., Drop penetration time into porous powder beds, Journal of Colloid and Interface Science, 253 (2002) 353-366.

[7] Hapgood, K.P., Nguyen, T., Shen, W., Drop penetration time in heterogeneous powder beds, Chem. Eng. Sci., 64 (2009) 5210-5221.

[8] Iveson, S.M., Litster, J.D., Growth regime map for liquid-bound granules, AIChE J., 44 (1998) 1510-1518.

[9] Kristensen, H.G., Holm, P., Schaefer, T., Mechanical properties of moist agglomerates in relation to granulation mechanisms: Part 1. Deformability of moist, densified agglomerates, Powder Technology, 44 (1985) 227-238.

[10] Plank, R., Diehl, B., Grinstead, H., Zega, J., Quantifying liquid coverage and powder flux in high-shear granulators, Powder Technology, 134 (2003) 223-234.

[11] Faure, A., York, P., Rowe, R.C., Process control and scale-up of pharmaceutical wet granulation processes: a review, Eur. J. Pharm. Biopharm., 52 (2001) 269-277.

[12] Terashita, K., Watano, S., Miyanami, K., Determination of end-point by frequency analysis of power consumption in agitation granulation, Chem. Pharm. Bull., 38 (1990) 3120-3123.

[13] Knight, P.C., Johansen, A., Kristensen, H.G., Schaefer, T., Seville, J.P.K., An investigation of the effects on agglomeration of changing the speed of a mechanical mixer, Powder Technology, 110 (2000) 204-209.

[14] Zinchuk, A., Mullarney, M., Hancock, B., Simulation of roller compaction using a laboratory scale compaction simulator, Int. J. Pharm., 269 (2004) 403-415.

[15] Forsmo, S.P.E., Vuori, J.P., The determination of porosity in iron ore green pellets by packing in silica sand, Powder Technology, 159 (2005) 71-77.

[16] Ghadiri, M., Rahmanian, N., Jia, X., Stepanek, F., Characterisation of granule structure and strength made in a high shear granulator, Powder Technology, 192 (2009) 184-194.

[17] Litster, J.D., Ramachandran, R., Poon, J., Sanders, C., Glaser, T., Immauel, C., III, F.D., Stepanek, F., Wang, F., Cameron, I., Experimental studies on distributions of granule size, binder content and porosity in batch drum granulation: Inferences on process modelling requirements and process sensitivities, Powder Technology, 188 (2008) 89-101.

[18] Carvajal, M.T., Macias, K.A., The influence of granule density on granule strength and resulting compact strength, Chem. Eng. Sci., 72 (2012) 205-213.

[19] Ghadiri, M., Rahmanian, N., Naji, A., Effects of process parameters on granule properties produced in a high shear granulator, Chemical Engineering Research and Design, 89 (2011) 512-518.

[20] Plantard, G., Goetz, V., Py, X., A direct method for porous particle density characterization applied to activated carbon, Advanced Powder Technology, 21 (2010) 592-598.

[21] Marston, J.O., Sprittles, J.E., Zhu, Y., Li, E.Q., Vakarelski, I.U., Thoroddsen, S.T., Drop spreading and penetration into pre-wetted powders, Powder Technology, 239 (2013) 128-136.

[22] Gift, A.D., Lunar, P.E., Luedeman, L., Taylor, L.S., Manipulating hydrate formation during high shear wet granulation, J. Pharm. Sci., 98 (2009) 4670-4683.

[23] Morris, K.R., Davis, T.D., Huang, H., Peck, G.E., Stowell, J.G., Eisenhauer, B.J., Hilden, J.L., Gibson, D., Byrn, S.R., *In situ* monitoring of wet granulation using online X-ray powder diffraction, Pharm. Res,, 20 (2003) 1851-1857.

[24] Michaels, J.N., Farber, L., Wong, G.S., Hapgood, K., Heidel, S.J., Farabaugh, J., Chou, J.-H., Tardos, G.I., Steady states in granulation of pharmaceutical powders with application to scale-up, Powder Technology, 189 (2009) 295-303.

[25] Vemavarapu, C., Surapaneni, M., Hussain, M., Badawy, S., Role of drug substance material properties in the processability and performance of a wet granulated product, Int. J. Pharm., 374 (2009) 96-105.

[26] Kristensen, H.G., Holm, P., Jaegerskou, A., Schaefer, T., Granulation in high shear mixers, Part 4: Effect of liquid saturation on the agglomeration, Pharm. Ind., 46 (1984) 763-766.

[27] Schaefer, T., Holm, P., Kristensen, H.G., Melt granulation in a laboratory scale high shear mixer, Drug Dev. Ind. Pharm., 16 (1990) 1249-1277.

[28] Shi, L., Feng, Y., Sun, C.C., Initial moisture content in raw material can profoundly influence high shear wet granulation process, Int. J. Pharm., 416 (2011) 43-48.

[29] Leuenberger, H., Scale-up of granulation processes with reference to process monitoring, Acta Pharm. Technol., 29 (1983) 274-280.

[30] Landin, M., York, P., Cliff, M.J., Rowe, R.C., Wigmore, A.J., Scale-up of a pharmaceutical granulation in a fixed bowl mixer-granulator, Int. J. Pharm., 133 (1996) 127-131.

[31] Reynolds, O., An Experimental Investigation of the Circumstances which Determine Whether the Motion of Water Shall Be Direct of Sinusous and of the Law of Resistance in Parallel Channels, Philos Trans. R. Soc. London, 174 (1883) 935-982.

[32] Vromans, H., Horsthuis, G.J.B., vanLaarhoven, J.A.H., vanRooji, R.C.B.M., Studies on upscaling parameters of the Gral high shear granulation process, Int. J. Pharm., 92 (1993) 143-150.

[33] Tardos, G.I., Hapgood, K.P., Ipadeola, O.O., Michaels, J.N., Stress measurements in high-shear granulators using calibrated "test" particles: application to scale-up, Powder Technology, 140 (2004) 217-227.

[34] Farber, L., Tardos, G.I., Michaels, J.N., Use of X-ray tomography to study the porosity and morphology of granules, Powder Technology, 132 (2003) 57-63.

[35] Faure, A., Grimsey, I.M., Rowe, R.C., York, P., Cliff, M.J., Applicability of a scale-up methodology for wet granulation processes in Collette Gral high shear mixer-granulators, Eur. J. Pharm. Sci., 8 (1999) 85-93.

[36] Campbell, G.A., Clancy, D.J., Zhang, J.X., Gupta, M.K., Oh, C.K., Closing the gap in series scale up of high shear wet granulation process using impeller power and blade design, Powder Technology, 205 (2011) 184-192.

[37] Knight, P.C., Seville, J.P.K., Wellm, A.B., Instone, T., Prediction of impeller torque in high shear powder mixers, Chem. Eng. Sci., 56 (2001) 4457-4471.

[38] Kayrak-Talay, D., Dale, S., Wassgren, C., Litster, J., Quality by design for wet granulation in pharmaceutical processing: Assessing models for *a priori* design and scaling, Powder Technology, 240 (2013) 7-18.

[39] Vervaet, C., Remon, J.P., Continuous granulation in the pharmaceutical industry, Chemical Engineering Science, 60 (2005) 3949-3957.

[40] Thompson, M.R., Sun, J., Wet granulation in a twin extruder: implications of screw design, J. Pharm. Sci., 99 (2010) 2090-2103.

[41] Dhenge, R.M., Fyles, R.S., Cartwright, J.J., Doughty, D.G., Hounslow, M.J., Salman, A.D., Twin screw granulation: granule properties, Chemical Engineering Journal, 164 (2010) 322-329.

[42] El-Hagrasy, A.S., Hennenkamp, J.R., Burke, M.D., Cartwright, J.J., Litster, J.D., Twin screw wet grnaulation: Influence of formulation parameters on granule properties and growth behavior, Powder Technology, 238 (2013) 108-115.

[43] Emady, H.N., Kayrak-Talay, D., Schwerin, W.C., Litster, J.D., Granule formation mechanisms and morphology from single drop impact on powder beds, Powder Technology, 212 (2011) 69-79.

[44] Wildeboer, W.J., Koppendraaier, E., Litster, J.D., Howes, T., Meesters, G., A novel nucleation apparatus for regime-separated granulation, Powder Technology, 171 (2007) 96-105.

[45] ICH Q8(R2), 2009, Pharmaceutical Development, http://www.ich.org/fileadmin/Public_Web_Site/ICH_Products/Guidelines/Quality/Q8_R1/Step4/Q8_R2_Guideline.pdf).

[46] ICH Q9, 2005, Quality Risk Management, http://www.ich.org/fileadmin/Public_Web_Site/ICH_Products/Guidelines/Quality/Q9/Step4/Q9_Guideline.pdf).

[47] ICH Q10, 2008, Pharmaceutical Quality Systems, http://www.ich.org/fileadmin/Public_Web_Site/ICH_Products/Guidelines/Quality/Q10/Step4/Q10_Guideline.pdf).

[48] Food and Drug Administration, 2004, Guidance for Industry PAT - A framework for innovative pharmaceutical development, manufacturing and quality assurance, http://www.fda.gov/CDER/GUIDANCE/6419fnl.htm).